FLUXES OF DISSOLVED ORGANIC CARBON DURING STORM EVENTS IN THE NEPONSET RIVER WATERSHED

A Dissertation Presented

by

KEITH THOMAS CIALINO

Submitted to the Office of Graduate Studies,
University of Massachusetts Boston,
in partial fulfillment of the requirements for the degree of

DOCTOR OF PHILOSOPHY

June 2015

Environmental Science Program

FLUXES OF DISSOLVED ORGANIC CARBON DURING

STORM EVENTS IN THE NEPONSET RIVER WATERSHED

A Dissertation Presented

by

KEITH THOMAS CIALINO

Approved as to style and content by:

_____

Robert F. Chen, Professor
Chairperson of Committee

_____

Ellen M. Douglas, Associate Professor
Member

_____

Crystal B. Schaaf, Professor
Member

_____

George B. Gardner, Adjunct Associate Professor
Member

_____

Ferdi L. Hellweger, Associate Professor, Northeastern University
Member

_____

Ellen M. Douglas, Graduate Program Director
School for the Environment

_____

Robyn Hannigan, Dean
School for the Environment

ABSTRACT

FLUXES OF DISSOLVED ORGANIC CARBON DURING STORM EVENTS IN THE NEPONSET RIVER WATERSHED

June 2015

Keith Thomas Cialino, B.A., La Salle University
M.S., University of Massachusetts Boston
Ph.D., University of Massachusetts Boston

Directed by Professor Robert F. Chen

The transport of dissolved organic carbon (DOC) and chromophoric dissolved organic matter (CDOM) from land to coastal environments strongly influences coastal ecosystems. The presence of first flush phenomena due to rainwater runoff traveling from land into waterways can greatly affect carbon fluxes to coastal areas. This research utilizes sensors, autosamplers, and standard watershed sampling in order to assess for the presence of first flush and its significance.

A rainfall simulator was built in order to collect runoff on two land use types. Time series data suggest that first flush of dissolved organic carbon was present for all rainfall intensities simulated on an impervious surface. At this location, approximately 40% to 51% of DOC flux occurred within the first 20% of runoff. At the permeable sampling location, first flush was observed in surface runoff collected during 12.7 and

25.4 mm hr^{-1} simulated storms, with 31% and 26% of DOC flux occurring within the first 22% of runoff.

Seven storm events at two locations in the Neponset River Watershed, Massachusetts, USA were monitored to study the impact of storm events on DOC export from an urban watershed. Real-time CDOM fluorescence sensor measurements were better able to capture the variability present in riverine DOC and CDOM concentrations due to runoff influxes. Using modeled flow data, estimates of total DOC export fluxes during storms were compared to estimated total annual export. Based on these calculations, the seven sampled storm events account for 7 to 10 percent of the calculated yearly flux during 4 to 5 percent of the year. Additional work is needed to collect consistent year round data using sensors at these locations.

DOC was sampled throughout the Neponset River Watershed monthly for seven years. Increased concentrations were observed following storm events and snowmelt, and were an average of 28% greater than concentrations observed during dry periods. Based on daily sampling data in September 2011, monthly fluxes may be underestimated by 38% or overestimated by 35%. More frequent sampling allows for better certainty in estimations of monthly and yearly fluxes from the watershed, but must be balanced with logistical and cost constraints.

ACKNOWLEDGEMENTS

I would like to thank Bob Chen, my graduate advisor and the chair of my committee. This research would not have been possible without his encouragement, support, and guidance.

I also appreciate the time donated by the members of my committee - Bernie Gardner, Ellen Douglas, Crystal Schaaf, and Ferdi Hellweger - whose advice helped to shape this manuscript. Thank you.

Thank you to Francesco Peri for his invaluable assistance with all things technical. Most of this research would have never gotten off the ground without his help.

This work would not have been completed without help from the Chen Lab and School for the Environment graduate students, faculty, and staff, including Wei Huang, Hayley Schiebel, Jason Olavesen, Yun Yang, Benjamen Wetherill, Jaclyn O'Riley, Thomas Heath, and Marin Kress.

Thanks to Blue Hill Observatory and Science Center for allowing me access to their weather data, and to Massachusetts Department of Conservation and Recreation for allowing me to conduct research within Blue Hills Reservation.

The National Science Foundation GK-12 Program Watershed Integrated Science Partnership, University of Massachusetts Boston School for the Environment, Office of Graduate Studies Doctoral Dissertation Research Grant Program, and the Graduate Student Assembly provided financial support.

During my graduate career, I had the chance to pursue several great opportunities, including the Harvard University Kennedy School of Government Rappaport Public

Policy Fellowship and the NOAA Sea Grant John A. Knauss Marine Policy Fellowship. Thank you to all my employers – COSMIC, EPA Region 1, NMFS Office of International Affairs, Urban Harbors Institute, and the NOAA Marine Debris Program.

My family has been supportive and understanding through everything, and I would not be where I am today without their lifelong love, support and encouragement. Thank you.

Thank you to my fiancée, Betsie, for her help and encouragement, and for supporting me throughout this process.

To all others not acknowledged by name that assisted me during my graduate career, thank you.

DEDICATION

To my parents, Ronald and Jacqueline

TABLE OF CONTENTS

CHAPTER Page

LIST OF FIGURES

Figure Page

Figure Page

Figure Page

Figure Page

Figure Page

Figure Page

Figure Page

Figure Page

Figure Page

LIST OF TABLES

Table Page

LIST OF ABBREVIATIONS

°C	degrees Celsius
BOD	biological oxygen demand
C	carbon
CDOM	chromophoric dissolved organic matter
CWMN	Citizens Water Monitoring Network
DN	dissolved nitrogen
DO	dissolved oxygen
DOC	dissolved organic carbon
DOM	dissolved organic matter
FAO	Food and Agriculture Organization of the United Nations
GIS	Geographic Information System
HCl	hydrochloric acid
in hr^{-1}	inches per hour
J	Joules
km^2	square kilometers
m^2	square meters
mg/L	milligrams per liter
mm	millimeter(s)
mm hr^{-1}	millimeters per hour
MWRA	Massachusetts Water Resources Authority
NepRWA	Neponset River Watershed Association
NOAA	National Oceanic and Atmospheric Administration
PP	pour point
psi	pounds per square inch
QSU	quinine sulfate units
t_c	time of concentration
USGS	United States Geological Survey
UV	ultraviolet
λ	wavelength
μM	micromolar

CHAPTER 1

INTRODUCTION

The transport of dissolved organic carbon and chromophoric dissolved organic matter from land to coastal environments strongly influences coastal ecosystems. Episodic events cause increased transport due to rainwater runoff traveling from land into waterways. The presence of first flush phenomena during storm events can greatly affect carbon fluxes to coastal areas. Sensor networks and high resolution sampling protocols can be used to assess the presence of first flush and its significance.

The Carbon Cycle

Carbon is the fourth most abundant element on earth by mass and fifteenth most abundant element in the Earth's crust, and carbon dioxide is the fourth most abundant gas in the atmosphere by volume (Chang and Goldsby, 2012). Due to its abundance and ability to form bonds, carbon is considered the building block of life. It is present in all living organisms. Carbon is tetravalent, having four electrons able to form covalent bonds and a wide diversity of molecules and biomolecules (Chang and Goldsby, 2012). There are three naturally occurring isotopes – ^{12}C, ^{13}C, and ^{14}C. ^{12}C and ^{13}C are stable, while ^{14}C is radioactive. ^{14}C is used for radiometric dating of biological material and

groundwater. The ratio of ^{12}C and ^{13}C can be used to determine differential uptake in living organisms. The sources of surface and ground water can also be identified using ^{12}C and ^{13}C ratios (Levin and Hesshaimer, 2000; Chang and Goldsby, 2012).

Carbon is found in the environment in multiple forms, such as carbonate ($CaCO_3$) in rocks, carbon dioxide (CO_2) in the atmosphere, dissolved as bicarbonate (HCO_3^-) in water, and stored in fossil fuels and other dead organic matter in soils and sediments. Carbon enters the biosphere through photo- or chemosynthesis by autotrophs, which are able to convert inorganic carbon into organic forms. Respiration returns the organic carbon to the environment. The carbon cycle (Figure 1.1) details the movement and transformations of carbon in the environment.

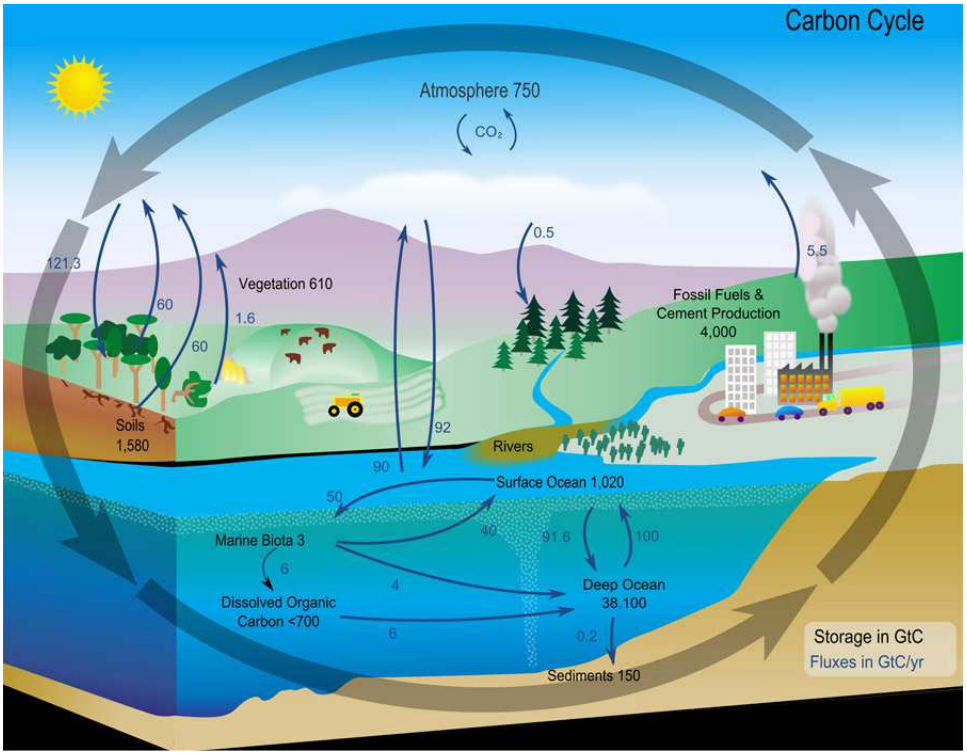

Figure 1.1: Global carbon cycle, showing carbon sinks and fluxes (Riebeek, 2011)

Carbon dioxide in the atmosphere helps to trap longwave radiation and creates about 25% of the greenhouse effect (Schneider, 1989; Karl and Trenberth, 2003). Without this process, the average temperature of the earth would be about 30 degrees Celsius cooler (Schlesinger and Bernhardt, 2013). Perturbations in the carbon cycle caused by the burning of fossil fuels and deforestation are causing an increase in greenhouse gases, which is causing global climate change (Schneider 1989; Karl and Trenberth 2003; Intergovernmental Panel on Climate Change 2007; Pachauri and Reisinger 2007; Cook et al. 2013; Intergovernmental Panel on Climate Change 2013). This imbalance in the cycle is partially balanced by sinks of carbon in terrestrial plants and the ocean. However, the increase of dissolved inorganic carbon in the ocean is causing ocean acidification (Fabry et al., 2008; Doney et al., 2009; Riebeek, 2011).

Coastal carbon represents a small, but important, part of the global carbon cycle. Coastal rivers and estuaries connect coastal watersheds with coastal oceans. There are active processes within these ecosystems that can influence nutrient availability. As climate change and its impacts have become widely publicized (Intergovernmental Panel on Climate Change, 2007; Pachauri and Reisinger, 2007; Anderegg et al., 2010; Cook et al., 2013), the importance of terrestrial dissolved organic matter (DOM) in the global carbon cycle has been recognized (Opsahl and Benner, 1997; Cole et al., 2007). However, the sources, transport, and processing of this DOM as it moves into the ocean requires further investigation (Hedges et al., 1997; Schlunz and Schneider, 2000; Chen and Gardner, 2004; Coble, 2007). Cole et al. (2007) emphasized that freshwater ecosystems are “an active component of the global carbon cycle”, rather than a “neutral pipe” that

funnels carbon from land to the ocean with few changes (Figure 1.2). Estuaries are also dynamic areas, where carbon is rapidly cycled (Figure 1.3), with autochthonous production, bacterial transformations, and photo-oxidation regulating and removing terrestrial carbon inputs (Wang et al., 2004; Yamashita et al., 2008; Dai et al., 2012; Bauer et al., 2013).

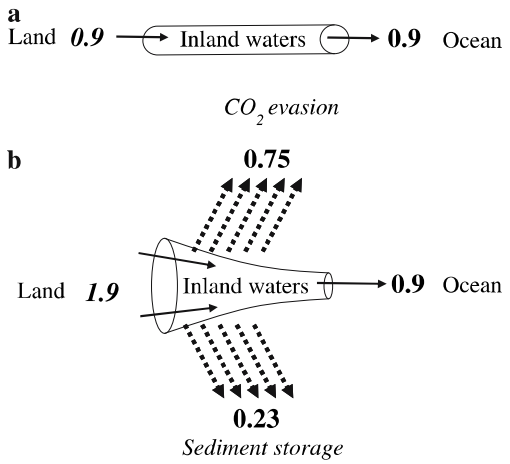

Figure 1.2: Schematic views of the role of inland aquatic systems in the global carbon cycle. a) The passive pipe theory, where organic and inorganic carbon is transferred to the ocean passively. b) An alternative view with inland waters as active components of the carbon cycle. Terrestrial carbon is stored in sediments and lost through processes to the atmosphere, in addition to transport to the ocean. Values in Pg C y-1. From Cole et al. (2007)

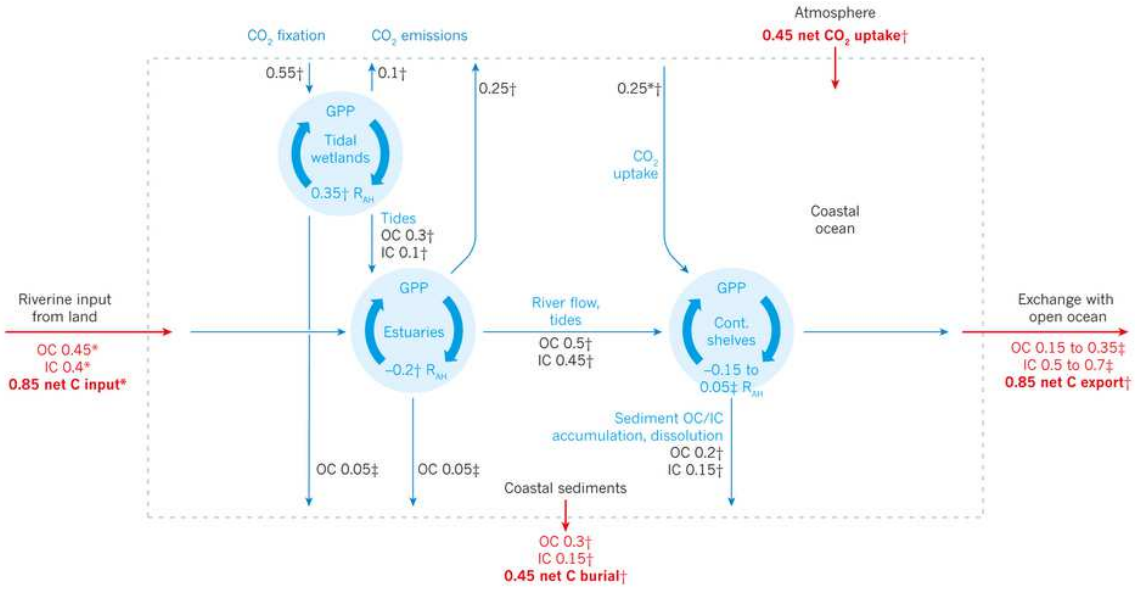

Figure 1.3: Carbon fluxes within (values in black) and across (values in red) the boundaries of the coastal ocean. All organic carbon (OC) and inorganic carbon (IC) fluxes are presented as positive values, arrows indicate direction of flux. Particulate and dissolved OC fluxes are presented as total OC values. The balance between gross primary production (GPP) and total system respiration (both autotrophic, A, and heterotrophic, H; RAH) is net ecosystem production (NEP), with negative values indicating conversion of OC to IC. The IC burial flux takes into consideration calcification. Typical uncertainties for carbon fluxes: *95% certainty that the estimate is within 50% of the reported value;†95% certainty that the estimate is within 100% of the reported value; ‡uncertainty greater than 100%. Units are Pg C yr−1 (1 Pg = 1015 g) rounded to ± 0.05 Pg C yr−1. Within-river fluxes and transformation of carbon are excluded from this analysis. From Bauer et al. (2013)

Dissolved organic carbon

Dissolved organic matter, including dissolved forms of carbon, nitrogen, and phosphorus, serves as a vehicle for the export of terrestrial carbon, nitrogen and phosphorus to coastal oceans (Qualls et al., 1991; Hedin et al., 1998; Kalbitz et al., 2000). As a result, knowledge about the riverine concentration of DOC and its transformation and movement through ecosystems is important. DOM represents an important source of nutrients for aquatic species (Jackson and Williams, 1985; Kemp et al., 1997; Gomi et al., 2002; Pace et al., 2004; Aller and Blair, 2006), enhances primary productivity (Rabalais

et al., 2002), and absorbs harmful UV radiation (Green and Blough, 1994; Morris et al., 1995). Opsahl and Benner (1997) state that while terrigenous DOM represents only 0.7-2.4% of the total DOM in the ocean, the rapid remineralization of terrigenous DOM leads to nutrients that could contribute to increased primary productivity in coastal waters.

While there are still some uncertainties surrounding estimates of riverine DOC transport to the ocean, there is 95% certainty that these estimates are within 50% of the reported value (Bauer et al., 2013). Depending on the study referenced and methods used, rivers transport approximately 0.17 to 0.45 Pg C y^{-1} (0.17 x 10^{15} g C to 0.45 x 10^{15}g C y^{-1}) as DOC from land to ocean annually (Schlunz and Schneider, 2000; Cole et al., 2007; Dai et al., 2012; Bauer et al., 2013; Schlesinger and Bernhardt, 2013). Many estimates are extrapolated from the measured fluxes from only the world's largest rivers (Schlunz and Schneider, 2000). For instance, Dai et al. (2012) used data from 118 rivers with available DOC concentrations, accounting for 48% of the global total riverine discharge, to estimate global DOC fluxes. This extrapolation may miss the influence of event-driven fluxes that may dominate water transport in many small watersheds that account for the other 52% of the global riverine discharge, but are currently unaccounted for in global river DOC fluxes.

The flux of DOC from rivers into coastal areas is highly variable and influenced by anthropologic perturbations, such as land use change, waterway modifications, and wetland loss (Findlay et al., 2001; Xenopoulos et al., 2003; Dai et al., 2012). Climate change also influences DOC export through changes in river discharge, sea-level height,

or the severity of storms. Climate change is expected to increase riverine carbon fluxes, and also lead to increased variability in these fluxes (Dai et al., 2012).

Urbanization and increased development can cause increased nutrient concentrations within a river (Howarth et al., 2002). Overland flows and sewer outfalls from developed watersheds often carry nutrients from fertilizers, as well as eroded soils and organic debris. This nutrient loading can result in increased algal growth. Excessive algal growth can cause low dissolved oxygen (hypoxia), unsightly appearance, odors, and degradation of aquatic habitat (Michaud, 1994; Howarth et al., 2002). In addition, ocean acidification effects can be amplified in estuaries that are nutrient-rich (Cai et al., 2011; Bauer et al., 2013). This can occur because increased respiration of organic matter by microbes produces carbon dioxide and increases acidity (Cai et al., 2011).

A better quantitative and qualitative understanding of the carbon exported from land to the ocean is important for coastal and global carbon budgets, as well as informing estimates of the global sink of anthropogenic carbon. Wahl, McKellar, and Williams (1997) compared DOC export from an urban stream and a forested stream in South Carolina. They found that mean annual DOC concentration in the urbanized stream was half that of the forested stream. However, due to greater runoff volumes in the urban catchment, the annual DOC fluxes from the streams were within 10%. In a study of DOC in Arizona, wastewater effluent was the dominant water flow, and responsible for the majority of the DOC flux (Westerhoff and Anning 2000). Tian et al. (2013) found that land surface processes (land-use type and density, hydrology and soil properties) are the primary factors controlling riverine DOC concentrations in small watersheds, particularly

watersheds within a single climate zone and where the inter-annual mean temperature variation is small (less than 2 ° C).

Yang et al. (2013) investigated the variation of DOC and dissolved nitrogen (DN) in surface runoff water during storms from different land use types in Florida. The land use types included residential, agricultural (vegetable farm, nursery, ranch, citrus grove), golf course, and forest. They found that land use type and the size and intensity of rainfall events strongly influenced the concentrations of DOC and DN, as well as the export of nitrogen, phosphorus, and metals in runoff. The largest export of DOC occurred during rain events.

Water quality

Protecting water quality in an urban watershed ensures safe drinking water (Makepeace et al., 1995), swimmable recreation areas (Pruss, 1998; Wade et al., 2003, 2006; Yau et al., 2009), and increased economic and aesthetic value to resource users (Greenley et al., 1981; Wiley et al., 2006). Water quality is mainly determined by the relative abundances of primary contaminants such as nutrients (including organic matter), heavy metals, microbial pathogens, sediment loading, and persistent organics. These contaminants are monitored by primary indicators such as dissolved oxygen (DO) levels, biological oxygen demand (BOD), nitrate and phosphate concentrations, *Escherichia coli*, turbidity and general appearance (foam, smell) (Peeler et al., 2006). Most monitoring of these indicators in surface waters occurs periodically in specific locations (Stewart et al., 2008).

Dissolved organic carbon in drinking water supplies can alter the efficacy of treatment efforts, and its presence can lead to harmful disinfection byproducts (Garvey and Tobiason, 2003; Kaplan et al., 2006). The fate and transport of pollutants, such as mercury, can be influenced by complexation with DOC (Ravichandran, 2004; Herngren et al., 2005; Selvendiran et al., 2008; Shanley et al., 2008). DOC also alters stream pH (Wigington Jr. et al. 1996).

Chromophoric Dissolved Organic Matter (CDOM)

Dissolved organic matter is composed of thousands of compounds, most of which have not been classified into compounds or compound classes. CDOM is the colored fraction of dissolved organic matter that absorbs light over a broad range of wavelengths, both visible and UV. CDOM is typically yellowish in color and fluoresces blue when irradiated with UV light. Due to its light absorbing properties, CDOM affects the light penetration of natural waters and can influence biogeochemical processes. CDOM is also useful as a tracer for DOC, as well as a "proxy for mixing" (Coble, 2007), in aquatic environments (Green and Blough, 1994; Stedmon et al., 2003; Chen and Gardner, 2004; Coble, 2007).

CDOM is composed of a mixture of humic substances, amino acids, and pigments from various sources. The primary source of CDOM in coastal waters is from rivers and groundwater carrying terrestrially-derived CDOM from soils. CDOM can also be produced *in situ* by plankton and bacteria. Upwelling, pore water advection, sediment resuspension, and anthropogenic sources, such as sewage effluent, can also be

contributors (Coble, 2007). CDOM typically behaves conservatively in relation to salinity in coastal areas. Non-conservative behavior may be evidence of estuarine production or removal (Gardner et al., 2005; Bowers and Brett, 2008).

Sinks of CDOM include photodegradation and microbial decomposition. The major products of degradation and decomposition are dissolved inorganic carbon and low molecular weight organic compounds, which are not colored. Photodegradation results in the release of labile, biologically available compounds, as well as the freeing of trace metals that might be associated with CDOM (Del Vecchio and Blough, 2002, 2004; Yamashita and Jaffé, 2008). In estuaries, it is possible for a surface layer of low salinity, high CDOM riverine water to remain on top of higher salinity estuarine water, although this varies by river system, and can vary with tide, season, and riverine discharge. For example, Gardner, Chen, and Berry (2005) found differences in CDOM spatial distribution within the Neponset Estuary depending on tidal period. Phytoplankton and bacteria can rapidly consume the nutrient flux within this freshwater layer, including labile DOC. CDOM photodegradation is also enhanced in this layer due to its exposure to direct sunlight. Other factors that influence CDOM in coastal areas include dilution, physical mixing, biological degradation, and in situ production (Coble, 2007). These processes can complicate the measurement of DOC and CDOM fluxes in coastal environments.

In terrestrially influenced areas, when the CDOM/DOC relationship is known, CDOM measurements can be used as a proxy for DOC concentration (Figure 1.4). CDOM fluorescence can be easily measured *in situ*, while DOC concentration requires

sample collection and laboratory analysis (Green and Blough, 1994; Coble, 2007). In situ measurement also allows for high resolution sampling. During episodic events, stormwater runoff can be a significant contributor to CDOM concentrations in rivers (Baker and Spencer, 2004; Huang and Chen, 2009).

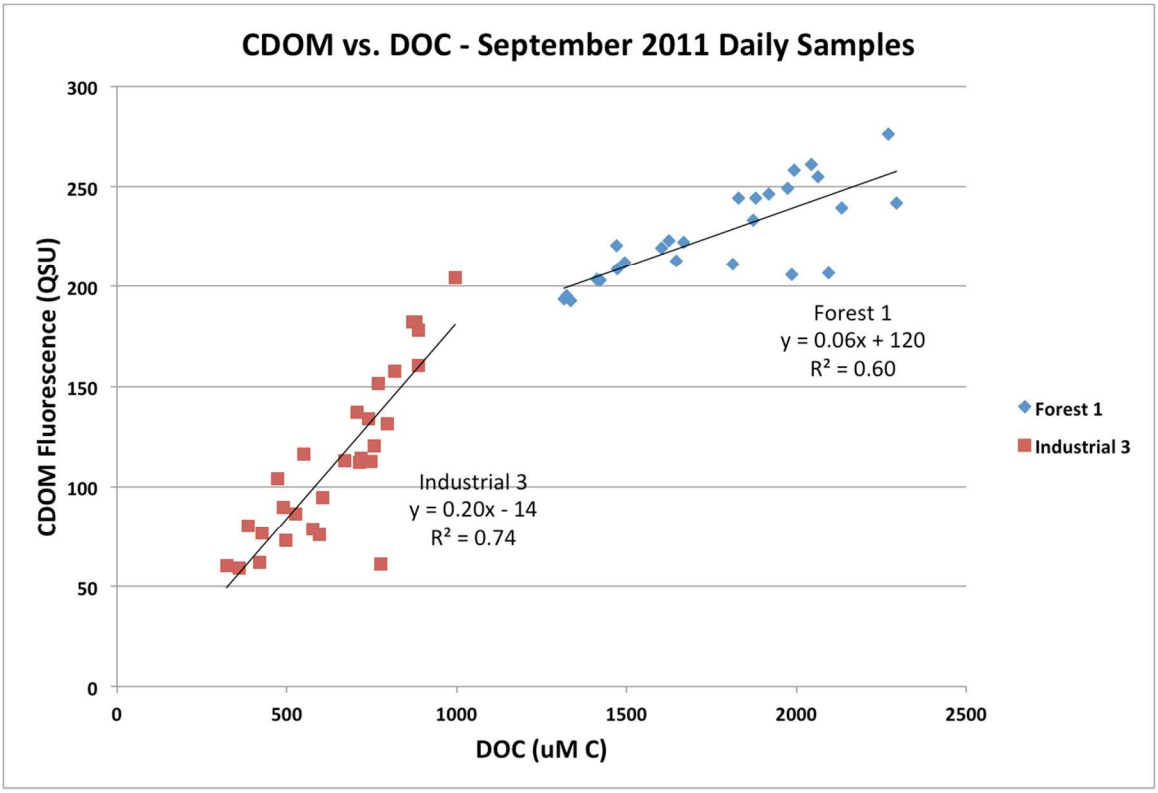

Figure 1.4: An example of the CDOM-DOC relationship from sample data collected during daily sampling at two Neponset Watershed locations in 2011

CDOM is also of interest for researchers examining ocean color using satellite-based sensors. The presence of CDOM in coastal areas complicates the measurement of chlorophyll *a* by remote sensing. CDOM absorbs strongly in the blue wavelengths, which is also where chlorophyll *a* light absorption is measured. In addition, remote observations only measure the return from the water surface, so knowing more about CDOM distribution and dynamics within an estuary allows for better assessment of the results

from these instruments (Coble, 2007). For example, better data about event-based estuarine stratification of a surface layer of low salinity, high CDOM riverine water on top of higher salinity estuarine water at a river mouth could result in a different interpretation of remotely sensed data.

First Flush

Contaminant levels and fluxes within a watershed are not constant over time, have multiple sources, and even vary rapidly over the course of a single rain event (Ahn et al., 2005). Previous studies have demonstrated that storm water runoff is a prime contributor to water quality degradation (Characklis and Wiesner, 1997; Buffleben et al., 2002; Ahn et al., 2005). During a phenomenon known as the "first flush," the initial runoff during a rainstorm can contain substantially elevated contaminant concentrations relative to runoff occurring later in the storm (Figure 1.5) (Lee and Bang, 2000; Lee et al., 2002; Kayhanian and Stenstrom, 2008).

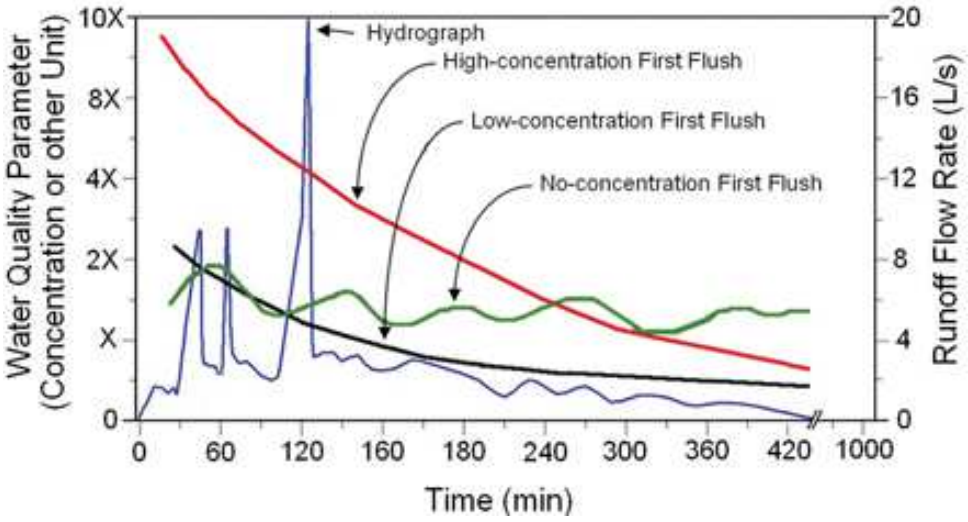

Figure 1.5: Generalized representation of first flush. From Kayhanian and Stenstrom (2008)

Hydrologic connectivity is defined as the linking of various parts of a watershed through subsurface water flow (Stieglitz et al., 2003). Stieglitz et al. (2003) used flow simulations to show that catchments are rarely connected, but connection throughout the watershed occurs during storm and snowmelt events when antedecent soil moisture is high.

In addition to subsurface flow, overland flow, or sheet flow can be a major transport pathway for water to rivers, ponds, and lakes during rain events. As a result, overland flows are also responsible for increased contaminant loadings to bodies of water (Miller and Gardner, 1981; Smith and Goodrich, 2005). Overland flow is a thin film of water that forms on a surface when the precipitation rate exceeds the infiltration rate. The infiltration rate depends on the permeability of the surface on which the precipitation is occurring. For natural surfaces, vegetation and sediment grain size influence the infiltration rate. Impervious surfaces, such as asphalt, reduce the infiltration rate and cause increased overland flow and flashy hydrologic response (Pitt, 1999).

One mechanism that causes first flush is the impact of raindrops on the ground resulting in the dislodging and movement of natural materials and pollutants. Many authors have studied the mechanism of rain falling to the ground and impacting surfaces. Soil erosion is typically caused by raindrop impact and overland flow (Hairsine and Rose, 1991). During raindrop impact, the drop depresses the soil surface. The kinetic energy of the drop is also transferred to lateral shear due to radial flow. A soil with a lower shear strength results in a larger depression and greater soil detachment due to the lateral shear of the radial flow (Aldurrah and Bradford, 1982). Some of the detached soil, and

interstitial waters, can be transported away from the impact site by overland flow (Hairsine and Rose, 1991).

For impervious surfaces, pollutants build up on the surface prior to a storm. Raindrops impacting these surfaces result in wash-off. Raindrop impact and sheer stress caused by surface runoff is responsible for loosening soluble or particulate pollutants and causing wash-off (Vaze and Chiew, 2003; Shaw et al., 2006). A storm event is only able to wash-off a fraction of the surface pollutant load. This fraction varies with rainfall intensity, rainfall kinetic energy, and the type of pollutant (Vaze and Chiew, 2002; Egodawatta et al., 2007). In addition, rainfall impact energy is very important at the beginning of a storm for detaching surface pollutants. The availability of easily detachable and transportable fractions of the surface pollutant decreases over the storm (Vaze and Chiew, 2003).

The magnitude of the first flush depends on site-specific conditions, such as land use, the amount of rainfall, antecedent precipitation, and the contaminant being studied (Makepeace et al., 1995; Appel and Hudak, 2001; Stenstrom and Kayhanian, 2005; Kayhanian and Stenstrom, 2008). Antecedent precipitation affects the amount of water and contaminant concentrations within surface soils. It has an impact on the amount of runoff that occurs during a subsequent rain event, and also influences the non-linearity of runoff during storms of similar intensity and duration. Antecedent precipitation has a greater influence when soil moisture and groundwater are major contributors to runoff (Jakeman and Hornberger, 1993; Beven, 2011). Time of concentration (t_c) can be calculated for a watershed. This is defined as the time required for water to travel from

the most hydrologically remote point in the watershed to the point of sample collection. Impervious surfaces reduce t_c by significantly reducing transport times within watersheds (Kang et al., 2008).

First flush can be difficult to measure in large watersheds because of the combination of many first flushes from different areas of the watershed. This is known as the "variable source area theory" of runoff generation (Hewlett and Hibbert, 1967). For instance, a monitoring point at the mouth of a river samples many different times of travel. This means that the runoff generated in one part of the watershed is reaching the collection point at a different time than runoff generated later in the storm. Kayhanian and Stenstrom (2008) observed first flush of pollutants typically "within the first few minutes to the first hour after observable runoff." This is why stormwater best management practices encourage local collection and treatment of runoff, and why monitoring for first flush must be done at a subwatershed scale.

Standard watershed monitoring programs can underestimate or completely miss the first flush because sampling strategies are not designed to capture episodic events, or these events are not sampled effectively. Several studies have shown the value of using high resolution sampling for different contaminants, but they did not examine first flush specifically (Grant et al. 2001; Boehm et al. 2002; Schiff and Tiefenthaler 2003; Gersberg, Daft, and Yorkey 2004; Ahn et al. 2005; Jeong, Sanders, and Grant 2006; Hellweger 2007; Eckley et al. 2008; Eckley and Branfireun 2008; Hellweger and Masopust 2008; Sheng, Ying, and Sansalone 2008; Zhang et al. 2008; He et al. 2010; Lee et al. 2011). Other studies have examined sampling strategies to capture the first flush.

Hathaway and Hunt (2010) evaluated the influence of first flush on total suspended solids and fecal indicator bacteria in an urban watershed. Tiefenthaler, Schiff, and Bay (2001) focused on total suspended solids and total organic carbon during first flush in an urban watershed (Figure 1.6).

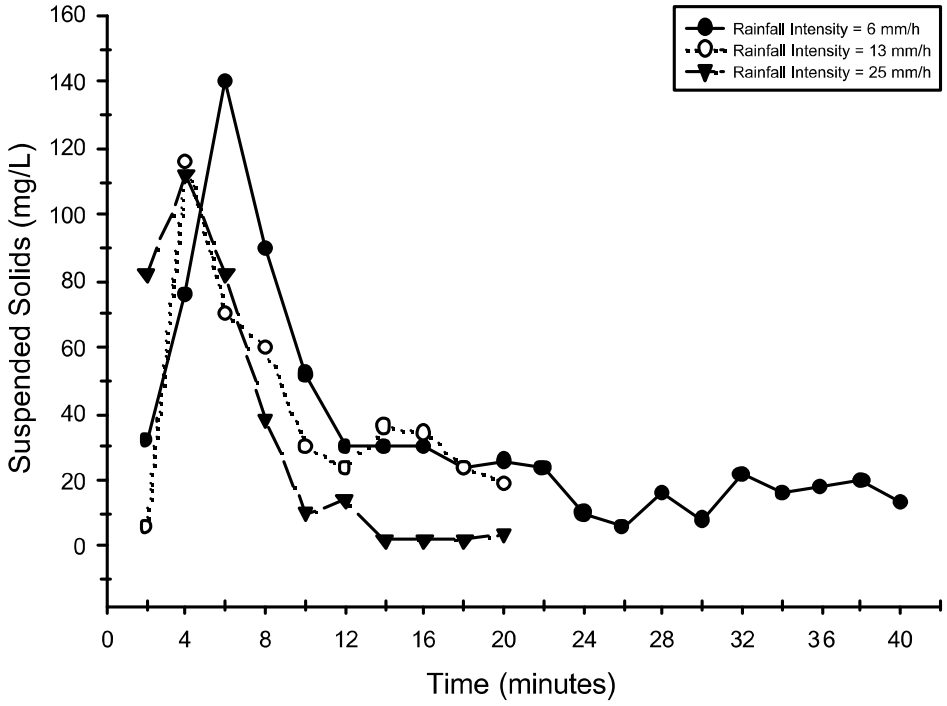

Figure 1.6: Time-concentration series of suspended solids concentrations (mg/L) for 6.3, 12.7, and 25.4 mm hr^{-1} simulated rainfall intensities. From Tiefenthaler and Schiff (2003).

Defining First Flush

Kayhanian and Stenstrom (2008) define a "concentration first flush" as initial storm runoff having a higher concentration relative to runoff later in the storm. A "mass first flush" is flow-related, and occurs when both the concentration and flow amount are elevated relative to the concentration and flow later in the storm. The authors state that "[c]oncentration first flushes have been frequently reported, but mass first flushes have

rarely been quantified." This is due to storm dynamics. In general, lower flows with higher concentrations may occur at the beginning of the storm, but greater flows with low concentrations during the middle of the storm result in a greater mass flux (Kayhanian and Stenstrom, 2008).

Deletic (1998) defines first flush as the percentage of total event pollution load transported by the first 20 percent of storm runoff volume. First flush is present if the first flush pollution load for an event is significantly greater than 20 percent. However, Deletic does not define what value is significant. A later study that Deletic coauthored (Bach, McCarthy, and Deletic 2010) reviews the problems with the variety of first flush definitions present in scientific literature. The presence or absence of first flush is determined by the definition used, which often uses arbitrary values set by the researcher. In most studies, dimensionless cumulative pollutant load vs. cumulative runoff volume curves are utilized. This curve is then used to define first flush as, for example, the first 25-30% of runoff transporting 70–80% of total pollutant mass. Other studies utilize a concept called Mass First Flush Ratio (MFFR), which compares the proportion of pollutant mass with the cumulative runoff volume at a particular point (Stenstrom and Kayhanian, 2005).

Using these methods ignores the impact of storm volume. A short-term pollutant source is defined by Kang, Kayhanian, and Stenstrom (2008) as pollution that accumulates between rain events and can be depleted by storms that are long and intense enough. A long-term pollution source is the watershed's background pollutant levels, which are not depleted. A small rain event may have consistently high concentrations

throughout the storm because the short-term pollution load dominates the concentrations. This would lead to a conclusion that a small event did not have a first flush.

First flush is traditionally defined based on the changes in contaminant fluxes during an event and is not compared to the catchment's background concentrations, or long-term pollution source. Bach, McCarthy, and Deletic (2010) give the example that 80% of the total load in a short event may be diluted in a longer event and thus represent only 60% at the same cumulative runoff. Other events display an "end flush", which is an increase in concentration at the end of a storm. The increased concentration at the end of the storm can mask the presence of a first flush.

During storm events, the relationship between concentration and discharge is rarely linear. Hysteresis occurs when there is a temporal difference in the response of a dissolved component compared to discharge. Evans and Davies (1998) present an overview of possible hysteresis scenarios using a three-component model. The model considers the concentrations of groundwater, soil water, and surface event water (runoff). In a clockwise loop (Figure 1.7, a-c), the total concentration is higher during the rising limb of the discharge, with the surface event water concentration greater than the soil water concentration. In an anticlockwise loop (Figure 1.7, d-f), the opposite is true.

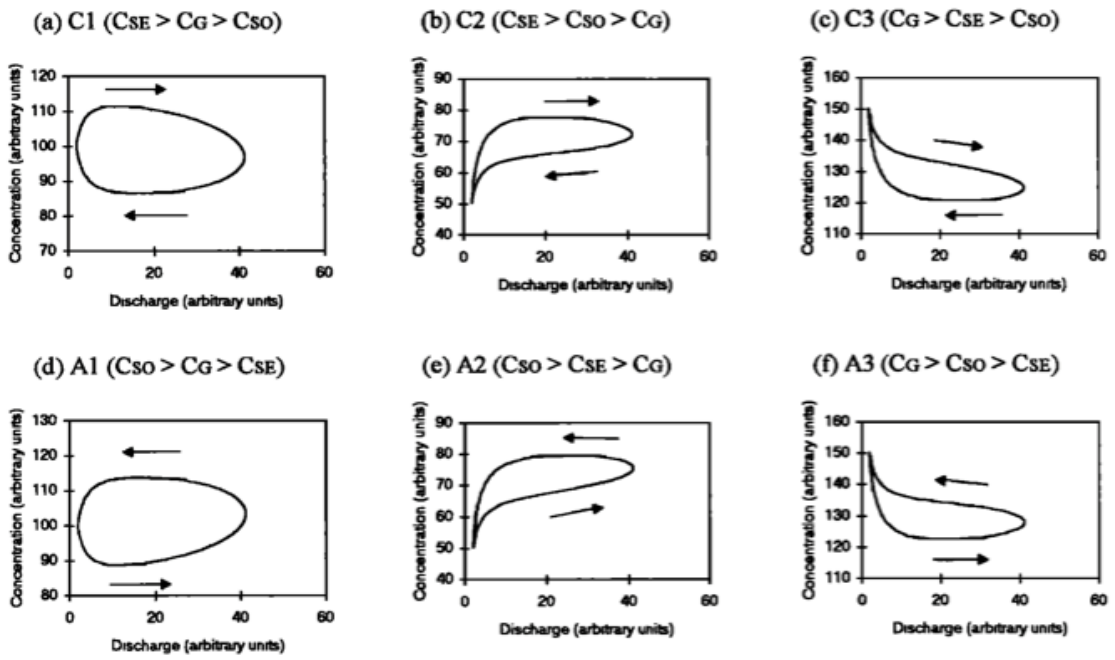

Figure 1.7: Examples of concentration/discharge hysteresis loops. C_{SE} is the concentration from surface event water, C_G is the concentration from groundwater, and C_{SO} is the concentration of the soil water. Image from Evans and Davies (1998).

Dissolved Organic Carbon in Runoff

Several studies have examined the effect of storms on DOC and CDOM export to rivers. Raymond and Saiers (2010) performed a metadata analysis encompassing 30 small eastern United States forested watersheds and found that 86% of DOC was exported during rain events. 70% of this export occurred during the rising hydrograph (Figure 1.8). Other studies highlight the complicated interactions between carbon source, land use type, soil type, bacterial activity, runoff flow path, and seasonality on DOC export. A summary of these key studies is presented here.

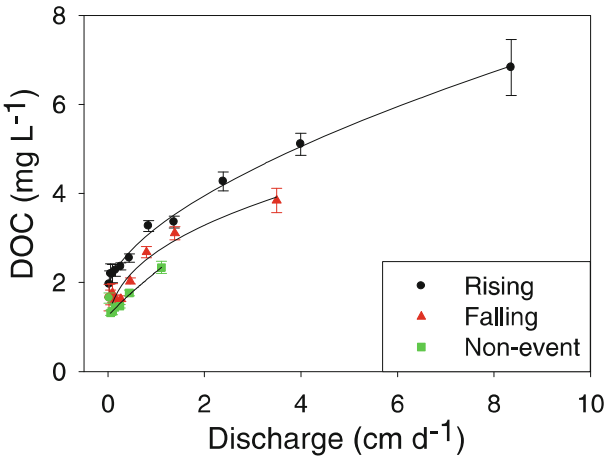

Figure 1.8: Relationship between stream discharge and stream water DOC concentrations for forested watersheds of the eastern United States. The error bars are standard errors. From Raymond and Saiers (2010).

In most of these studies, the path that water takes into a river, or other water body, is considered. Overland flow is just one source of water to a water body during a rain event. Other flow paths, particularly subsurface flow in riparian soils, can carry large amounts of high DOC concentration water to rivers. When the subsurface flow is in contact with soils with high organic matter content for longer periods of time, the DOC export is higher. Hinton, Schiff, and English (1998) found that these dynamics vary from catchment to catchment and storm to storm. However, they hypothesized that "positive correlations between DOC concentrations and stream discharge will be strongest in watersheds with large riparian DOC sources and without significant wetland area" (Hinton et al., 1998).

Utilizing artificial rain experiments, Boissier and Fontvieille (1993; 1995) analyzed DOC export from two different soil types using biodegradable DOC (BDOC) measurements. Short-term incubations were used to determine bacterial activity within

DOC samples. They found that DOC fluxes were not different between the two soils, but BDOC and enzymatic activity did vary. When soils were relatively dry, rain events caused seepage water to carry labile organic matter to deeper soil layers or nearby aquatic systems. When soils were already wet and a rain event occurred, enzymatic activity remained high and bioavailable DOC was consumed quickly while refractory DOC was exported in seepage water.

Hinton, Schiff, and English (1998) examined DOC export from areas adjacent to streams during storms. They found that depth of the water table, presence of wetlands, and topography strongly influence DOC dynamics and export. In catchments with wetlands, DOC transport was strongly dependent on DOC leaching and subsequent export at the wetland surface. As a result, DOC export decreased with subsequent storms. In riparian soils, subsurface flow paths and groundwater discharge were correlated with DOC concentrations and export. The authors encouraged further examination of overland flow, as their data showed that it might be a significant source. Other sources during storms included precipitation, throughfall (precipitation falling through the tree canopy), and stemflow (water running down tree trunks), but these sources accounted for less than 20% of DOC export. In-stream production was minimal.

Barrett et al. (1998) investigated the water quality of highway runoff in Austin, Texas. They studied three sites with different highway traffic volumes, surrounding land use, and drainage systems. They found that the water quality at all the sites was similar to median values found in Driscoll, Shelley, and Strecker's (1990) nationwide study of highway runoff water quality. Median dissolved total carbon was between 11-25 mg C/L.

The authors state that a first flush effect was noticeable "during selected events, but was generally limited to small volumes of runoff." The first flush effect was most pronounced during short, constant intensity storms. Data is only provided for total suspended solids, with the first flush occurring during the first 5 mm of runoff. The overall effect of first flush was found to be small or negligible when the authors considered all sampled events.

Wada et al. (2006) analyzed urban first flush runoff for organic carbon and demonstrated an experimental treatment system. They found that stormwater runoff entering Lake Biwa, near Kyoto, Japan, had a high level of refractory DOC. In addition, the first flush runoff had an elevated concentration of DOC as compared to runoff occurring later in the storm – up to 50% of the DOC export in the first 2 mm. The first flush runoff also contained about 90% of the particulates exported during the rain event. The treatment system captured the first 2mm of stormwater runoff, percolated this first flush through a soil chamber, and effectively reduced the runoff loading by about 4-6 times. Delpla et al. (2011) examined runoff water quality, including dissolved organic carbon (DOC), in agricultural environments in temperate areas. The researchers set up plots treated with cattle or pig manure and observed high DOC concentrations in runoff from high intensity storms.

Neff and Asner (2001) summarized known information about DOC fluxes through soils, and models used to simulate fluxes. They conclude that DOC soil fluxes are a large contributor of carbon for microbial activity and are a small but important carbon loss pathway. The authors call for additional investigation of sorption estimates, the duration of sorption, and the influence of storm events on DOC fluxes.

Findlay et al. (2001) studied near-stream flow paths in several land use types in New Zealand. They found that riparian flow paths and land use affect the concentration, quality and bioavailability of DOC exported to streams. They also found that ultraviolet exposure may result in changes in DOC bioavailability. Xenopoulos et al. (2003) examined watershed characteristics and their relation to dissolved organic carbon concentrations in temperate lakes in the Upper Great Lakes region. They found that, regionally and globally, wetlands are the best predictor of DOC. However, the influence of land use type varied regionally.

McKnight et al. (1993) found that DOC concentrations varied seasonally in an alpine stream in Colorado. The decomposition of leaf litter under snowpack results in the build up of leached DOC within the leaf litter, at the interface of the snowpack and litter, or within the soil. As the snow melts, this built up DOC might contribute to elevated stream concentrations. The authors observed maximum DOC concentrations during early spring snowmelt, several weeks before the stream reached maximum discharge.

In order to assess DOC export, sampling methods must take into account the complex interactions between carbon source, land use type, soil type, bacterial activity, runoff flow path, and seasonality. Utilizing sensors to better capture DOC concentration changes during storm events is also important for fully assessing DOC export.

Sensors

Monitoring fluxes of contaminants or DOC can be difficult during storms. Due to the dynamic nature of contaminants, nutrients, and DOM during storms, a large number of samples must be taken in quick succession. Storms are often unpredictable, and

deploying field equipment for every storm can be cost prohibitive and logistically difficult. Sensor networks offer the ability to take high resolution samples at minimal cost and manpower (Hart and Martinez, 2006; Rundel et al., 2009; Zia et al., 2013). Sensor arrays can be deployed in the field for long periods of time and programmed to take continuous high resolution samples (Hart and Martinez, 2006; Rundel et al., 2009; Zia et al., 2013). Several studies have shown the efficacy of using sensors to capture the effect of storms on various water quality parameters (Ahn et al., 2005; Jeong et al., 2006; Zhang et al., 2008; Eckley and Branfireun, 2009; He et al., 2010).

Due to its optical properties, CDOM can be easily measured *in situ* with commercially available sensors (Chen, 1999; Keith et al., 2002; Conmy et al., 2004; Downing et al., 2009; Saraceno et al., 2009). CDOM can often be used as a proxy for DOC given a handful of samples to characterize the relationship in a given environment and through a given event (Green and Blough, 1994; Coble, 2007). Other sensors can be used to measure water quality parameters such as temperature, dissolved oxygen, pH, and conductivity (Rundel et al., 2009). These parameters do not always change during storm events, but can vary depending on a number of conditions (Deletic, 1998; Boehm et al., 2002).

Neponset River Watershed

Many small catchments are located in urban settings. The Neponset River is located in an urban area close to Boston and empties into Boston Harbor. The watershed covers about 300 square kilometers and is comprised of 14 cities and towns with a population of about 330,000 (Neponset River Watershed Association, 2014a). The

Neponset River Estuary often fails to meet state water quality standards, due to the impacts of combined sewer overflows (CSO) and urban stormwater runoff (MWRA, 2014). The watershed is dominated by five land use types: residential (38%), forest (34%), industrial (5%), wetland (4%) and golf courses (2%). 16 other land use types classified by MassGIS account for less than 2% each (Huang and Chen, 2009). By examining the Neponset River Watershed, an estimate of the influence of first flush on DOC export to coastal waters can be constructed. With this new understanding, basic predictions for future impacts of urbanization and climate change on DOC export can be made.

Table 1.1: Data and estimates used for the Neponset River Watershed flux calculation

Variable	Value	Source
Mean annual precipitation, Neponset River	123.49 cm (48.62 in)	http://www.bluehill.org
Baseline DOC concentration	4.8 mg C (400 uM C)	Neponset sample data (Appendix B)
Storm DOC concentration	12 mg C (1200 uM C)	Neponset sample data (Appendix B)
Concentration increase	2-3 times	Neponset sample data (Appendix B); Hood, Gooseff, and Johnson (2006)
Baseline flow	2.83 m^3 sec^{-1} (100 ft^3 sec^{-1})	http://waterdata.usgs.gov/usa/nwis/uv?011055566
Storm flow	8.5 m^3 sec^{-1} (300 ft^3 sec^{-1})	http://waterdata.usgs.gov/usa/nwis/uv?011055566

For the calculation, the following assumptions were made:

- Increased concentrations occur during thirty 25.4 mm (1 inch) storms
- Concentrations are not influenced by remaining storms that deliver approximately 48.3 cm (19 inches) of rain per year
- Concentration and discharge increases occur for 10 hours during each storm (300 hours total)
- Normal flow occurs during 96.58% of the year (8460 hours)

An estimate of the normal flow flux is obtained by multiplying the average baseline flow and concentration by the percentage of the year (96.58%) (Equation 1.1).

$$\frac{2.83\ m^3}{sec} \times \frac{31536000\ sec}{1\ year} \times \frac{4.8\ mg\ C}{1\ liter} \times \frac{1000\ liters}{1\ m^3} \times 0.9658 = 4.13 \times 10^{11} mg\ C\ yr^{-1} \quad (1.1)$$

The storm flux estimate is obtained by multiplying the storm flow and concentration by the percentage of the year (3.42%) (Equation 1.2).

$$\frac{8.5\ m^3}{sec} \times \frac{31536000\ sec}{1\ year} \times \frac{12\ mg\ C}{1\ liter} \times \frac{1000\ liters}{1\ m^3} \times 0.0342 = 1.10 \times 10^{11} mg\ C\ yr^{-1} \quad (1.2)$$

By dividing the two fluxes, the relative contribution of storms, as opposed to baseline flow, is determined (Equation 1.3).

$$\frac{1.10 \times 10^{11}}{5.23 \times 10^{11}} = 0.21 = 21\% \text{ of export during } 3.42\% \text{ of year} \quad (1.3)$$

From this rough estimate, the potential influence of first flush in the Neponset River is significant. Twenty-one percent of export during only 3.42% of the year is a large flux of dissolved organic carbon that might be missed by regular watershed sampling efforts. If this storm-influenced flux is occurring, current estimates of DOC export from the Neponset, and potentially other small, temperate rivers, are underestimated. Regular sampling during episodic events is needed in order to either validate or repudiate the estimate presented above.

Summary

Due to the importance of DOC and CDOM in riverine and coastal environments, first flush could significantly affect coastal carbon cycling. In addition, underestimation of carbon export from small rivers might have global significance. By studying a typical

urban river, the Neponset River near Boston, Massachusetts, it is possible to increase our understanding of the general dynamics of first flush of DOC and CDOM. An experimental setup to mimic rainstorms and collect first flush samples is discussed in Chapter 3. By examining high resolution sampling during storm events (Chapter 4) and monthly long-term (2006-2012) data (Chapter 5), better estimates of the influence of first flush on CDOM and DOC export to Boston Harbor from the Neponset River can be determined. Knowing if first flush occurs, either during a storm or seasonally, might allow decision makers to develop better pollutant reduction strategies. These results are then compared with the back-of-the-envelope calculation presented here to estimate the local and global significance of first flush in small urban rivers.

Chapter Summaries

Chapter 1 provides an overview of the carbon cycle and its global importance, as well as a review of significant literature relating to dissolved organic carbon, colored dissolved organic matter, water quality, the concept of first flush, and sensor measurements. A calculation of the potential influence of runoff from storm events on the annual export of dissolved organic carbon in the Neponset River, Massachusetts, USA is also presented.

Chapter 2 summarizes the methods used to conduct the research described in subsequent chapters including: rain simulator design, testing and deployment; event sampling with autosamplers and sensors; monthly watershed sampling; and discrete sample collection, laboratory processing and analysis.

A rainfall simulator used to mimic natural rain events under controlled environments and to characterize first flush events in permeable and impermeable environments is described in Chapter 3. Storm events in the Neponset River Watershed from 2012 are characterized using real-time sensors and autosamplers in Chapter 4. These events are placed into a longer timescale context by examining monthly sampling from 2006-212 throughout the Neponset in Chapter 5. Chapter 6 presents conclusions, management recommendations and suggestions for future research.

CHAPTER 2

METHODS

2.1 Introduction

First flush studies require high resolution sampling in order to evaluate concentration changes over time. This is a difficult task because storms can be unpredictable and deploying field equipment for every storm can be costly. This project utilized a mixture of sensors, autosamplers, and standard watershed sampling in order to capture data during as many storms as possible as effectively as possible. Sensor arrays were continuously deployed during the sampling season and serviced at least once per week. Autosamplers were stationed at the field sites and were programmed to capture discrete samples during storm events. Monthly sampling throughout the watershed allowed for comparison of storm concentrations to baseline concentrations. In addition, a rain simulator was built in order to collect runoff on two land use types while controlling for the variability present during storms.

Figure 2.1: Methods and approximate scales utilized in research

This chapter presents method details for the research described in subsequent chapters, including: controlled experiment design, testing and deployment; event

sampling with autosamplers and sensors; long-term monitoring on a watershed scale; and discrete sample collection, laboratory processing and analysis.

2.2 Controlled Experiments

Rainfall Simulator Design

The rain simulator was designed after a thorough literature review of previous projects that utilized rain simulators. Key design goals included the ability to reproduce a natural rain event, low cost, construction from easily available materials, and portability. For simplicity, a pressurized nozzle system was utilized, with a single nozzle mounted at 3 meters height on a canopy frame. Water was pumped to the nozzle with a 1 horsepower centrifugal pump (Wayne Water Systems, Harrison, Ohio) from a 55-gallon plastic drum (Baytec Containers, Houston, Texas). Two nozzles – Fulljet 1/4GG-10W and Fulljet 1/8GG-2.8W from Spraying Systems Co. (Wheaton, Illinois) – were selected for their conical spray pattern and flow rates at low pressures. Pressure gauges and flow controls were placed at several points in the pumping system in order to regulate flow to the nozzle.

Figure 2.2: Rain simulator in operation during drop dispersion testing

Figure 2.3: Pump system with modifications to control flow to nozzle

Rainfall Simulator Testing

Following the design and construction of the rain simulator, it was tested for spray characteristics, including drop size, drop velocity, intensity, and spray uniformity. These characteristics were tested in order to compare the simulated rainfall to natural rainfall in the study area. Drop size was tested using the oil method (Eigel and Moore, 1983). Water droplets were caught in a petri dish containing a mixture of 2 parts heavy gear oil and 1 part STP oil treatment. The mixture was prepared in a large beaker on a hot plate (approximately 80ºC). The heat aided in mixing the materials and removed air bubbles entrained in the mixture. The mixture was then cooled and poured into the petri dishes. Any remaining air bubbles were removed with a hypodermic needle. Each petri dish was placed near ground level underneath a cover under the rain simulator. The simulator was started and allowed to run for about 1 minute in order to clear any air from the pumping system. The cover over the petri dish was removed and the oil mixture was exposed to simulated rain for approximately 3 seconds before being covered again. The rain simulator was turned off and the dish containing raindrops was then photographed within 30 seconds of exposure. A millimeter scale was present in the photograph. The photographs were then projected onto a white board, and the millimeter scale was used to measure and enumerate the suspended drops.

The kinetic velocity of the drops was obtained using the measured drop sizes and drop velocities calculated by Laws (1941) and Gunn and Kinzer (1949). Drop dispersion was analyzed using the uniformity coefficient equation (Christiansen, 1942),

$$C_u = 100\left(1 - \frac{\sum x}{mn}\right), \quad (2.1)$$

where x is the deviation of the individual observations from the mean value m, and n is the number of observations. A 2 by 2 meter grid was constructed with pre-weighed cups (95.25 mm diameter; standard deviation 0.327-0.439 grams) spaced at 0.4 meter intervals with an additional cup directly under the nozzle (Figure 2.3). The grid was exposed to simulated rainfall for 15 minutes. The cups were then weighed to determine the amount of water collected. The mean value, *m,* was calculated from these measurements. The dispersion from each nozzle was tested twice.

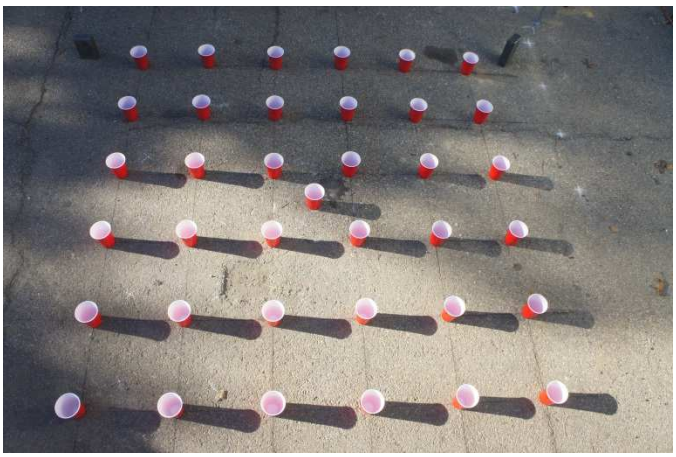

Figure 2.4: 2 by 2 meter grid with cups spaced at 0.4 meter intervals

Rainfall Simulator Deployment

Study Sites

Two contrasting sites were selected for rain simulator deployment - Parking Lot D at the University of Massachusetts Boston, Boston, MA and a forested site in the Blue

Hills Reservation, Canton, MA. Parking Lot D has an asphalt surface (Figure 2.5). The lot is about 15,000 m^2 and holds approximately 485 cars when full. The forested site in the Blue Hills Reservation was located in an area with minimal foot traffic (Figure 2.6). Ground cover consisted of grass and fallen leaves with several large deciduous trees surrounding the plot. Additional information about the study sites is available in Appendix A.

Figure 2.5: Parking lot study site with rain simulator in operation


Figure 2.6: Forested study site with rain simulator deployed

Plot Design

At both sites, the canopy structure was deployed and anchored down to prevent movement due to wind. The canopy top was placed on the frame to reduce the influence of wind on the simulated rainfall. At the parking lot site, the 55-gallon water drum was filled with tap water (143-161 uM C; <8 QSU) obtained from a spigot at the University of Massachusetts Boston. Electricity was available at the site. At the forested site, tap water was obtained from the Department of Conservation and Recreation Blue Hills Reservation headquarters (Fall 2012; 133 uM C; 4 QSU) or University of Massachusetts Boston (Summer 2013; 119-141 uM C; 7-23 QSU). A gasoline-powered generator was utilized to provide electricity for the pump.

Parking Lot Site

The site selected was a 2 by 2 meter plot near a storm drain in the travel lane of the parking lot. In order to collect runoff, the plot was isolated from the surrounding parking lot using pre-bent aluminum flashing (Figure 2.7). The flashing was secured to

the parking lot using silicon caulk and 3M Blue painter's tape. A collection point was set up at the storm drain located on one edge of the plot. This was an ideal collection point as the plot gently sloped toward the storm drain. The storm drain grate was removed and a piece of flashing was used to channel runoff to a collection point. This flashing was held in place with silicon caulk and 3M Blue painter's tape. The collection point was covered to avoid receiving spray directly from the nozzle.

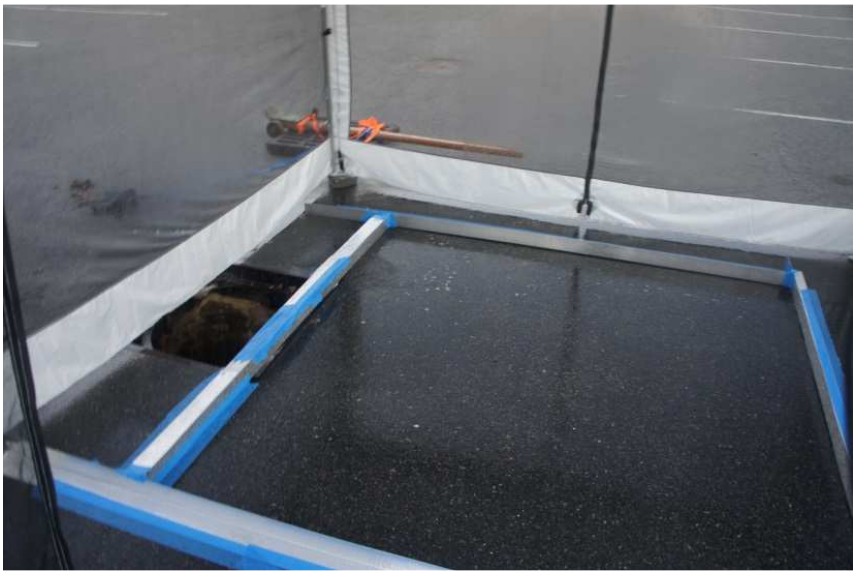

Figure 2.7: Parking lot study site, showing aluminum flashing and collection point

Forested Site

Pre-bent aluminum flashing was used to isolate the 2 by 2 meter forest plot (Figure 2.8). The plot was set up in a square shape, with a collection point at a corner. This was the lowest point of the plot. On the two upper sides, the flashing was pushed into the soil to a depth of 3 inches. On the lower two sides, a shallow channel was dug and the flashing was pushed into the soil to create a runoff channel. Care was taken to not disturb soil inside of the plot. Runoff was carried through these two channels to the collection point. A hole was dug at the collection point in order to place a collection

bottle at the outlet of the channel. Both channels and the collection point were covered to avoid receiving spray directly from the nozzle.

Figure 2.8: Forest study site, showing aluminum flashing. The collection point is at the lower right corner. The aluminum flashing on the right and bottom sides of the picture are the runoff channels. Due to the slope from the top left to the bottom right, the aluminum flashing on the left and top sides only isolate the plot and do not carry water to the collection point

2.3 Event Sampling

Two locations within the Neponset River Watershed with different land use types were selected for high-resolution sampling. The Neponset River is located in an urban area close to Boston, Massachusetts and empties into Boston Harbor. The watershed covers about 300 square kilometers and is comprised of 14 cities and towns with a population of about 330,000 (Neponset River Watershed Association, 2014a). The Neponset River estuary often fails to meet state water quality standards, due to the impacts of combined sewer overflows (CSO) and urban stormwater runoff (MWRA, 2014). The Massachusetts Water Resources Authority (MWRA) does not sample the freshwater sections of the Neponset River so less is known about the water quality of this

part of the river. The Neponset River Watershed Association's (NepRWA) Citizens Water Monitoring Network (CWMN) samples six times per year at 41 sites within the watershed. CWMN samples for E. coli, total nitrogen and phosphorus, orthophosphate, nitrate, chlorophyll, dissolved oxygen, pH, and water temperature, but does not sample for DOC or CDOM (Neponset River Watershed Association, 2014b).

The two selected sampling locations were already in use as part of a thirty-one site monthly sampling program within the Neponset River Watershed, described below. Forest 1 was located in Canton, MA, and samples were taken from a small creek running through forested land. The subwatershed is 1.96 km^2 and is mostly forested (>80%), with other land use types including low or very low density residential, forested wetland, and crop land. Industrial 3 was located in Norwood, MA near an industrial park and also received stormwater input from a nearby highway. Its subwatershed is approximately 1.4 km^2 and composed of industrial, commercial, forest, and medium density residential land use types. More details about the sampling locations are available in Appendix A.

Figure 2.9: Aerial view of Forest 1 sampling location (Google Earth)

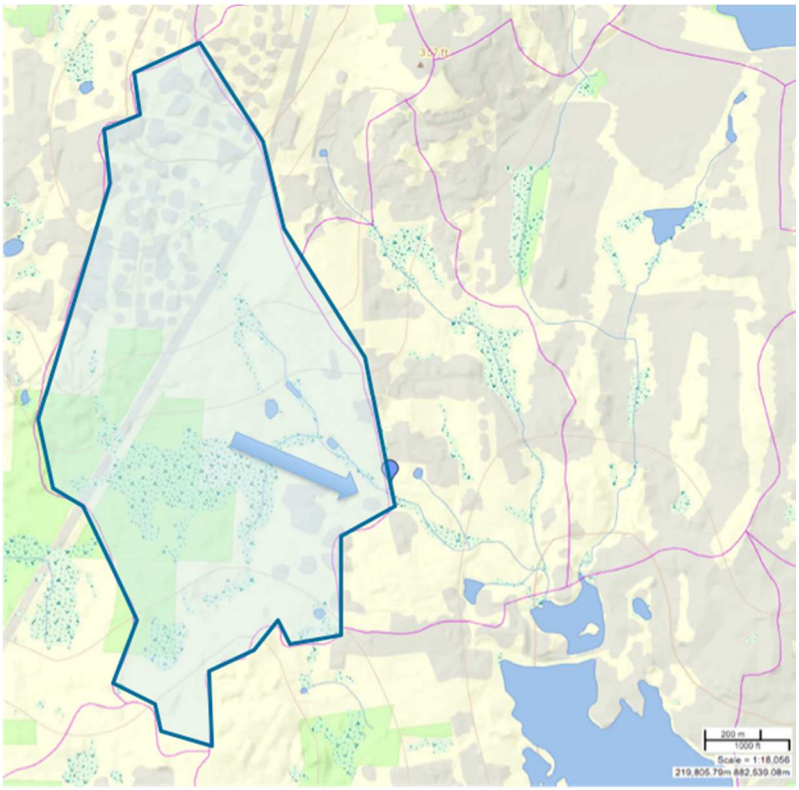
Figure 2.10: GIS map showing Forest 1 sampling location (blue pin) and general direction of water flow in the subwatershed. The sampling location is the outlet of the subwatershed. The thin purple line indicates the boundary of the subwatershed. GIS data from MassGIS OLIVER (http://maps.massgis.state.ma.us/map_ol/oliver.php)

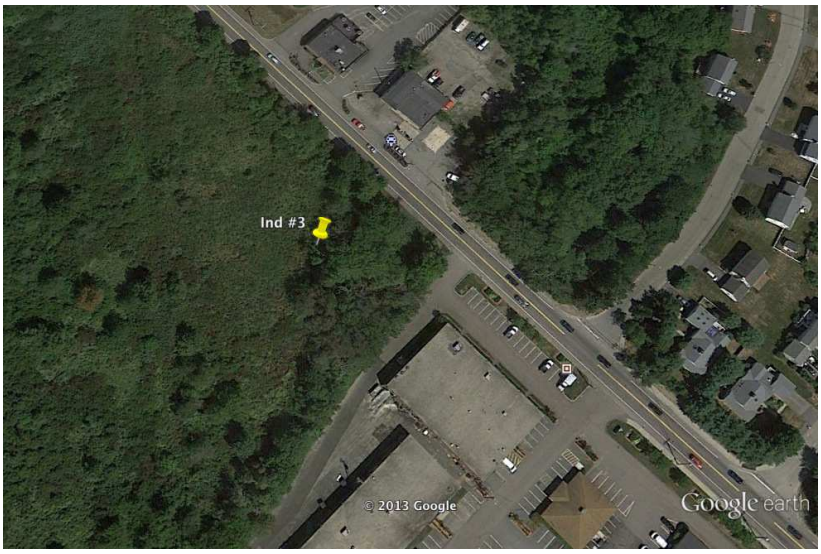

Figure 2.11: Aerial view of Industry 3 sampling location (Google Earth)

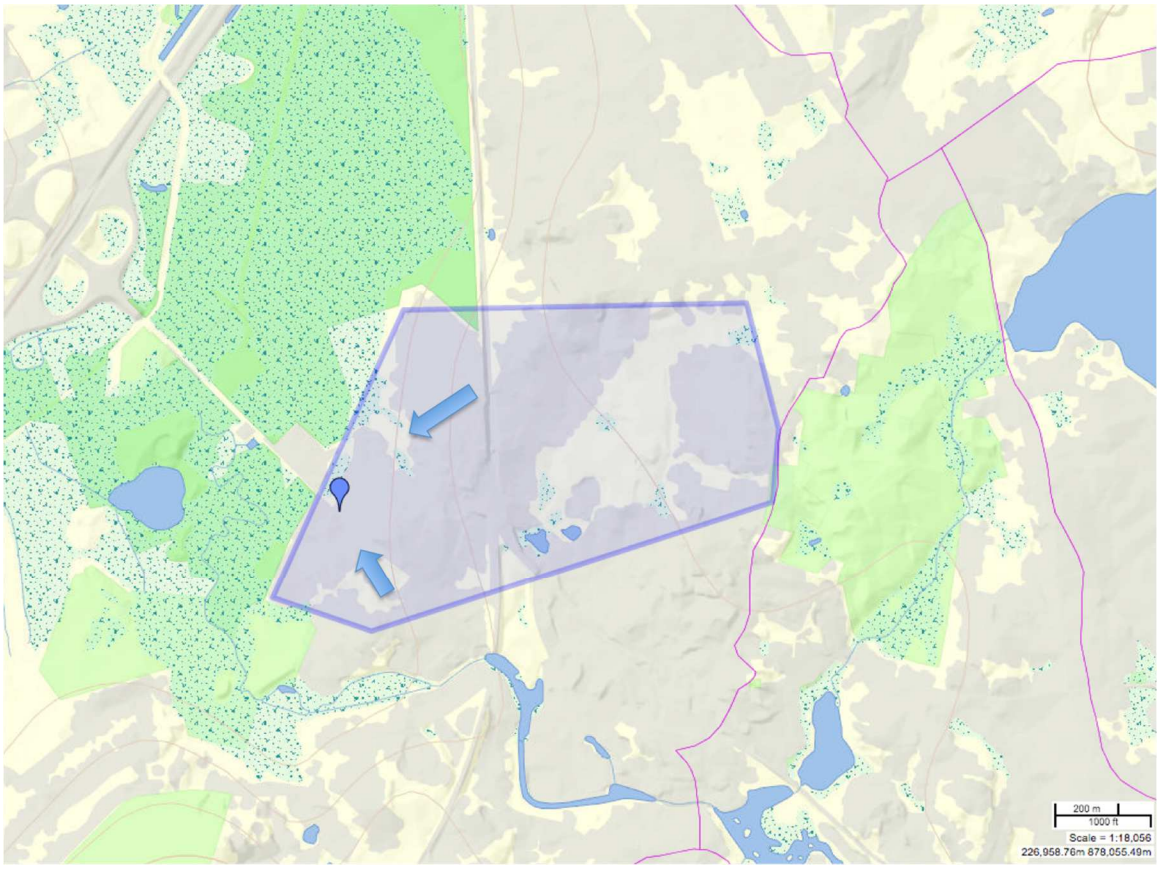

Figure 2.12: GIS map showing Industry 3 sampling location and general direction of flow of water in the subwatershed toward the sampling point. The polygon represents the approximate boundary of the drainage area that passes through the sampling point. GIS data from MassGIS OLIVER (http://maps.massgis.state.ma.us/map_ol/oliver.php)

Two *in situ* sensors were deployed at each site from March 6 through April 4, 2012 and May 7 through November 10, 2012. The sensors were removed in April to be deployed in Florida for an unrelated research project. One *in situ* sensor measured parameters including water temperature, conductivity, dissolved oxygen, and pH every 2 to 5 minutes (YSI Inc. 6-series V2 sonde). The frequency was reduced from 2 minutes to 5 minutes during the deployment due to battery and data storage limitations. The second sensor (Seapoint Sensors, Inc. Ultraviolet Fluorometer; Turner Designs Cyclops-7 Submersible CDOM Fluorometer) measured chromophoric dissolved organic matter (CDOM) fluorescence every 2 minutes. The sensors were mounted to a cinder block. An Onset Instruments HOBO U-12 datalogger was utilized for datalogging. The sensors and datalogging were powered by a swappable lead acid battery and charged with a solar powered charger. The battery and datalogging equipment was stored in a lockable waterproof housing near the sampling location. The solar panel was mounted on the waterproof housing.

A Hach Sigma SD900 portable autosampler was deployed at each site during the same time period. A lead acid battery was used to power the autosampler. During episodic events (i.e. rain events), the autosamplers were programmed to collect discrete water samples at timed intervals, typically every 30 to 60 minutes for 24 to 36 hours (Appel and Hudak, 2001), and were triggered manually prior to a storm. In order to know when a storm was approaching, precipitation alerts were set up on weather.com. During storm sampling, samples were collected through Tygon tubing (0.25 inch inside diameter) and pumped into 250 ml pre-combusted (500°C, 5 hours) glass bottles within

the sample chamber of the autosampler. The autosampler was programmed to rinse the tubing three times before collecting the sample. Samples were collected before, during, and after the storm using this method. Ice was placed around the sample bottles during warm weather. No preservatives, such as hydrochloric acid or mercuric chloride, were added to the samples following autosampler collection. Samples were retrieved after the storm ended and transferred into 300 ml pre-combusted (500°C, 5 hours) glass bottles with Teflon-lined caps.

Long-term Monitoring on Watershed Scale

Thirty-one freshwater sites within the Neponset River Watershed were sampled monthly from January 2008 to December 2012 (Figure 2.13). This was a continuation of a previous data set started in 2006 (Huang and Chen, 2009). Huang and Chen (2009) utilized land cover maps from MassGIS to determine the dominant land use types within the watershed and to select 30 sampling locations. From their results, the watershed was found to be dominated by five land use types: residential (38%), forest (34%), industrial (5%), wetland (4%) and golf courses (2%). Sixteen other land use types classified in MassGIS account for less than 2% each. Fifteen freshwater sites were selected as endmembers with an endmember subwatershed defined as an area that drains at least 80% from a unique land-cover type.

These sampling sites were named by land use and numbered to distinguish between sites in the same land use type (i.e. Forest 1, Wetland 3, etc.). Fifteen additional freshwater sites selected represent pour points, which are sites that represent drainage from a mixture of land use types. These sampling sites were labeled “PP” for pour point

and then numbered (i.e. PP1, PP10, etc.). The thirty-first site was added in January 2009 at the location where part of the Charles River is diverted into the Neponset River watershed through Mother Brook. This site was named Mother Brook, or MB for short. Discrete samples were collected monthly on a single day using a stainless steel pitcher that was cleaned in the laboratory with deionized water and rinsed three times with water from the sampling site.

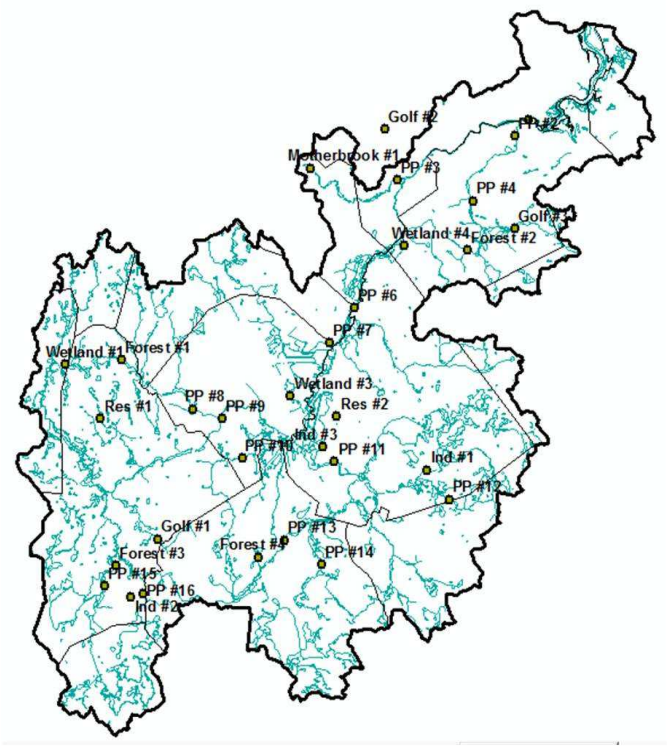

Figure 2.13: Map of the 31 sampling sites within the Neponset River Watershed

Climatic data, including precipitation, was obtained from records kept by the Blue Hill Observatory (http://www.bluehill.org) and available from the Blue Hill Observatory and NOAA's National Climatic Data Center (http://www.ncdc.noaa.gov/cdo-web/datasets/PRECIP_HLY/stations/COOP:190736/detail). Neponset Watershed

discharge data was obtained from streamflow data available from the United States Geological Survey (USGS) (http://waterdata.usgs.gov/usa/nwis/uv?011055566).

2.4 Discrete Samples

Discrete samples obtained from rainfall simulation, event sampling, and monthly watershed sampling were transported to the laboratory in 300 ml pre-combusted (500°C, 5 hours) glass bottles with Teflon-lined caps. Within 24 hours of sampling, each sample was filtered (high purity N_2 pressure filtered, <15 psi) at the laboratory through pre-combusted 0.7 μm glass fiber filters (Whatman GF/F). Dissolved organic carbon (DOC) and chromophoric dissolved organic matter (CDOM) samples were filtered into pre-combusted (500°C, 5 hours) 40 ml borosilicate glass vials with Teflon-lined caps. DOC samples were acidified to pH less than 2 with phosphoric acid and stored in clear vials at 4°C until analysis (Kaplan 1994). Absorbance and fluorescence samples were stored in amber vials at -4°C until analysis. All samples were analyzed at room temperature (21°C ± 1°).

2.5 Dissolved Organic Carbon (DOC)

A Shimadzu TOC-V analyzer was utilized for DOC analysis (Qian and Mopper, 1996). DOC standards were prepared using potassium hydrogen phthalate (KHP, Sigma Chemical) based on the instrument manual. The instrument was turned on and allowed to warm-up for at least one hour. Milli-Q water injections were then run until the instrument baseline stabilized at a peak area less than 2, similar to values obtained during analysis of

1 μM C Low Carbon Water. The instrument was then calibrated with a seven-point standard curve. Samples were run following a linear regression of the standard curve ($r^2 \geq 0.995$). On subsequent days, at least one random carbon standard was run and compared to the standard curve to ensure continued calibration.

While running samples, the instrument blank was checked with ultra high purity, low carbon Milli-Q UV water every 10 to 15 samples. The mean blank value was subtracted from the sample measurements (Stedmon et al., 2000). Low Carbon Water (LCW) and Deep Sea Water (DSW) standards from Dennis Hansell's lab at the University of Miami were also run to ensure data quality (http://yyy.rsmas.miami.edu/groups/biogeochem/CRM.html).

2.6 CDOM Fluorescence

Fluorescence samples were thawed and then analyzed on a Photon Technologies International (PTI) Quantum Master 1 spectrofluorometer. Excitation scans were conducted with excitation (λ_{ex}) 337 nm, a 1 cm quartz cell, and emission scans from 350 nm to 650 nm. Slits widths were set to 4 nm. A blank (Milli-Q water) was run each day and subtracted from sample spectra to remove the Raman scattering peak. Fluorescence spectra were integrated in the wavelength range of 350 - 650 nm. A seven-point quinine sulfate standard curve (pH = 2) was used to convert the area of the emission spectra to quinine sulfate units (QSU) (Green and Blough, 1994; Siegener and Chen, 2002; Stedmon et al., 2003; Chen and Gardner, 2004). One QSU was equivalent to the fluorescence of 1 μg/l quinine sulfate at pH 2.

Sensor CDOM voltages were converted to CDOM concentrations utilizing the discrete CDOM sample concentrations. Sensor CDOM concentrations were then converted to DOC concentrations utilizing the CDOM-DOC relationship from discrete samples from each event. Difficulties were encountered calibrating sensor data using the discrete samples. This could have been due to a slight time lag between discrete sample collection and sensor measurement. Data from each storm was separately calibrated in order to reduce error from these issues. This method limits the usefulness of the sensor data for non-storm periods without discrete samples. This was similar to the experience of another graduate student using similar sensors. Benjamen Wetherill found that there was a fairly large difference in calibrations between different sensors during deployments. There were also calibration differences between deployments of the same sensor (personal communication).

2.7 CDOM Absorption

Absorption samples were thawed and re-filtered through pre-cleaned 0.2 μm GE Osmonics polycarbonate filters before analysis to remove any glass fibers that may have become dislodged during the original filtration (Chen and Gardner, 2004). The polycarbonate filters were pre-washed with 2 M HCl prior to use (Stedmon et al., 2000). CDOM absorption spectra (200 – 800 nm) were measured with a Cary 50 spectrophotometer with a 1-cm path quartz cell. The precision of the instrument was +/- 0.002 absorption units.

All absorption calculations were completed after correcting the spectra by subtracting the average absorption in the 700 – 800 nm range (Green and Blough, 1994). The absorption coefficient (a, in m^{-1}) was computed using the following formula:

$$a_\lambda = 2.303 \times A(\lambda)/l \quad (2.2)$$

where $a(\lambda)$ is the measured optical density at a chosen wavelength, and l is the cuvette path length in meters (Green and Blough, 1994). For the purposes of this research, the wavelength was 337 nm.

The DOC-specific absorption coefficient (a^*) was calculated using the following formula (Zhang et al., 2007):

$$a^*_\lambda = a_\lambda / (\text{DOC concentration}) \quad (2.3)$$

where DOC is expressed in mg l^{-1}. The wavelength used was 337 nm.

Spectral slopes (S) were calculated using best-fit linear regression of the log transformed a spectra over two wavelength ranges (275 - 295 nm and 350 - 400 nm). S depends on the wavelength range chosen (Green and Blough, 1994; Ferrari, 2000). A parameter called the slope ratio, or S_R, was calculated using the ratio of the absorption slope from 275-295 nm compared to that of the slope from 350-400 nm. The slope ratio compares absorbance values that often change during transit, either over time or due to photodegradation, and can allow for insight into DOM molecular weight and source. Higher value, or steeper, slopes show a more rapid decrease in absorption with increasing wavelengths (Helms et al., 2008).

Fluorescence quantum yield was calculated with the relationship:

CDOM fluorescence / absorbance coefficient (2.4)

This relationship expresses the quantum efficiency of the fluorescence with respect to the absorption of a sample (Green and Blough, 1994). The CDOM versus DOC relationship was also graphed.

Spectral data were all corrected for the inner filter effect for samples with absorbance above 0.1. The inner filter effect occurs when dissolved species, including the fluorophore, absorb exciting or emitted radiation (Puchalski et al., 1991; Hu et al., 2002). To correct for this effect, dilution with Milli-Q water was conducted for all samples over 100 QSU (about 0.1 m^{-1}).

2.8 Soil testing

Wet/dry weight comparison

The soil series at the forested site is Canton fine sandy loam. This is a well-drained soil type, with high (50.8 to 152.4 mm hr^{-1}; 2.00 to 6.00 in hr^{-1}) capacity for the most limiting layer to transmit water (USDA, 2013a). The initial carbon content of the soil is estimated to be 175.1 to 225 megagrams C per 10,000 square meters (USDA, 2013b).

Soil samples were collected from the forested site in the Blue Hills Reservation where the rainfall simulator was deployed. Several soil columns (4 inches long by 1.5 inch diameter) were collected in a butyrate plastic core liner utilizing a soil core sampler with hammer attachment (AMS Inc., American Falls, ID). The soil columns were then

transported to the laboratory. Approximately 10 grams of soil were measured on aluminum weighing dishes. The dishes were then placed in a 90°C oven for 24 hours. The dry weight was then measured. The weight difference represents the water weight of the soil sample. Samples were left in the oven and weighed again after several weeks. Little difference was observed from the weights measured after 24 hours in the oven (less than 0.05 grams).

An experimental setup was utilized to assess saturation and infiltration rate in an intact soil column. In the lab, a nylon stocking was taped to the bottom of the plastic core liner. Ultra high purity, low carbon Milli-Q UV water was then poured slowly into the top of the column. The rate of water addition was about 5.1 mL min^{-1} during the hour-long experiment. Observations were made about the speed with which the water drained through the soil column. In addition, the water that filtered through was collected at the bottom of the column and analyzed for DOC and CDOM. Additional wet weight and dry weight measurements were obtained for samples of soil from the top and bottom of the column after the saturation experiment.

2.9 Materials Testing

Laboratory tests were conducted in December 2014 to determine the potential DOC and CDOM contribution of 3M Blue painter's tape and silicone caulk. These materials were utilized for rainfall simulator plot isolation and collection at the parking lot site. While the materials were not fully submerged in water for 4 hours during the parking lot experiment, the following procedure was used to mimic the conditions in the

parking lot as best as possible. For the Blue painter's tape, 2 inch square pieces of tape were soaked in 100 mL Milli-Q water, with samples taken at 30, 60, 240, and 1440 minutes. For the silicone caulk, 5.14 grams were placed in 125 mL of Milli-Q in a beaker, with samples taken at 30, 60, 240, and 1440 minutes. A separate 5.18 grams of silicone caulk was allowed to cure for the manufacturer-recommended 60 minutes in a beaker, then 125 mL of Milli-Q was added to the beaker, with samples taken at 30, 60, 240, and 1440 minutes. All samples were processed using standard DOC and CDOM collection, filtering, and processing methods.

2.10 Conclusions

The methods detailed here include novel developments, as well as the use of common methods. While rainfall simulators are often used in erosion research, the design presented here is new and can be built to replicate storms of varying intensities. The utilization of the rainfall simulator to collect dissolved organic carbon samples from two land use types has not previously been done. The collection of discrete samples, autosampler and sensor deployments, and laboratory methods have been utilized in previous studies. The locations for watershed sampling were previously identified by Huang and Chen (2009).

The sensor methods need additional development. Battery depletion occurred even with solar charging, and resulted in several periods without sensor data. For future work, finding ways to maximize battery life and recharging should be a priority. The rainfall simulator deployment methods also need additional development in order to seal

the impervious plot from the rest of the parking lot without contributing to runoff dissolved organic carbon concentrations.

CHAPTER 3

DESIGN, CONSTRUCTION, AND TESTING OF A RAINFALL SIMULATOR FOR EVALUATING DISSOLVED ORGANIC CARBON CONCENTRATIONS DURING SIMULATED EPISODIC EVENTS

3.1 Abstract

A rainfall simulator was designed and built in order to mimic natural rain events. The rainfall simulator was then deployed on two different land use types. Under controlled conditions, runoff samples were collected in a forested site and an impermeable site (parking lot). Time series data suggest that first flush of dissolved organic carbon was present for all rainfall intensities for the parking lot simulations. Approximately 40-51% of DOC flux occurred within the first 20% of runoff. For the forested site, first flush was present in two of three simulations, but is only indicative of fluxes due to overland flow and does not capture soil water fluxes resulting from rainfall simulation.

3.2 Introduction

Contaminant levels and fluxes within a watershed are not constant over time, have multiple sources, and even vary rapidly over the course of a single rain event (Ahn et al., 2005). Previous studies have demonstrated that storm water runoff is a prime contributor to water quality degradation (Characklis and Wiesner, 1997; Buffleben et al., 2002; Ahn

et al., 2005). During a phenomenon known as the "first flush," the initial runoff during a rainstorm can contain substantially elevated contaminant concentrations relative to runoff occurring later in the storm (Lee and Bang, 2000; Lee et al., 2002; Kayhanian and Stenstrom, 2008).

DOC Movement in Natural Systems

Several studies have examined the effect of storms on DOC and CDOM export to rivers. Raymond and Saiers (2010) performed a metadata analysis encompassing 30 small eastern forested watersheds and found that 86% of DOC was exported during high-discharge events. Hydrologic events were defined as days where the quickflow - stream discharge related to precipitation or snowmelt - was greater than the baseflow of the river. 70% of this event-related export occurred during the rising hydrograph.

Other studies highlight the complicated interactions between carbon source, land use type, soil type, bacterial activity, runoff flow path, and seasonality on DOC export. In most of these studies, the path that water takes into a river, or other water body, is considered. Some connections can be made between first flush and overland flow, or sheet flow. Overland flow is a thin film of water that forms on a surface when the precipitation rate exceeds the infiltration rate. The infiltration rate depends on the permeability of the surface on which the precipitation is occurring. Vegetation and sediment grain size influence the infiltration rate. Impervious surfaces, such as asphalt, reduce the infiltration rate and cause increased overland flow. Overland flow is important because it can be a major source of water to rivers, ponds, and lakes during rain events.

As a result, overland flows are also responsible for increased contaminant loadings to bodies of water (Miller and Gardner, 1981; Smith and Goodrich, 2005).

Overland flow is just one source of water to a water body during a rain event. Other flow paths, particularly subsurface flow in riparian soils, can carry large amounts of high DOC concentration water to rivers. When the subsurface flow is in contact with soils with high organic matter content for longer periods of time, the DOC export is generally higher (Hinton et al., 1998). The authors found that these dynamics vary from catchment to catchment and storm to storm. However, they hypothesized that "positive correlations between DOC concentrations and stream discharge will be strongest in watersheds with large riparian DOC sources and without significant wetland area" (Hinton et al., 1998).

Simulated Rainfall

The presence and magnitude of the first flush depends on site-specific conditions, such as land use, the amount of rainfall, antecedent precipitation, and the contaminant being studied (Makepeace et al., 1995; Appel and Hudak, 2001; Stenstrom and Kayhanian, 2005; Kayhanian and Stenstrom, 2008). In order to control for the unpredictability and natural variability among rain events, a rainfall simulator can be utilized to mimic a rain event (Tiefenthaler et al., 2001b; Tiefenthaler and Schiff, 2003). A rain simulator is able to distribute a controlled amount of water uniformly over a given area. Samples of the runoff can then be collected for analysis. Several benefits of rainfall simulators are outlined in the Food and Agriculture Organization of the United Nations (FAO) publication, *Field measurement of soil erosion and runoff*, including taking many

measurements quickly without having to wait for natural rain; and working with constant controlled rain, thereby eliminating the erratic and unpredictable variability of natural rain (Hudson, 1993). Most disadvantages are related to the scale of the treatment area, which is limited to the size of the rainfall simulator and availability of water.

A rainfall simulator must be able to mimic a natural rain event. According to Meyer (1979), an ideal rain simulator should have the following characteristics:

1. Drop size distribution near that of natural rainfall
2. Drop impact velocities near those of natural rainfall
3. Intensities in the range of storms for which results are of interest
4. Research area of sufficient size to satisfactorily represent the treatments and conditions to be evaluated
5. Drop characteristics and intensity of application fairly uniform over the study area
6. Raindrop application nearly continuous throughout the study area
7. Angle of impact not greatly different from vertical for most drops
8. Capability to reproduce the rainstorm durations of interest at selected intensities
9. Satisfactory characteristics when used during common field conditions such as high temperatures and moderate winds
10. Portability for movement from research site to site.

Characteristics of Natural Rainfall

Natural rainfall drop sizes can range from almost zero to about 7 mm in diameter. Larger drops are observed with greater intensities but eventually level off due to very large drops breaking apart (Meyer, 1979). Drop sizes for various storm intensities, as

measured by Laws and Parsons (1943) for natural rainstorms in the Washington, D.C. area, are presented in Figure 3.1. The authors derived values for rainfall rates of 0.01 and 4.0, and for raindrops smaller than 0.5 mm, by extrapolation. Approximate median drop sizes are presented in Table 3.1.

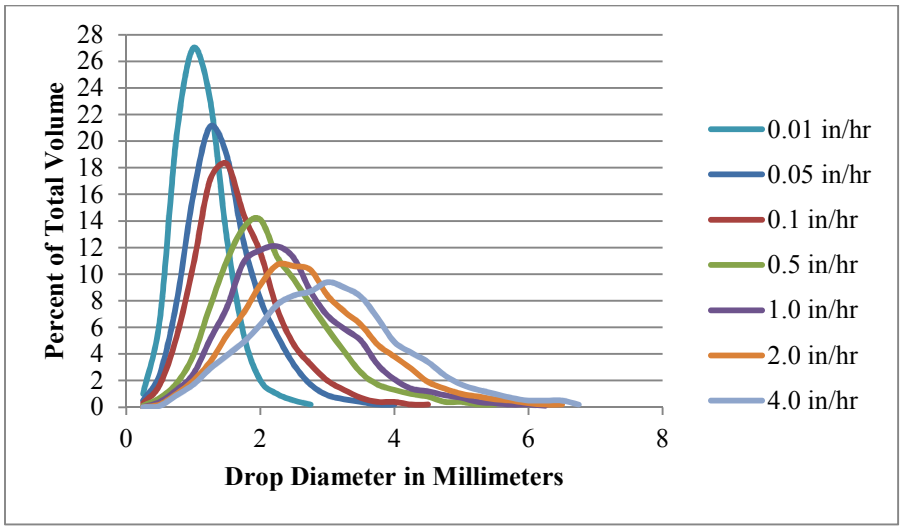

Figure 3.1: Average drop sizes for various storm intensities. Data from Laws and Parsons (1943)

Table 3.1: Approximate median drop sizes from Laws and Parsons (1943) data

Storm intensity (in hr^{-1})	Median drop size (mm)
0.01	1
0.05	1.25
0.1	1.4
0.5	2
1.0	2.25
2.0	2.6
4.0	2.8

Drop velocities can range from close to zero to more than 9 meters per second for larger droplets (Figure 3.2). According to Meyer (1979), a drop with a 2 mm diameter falls at about 6 to 7 meters per second. For pressurized nozzle systems, greater pressure at the nozzle will increase the velocity of the drops but reduce the drop size. If a pressurized system releases small drops at greater than terminal velocity and larger drops at less than their terminal velocity, the drops tend to approach their terminal velocity during the fall (Meyer, 1979). Kinetic energy can be estimated using the rainfall intensity. Miller (1987) built a rainfall simulator with a kinetic energy of 23.1 J m^2 mm^1, whereas Lascano et al. (1997) was able to produce kinetic energies ranging from 15 to 23.5 J m^2 mm^1.

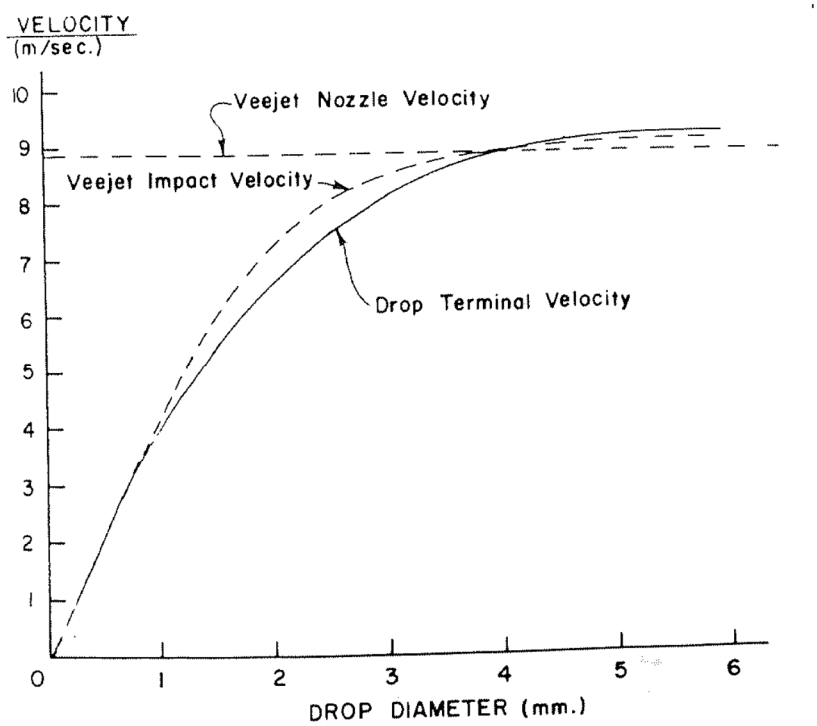

Figure 3.2: Drop impact velocities compared with terminal drop velocities for Veejet nozzles spraying downward from 3 meters height and at a pressure of 41 N m-2 (approximately 6 psi). Adapted from Gunn and Kinzer (1949) by Meyer and Harmon (1979).

Rainfall Simulator Designs

There are two basic types of rainfall simulators – drop-forming simulators and pressurized nozzle simulators. A drop-forming simulator uses tubes made from glass, polyethylene, or metal to form drops that then fall onto the plot due to gravity. Most of these simulators produce drops at a constant size unless a variety of tube sizes are utilized. Drawbacks to these simulators include the consistent drop size, high fall distances needed to have drops reach terminal velocity, and small plot sizes due to the number of tubes needed to get a high intensity (Bubenzer, 1979; Meyer, 1979).

Pressurized nozzle simulators allow for a larger variation in rainfall intensity than drop-forming simulators. The initial velocity of the drop is higher due to the exit pressure at the nozzle and therefore less distance is needed for the drops to reach terminal velocity. Rain intensity varies with nozzle size, pressure at the nozzle, the number of nozzles utilized, and nozzle movement (Meyer, 1979). An issue with continuous spray simulators is that the intensity is often too high. In order to control the intensity, water flow to the nozzle(s) can be solenoid-controlled or the nozzles can be placed on a rotating disc or an oscillating boom (Miller, 1987; Pérez-Latorre et al., 2010).

Numerous pressurized nozzle simulators were examined for their applicability (Table 3.3). Most of the designs studied were deemed too expensive, too complicated, or not portable enough. In a quote obtained by Long and Demars (2005), a professionally built rain simulator cost $12,000 to $15,000, and this estimate did not include the cost of a generator, pump, water tank and multiple connections. Others did not meet the desired rainfall intensity for this study of 25.4 mm hr^{-1} (1 in hr^{-1}) or less. Oscillating boom type

simulators can be complicated and expensive, requiring an electric motor and a computer controller to modulate the boom swing. In addition, the application of water on the plot is intermittent, rather than constant.

Many simulator designs published in the literature are unable to reproduce a realistic natural rainfall rate. While the design presented in Herngren, Goonetilleke, and Ayoko (2005) is simple, inexpensive and designed for studying urban water quality, the design was most effective at intensities of 60 to 100 mm hr^{-1} (2.36 to 3.94 in hr^{-1}). The design detailed in Edwards et al. (2002) was also inexpensive to build but unable to mimic a rain event of less than 70 mm hr^{-1} (2.8 in hr^{-1}). Storms of these magnitudes are highly unusual for the New England area, as the average monthly precipitation in New England is about 103 mm per month (Table 3.2).

Table 3.2: Mean and Extreme Precipitation, Blue Hill Meteorological Observatory, 1891-2010. All values in millimeters

Month	Mean	Record Highest (Year)	Record Lowest (Year)	24 Hour Maximum (Year)
January	108	295 (1979)	23 (1955)	78.7 (1889)
February	100	237 (1969)	18 (1987)	123 (1886)
March	117	478 (2010)	1.5 (1915)	168 (1968)
April	103	263 (1987)	23 (1892)	81.0 (1991)
May	94.0	257 (2006)	13 (1944)	128 (1984)
June	93.7	440 (1998)	3.6 (1999)	155 (1998)
July	92.5	296 (1938)	3.3 (1952)	119 (1979)
August	104	477 (1955)	14 (1981)	252 (1955)
September	100	314 (1999)	11 (1914)	149 (1961)
October	101	374 (2005)	5.6 (1924)	188 (1996)
November	111	248 (1983)	14 (1976)	129 (1955)
December	112	320 (1969)	23 (1955)	144 (1969)
Year	1235	1803 (1998)	685 (1965)	252 (1955)
From http://www.bluehill.org/climate/meanandextreme_1891-2010.html				

Table 3.3: Summary of Pressurized Nozzle Rainfall Simulator Designs

Source	**Use**	**Type**	**Nozzle**	**Rainfall intensity (mm hr^{-1})**	**Drop size (mm)**	**Uniformity (%)**	**Plot size (m)**	**Cost**
Herngren, Goonetilleke, and Ayoko (2005)	Urban water quality – impervious surfaces	Oscillating boom, three nozzles	Veejet 80100	60 – 100	0.05 – 5.6 (median 2.1)	95	2 x 1.5	Not stated
Loch et al. (2001)	Erosion and infiltration	Oscillating boom, three nozzles	Veejet 80100	Not stated, 40-60 or more?	Not stated	86.6 - 87.8	2 x 1.5	Not stated
Blanquies, Scharff, and Hallock (2003)	Vegetative and erosion control research	Oscillating boom, four nozzles	Floodjet 3/8 K SS45	< 50	1 – 7 (median 1.7)	> 90	1 x 3.56	Less than $7000
Wilcox et al. (1986)	Erosion	Fixed, single nozzle	Fulljet 1/4 G10	69 – 200	0.8 – 2.8 (median 1.2)	Not stated	1 x 1	$60
Edwards et al. (2002)	Phosphorus runoff	Fixed, single nozzle	Fulljet HH50WSQ	70	1.0 – 4.5 (median 1.9)	93	1.5 x 2	$1,500

Source	Use	Type	Nozzle	Rainfall intensity (mm hr^{-1})	Drop size (mm)	Uniformity (%)	Plot size (m)	Cost
Miller (1987)	Erosion and infiltration	Fixed, single or triple nozzle system; solenoid controlled	Fulljet 30WSQ	Single: 12.7 – 86.4 Triple: 43.2 – 115.8	1.0 – 2.75 (mean 2.25 - 2.5)	Single: 90 - 95 Triple: 85 – 90	Single: 1 x 1 Triple: 1 x 3	Approx. $1000
Pérez-Latorre, de Castro, and Delgado (2010)	Nutrient runoff	Single nozzle, solenoid controlled; triple nozzle, manual control	Single: Fulljet 35W; Triple VYR 118-2	Single: 21 - 83 Triple: 20 – 59	Single: 0.5 – 2.8 Triple: 0.5 – 2.0	Single: 80 – 92 Triple: 80 - 86	Single: 1.6 x 1.6 Triple: 1.2 x 1.2	Not stated
Shelton, Von Bernuth, and Rajbhandari (1985)	Erosion	Single nozzle, air injection	Fulljet 50WSQ	76 – 168	0.5 – 4.0 (median 1.8)	Minimum 84	6 x 6	Not stated
Thomas and El Swaify (1989)	Erosion, infiltration and runoff	Rotating disk	Spraying Systems 1-5H 30	15 – 150	Not stated	91.2 – 94.3	1.5 x 1.5	Not stated

3.3 Methods

Simulator design

The simulator design was based on the designs summarized in Table 3.3. Key design goals included the ability to mimic intensities in the range of storms in the New England area (25.4 mm hr^{-1} (1 in hr^{-1}) or less), uniform application over the study area, low cost, construction from easily available materials, and portability. For simplicity, a pressurized nozzle system was utilized, with a single, interchangeable nozzle mounted at 3 meters height on a canopy frame. Water was pumped to the nozzle with a 1 horsepower centrifugal pump (Wayne Water Systems, Harrison, Ohio) from a 55-gallon plastic drum (Baytec Containers, Houston, Texas). Two nozzles – Fulljet 1/4GG-10W and Fulljet 1/8GG-2.8W from Spraying Systems Co. (Wheaton, Illinois) – were selected for their conical spray pattern and flow rates at low pressures.

Simulator testing

Following the design and construction of the rain simulator, it was tested for spray characteristics, including drop size, drop velocity, intensity, and spray uniformity. These characteristics were tested in order to compare the simulated rainfall to natural rainfall in the study area. Drop size was tested using the oil method (Eigel and Moore, 1983). Water droplets were caught in a petri dish containing a mixture of 2 parts heavy gear oil and 1 part STP oil treatment. The mixture was prepared in a large beaker on a hot plate (approximately 80ºC). The heat aided in mixing the materials and removed air bubbles entrained in the mixture. The mixture was then cooled and poured into the petri dishes. Any remaining air bubbles were removed with a hypodermic needle. Each petri dish was

placed near ground level underneath a cover under the rain simulator. The simulator was started and allowed to run for about 1 minute in order to clear any air from the pumping system. The cover over the petri dish was removed and the oil mixture was exposed to simulated rain for approximately 3 seconds before being covered again. The rain simulator was turned off and the dish containing raindrops was then photographed within 30 seconds of exposure. A millimeter scale was present in the photograph. The photographs were then projected onto a white board, and the millimeter scale was used to measure and enumerate the suspended drops.

The equation from Van Dijk, Bruijnzeel, and Rosewell (2002) was used to calculate kinetic energy, in J m^{-2} mm^{-1}, for the different rainfall intensities.

$$e_K = 28.3\ [1\text{-}0.52\ \exp\ (\text{-}0.042R)], \tag{3.1}$$

where R is rainfall intensity in mm hr^{-1}.

Drop dispersion was analyzed using the uniformity coefficient equation (Christiansen, 1942),

$$C_u = 100\left(1 - \frac{\sum x}{mn}\right), \tag{3.2}$$

where x is the deviation of the individual observations from the mean value m, and n is the number of observations. A 2 by 2 meter grid was constructed with pre-weighed cups (95.25 mm diameter; standard deviation 0.327-0.439 grams) spaced at 0.4 meter intervals with an additional cup directly under the nozzle (Figure 2.3). The grid was exposed to simulated rainfall for 15 minutes. The cups were then weighed to determine the amount of water collected. The mean value, *m,* was calculated from these measurements. The dispersion from each nozzle was tested twice.

Figure 3.3: Photograph showing raindrops collected using the Fulljet 1/4GG-10W nozzle

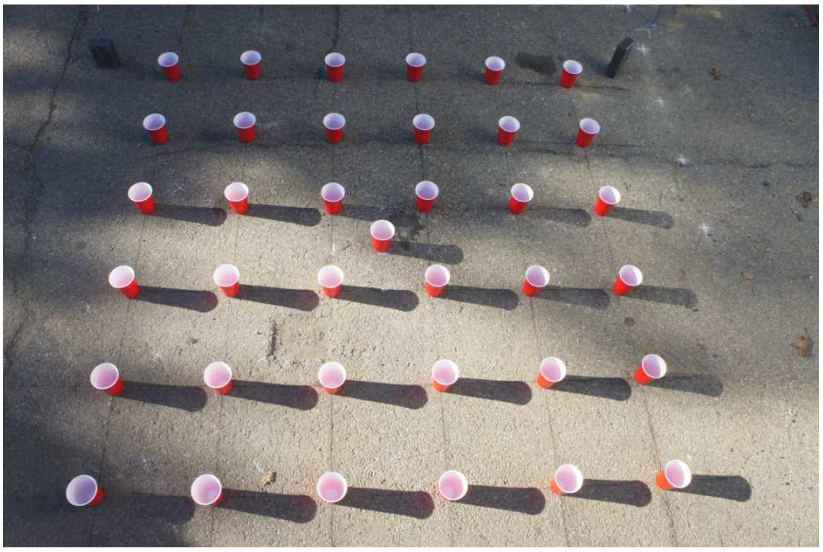

Figure 3.4: 2 by 2 meter grid with cups spaced at 0.4 meter intervals


Figure 3.5: Rain simulator in operation during drop dispersion testing

Study Sites

Two contrasting sites were selected for rain simulator deployment - Parking Lot D at the University of Massachusetts Boston, Boston, MA and a forested site in the Blue Hills Reservation, Canton, MA. Parking Lot D has an asphalt surface (Figure 3.6). The lot is about 15,000 m^2 and holds approximately 485 cars when full. The forested site in the Blue Hills Reservation was selected because it was relatively flat, treeless, and located in an area with minimal foot traffic (Figure 3.7). Ground cover consisted of grass and fallen leaves with several large deciduous trees surrounding the plot. Additional location information is available in Appendix A.

Figure 3.6: Parking lot study site with rain simulator in operation

Figure 3.7: Forested study site with rain simulator deployed

Plot design

At both sites, the canopy structure was deployed and anchored down to prevent movement due to wind. The canopy top was placed on the frame to reduce the influence of wind on the simulated rainfall. At the parking lot site, the 55-gallon water drum was filled with tap water (143-161 uM C; <8 QSU) obtained from a spigot at the University of Massachusetts Boston. Electricity was available at the site. At the forested site, water used was from the Department of Conservation and Recreation Blue Hills Reservation headquarters tap water (Fall 2012; 133 uM C; 4 QSU) or University of Massachusetts Boston tap water (Summer 2013; 119-141 uM C; 7-23 QSU). A gasoline-powered generator was utilized to provide electricity for the pump.

Parking lot site

The site selected was a 2 by 2 meter plot near a storm drain in the travel lane of the parking lot. In order to collect runoff, the plot was isolated from the surrounding parking lot using pre-bent aluminum flashing (Figure 3.8). The flashing was secured to the parking lot using silicon caulk and 3M Blue painter's tape. Potential contamination from these materials is addressed in the Results and Discussion section under "Materials Testing." A collection point was set up at the storm drain located on one edge of the plot. This was an ideal collection point as the plot gently sloped toward the storm drain. The storm drain grate was removed and a piece of flashing was used to channel runoff to a collection point. This flashing was held in place with silicon caulk and 3M Blue painter's tape. The collection point was covered to avoid receiving spray directly from the nozzle.

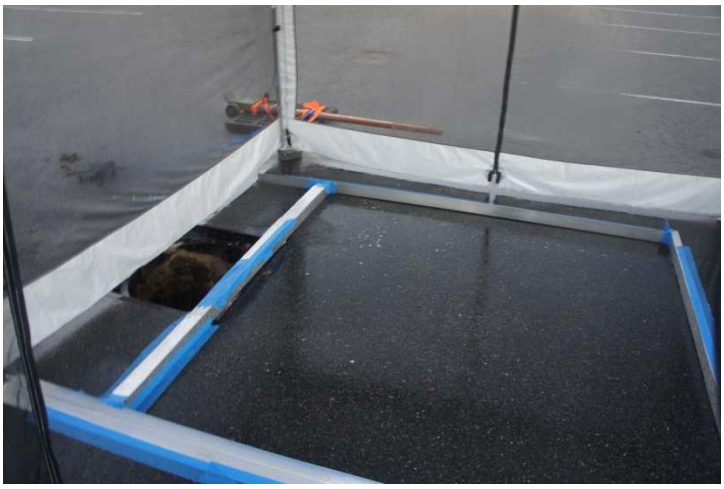

Figure 3.8: Parking lot study site, showing aluminum flashing and collection point

Forest site

Pre-bent aluminum flashing was used to isolate the 2 by 2 meter forest plot (Figure 3.9). The plot was set up in a square shape, with a collection point at a corner. This was the lowest point of the plot. On the two upper sides, the flashing was pushed into the soil to a depth of 3 inches. On the lower two sides, a shallow channel was dug and the flashing was pushed into the soil to create a runoff channel. Care was taken to not disturb soil inside of the plot. Runoff was carried through these two channels to the collection point. A hole was dug at the collection point in order to place a collection bottle at the outlet of the channel. Both channels and the collection point were covered to avoid receiving spray directly from the nozzle.

Figure 3.9: Forest study site, showing aluminum flashing. The collection point is at the lower right corner. The aluminum flashing on the right and bottom sides of the picture are the runoff channels. Due to the slope from the top left to the bottom right, the aluminum flashing on the left and top sides only isolate the plot and do not carry water to the collection point

Soil samples

In order to assess soil moisture, several soil samples were collected from an area close to the forested site in the Blue Hills Reservation. Several soil columns (4 inches long by 1.5 inch diameter) were collected in a butyrate plastic core liner utilizing a soil core sampler with hammer attachment (AMS Inc., American Falls, ID). The soil columns were then transported to the laboratory. Approximately 10 grams of soil were measured on aluminum weighing dishes. The dishes were then placed in a 90°C oven for 24 hours. The dry weight was then measured. The weight difference represents the water weight of the soil sample. Samples were left in the oven and weighed again after several weeks. Little difference (less than 0.05 grams) was observed from the weights measured after 24 hours in the oven.

An experimental setup was utilized to assess saturation and infiltration rate in an intact soil column (Figure 3.10). In the lab, a nylon stocking was taped to the bottom of the plastic core liner. Ultra high purity, low carbon Milli-Q UV water was then poured slowly into the top of the column. The rate of water addition was approximately 5.1 mL min^{-1} during the hour-long experiment. Observations were made about the speed with which the water drained through the soil column. In addition, the water that filtered through was collected at the bottom of the column and analyzed for DOC and CDOM. Additional soil moisture analyses were conducted on samples of soil from the top and bottom of the column after the saturation experiment.

Figure 3.10: Soil column setup for infiltration testing

3.4 Discrete Samples

Discrete samples were collected in 300 ml pre-combusted (500°C, 5 hours) glass bottles with Teflon-lined caps. Within 24 hours of sampling, each sample was filtered (high purity N_2 pressure filtered, <15 psi) at the laboratory through pre-combusted 0.7

μm glass fiber filters (Whatman GF/F). Dissolved organic carbon (DOC) and chromophoric dissolved organic matter (CDOM) samples were filtered into pre-combusted (500°C, 5 hours) 40 ml borosilicate glass vials with Teflon-lined screw caps. DOC samples were acidified to pH less than 2 with phosphoric acid and stored in clear vials at 4°C until analysis (Kaplan 1994). Absorbance and fluorescence samples were stored in amber vials at -4°C until analysis. All samples were analyzed at room temperature (21°C ± 1°).

3.5 Dissolved Organic Carbon (DOC)

A Shimadzu TOC-V analyzer was utilized for DOC analysis (Qian and Mopper, 1996). DOC standards were prepared using potassium hydrogen phthalate (KHP, Sigma Chemical) based on the instrument manual. The instrument was turned on and allowed to warm-up for at least one hour. Milli-Q water injections were then run until the instrument baseline stabilized with a peak area of 2 or less. The instrument was then calibrated with a seven-point standard curve. Samples were run following a linear regression of the standard curve ($r^2 \geq 0.995$). On subsequent days, at least one random carbon standard was run and compared to the standard curve to ensure continued calibration.

While running samples, the instrument blank was checked with ultra high purity, low carbon Milli-Q UV water every 10 to 15 samples. The mean blank value was subtracted from the sample measurements (Stedmon et al., 2000). Low Carbon Water (LCW) and Deep Sea Water (DSW) standards provided by Dennis Hansell's lab at the University of Miami were also run to ensure data quality.

3.6 CDOM Fluorescence

Fluorescence samples were thawed and then analyzed on a Photon Technologies International (PTI) Quantum Master 1 spectrofluorometer. Excitation scans were conducted with excitation (λ_{ex}) 337 nm, a 1 cm quartz cell, and emission scans from 350 nm to 650 nm. Slits widths were set to 4 nm. A blank (Milli-Q water) was run each day and subtracted from sample spectra to remove the Raman scattering peak. Fluorescence spectra were integrated in the wavelength range of 350 - 650 nm. A seven-point quinine sulfate standard curve (pH = 2) was used to convert the area of the emission spectra to quinine sulfate units (QSU) (Green and Blough, 1994; Siegener and Chen, 2002; Stedmon et al., 2003; Chen and Gardner, 2004). One QSU was equivalent to the fluorescence of 1 μg/l quinine sulfate at pH 2.

3.7 CDOM Absorption

Absorption samples were thawed and re-filtered through pre-cleaned 0.2 μm GE Osmonics polycarbonate filters before analysis to remove any glass fibers that may have become dislodged during the original filtration (Chen and Gardner, 2004). The polycarbonate filters were pre-washed with 2 M HCl prior to use (Stedmon et al., 2000). CDOM absorption spectra (200 – 800 nm) were measured with a Cary 50 spectrophotometer with a 1-cm path quartz cell. The precision of the instrument was +/- 0.002 absorption units.

All absorption calculations were completed after correcting the spectra by subtracting the average absorption in the 700 – 800 nm range (Green and Blough, 1994). The absorption coefficient (a, in m^{-1}) was computed using the following formula:

$$a_\lambda = 2.303 \times A(\lambda)/l \quad (3.3)$$

where A(λ) is the measured optical density at a chosen wavelength, and l is the cuvette path length in meters (Green and Blough, 1994). For the purposes of this research, the wavelength was 337 nm and the cuvette path length was 0.01 meters.

The DOC-specific absorption coefficient (a^*) was calculated using the following formula (Zhang et al., 2007):

$$a^*_\lambda = a_\lambda / (\text{DOC concentration}) \quad (3.4)$$

where DOC is expressed in mg l^{-1}. The wavelength used was 337 nm.

Spectral slopes (S) were calculated using best-fit linear regression of the log transformed a spectra over two wavelength ranges (275 - 295 nm and 350 - 400 nm). S depends on the wavelength range chosen (Green and Blough, 1994; Ferrari, 2000). A parameter called the slope ratio, or S_R, was calculated using the ratio of the absorption slope from 275-295 nm compared to that of the slope from 350-400 nm. The slope ratio compares absorbance values that often change during transit, either over time or due to photodegradation, and can allow for insight into DOM molecular weight and source. Higher value, or steeper, slopes show a more rapid decrease in absorption with increasing wavelengths (Helms et al., 2008).

Fluorescence quantum yield was calculated with the relationship:

CDOM fluorescence / absorbance coefficient (3.5)

This relationship expresses the quantum efficiency of the fluorescence with respect to the absorption of a sample (Green and Blough, 1994). The CDOM versus DOC relationship was also graphed.

Spectral data were all corrected for the inner filter effect for samples with absorbance above 0.1. The inner filter effect occurs when dissolved species, including the fluorophore, absorb exciting or emitted radiation (Puchalski et al., 1991; Hu et al., 2002). To correct for this effect, dilution with Milli-Q water was conducted for all samples over 100 QSU (about 0.1 m^{-1}).

3.8 Results and Discussion

Simulator testing

Based on the test results, the rainfall simulator satisfied the design requirements of this study, including rain rate, drop dispersion, and uniformity. The results are presented in Table 3.4. Parameters tested included volume, rainfall intensity, dispersion uniformity, and drop size. Kinetic energy was calculated using Equation 3.1. The uniformity of the higher flow nozzle (Fulljet 1/4GG-10W) was comparable to other studies with uniformities around 85% (Bubenzer et al., 1985; Shelton et al., 1985; Miller, 1987). The Fulljet 1/8GG-2.8W created less uniform spray but still delivered water to the entire 2 by 2 meter plot. The observed average drop sizes from both nozzles were smaller than an average rainstorm in the New England region.

The kinetic energy of the simulated rain was similar to other studies based on calculations using rainfall intensity. Since a pressurized rainfall simulator was utilized, the actual velocities may have been close to velocities calculated by others, such as Meyer and Harmon (1979) and Parsakhoo et al. (2012). Drop velocity is important when examining the impact that raindrop cratering has on erosion. This study was not intended to cause erosion in the test plots. While soil disturbance has implications for the release of DOC from the top layer of soil, the runoff results show that DOC was mobilized during the experiments.

Table 3.4: Rainfall simulator testing results

Nozzle	**Pressure (psi) (at nozzle / at pump)**	**Volume (L/min)**	**Intensity (mm hr^{-1})**	**Uniformity (% over 4m^2 plot)**	**Drop size range (mm)**	**Average drop size (mm)**	**Kinetic energy (J m^{-2} mm^{-1})**
Fulljet 1/4GG-10W	10 / 15	4.1	25.4	83.2	<0.25 to 2.25	0.59	23.24
Fulljet 1/8GG-2.8W	27-30 / 30	1.95	12.7	Not evaluated	Not evaluated	Not evaluated	19.67
Fulljet 1/8GG-2.8W	10 / 12.5	1.05	6.35	58.3	<0.25 to 1.125	0.47	17.03

Materials Testing

Blue painter's tape (3M Company) and silicon caulk were used to hold the pre-bent aluminum flashing in place at the Parking Lot location. Most of the Blue tape was located outside of the plot area. Silicon caulk was used underneath the aluminum flashing and to hold the flashing that was used to channel runoff at the collection point. Contact of the simulated rain with these substances was minimal, but did occur.

Laboratory tests were conducted in December 2014 to determine the potential DOC and CDOM contribution of both materials. While the materials were not fully submerged in water for 4 hours during the parking lot experiment, the following procedure was used to mimic the conditions in the parking lot as best as possible. For the Blue painter's tape, 2 inch square pieces of tape were soaked in 100 mL Milli-Q water, with samples taken at 30, 60, 240, and 1440 minutes. For the silicone caulk, 5.14 grams were placed in 125 mL of Milli-Q in a beaker, with samples taken at 30, 60, 240, and 1440 minutes. A separate 5.18 grams of silicone caulk was allowed to cure for the manufacturer-recommended 60 minutes in a beaker, then 125 mL of Milli-Q was added to the beaker, with samples taken at 30, 60, 240, and 1440 minutes. All samples were processed using standard DOC and CDOM collection, filtering, and processing methods. The Blue painter's tape testing resulted in high DOC values (182-644 uM C), with increasing concentrations with time (Figure 3.11). CDOM concentrations were between 10 and 37 QSU, with concentrations increasing with time (Figure 3.12).

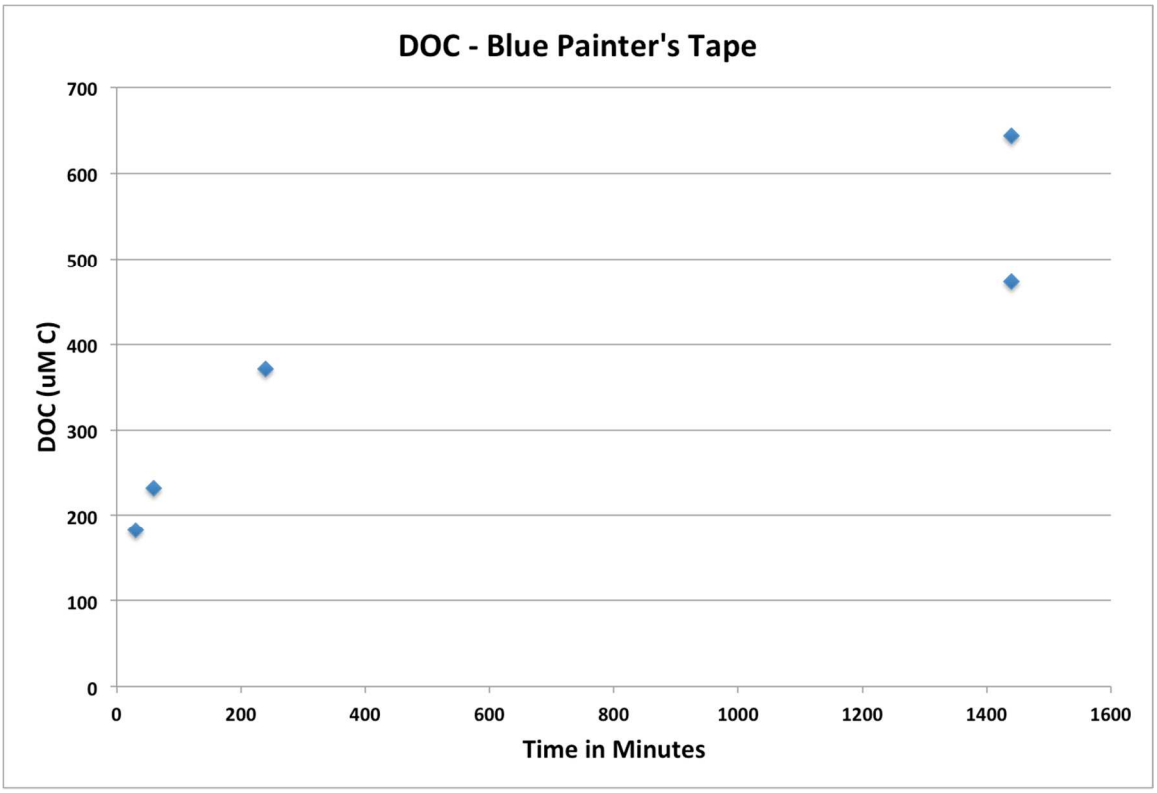

Figure 3.11: DOC concentration results from laboratory testing of Blue painter's tape

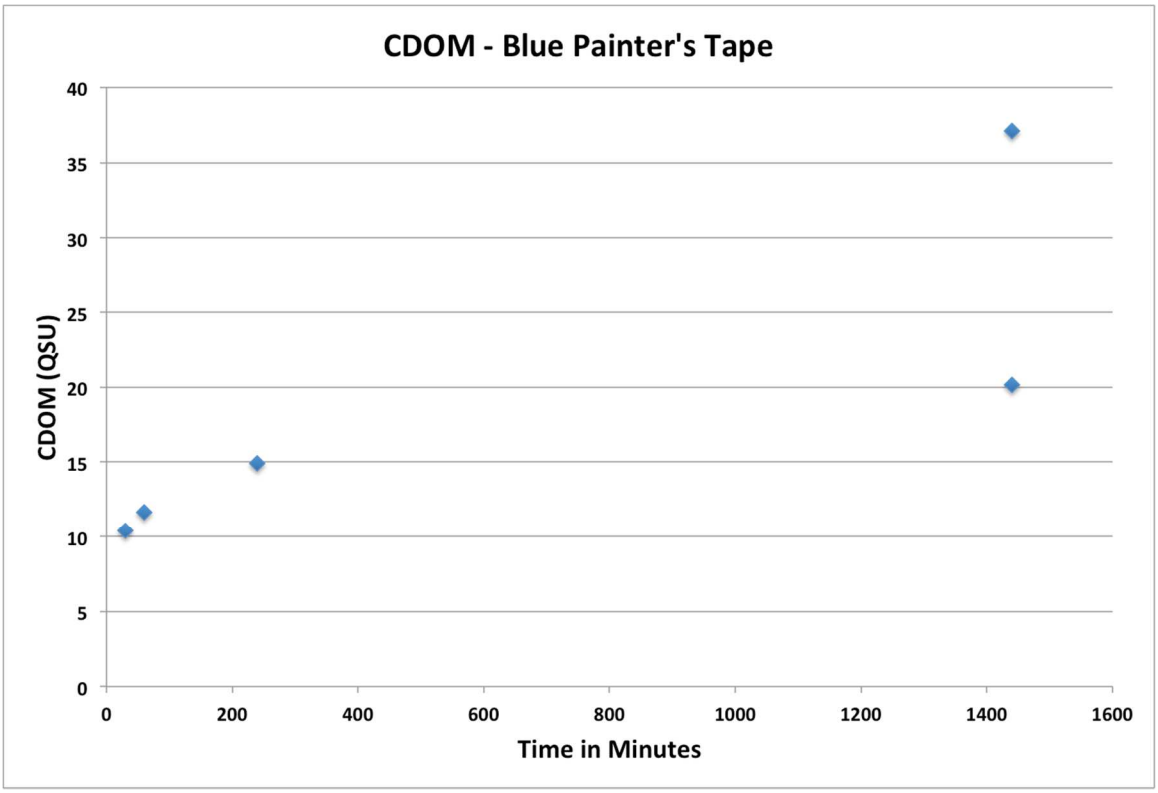

Figure 3.12: CDOM concentration results from laboratory testing of Blue painter's tape

The silicone caulk testing resulted in extremely high DOC values (354-71059 uM C), with increasing concentrations with time (Figure 3.13). Even if the samples taken at 1440 minutes (24 hours) are excluded, the concentrations are still very high (354-5423 uM C), with slightly higher values for the cured samples (Figure 3.14). Low CDOM concentrations and absorption coefficients contrast with the high DOC contributions from both materials. All CDOM samples were less than 1 QSU (Figure 3.15). The absorption coefficients for both materials were low (Figure 3.16). The high DOC values may be the result of acetic acid being released during the silicon caulk curing process, as described by the packaging material.

Based on the laboratory testing, the high concentration values for the 5 grams of silicone soaked in Milli-Q water were equivalent to approximately 0.78 g C per liter (~65000 uM C). Assuming that 100 grams were used in the Parking Lot plot, with 50 grams exposed to precipitation and runoff, the potential influence of the silicone in the large simulated event (~500 liters) could be 1300 uM C. For the smaller rain events (~150 liters), the contribution from the silicone could account for 4350 uM C.

These concentration values are very similar to the concentration observed the beginning of the simulated rain events. In effect, the silicone caulk may have seeded the plot with extra DOC that was washed off during the simulated event. While there are concerns that the materials used strongly influenced the runoff DOC concentrations, the results presented here are a valid demonstration of the capabilities of the designed rainfall simulator for creating runoff on an impervious surface and then collecting the runoff for analysis.

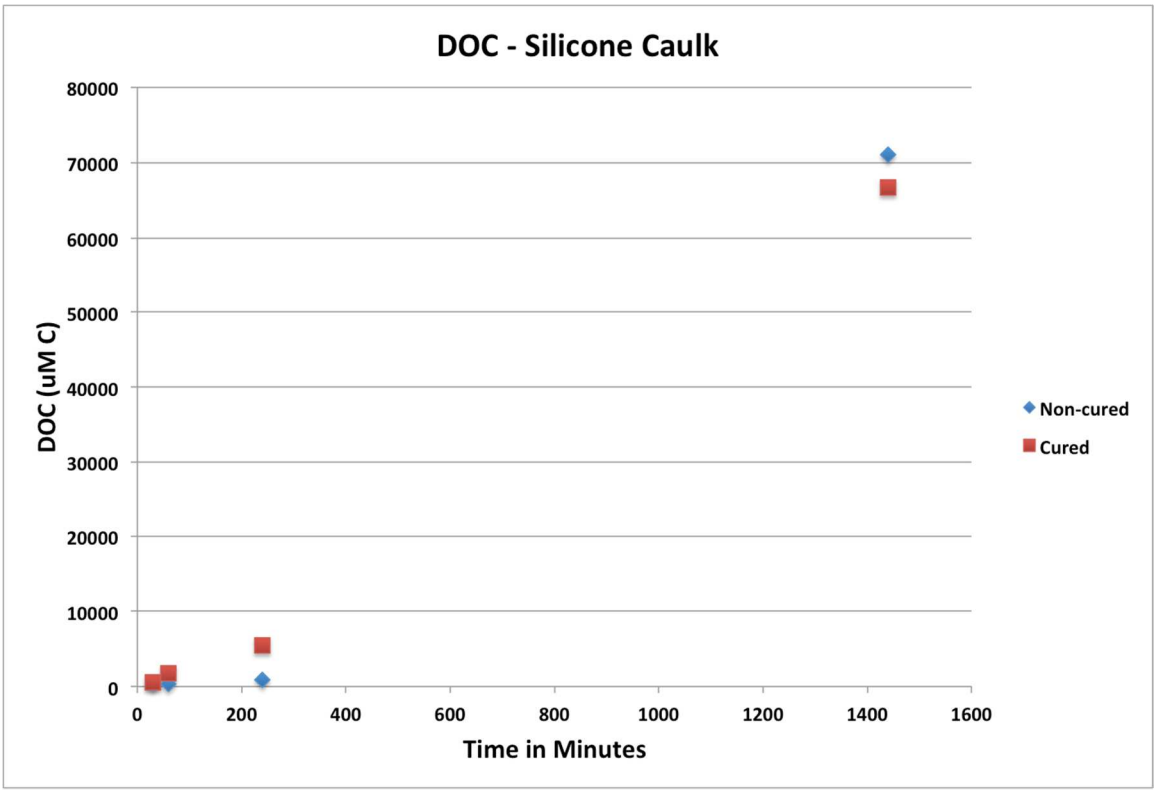

Figure 3.13: DOC concentration results from laboratory testing of silicone caulk. Graph includes very high concentration samples taken at 1440 minutes

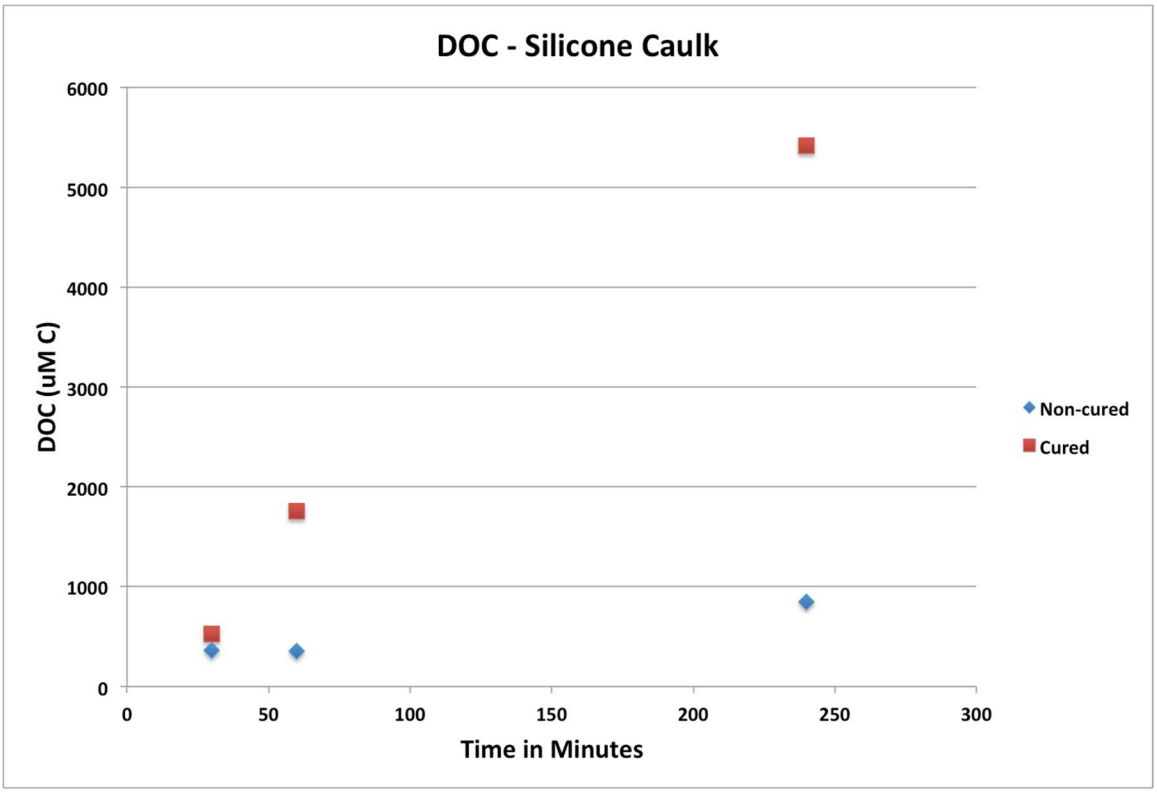

Figure 3.14: DOC concentration results from laboratory testing of silicone caulk. Graph excludes very high concentration samples taken at 1440 minutes

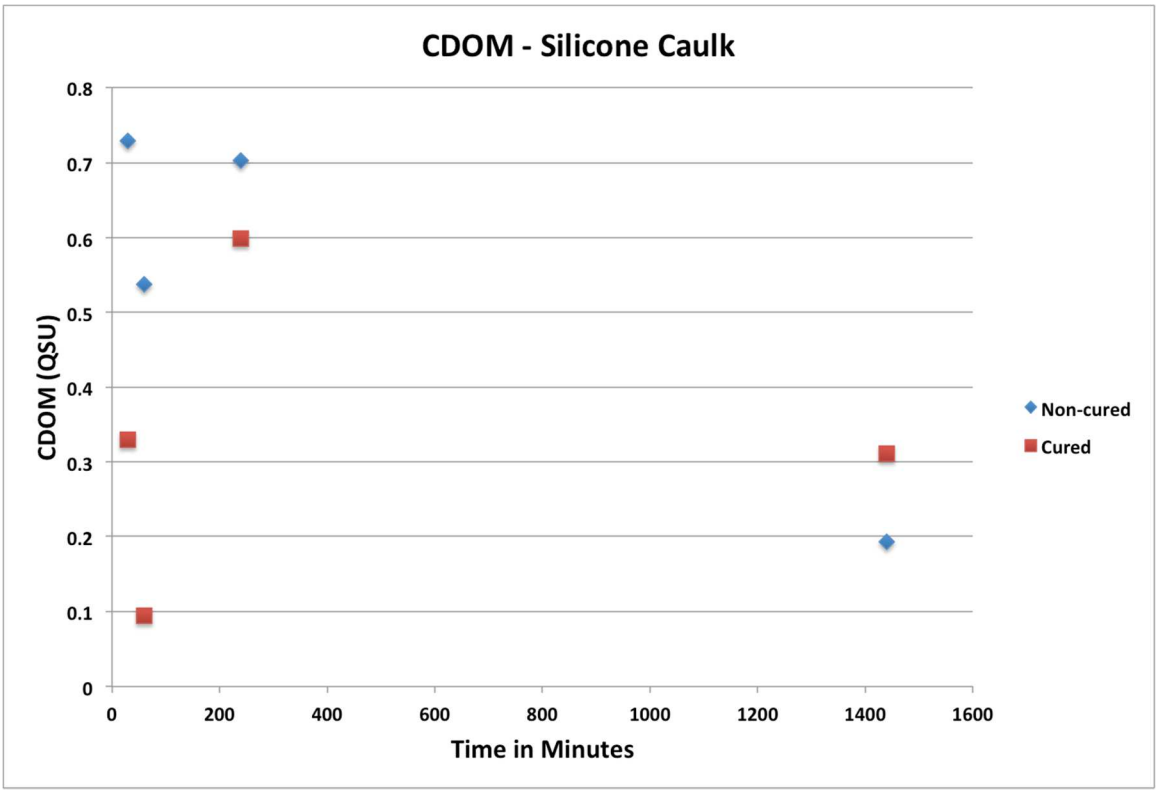

Figure 3.15: CDOM concentration results from laboratory testing of silicone caulk

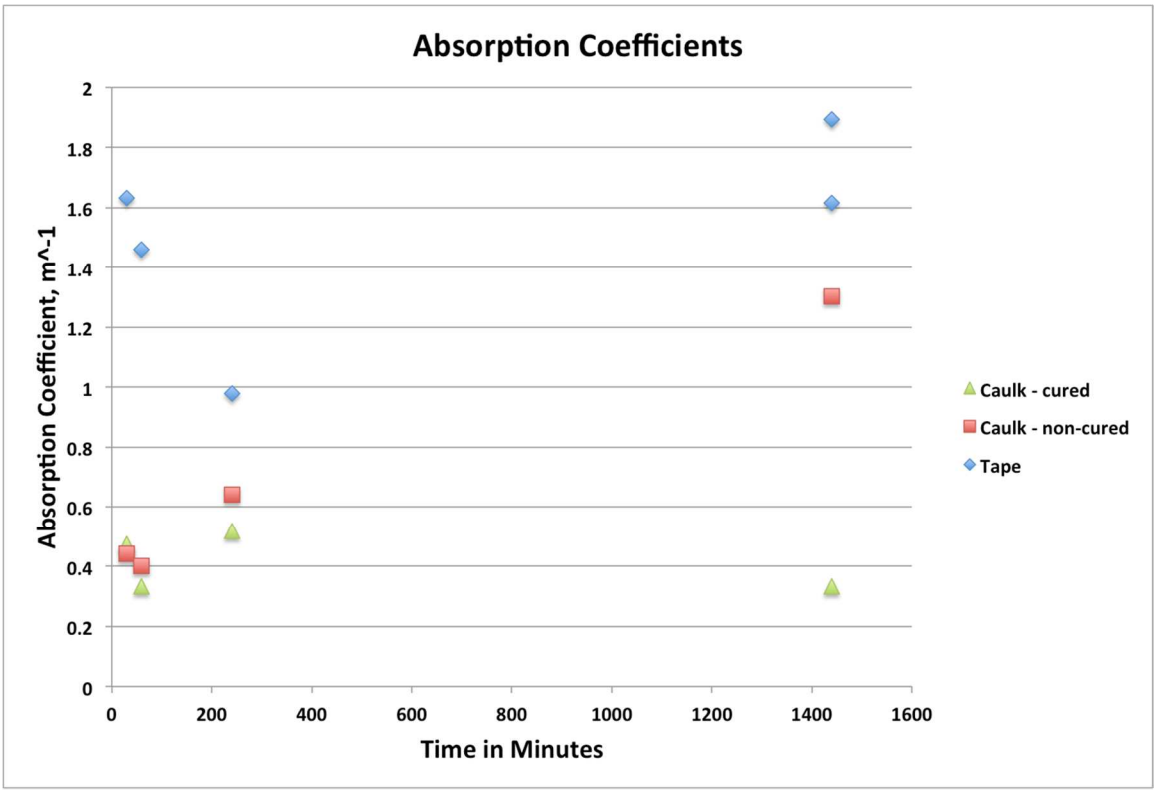

Figure 3.16: Absorption coefficients for materials testing samples

Simulator Deployment

The rainfall simulator was deployed four times each at the two study sites. More information about the deployments is presented in Table 3.5.

Table 3.5: Information about rainfall simulator deployments

Experiment	Date	Antecedent Rainfall	Testing Conditions
Parking Lot I	11/17/12	10.92 mm; 11/12/12	25.4 mm hr^{-1}; 1 hour
Parking Lot II	6/30/13	12.45 mm; 6/28-6/29/13	25.4 mm hr^{-1}; 4 hours
Parking Lot III	7/7/13	4.57 mm; 6/30-7/1/13	12.7 mm hr^{-1}; 4 hours
Parking Lot IV	7/14/13	11.94; 7/11/13	6.35 mm hr^{-1}; 4 hours
Forest I	11/18/12	10.92 mm; 11/12/12	25.4 mm hr^{-1}; 1 hour
Forest II	8/14/13	57.15 mm; 8/9/13	6.35 mm hr^{-1}; 4 hours
Forest III	8/15/13	57.15 mm; 8/9/13	12.7 mm hr^{-1}; 4 hours
Forest IV	8/16/13	57.15 mm; 8/9/13	25.4 mm hr^{-1}; 4 hours

Parking Lot I – Thursday, 11/17/12 – 25.4 mm hr^{-1} (1 in hr^{-1})

At the parking lot site, runoff did not start to drain at the collection site until 1 minute 50 seconds after the rain started. At the collection point, approximately 3 liters per minute were draining into the storm drain (measured at 16:30, 25:30, and 41:30). Large sediment grains were observed in samples 1 through 5, with less sediment in 6 through 8,

and hardly any in samples 9 through 20. DOC concentrations ranged from 51 to 1164 μm C, with the highest concentration in the first sample (Figure 3.17). CDOM concentrations showed a similar trend to DOC, with the highest concentration (75 QSU) in the first sample and lower concentrations in subsequent samples (Figure 3.18). There is lower concentration (41 QSU) in the second sample, and then an increase in concentration for the third and fourth samples, but then a steady decreasing trend is observed.

A blank was not collected on this day, so the DOC and CDOM concentration of the tap water is unknown. The average DOC concentration for 2013 for water from the same tap was 155 uM C. The average CDOM concentration for 2013 for water from the same tap was 12 QSU. For comparison, the 2013 blank values were subtracted from the 2012 parking lot data.

Parking Lot II – Sunday, 6/30/13 – 25.4 mm hr^{-1} (1 in hr^{-1})

Runoff started to drain at the collection site approximately 2 minutes after the rain started. At the collection point, approximately 3 liters per minute were draining into the storm drain. Sediment grains were observed in samples 1 through 5, with less sediment in subsequent samples. DOC concentrations ranged from 89 to 1868 μm C, with the highest concentration in the first sample (Figure 3.17). The concentrations decrease until sample 16 (2 hours 15 minutes, 89 uM C). Then, the concentrations rise slightly, but do not go above 200 uM C through the end of the experiment. There was a large decrease in concentration between samples 7 (10 minutes, 1080 uM C) and 8 (20 minutes, 490 uM C). The CDOM analysis shows a similar trend. Concentrations range between 24 and 192 QSU, with the highest concentration in the first sample (Figure 3.18). The CDOM

concentrations rise towards the end of the experiment after holding at about 25 QSU between 1 hour and 2 hours 30 minutes. Field blanks of 152 uM C and 6 QSU were subtracted to arrive at the final DOC and CDOM values, respectively.

Parking Lot III – Sunday, 7/7/13 – 12.7 mm hr^{-1} (0.5 in hr^{-1})

Runoff started to drain at the collection site approximately 3 minutes after the rain started. At the collection point, approximately 0.66 liters per minute were draining into the storm drain (measured during minute 25). DOC concentrations ranged from 335 to 4398 μm C, with the highest concentration in the first sample (Figure 3.17). Concentrations tended to decrease, with several small increases, until sample 18 (2 hours 15 minutes, 335 uM). Then, concentrations increase slightly to between 349 and 527, with a single large increase to 902 uM C observed at 3 hours 30 minutes. CDOM concentrations were between 97 and 680 QSU, with the highest concentration in the first sample (Figure 3.18). There is a steady decrease in concentration until 1 hour 30 minutes. Then, concentrations level off between 97 and 146 QSU until the end of the experiment. A slight increase is observed in the sample at 3 hours 30 minutes, but is not as great an increase as observed in the corresponding DOC sample. Field blanks of 156.5 uM C and 7 QSU were subtracted to arrive at the final DOC and CDOM values, respectively.

Parking Lot IV – Sunday, 7/14/13 – 6.35 mm hr^{-1} (0.25 in hr^{-1})

Runoff started to drain at the collection site approximately 3.5 minutes after the rain started. At the collection point, approximately 0.66 liters per minute were draining into the storm drain (measured during minute 48). DOC concentrations ranged from 156 to 3751 μm C, with the highest concentration in the first sample (Figure 3.17).

Decreasing DOC concentrations were observed through sample 17 (2 hours, 245 uM C). Then, concentrations varied between 146 (sample 20, 2 hours 45 minutes) and 365 (sample 18, 2 hours 15 minutes). The CDOM data is very similar to the DOC data, although the highest concentration (436 QSU) is observed in the second sample (Figure 3.18). A steady decrease in concentration occurs through sample 17 (2 hours, 54 QSU). Then, concentrations are between 45 and 89 QSU. Field blanks of 155 uM C and 7 QSU were subtracted to arrive at the final DOC and CDOM values, respectively.

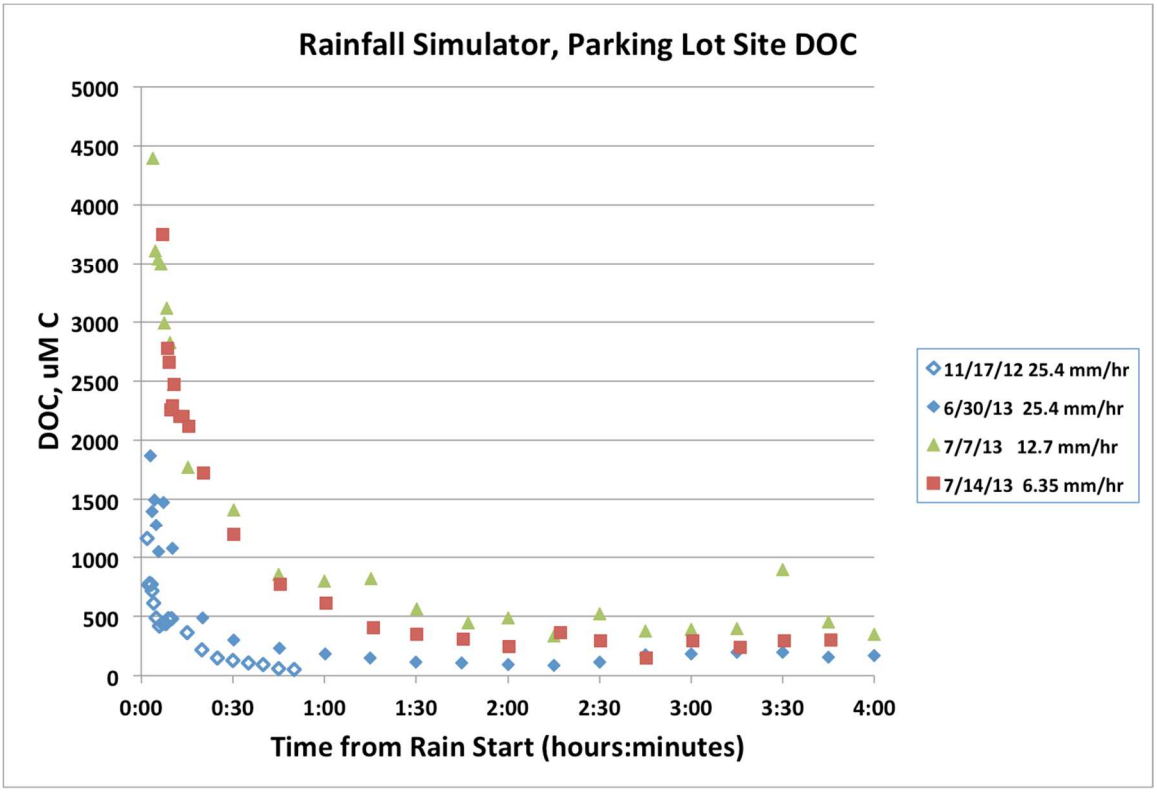

Figure 3.17: Comparison of DOC concentrations over time for all parking lot deployments

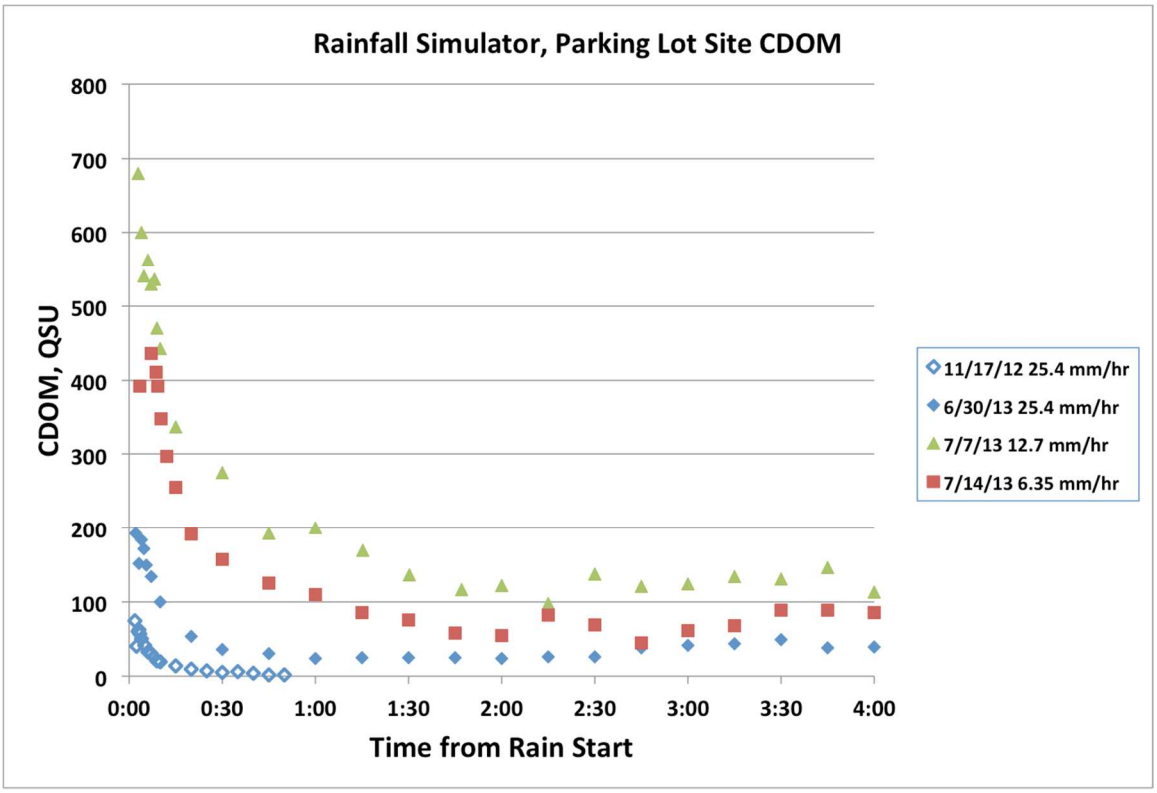

Figure 3.18: Comparison of CDOM concentrations over time for all parking lot deployments

For the three parking lot deployments in 2013, rainfall intensity and antecedent rainfall seem to influence DOC and CDOM concentrations. It is difficult to assess the total influence because there is a week of time between each of the simulated storms. During these different periods, varying amounts of organic compounds may have deposited on the test plot. Sediment was observed on filters, but was not collected for particulate organic carbon analysis. However, it is important to note that Parking Lot II has the closest antecedent rainfall and the lowest DOC and CDOM concentrations. This may be due to the washing of the surface by the antecedent rainfall or dilution by the higher simulated rainfall intensity. Parking Lot III has the highest DOC and CDOM concentrations, and was preceded by the driest period of the three 2013 sampling dates.

Parking Lot IV has high DOC and CDOM concentrations, even with the lowest rainfall intensity, and antecedent rainfall three days before sampling.

The different slopes of the CDOM versus DOC graph may be the result of different types of organic compounds depositing on the test plot between storms (Figure 3.19). Leaching from the silicone caulk used to isolate the sampling plot from the surrounding parking lot may also influence DOC concentrations. The caulk has a high DOC concentration, but low CDOM concentration. This is discussed further in "Materials Testing."

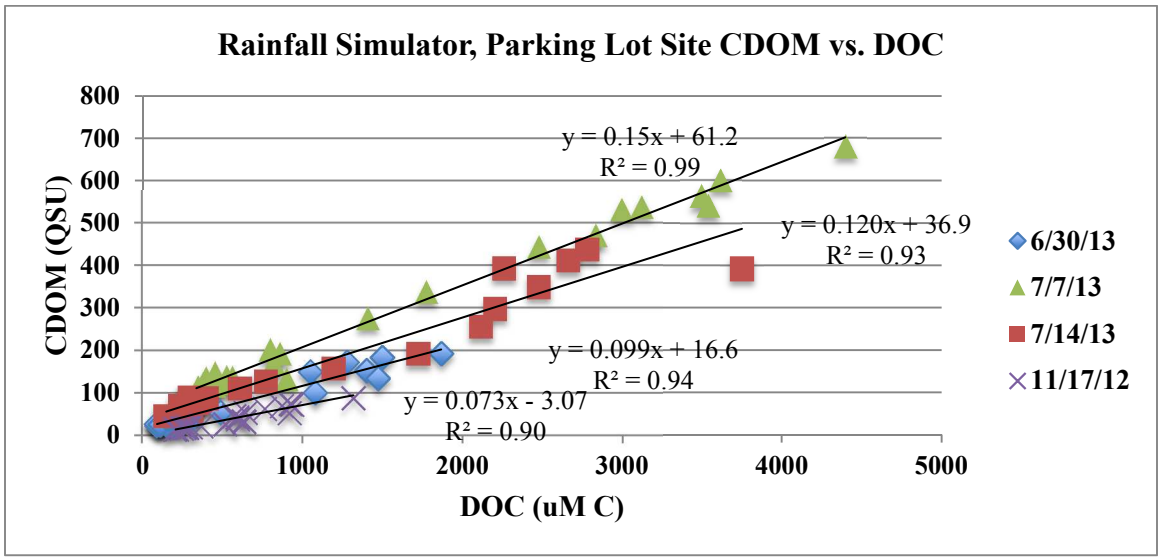

Figure 3.19: CDOM versus DOC comparison for all parking lot deployments

Parking lot absorption coefficients decrease with time, with a slight increase towards the end of the storm (Figure 3.20). The pattern is similar to the exponential decrease in DOC and CDOM concentrations also observed at the parking lot site. This decrease in absorption may be the result of the wash-off of DOM from the parking lot at the beginning of the storm. As the DOM is depleted, samples towards the end of the

storm would be more rainwater and have a lower concentration of contaminants. Spectral slopes are fairly consistent, with a slight increasing trend visible (Figure 3.21). Higher value, or steeper, slopes correspond to a more rapid decrease in absorption with increasing wavelengths. Since absorption decreases during the simulated storms, higher spectral slope values would be expected to occur towards the end of the storms.

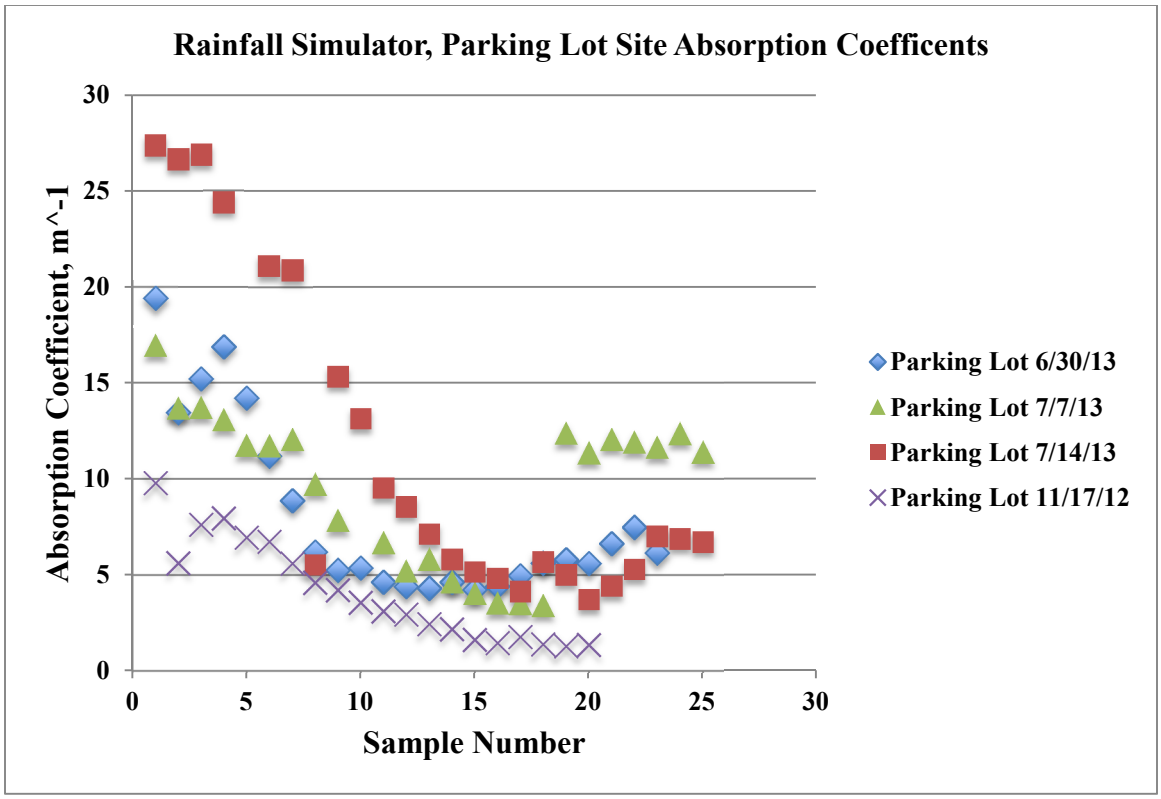

Figure 3.20: Comparison of absorption coefficients over time for all parking lot deployments

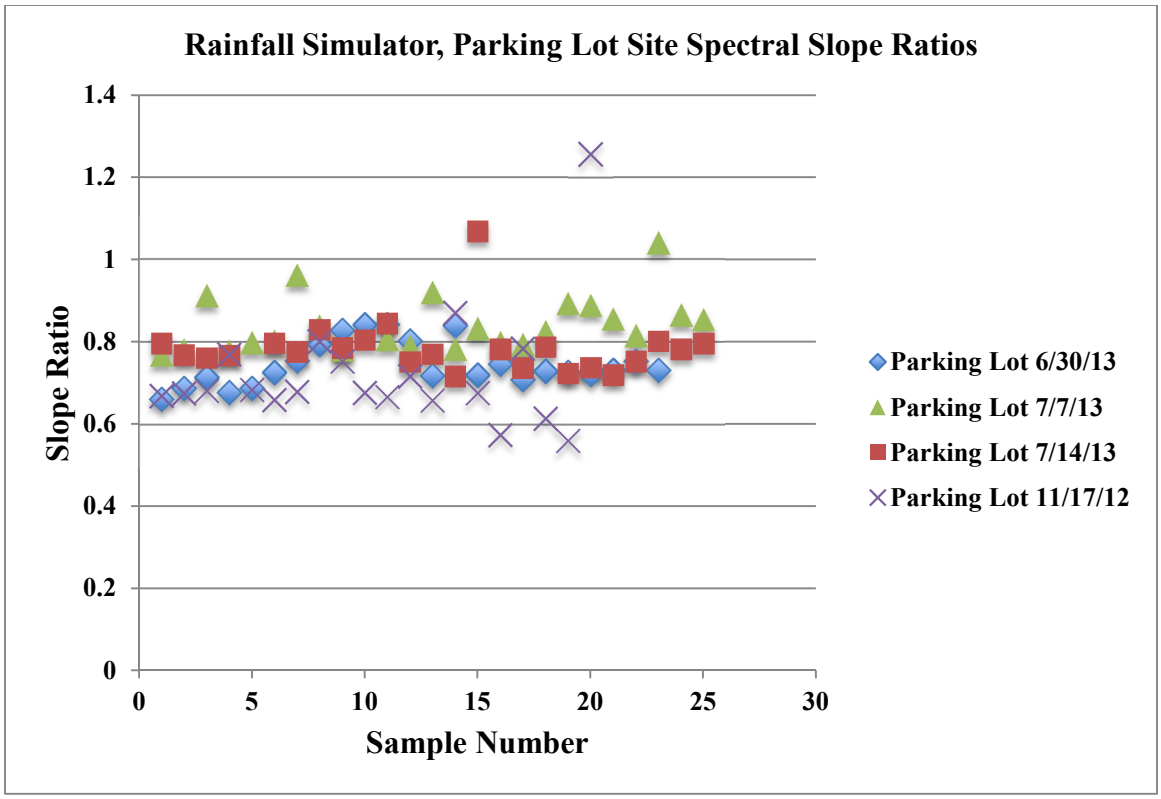

Figure 3.21: Comparison of spectral slope ratios over time for all parking lot deployments

The rain application over the parking lot plot is between 58.3 to 83.2% uniform (depending on the nozzle), but the edges of the plot receive less rain than the center. As a result, the center of the parking lot plot may have a greater flux and contributes to the beginning of the runoff. The outer edges of the plot receive a lower flow and contribute to the runoff only after a period of pooling. The release of water from this pool may account for the spikes in concentration observed within the first 10 minutes in the four parking lot deployments. The parking lot experiments also show an increase in concentration at the end of the experiments. However, this end flush is not large enough to mask the first flush present during the simulated storms.

Forest I – Friday, 11/18/12 – 25.4 mm hr^{-1} (1 in hr^{-1})

At the forested site, runoff was observed 18 minutes 20 seconds after starting the rain simulator. Samples were collected approximately every 5 minutes after runoff started. The amount of runoff that reached the collection point was much less than at the parking lot site. DOC concentrations were much higher than at the parking lot site, ranging from 1492 to 2942 μm C (Figure 3.22). A slight concentration increase was observed in the second sample with all subsequent samples decreasing in concentration. For the CDOM samples, a slight increasing trend is observed (Figure 3.23). Concentrations are greater than those at the parking lot, ranging between 104 and 198 QSU. All sample values were corrected for the DOC concentration (133 uM C) or the CDOM concentration (4 QSU) of the tap water used in the field.

Forest II – 8/14/13 – 6.35 mm hr^{-1} (0.25 in hr^{-1})

With a 6.35 mm hr^{-1} (0.25 in hr^{-1}) rain rate, runoff was observed 25 minutes after starting the rain simulator. The amount of runoff that reached the collection point was much less than at the parking lot site. DOC concentrations ranged from 958 to 3159 μm C (Figure 3.22). The lowest concentrations were observed at the beginning of the experiment, with a peak concentration at the 2-hour mark, and a slight decreasing trend to the end of the experiment. The CDOM concentrations exhibited the same trends, with concentrations between 112 and 305 QSU (Figure 3.23). Field blanks of 140.5 uM C and 9 QSU were subtracted to arrive at the final DOC and CDOM values, respectively.

Forest III – 8/15/13 – 12.7 mm hr^{-1} (0.5 in hr^{-1})

With a 12.7 mm hr^{-1} (0.5 in hr^{-1}) rain rate, runoff was observed 29 minutes and 20 seconds after starting the rain simulator. The amount of runoff that reached the collection point was much less than at the parking lot site. DOC concentrations ranged from 1297 to 4910 μm C (Figure 3.22). The highest concentration was observed at the beginning of the experiment, with concentrations showing a decreasing trend until the end of the experiment. CDOM concentrations ranged from 129 to 325 QSU, and followed the same trends as DOC (Figure 3.23). Field blanks of 124 uM C and 7 QSU were subtracted to arrive at the final DOC and CDOM values, respectively.

Forest IV – 8/16/13 – 25.4 mm hr^{-1} (1 in hr^{-1})

With a 25.4 mm hr^{-1} (1 in hr^{-1}) rain rate, runoff was observed approximately 20 minutes after starting the rain simulator. The amount of runoff that reached the collection point was much less than at the parking lot site. DOC concentrations ranged from 491 to 937 μm C (Figure 3.22). The highest concentration was observed at the beginning of the experiment, with concentrations showing a decreasing trend until 3 hours and then increasing for the last hour. CDOM concentrations were between 74 and 159 QSU (Figure 3.23). However, low concentrations were observed at the beginning of the experiment, increasing until 1 hour 10 minutes (147 QSU). Then, concentrations show a slight decreasing trend until 3 hours and increase for the last hour, with the highest concentration observed at 3 hours 20 minutes. Field blanks of 126 uM C and 20 QSU were subtracted to arrive at the final DOC and CDOM values, respectively.

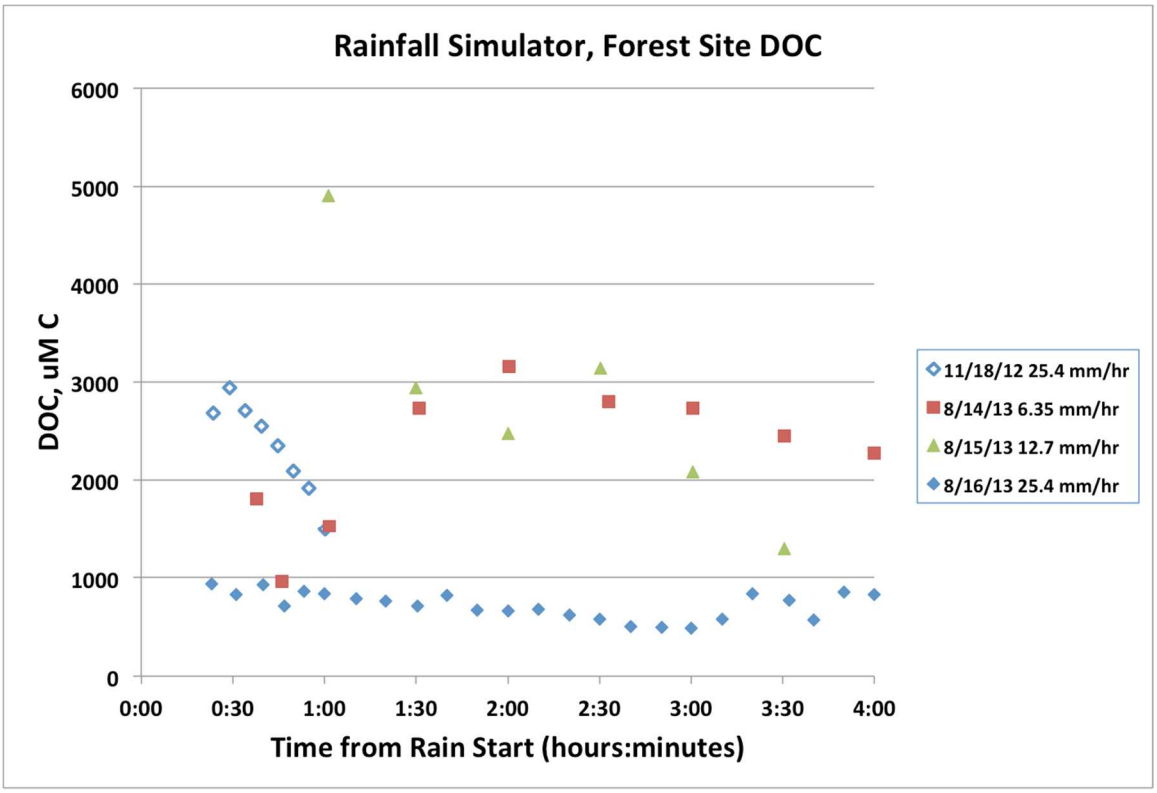

Figure 3.22: Comparison of DOC concentrations over time for all forested site deployments

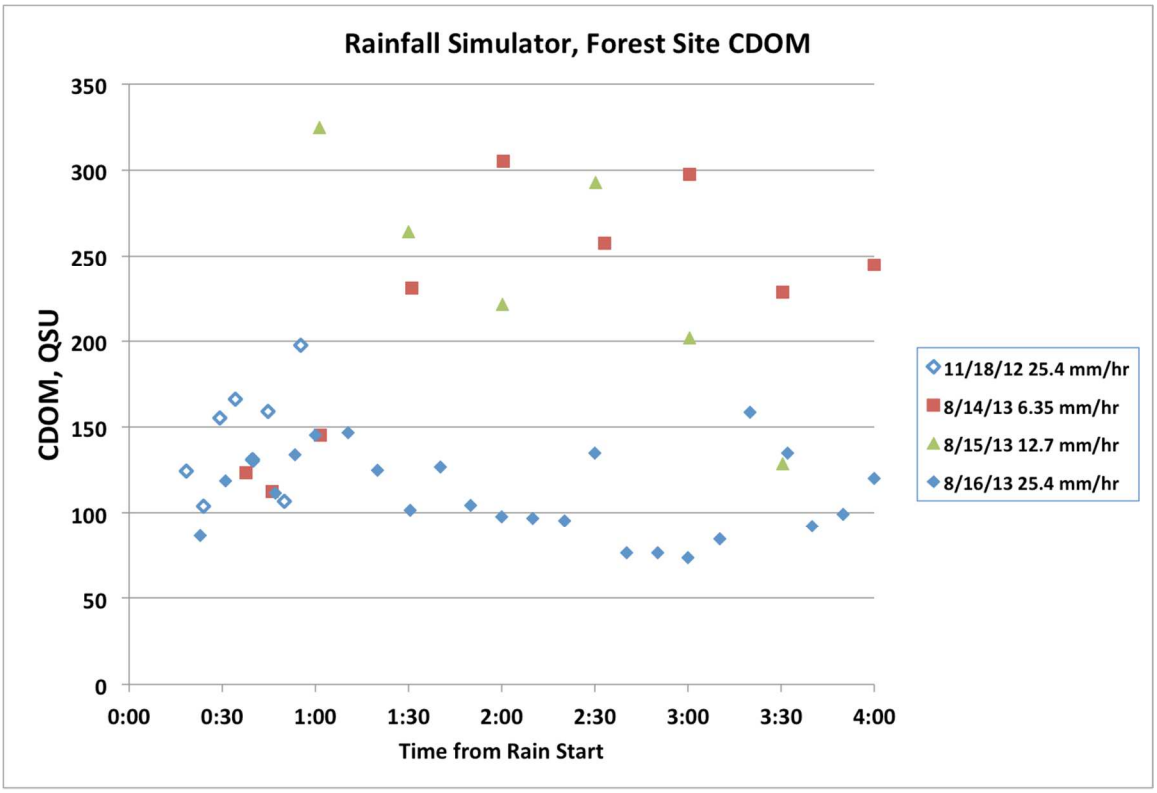

Figure 3.23: Comparison of CDOM concentrations over time for all forested site deployments

For the three forest site deployments in 2013, rainfall intensity and antecedent rainfall seem to influence DOC and CDOM concentrations. The antecedent storm was 57.15 mm on 8/9/13, which is five days prior to the first simulated rain event. The first simulated event, Forest II, is the lowest intensity but collected runoff has very high DOC and CDOM concentrations. Concentrations show an increasing trend through the simulated storm. Approximately 261 milliliters of runoff were collected during the Forest II experiment. Forest III has similar concentrations to Forest I, but concentrations show a decreasing trend through the storm. Approximately 169 milliliters of runoff were collected during the Forest III experiment. Forest II and III may have resulted in the wash-off of the most labile DOM, as detailed by McLaughlin and Kaplan (2013). Forest

IV is the highest intensity storm, with lower concentrations than Forest II and III, but a higher total flux due to more runoff. Approximately 1356 milliliters of runoff were collected during the Forest IV experiment. Forest IV concentrations may be close to the background, or baseline, concentrations for the forest site following the depletion of higher concentration DOM during the two antecedent simulated storms.

Data collected in 2012 has a very different CDOM-DOC slope than data collected in 2013. This may be the result of the time of year when the experiments were conducted. In November 2012 during Forest I, the forest plot had a layer of leaf litter. This may have resulted in CDOM concentrations being a higher proportion of the DOM pool (Hongve, 1999) (Figure 3.24). Forest II, III, and IV samples were collected in August 2013. The surface of the forest plot was mostly grass, with little leaf litter present.

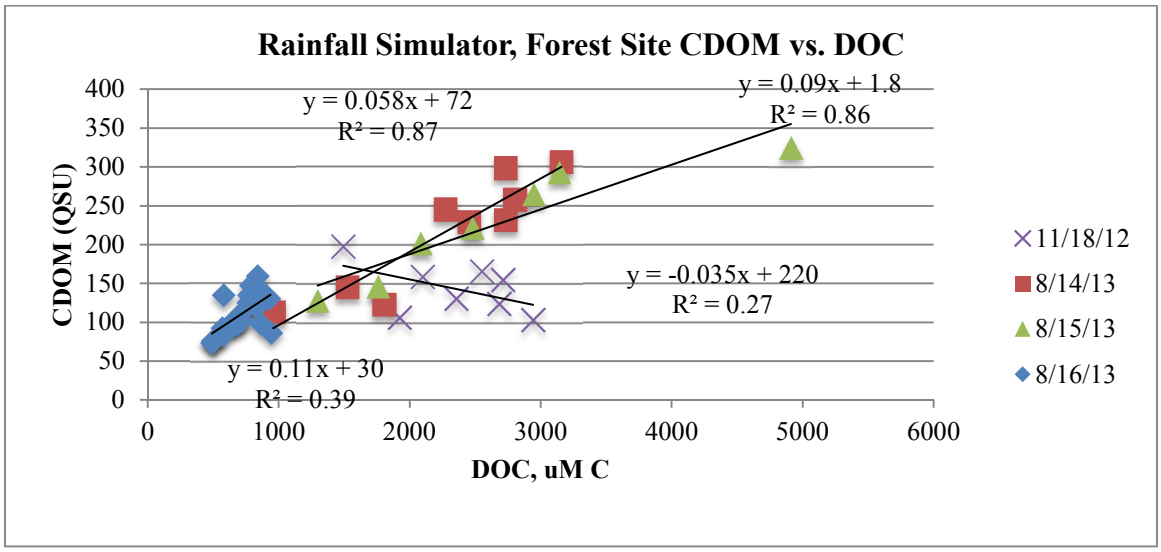

Figure 3.24: CDOM versus DOC comparison for all deployments

Forest site absorption coefficients decrease slightly with time (Figure 3.25). Spectral slopes appear to increase through the storms (Figure 3.26). Higher value, or

steeper, slopes correspond to a more rapid decrease in absorption with increasing wavelengths. Since absorption decreases during the simulated storms, higher spectral slope values would be expected to occur towards the end of the storms.

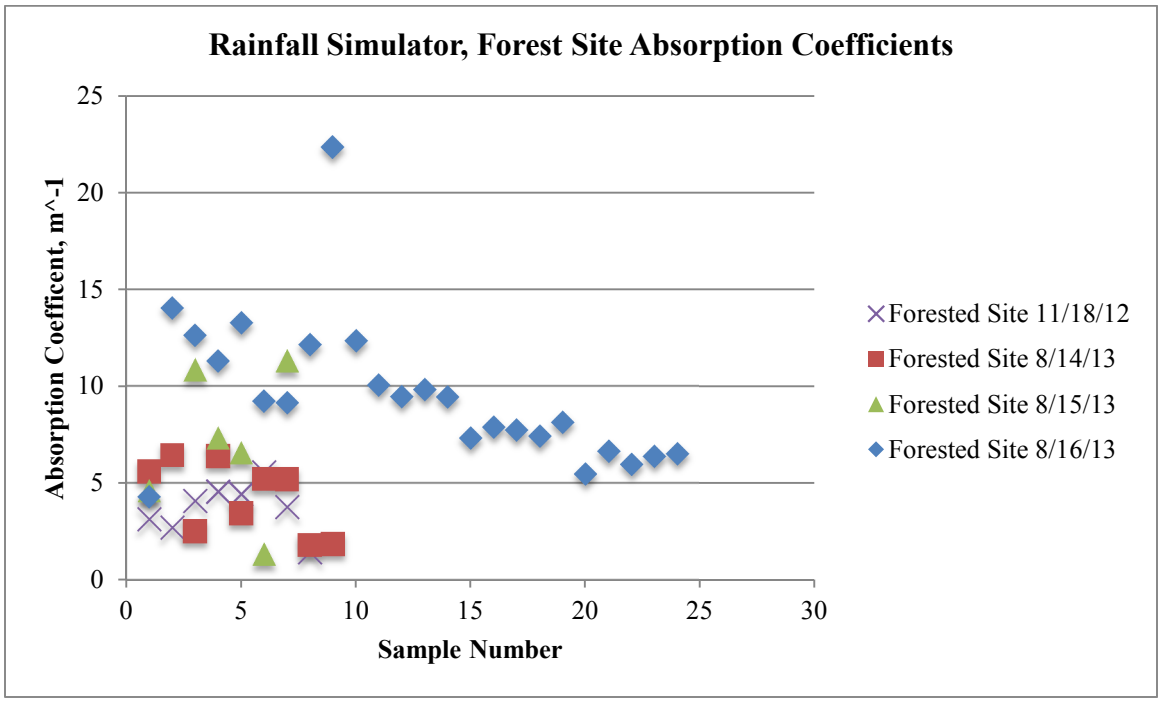

Figure 3.25: Comparison of forested site absorption coefficients over time for all deployments

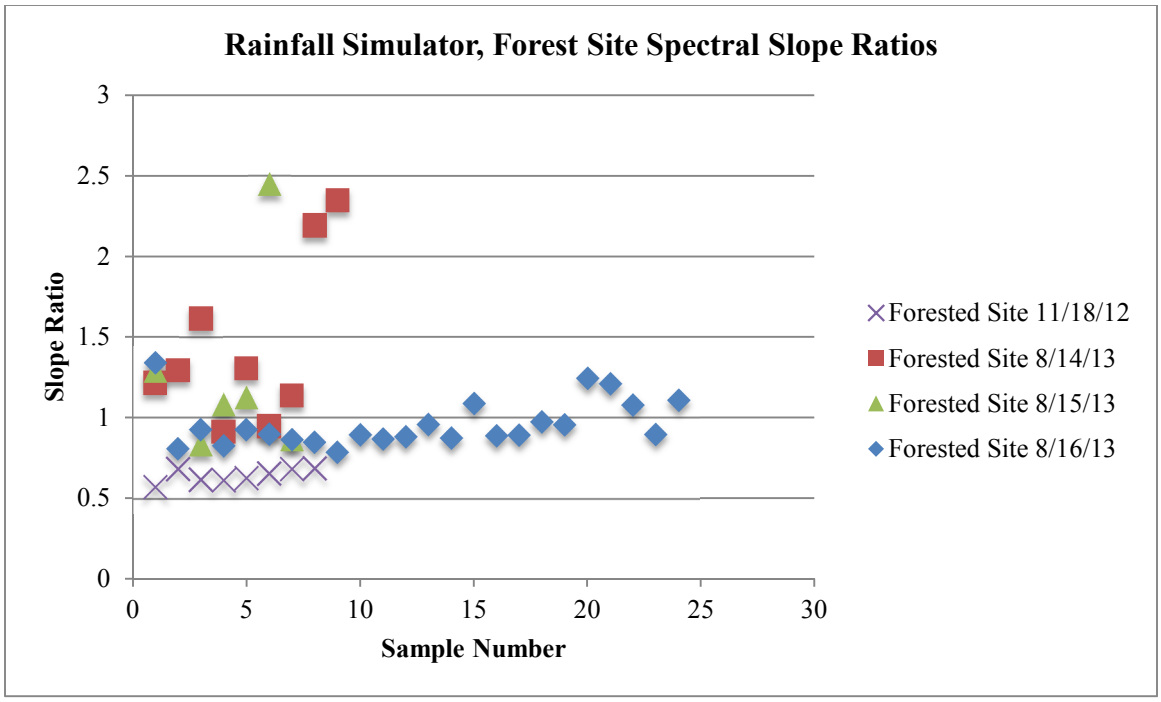

Figure 3.26: Comparison of spectral slope ratios over time for all deployments

First flush

The presence of first flush is typically determined by comparing measurements of the cumulative fraction of total pollutant mass to the total cumulative runoff volume for a rain event. This is difficult without continuous runoff flow measurements. For the parking lot experiments, continuous flow measurements were not taken. For the following calculations, the runoff flow was assumed to be constant during sample collection and each sample concentration was averaged over the time since the previous sample. Rough 4-hour flux estimates from the parking lot rain simulations of 25.4 mm hr^{-1}, 12.7 mm hr^{-1}, and 6.35 mm hr^{-1} are 1837, 1350, and 1012 mg C respectively.

Deletic (1998) defines first flush as the percentage of total event pollution load transported by the first 20 percent of storm runoff volume. First flush is present if the first

flush pollution load for an event is significantly greater than 20 percent. Based on this definition, first flush of dissolved organic carbon was present for all rainfall intensities for the parking lot simulations. The 20 percent runoff volume occurred near the 45-minute mark for the three simulations (Table 3.6).

Table 3.6: Rainfall intensity, runoff volume, and corresponding DOC flux percentages during the parking lot deployments

Rainfall intensity	Runoff volume (%)	Flux of DOC (%)
25.4 mm hr^{-1}	18.1	43.3
12.7 mm hr^{-1}	17.8	39.5
6.35 mm hr^{-1}	17.7	51.1

For the forested site, the total flux is unknown because most of the simulated rain soaked into the soil and did not become surface runoff. There was a much smaller runoff flow during the simulations at the forested site, only 261, 169, and 1346 milliliters total respectively for the 4 hour experiments. As a result, the entire volume of runoff reaching the collection point was collected. From the collected surface runoff, the 4-hour flux estimates for 25.4 mm hr^{-1}, 12.7 mm hr^{-1}, and 6.35 mm hr^{-1} are 7, 5, and 12 mg C respectively. Using Deletic's (1998) definition, first flush is present in the 25.4 and 12.7 mm hr^{-1} experiments, but not in the 6.35 mm hr^{-1} experiment (Table 3.7).

Table 3.7: Rainfall intensity, runoff volume, and corresponding DOC flux percentages during the forest deployments

Rainfall intensity	Runoff volume (%)	Flux of DOC (%)	Time (hours:min:sec)
25.4 mm hr^{-1}	21.5	25.5	00:53:20
12.7 mm hr^{-1}	20.6	30.8	01:30:00
6.35 mm hr^{-1}	22.7	19.1	00:37:40

Soil column tests

305 milliliters of water were filtered through the 4 inches long by 1.5 inches diameter soil column in one hour. This corresponds to approximately 10.52 inches of rain per hour, over a catchment area of 1.767 in^2 (1.5 in. diameter column) (Table 3.8). Samples taken immediately after the saturation test showed that the top portion of the soil column was 53% saturated and the bottom was 27% saturated. Soil columns not used for the saturation test showed 27% saturation (Table 3.9).

Table 3.8: Rainfall intensity calculation for soil column testing

Total volume	330	mL
Infiltration rate	5.08	mL/minute
	304.6	mL/hour
	10.52	in/hour*

*Calculated based on a catchment area of 1.767 in^2 (1.5 in. diameter column)

Table 3.9: Wet and dry weights of soil samples

Sample	Notes	Wet weight (g)	Dry weight (g) – 24 hours	Weight difference (g)	% water
1 A	From top of saturation column	15.3769	7.2517	8.1252	52.84
1 B	From bottom of saturation column	19.2963	14.0048	5.2915	27.42
3	No experiment	8.9792	7.5800	2.3955	26.68
4	No experiment	8.0287	8.0287	2.5546	26.70

DOC and CDOM samples collected during the saturation test display a decreasing trend as DOC is carried from the pore water and leached from the soil in the column (Figures 3.27 and 3.28). The DOC concentrations seem to level out at about 900 uM. CDOM levels out at approximately 170 QSU. A longer experiment time period would help to determine if the decrease in concentration is the depletion of the short-term pollutant source as described by Kang, Kayhanian, and Stenstrom (2008). When the

concentration levels out, this may be the long-term pollution source, the background pollutant levels for the location. DOC and CDOM concentrations of forested site samples (averages of 1410 uM and 155 QSU) collected during simulated rainfall were similar to the soil test results (875-2200 uM; 170-210 QSU). The DOC and CDOM concentrations obtained from the soil column test are also comparable to samples collected during storms at a forested site (Forest 1) within the same watershed (averages of 970 uM and 127 QSU).

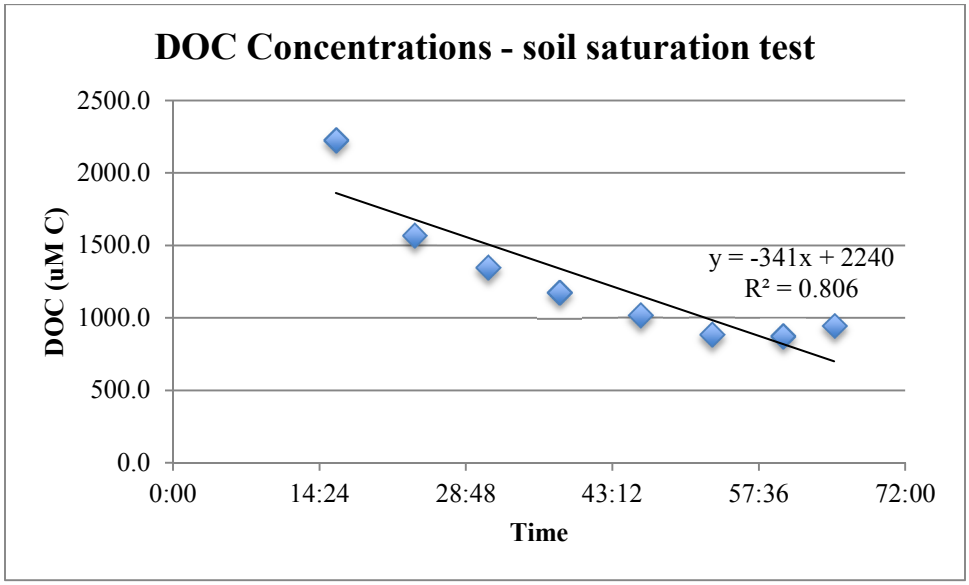

Figure 3.27: DOC concentration over time during the soil saturation test

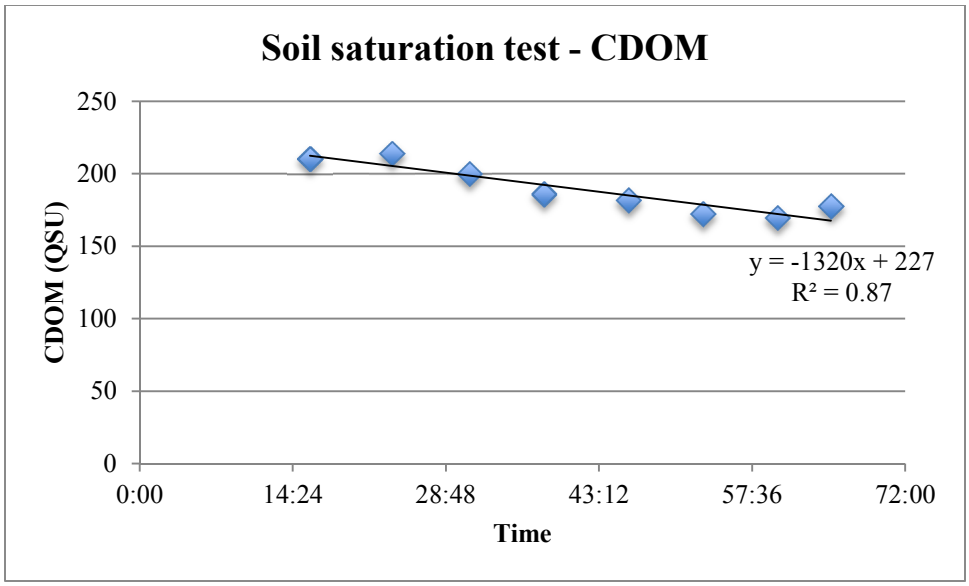

Figure 3.28: CDOM concentration over time during the soil saturation test

3.9 Conclusions

For the two sites studied, both have an initial capacity to hold water. Runoff occurs after a threshold amount of precipitation, which is dependent on site conditions. The parking lot site is impervious, and runoff started soon after the rain started. Little of the rainwater was retained on the plot, resulting in large quantities of runoff at the collection point. In general, the resulting runoff from the parking lot contains high concentrations of DOC and CDOM that rapidly decrease as the parking lot is "washed" by the rainfall. Parking lot rainfall rates of 25.4 mm hr^{-1}, 12.7 mm hr^{-1}, and 6.35 mm hr^{-1} resulted in 4-hour flux estimates of 1837, 1350, and 1012 mg C respectively. Runoff concentrations from the parking lot appear to be a function of the rain intensity, and the amount of DOC/CDOM built up on the parking lot surface, which is dependent on the amount of time since the previous rain event (Figure 3.29). The use of silicone caulk and

Blue painter's tape may have also increased the concentrations present in parking lot samples.

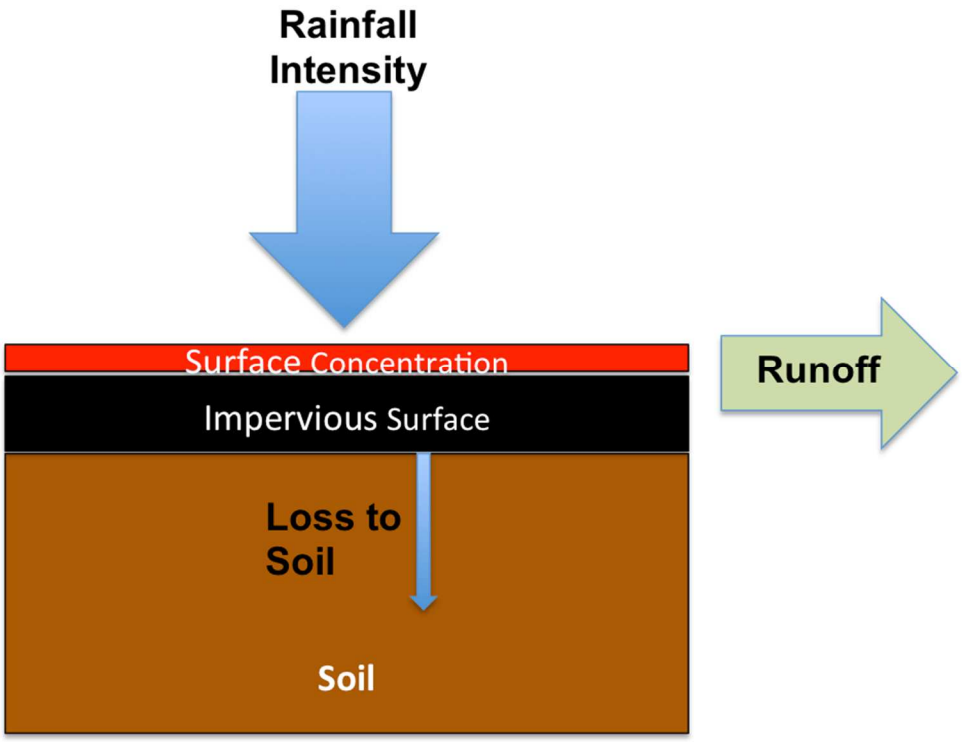

Figure 3.29: Conceptual runoff model for impervious surfaces

In comparison, the majority of the simulated rainfall at the forested site was absorbed by the soil. Between 150 and 600 liters were rained on the plot each experiment day, depending on the chosen rain rate, but the greatest amount of runoff collected was less than 1.4 liters. This is less than 1% of the water applied to the plot. As a result, the entire volume of surface runoff reaching the collection point was sampled. From the collected runoff, rain rates of 25.4 mm hr^{-1}, 12.7 mm hr^{-1}, and 6.35 mm hr^{-1} resulted in 4-hour flux estimates of 7, 5, and 12 mg C respectively. These estimates do not include any subsurface fluxes.

In forested land use types, greater amounts of surface runoff are more likely in a scenario where the rainfall intensity is greater than the infiltration rate of the soil. In this situation, there is the chance that the soil will become saturated and runoff will occur. However, based on the laboratory tests of the soil column, the rain intensity would have to be very high to cause saturation of the upper 4 inches of soil. This agrees with what is known about the soil type at the forested location. The soil is Canton fine sandy loam, which is a well-drained soil type, with high (50.8 to 152.4 mm hr^{-1}; 2.00 to 6.00 in hr^{-1}) capacity for the most limiting layer to transmit water (USDA, 2013a). Soil that is highly saturated at the beginning of a rainstorm might also result in greater amounts of runoff, making antecedent rainstorms important for forested site runoff estimates. Runoff concentrations from the forested site are a function of the rain intensity, initial soil moisture, time since last rain event, and initial DOC/CDOM within the soil (which is a factor of the soil organic carbon, time since last rain, and temperature/bacterial activity) (Figure 3.30).

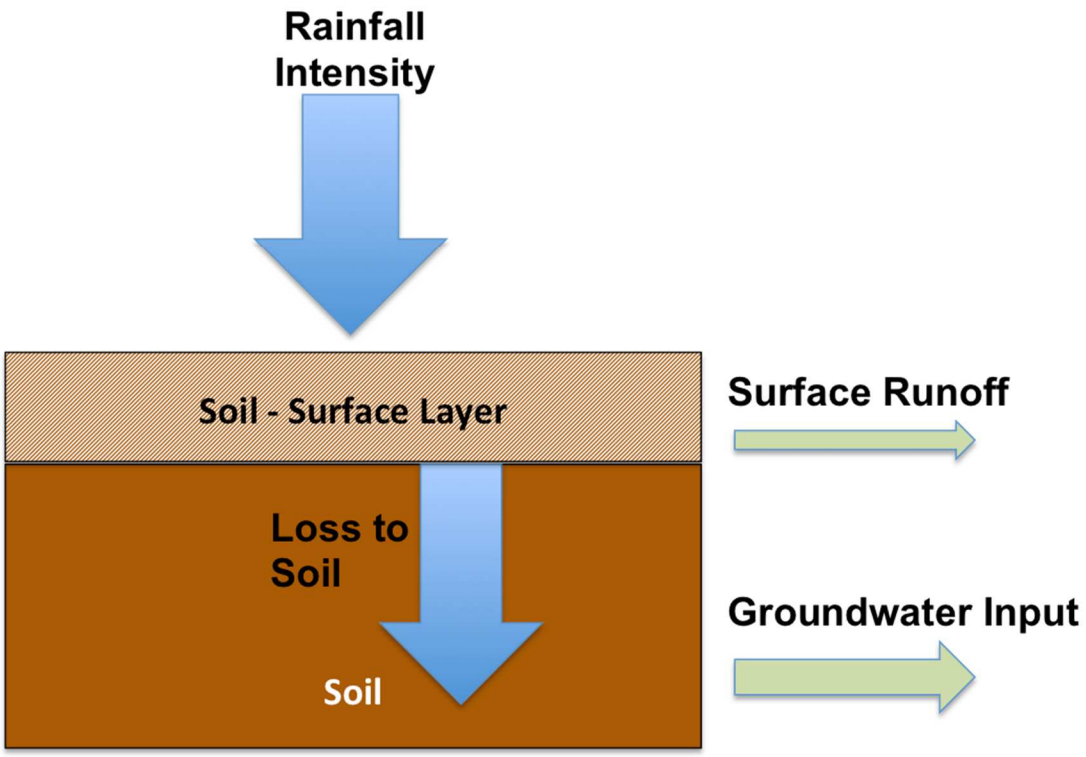

Figure 3.30: Conceptual runoff model for permeable (natural) surfaces

There is no known published study that uses a rainfall simulator to test for the presence or absence of dissolved organic carbon in the first flush on different land use types. Herngren, Goonetilleke, and Ayoko (2005) measured DOC, as well as heavy metals, in simulated runoff collected from impervious surfaces and found an average DOC concentration of 8.81 mg/L (approximately 734 uM C). This value was obtained from a composite of all samples collected during the simulated event. For the research detailed here, the parking lot experiments had an average concentration of 1120 uM. The forested site experiments had an average concentration of 1410 uM.

Other studies have demonstrated first flush effects of other constitutents in simulated runoff on impervious surfaces. Eckley and Branfireun (2009) showed that

mercury concentrations were highest at the beginning of simulated storm events, with almost 50% of the total mercury flux occurring during the first minutes of runoff. Vaze and Chiew (2003) observed high concentrations of total phosphorus, total nitrogen, and total suspended solids in runoff at the beginning of simulated rainstorms on impervious surfaces. The authors used laboratory results to develop characteristic curves that allow for loading calculations based on storm intensities and durations. Schiff and Tiefenthaler (2003) demonstrated first flush of suspended solids, trace metals, and polycyclic aromatic hydrocarbons (PAH) from impervious surfaces.

The rainfall simulator detailed here satisfied the design requirements of this study, including rain rate, drop dispersion, and uniformity. The simulator was designed, tested and deployed for about $1500. Other expenses, such as travel expenses, gasoline, and truck and water trailer rentals, are not included in this total. The total for design, testing, and eight deployments was about $3200 when these expenses are included. The design is simple, utilizing a single, fixed, interchangeable nozzle and commercially available parts. The simulator is portable and can be deployed easily by two people in varying terrains. For future measurement of DOC and CDOM concentrations on impervious surfaces, carbon-clean (non-organic) materials should be utilized if possible.

CHAPTER 4

HIGH RESOLUTION MONITORING OF DISSOLVED ORGANIC CARBON CONCENTRATIONS DURING STORM EVENTS

4.1 Abstract

Seven storm events at two locations in the Neponset River Watershed, Massachusetts, USA were monitored to study the impact of storm events on dissolved organic carbon (DOC) export from an urban watershed. Real-time chromophoric dissolved organic matter (CDOM) fluorescence sensor data was calibrated using discrete DOC samples collected by autosamplers. Compared to discrete samples, sensor measurements captured more of the variability in riverine DOC and CDOM concentrations that occurred due to runoff influxes. Using modeled flow data, estimates of total DOC export fluxes were calculated at these two sites during storms and compared to total annual export. Based on these calculations, the seven sampled storm events account for 7.1% to 10% of the calculated yearly flux. Additional work is needed to collect consistent year round data using sensors at these locations.

4.2 Introduction

Contaminant levels and fluxes within a watershed are not constant over time, have multiple sources, and even vary rapidly over the course of a single rain event (Ahn et al.,

2005). Previous studies have demonstrated that storm water runoff is a prime contributor to water quality degradation (Characklis and Wiesner, 1997; Buffleben et al., 2002; Ahn et al., 2005). During a phenomenon known as the "first flush," the initial runoff during a rainstorm can contain substantially elevated contaminant concentrations relative to runoff occurring later in the storm (Lee and Bang, 2000; Lee et al., 2002; Kayhanian and Stenstrom, 2008).

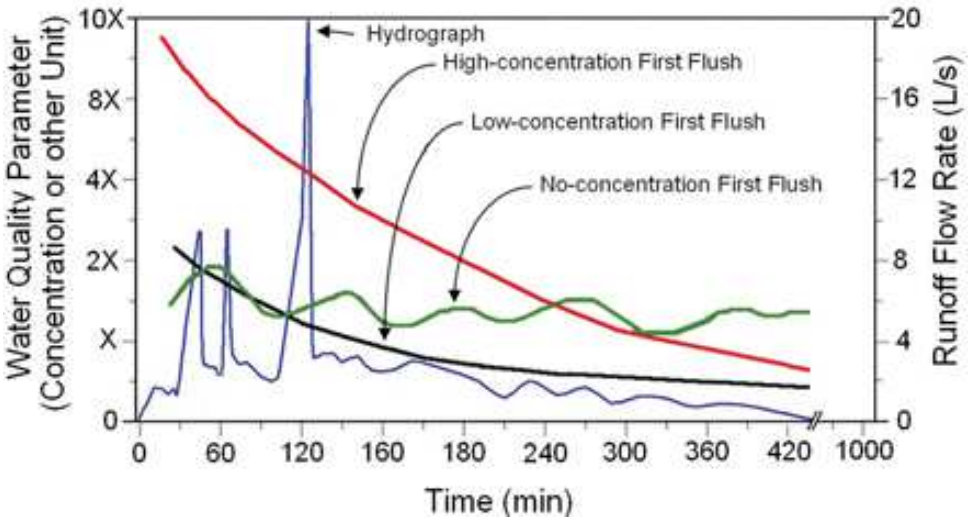

Figure 4.1: Generalized representation of first flush. From Kayhanian and Stenstrom (2008)

Several studies have examined the effect of storms on DOC and CDOM export to rivers. Raymond and Saiers (2010) performed a metadata analysis encompassing 30 small eastern United States forested watersheds and found that 86% of DOC was exported during rain events. 70% of this export occurred during the rising hydrograph. Other studies highlight the complicated interactions between carbon source, land use type, soil type, bacterial activity, runoff flow path, and seasonality on DOC export (Miller and Gardner, 1981; Boissier and Fontvieille, 1993, 1995; McKnight et al., 1993; Hinton et al.,

1998; Findlay et al., 2001; Neff and Asner, 2001; Xenopoulos et al., 2003; Smith and Goodrich, 2005; Wada et al., 2006; Delpla et al., 2011).

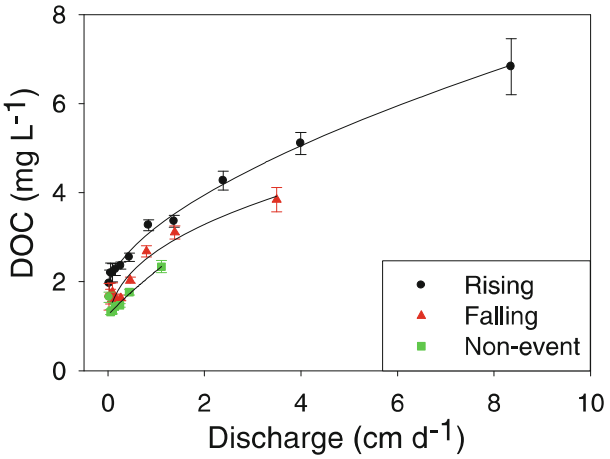

Figure 4.2: Relationship between stream discharge and stream water DOC concentrations for forested watersheds of the eastern United States. The error bars are standard errors. From Raymond and Saiers (2010).

Standard watershed monitoring programs can underestimate or completely miss the first flush because sampling strategies are not designed to capture episodic events, or these events are not sampled effectively. Several studies have shown the value of using high resolution sampling for different contaminants, but they did not examine first flush specifically (Grant et al., 2001; Boehm et al., 2002; Schiff and Tiefenthaler, 2003; Gersberg et al., 2004; Ahn et al., 2005; Jeong et al., 2006; Hellweger, 2007; Eckley et al., 2008; Eckley and Branfireun, 2008; Hellweger and Masopust, 2008; Sheng et al., 2008; Zhang et al., 2008; He et al., 2010; Lee et al., 2011). Other studies have examined sampling strategies to capture the first flush. Hathaway and Hunt (2010) evaluated the influence of first flush on total suspended solids and fecal indicator bacteria in an urban

watershed. Tiefenthaler et al. (2001) focused on total suspended solids and total organic carbon during first flush in an urban watershed.

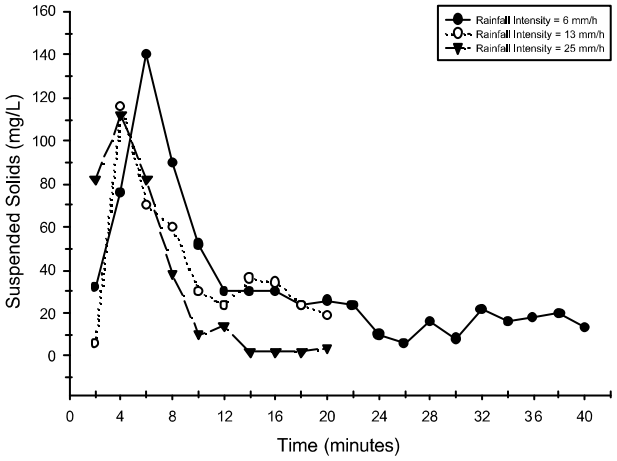

Figure 4.3: Time-concentration series of suspended solids concentrations (mg/L) for 6.3, 12.7, and 25.4 mm hr^{-1} simulated rainfall intensities. From Tiefenthaler and Schiff (2003).

During storm events, the relationship between concentration and discharge is rarely linear. Hysteresis occurs when there is a temporal difference in the response of a dissolved component compared to discharge. Evans and Davies (1998) present an overview of possible hysteresis scenarios using a three-component model. The model considers the concentrations of groundwater, soil water, and surface event water (runoff). In a clockwise loop (Figure 4.4, a-c), the total concentration is higher during the rising limb of the discharge, with the surface event water concentration greater than the soil water concentration. In an anticlockwise loop (Figure 4.4, d-f), the opposite is true.

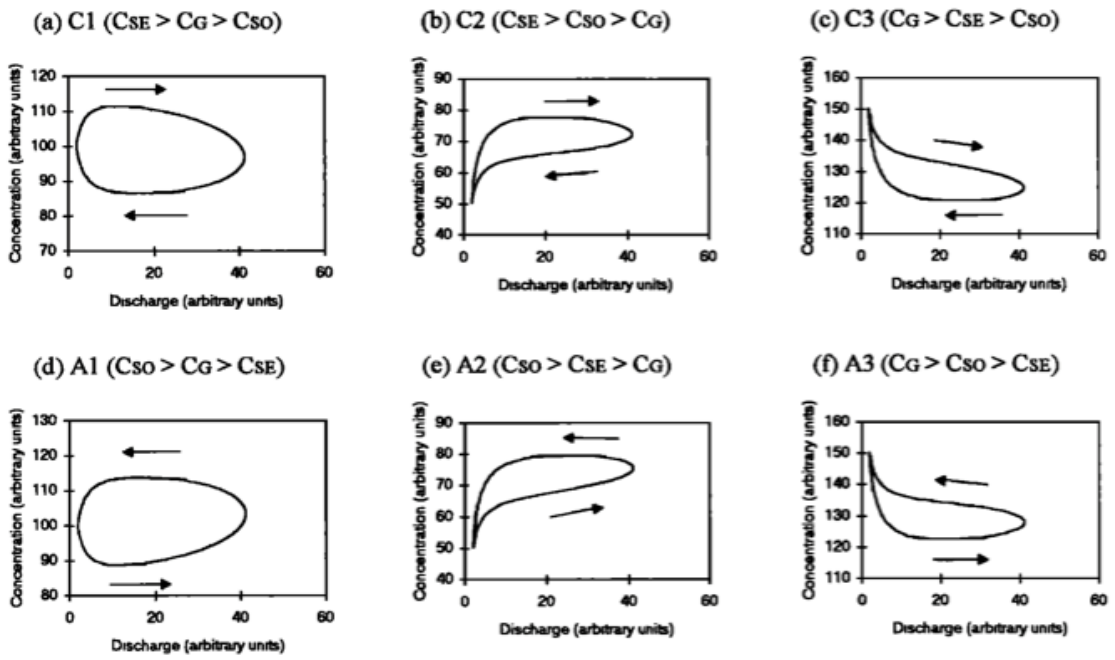

Figure 4.4: Examples of concentration/discharge hysteresis loops. C_{SE} is the concentration from surface event water, C_G is the concentration from groundwater, and C_{SO} is the concentration of the soil water. Image from Evans and Davies (1998).

Kayhanian and Stenstrom (2008) define a "concentration first flush" as initial storm runoff having a high concentration relative to runoff later in the storm. A "mass first flush" is flow-related, and occurs when both the concentration and flow amount are elevated relative to the concentration and flow later in the storm. The authors state that "[c]oncentration first flushes have been frequently reported, but mass first flushes have rarely been quantified." This is due to storm dynamics. In general, lower flows with higher concentrations may occur at the beginning of the storm, but greater flows with low concentrations during the middle of the storm result in a greater mass flux (Kayhanian and Stenstrom, 2008).

Monitoring fluxes of contaminants or DOC can be difficult during storms. Due to the dynamic nature of contaminants, nutrients, and DOM during storms, a large number of samples must be taken in quick succession. Storms are often unpredictable, and deploying field equipment for every storm can be cost prohibitive and logistically difficult. Sensor networks offer the ability to take high resolution samples at minimal cost and manpower (Hart and Martinez, 2006; Rundel et al., 2009; Zia et al., 2013). Sensor arrays can be deployed in the field for long periods of time and programmed to take continuous high resolution samples (Hart and Martinez, 2006; Rundel et al., 2009; Zia et al., 2013). Several studies have shown the efficacy of using sensors to capture the effect of storms on various water quality parameters (Ahn et al., 2005; Jeong et al., 2006; Zhang et al., 2008; Eckley and Branfireun, 2009; He et al., 2010).

Due to its optical properties, CDOM can be easily measured *in situ* with commercially available sensors (Chen, 1999; Keith et al., 2002; Conmy et al., 2004; Downing et al., 2009; Saraceno et al., 2009). CDOM can often be used as a proxy for DOC given a handful of samples to characterize the relationship in a given environment and through a given event (Green and Blough, 1994; Coble, 2007). Other sensors can be used to measure water quality parameters such as temperature, dissolved oxygen, pH, and conductivity (Rundel et al., 2009). These parameters do not always change during storm events, but can vary depending on a number of conditions (Deletic, 1998; Boehm et al., 2002).

4.3 Event sampling

Two locations within the Neponset River Watershed with different land use types were selected for high-resolution sampling. The Neponset River is located in an urban area close to Boston, Massachusetts and empties into Boston Harbor. The watershed covers about 300 square kilometers and is comprised of 14 cities and towns with a population of about 330,000 (Neponset River Watershed Association, 2014a). The Neponset River estuary often fails to meet state water quality standards, due to the impacts of combined sewer overflows (CSO) and urban stormwater runoff (MWRA, 2014). The Massachusetts Water Resources Authority (MWRA) does not sample the freshwater sections of the Neponset River so less is known about the water quality of this part of the river. The Neponset River Watershed Association's (NepRWA) Citizens Water Monitoring Network (CWMN) samples six times per year at 41 sites within the watershed. CWMN samples for E. coli, total nitrogen and phosphorus, orthophosphate, nitrate, chlorophyll, dissolved oxygen, pH, and water temperature, but does not sample for DOC or CDOM. The sampling dates are selected in advance and do not specifically sample during or immediately after a storm event (Neponset River Watershed Association, 2014b).

The two selected sampling locations were already in use as part of a thirty-one site monthly sampling program within the Neponset River Watershed. Huang and Chen (2009) utilized land cover maps from MassGIS to determine the dominant land use types within the watershed. From their results, the watershed was found to be dominated by five land use types: residential (38%), forest (34%), industrial (5%), wetland (4%) and

golf courses (2%). Huang and Chen (2009) identified endmember subwatersheds, which were defined as areas that drain at least 80% from a unique land-cover type. As a result, sampling locations were named for their dominant land use type.

A site classified as more natural (Forest 1) and a site classified as industrial (Industrial 3) were selected for the event sampling locations. These locations were selected in order to compare the runoff from two different land use types. Also, in another piece of this research, runoff from simulated rain events was collected from a parking lot site and a forested site, so the two locations selected here have similar land use characteristics. In addition, the two locations were easily accessible, seemed safe for leaving equipment relatively unsecured, and allowed for sample collection from narrow stream channels.

Forest 1 was located in Canton, MA, and samples were taken from a small creek running through forested land (Figure 4.5). The subwatershed is 1.96 km^2 and is mostly forested (>80%), with other land use types including low or very low density residential, forested wetland, and crop land. Industrial 3 was located in Norwood, MA near an industrial park and also received stormwater input from a nearby highway (Figure 4.6). Its subwatershed is approximately 1.4 km^2 and composed of industrial, commercial, forest, and medium density residential land use types. Industrial 3 was occasionally dry during the sampling period. More details about the sampling locations are available in Appendix A.

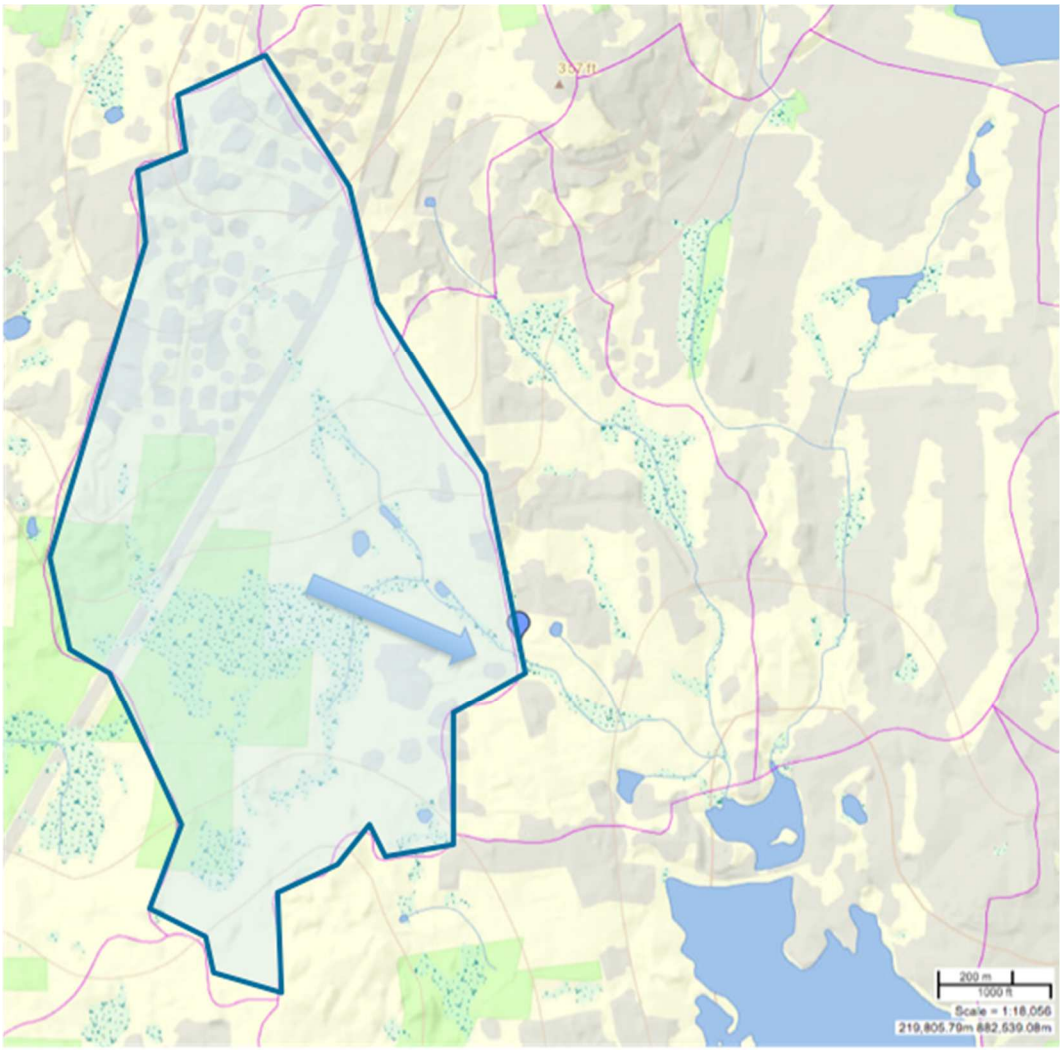

Figure 4.5: GIS map showing Forest 1 sampling location (blue pin) and general direction of water flow in the subwatershed. The sampling location is the outlet of the subwatershed. The thick blue line indicates the boundary of the subwatershed. GIS data from MassGIS OLIVER (http://maps.massgis.state.ma.us/map_ol/oliver.php)

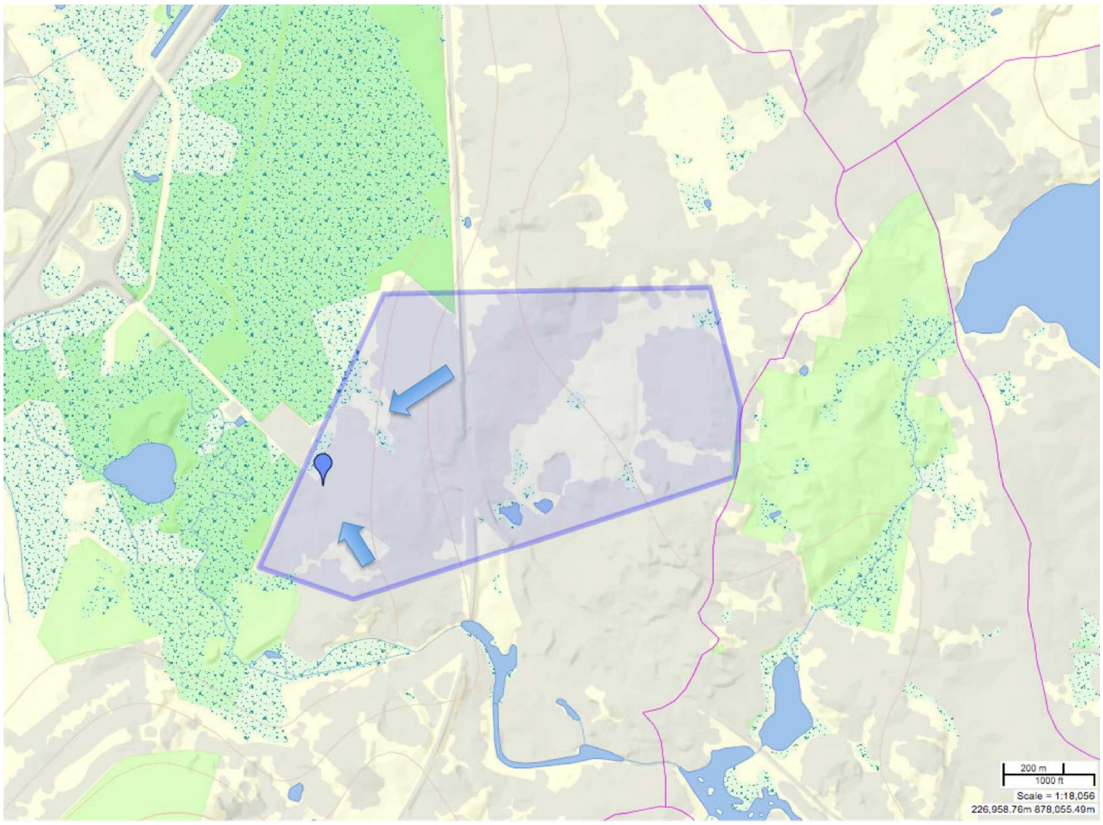

Figure 4.6: GIS map showing Industry 3 sampling location and general direction of flow of water in the subwatershed toward the sampling point. The polygon represents the approximate boundary of the drainage area within the subwatershed that passes through the sampling point. GIS data from MassGIS OLIVER (http://maps.massgis.state.ma.us/map_ol/oliver.php)

Two *in situ* sensors were deployed at each site from March 6 through April 4, 2012 and May 7 through November 10, 2012. The sensors were removed in April to be deployed in Florida for an unrelated research project. One *in situ* sensor measured parameters including water temperature, conductivity, dissolved oxygen, and pH every 2 to 5 minutes (YSI Inc. 6-series V2 sonde). The frequency was reduced from 2 minutes to 5 minutes during the deployment due to battery and data storage limitations. The second sensor (Seapoint Sensors, Inc. Ultraviolet Fluorometer; Turner Designs Cyclops-7

Submersible CDOM Fluorometer) measured chromophoric dissolved organic matter (CDOM) fluorescence every 2 minutes. The sensors were mounted to a cinder block (Figure 4.7) and removed from the water for cleaning approximately once per week. This was to clean any biofouling or sediments from the sensors.

Figure 4.7: YSI sonde deployed at Forest 1. The sonde is mounted on a cinder block. The fluorometer is mounted below the YSI sonde and not visible in this picture

An Onset Instruments HOBO U-12 datalogger was utilized for datalogging. The sensors and datalogging were powered by a swappable lead acid battery and charged with a solar powered charger. The battery and datalogging equipment was stored in a lockable waterproof housing near the sampling location. The solar panel was mounted on the waterproof housing (Figure 4.8). There were no signs of tampering or vandalism during the deployment.

Figure 4.8: Image showing the waterproof housing at Forest 1 that contains the battery and datalogging equipment. The solar panel is mounted on the outside of the housing

A Hach Sigma SD900 portable autosampler was deployed at each site during the same time period. A lead acid battery was used to power the autosampler. During episodic events (i.e. rain events), the autosamplers were programmed to collect discrete water samples at timed intervals, typically every 30 to 60 minutes for 24 to 36 hours (Appel and Hudak, 2001), and were triggered manually prior to a storm. In order to know when a storm was approaching, precipitation alerts were set up on weather.com. During storm sampling, samples were collected through Tygon tubing (0.25 inch inside diameter) and pumped into 250 ml pre-combusted (500°C, 5 hours) glass bottles within the sample chamber of the autosampler (Figure 4.9). The autosampler was programmed to rinse the tubing three times before collecting the sample. Samples were collected before, during, and after the storm using this method. Ice was placed around the sample bottles during warm weather. No preservatives, such as hydrochloric acid or mercuric chloride, were added to the samples following autosampler collection. Samples were

retrieved typically within 24 hours of collection, although during longer duration storms, some samples were stored for up to 50 hours. The effect of long-term storage was not tested but there was no indication of storage effects. Samples were transferred in the field into 300 ml pre-combusted (500°C, 5 hours) glass bottles with Teflon-lined caps.

Figure 4.9: Interior of autosampler sample chamber with samples collected during a storm event

Within 24 hours of arriving at the laboratory, each sample was filtered (high purity N_2 pressure filtered, <15 psi) through pre-combusted 0.7 μm glass fiber filters (Whatman GF/F). Dissolved organic carbon (DOC) and chromophoric dissolved organic matter (CDOM) samples were filtered into pre-combusted (500°C, 5 hours) 40 ml borosilicate glass vials with Teflon-lined screw caps. DOC samples were acidified to pH less than 2 with phosphoric acid and stored in clear vials at 4°C until analysis (Kaplan 1994). Absorbance and fluorescence samples were stored in amber vials at -4°C until analysis. All samples were analyzed at room temperature (21°C ± 1°).

Climatic data, including precipitation, was obtained from records kept by the Blue Hill Observatory (http://www.bluehill.org) and available from the Blue Hill Observatory and NOAA's National Climatic Data Center (http://www.ncdc.noaa.gov/cdo-web/datasets/PRECIP_HLY/stations/COOP:190736/detail). Neponset Watershed discharge data was obtained from streamflow data available from the United States Geological Survey (USGS) (http://waterdata.usgs.gov/ma/nwis/current/?type=flow). GIS data was obtained from MassGIS (http://maps.massgis.state.ma.us/). Flow data for 2012 at the two sampling locations was obtained from modeled flows obtained from a Regional Hydro-Ecologic Simulation System (RHESSys) model developed for the Neponset by Yang (2013).

4.4 Dissolved Organic Carbon (DOC)

A Shimadzu TOC-V analyzer was utilized for DOC analysis (Qian and Mopper, 1996). DOC standards were prepared using potassium hydrogen phthalate (KHP, Sigma Chemical) based on the instrument manual. The instrument was turned on and allowed to warm-up for at least one hour. Milli-Q water injections were then run until the instrument baseline stabilized at a peak area less than 2, similar to values obtained during analysis of 1 μM C Low Carbon Water. The instrument was then calibrated with a seven-point standard curve. Samples were run following a linear regression of the standard curve ($r^2 \geq$ 0.995). On subsequent days, at least one random carbon standard was run and compared to the standard curve to ensure continued calibration.

While running samples, the instrument blank was checked with ultra high purity, low carbon Milli-Q UV water every 10 to 15 samples. The mean blank value was subtracted from the sample measurements (Stedmon et al., 2000). Low Carbon Water (LCW) and Deep Sea Water (DSW) standards from Dennis Hansell's lab at the University of Miami were also run to ensure data quality (http://yyy.rsmas.miami.edu/groups/biogeochem/CRM.html).

4.5 CDOM Fluorescence

Fluorescence samples were thawed and then analyzed on a Photon Technologies International (PTI) Quantum Master 1 spectrofluorometer. Excitation scans were conducted with excitation (λ_{ex}) 337 nm, a 1 cm quartz cell, and emission scans from 350 nm to 650 nm. Slits widths were set to 4 nm. A Milli-Q water blank was run each day and subtracted from sample spectra to remove the Raman scattering peak. Fluorescence spectra were integrated in the wavelength range of 350 - 650 nm. A seven-point quinine sulfate standard curve (pH = 2) was used to convert the area of the emission spectra to quinine sulfate units (QSU) (Green and Blough, 1994; Siegener and Chen, 2002; Stedmon et al., 2003; Chen and Gardner, 2004). One QSU was equivalent to the fluorescence of 1 μg/l quinine sulfate at pH 2.

4.6 CDOM Absorption

Absorption samples were thawed and re-filtered through pre-cleaned 0.2 μm GE Osmonics polycarbonate filters before analysis to remove any glass fibers that may have

become dislodged during the original filtration (Chen and Gardner, 2004). The polycarbonate filters were cleaned with 2 M HCl prior to use (Stedmon et al., 2000). CDOM absorption spectra (200 – 800 nm) were measured with a Cary 50 spectrophotometer with a 1-cm path quartz cell. The precision of the instrument was +/- 0.002 absorption units.

All absorption calculations were completed after correcting the spectra by subtracting the average absorption in the 700 – 800 nm range (Green and Blough, 1994). The absorption coefficient (a, in m^{-1}) was computed using the following formula:

$$a_\lambda = 2.303 \times A(\lambda)/l \quad (4.1)$$

where $A(\lambda)$ is the measured optical density at a chosen wavelength, and l is the cuvette path length in meters (Green and Blough, 1994). For the purposes of this research, the wavelength was 337 nm and the cuvette path length was 0.01 meters.

The DOC-specific absorption coefficient (a^*) was calculated using the following formula (Zhang et al., 2007):

$$a^*_\lambda = a_\lambda / (\text{DOC concentration}) \quad (4.2)$$

where DOC is expressed in mg l^{-1}. The wavelength used was 337 nm.

Spectral slopes (S) were calculated using best-fit linear regression of the log transformed a spectra over two wavelength ranges (275 - 295 nm and 350 - 400 nm). S depends on the wavelength range chosen (Green and Blough, 1994; Ferrari, 2000). A parameter called the slope ratio, or S_R, was calculated using the ratio of the absorption slope from 275-295 nm compared to that of the slope from 350-400 nm. The slope ratio compares absorbance values that often change during transit, either over time or due to

photodegradation, and can allow for insight into DOM molecular weight and source. Higher value, or steeper, slopes show a more rapid decrease in absorption with increasing wavelengths (Helms et al., 2008).

Fluorescence quantum yield was calculated with the relationship:

CDOM fluorescence / absorbance coefficient (4.3)

This relationship expresses the quantum efficiency of the fluorescence with respect to the absorption of a sample. The CDOM versus DOC relationship was also graphed.

Spectral data were all corrected for the inner filter effect for samples with absorbance above 0.1. The inner filter effect occurs when dissolved species, including the fluorophore, absorb exciting or emitted radiation (Puchalski et al., 1991; Hu et al., 2002). To correct for this effect, dilution with Milli-Q water was conducted for all samples over 100 QSU (about 0.1 m^{-1}).

4.7 Results and Discussion

Selected discrete sample data, as well as sensor data, are presented here from samples collected between Spring 2012 and Fall 2012 during seven episodic events (Figure 4.10). Due to high resolution sampling, trends are noticeable during rain events that would be missed by standard monthly watershed sampling. All sampled storms occurred in relatively dry periods, with antecedent rainfall occurring no sooner than 72 hours prior to the sampled event. The Industrial 3 sampling site was intermittently dry between storm events.

Table 4.1: List of sampled events, including date(s), storm amount, storm duration, calculated storm intensity, and antecedent rainfall details

Event	Date	Storm amount (mm)	Storm duration (hours)	Avg. storm intensity (mm hr^{-1}) (calculated)	Antecedent* rainfall (time/amount/date)
1	5/8-5/11/12	38.4	56	0.69	72 hours, 20.8 mm, 5/1-5/5/12
2	6/12-6/14/12	15.7	24	0.65	95 hours, 49.0 mm, 6/2-6/8/12
3	7/18-7/19/12	36.6	4	9.15	341 hours, 9.4 mm, 7/4/12
4	8/27-8/28/12	25.4	10	2.54	221 hours, 5.6 mm, 8/18/12
5	9/18-9/19/12	26.2	21	1.25	216 hours, 10.2 mm, 9/8-9/9/12
6	10/29-10/31/12	83.6	69	1.21	189 hours, 7.9 mm, 10/19-10/20/12
7	11/7-11/8/12	26.4	36	0.73	164 hours, 83.6 mm, 10/29-10/31/12

* Antecedent rainfall only counted for storms larger than 2.54 mm (0.1 in)

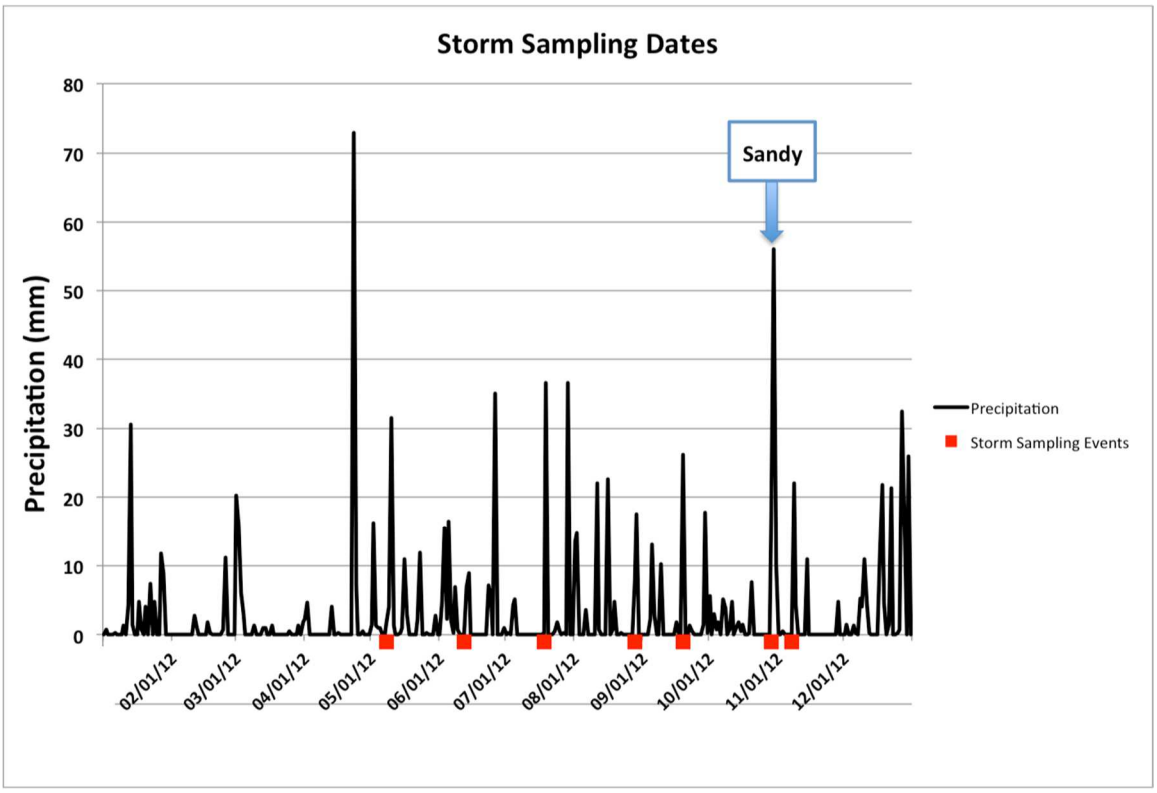

Figure 4.10: Precipitation record for 2012 at Blue Hill, with storm sampling dates indicated along the x-axis

Table 4.2: Forested site discrete sample information

Event	Sample start date	Sample start time	Sample end date	Sample end time	Discrete samples collected
1	5/8/12	0200	5/11/12	1120	34
2	6/12/12	1925	6/14/12	1120	24
3	7/18/12	1534	7/19/12	1135	20
4	8/27/12	2030	8/28/12	1403	17
5	9/18/12	0932	9/19/12	1300	12
6	10/28/12	1445	10/31/12	1140	15
7	11/7/12	1212	11/8/12	0957	22

Table 4.3: Industrial site discrete sample information

Event	Sample start date	Sample start time	Sample end date	Sample end time	Discrete samples collected
1	5/8/12	0200	5/11/12	1225	35
2	6/12/12	2045	6/14/12	1300	26
3	7/18/12	1603	7/18/12	1915	5
4	8/28/12	0200	8/28/12	1451	10
5	9/19/12	0100	9/19/12	1350	10
6	10/29/12	0900	10/31/12	1235	25
7	11/7/12	1304	11/8/12	1055	22

Forested versus Industrial

In a comparison of all storm samples and samples collected monthly at each site, the large range of concentrations that occur during storms are noticeable (Figure 4.11). The storm responses at Forest 1 are muted, and the monthly sample concentrations are close to the storm sample concentrations. The muted response may be the result of less connectivity due to much of the precipitation soaking into the soil and not running off. Subsurface runoff may take longer to reach the river, also muting concentration responses due to storms. The higher storm concentrations in October and November could be the result of the contribution of leaf litter, plus the impact of the long duration precipitation event at the end of October (Hurricane Sandy).

The Industrial 3 storm samples show a wide range of concentrations, and the monthly samples often do not capture this variability. The wider range of concentrations during storms is the result of high concentration runoff from impervious surfaces entering the river. The majority of any runoff generated reaches the river, and is less impeded in its travel. Another reason the storm samples capture the concentration better is that during the monthly sampling dates in August and September, the site was dry. However, during storms in those months, water flowing through the site was captured by the autosampler and sensor measurements.

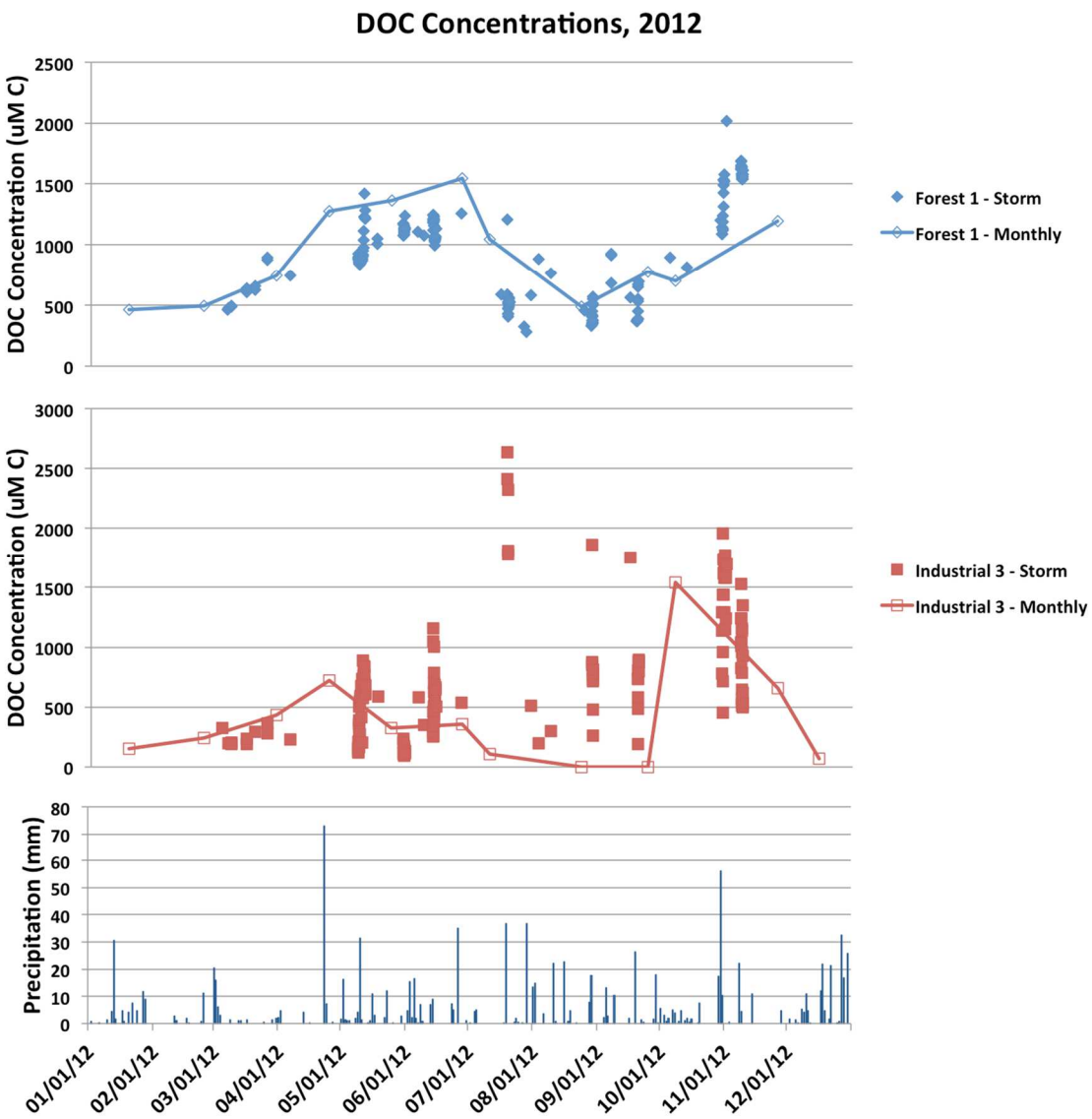

Figure 4.11: Storm sampling concentrations compared to monthly sample values. A line connects monthly samples, while storm samples and samples collected during routine cleanings are not connected.

Evidence of First Flush

Industrial 3 data from Event 2 shows a sharp increase in DOC concentration at the beginning of the storm with only about 2 mm of precipitation (Figure 4.12). The increase is almost sixfold in an hour. The CDOM trend for Industrial 3 is similar to the DOC

samples (Figure 4.13). Forest 1 DOC and CDOM do not show sharp concentration increases at the beginning of the storm. This lack of response to the rainstorm supports the theory that much of the precipitation is soaking into the soil and not running off.

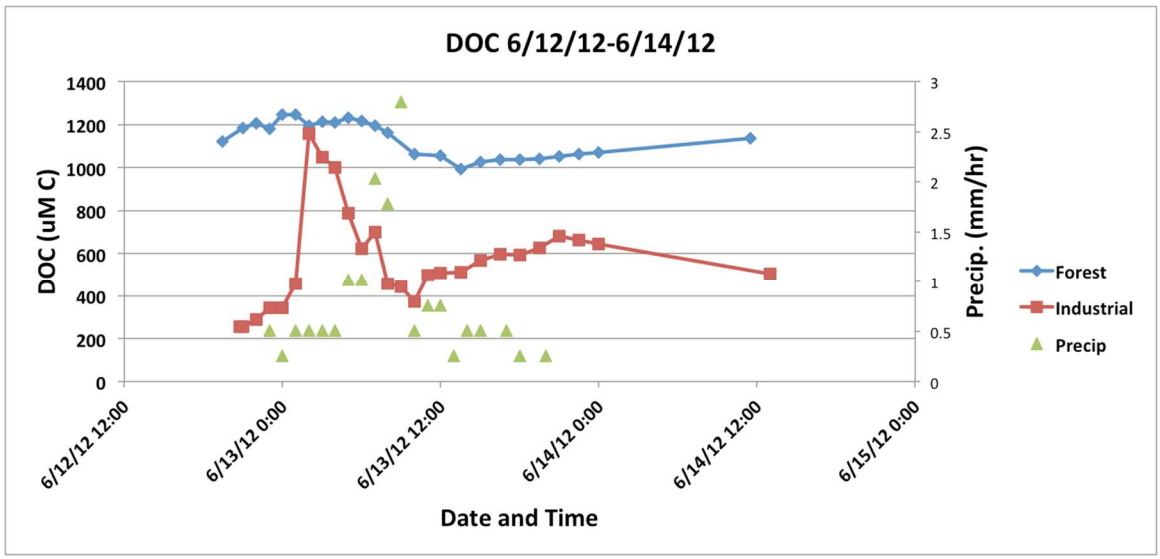

Figure 4.12: Discrete samples showing DOC concentration over time

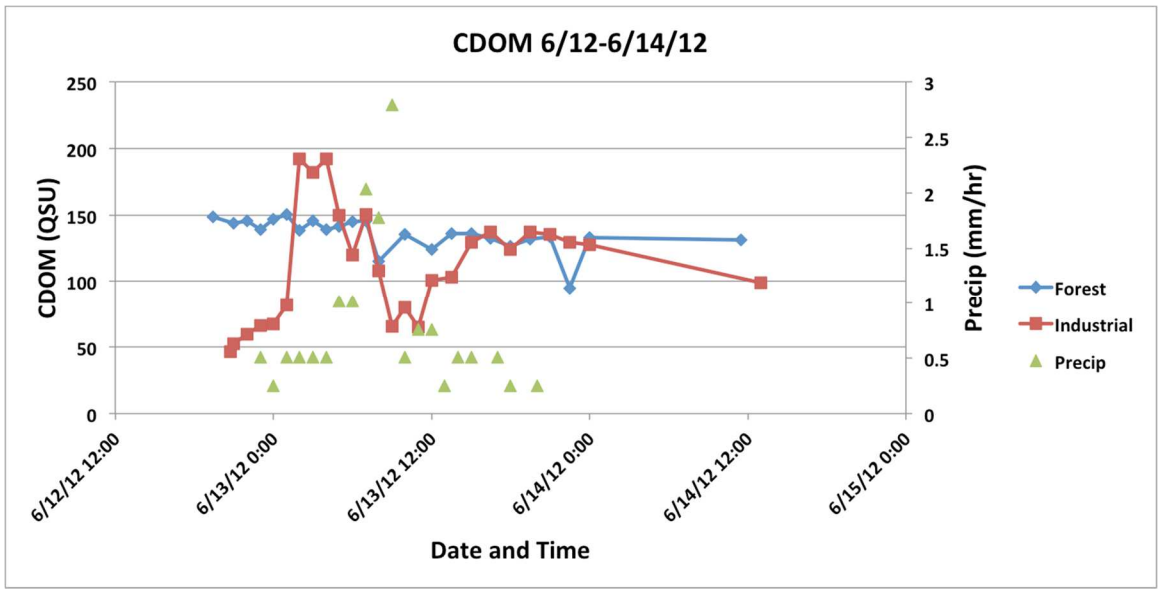

Figure 4.13: Discrete samples showing CDOM concentration over time

Impact of Antecedent Rainfall and Storm Intensity

Event 1 was the closest storm event to a preceding storm, with the prior storm ending approximately 72 hours prior. The antecedent storm had 20.8 mm of precipitation from 5/1-5/5/12. In comparison, Event 3 occurred approximately 2 weeks (341 hours) after the last rainfall. The preceding storm was small, with 9.4 mm of precipitation on 7/4/12. Event 1 and Event 3 were similar in rain amounts – 38.4 mm and 36.6 mm respectively - but Event 1 was one of the lower average intensity storms sampled, while Event 3 was the most intense storm sampled. During Event 3, only four samples were collected at Industry 3, due to the site being dry at all other times.

The very dry conditions and high storm intensity result in a large amount of wash-off from impermeable surfaces over a short period of time and could be the cause of the high concentrations present at the start of Event 3 (Figure 4.14). During Event 1, concentrations at both Forest 1 and Industrial 3 increase gradually, which may be the result of the lower rainfall intensity. In future work, measurement of soil moisture before, during, and after storms would help to determine whether antecedent soil moisture plays a role in runoff amounts and concentrations.

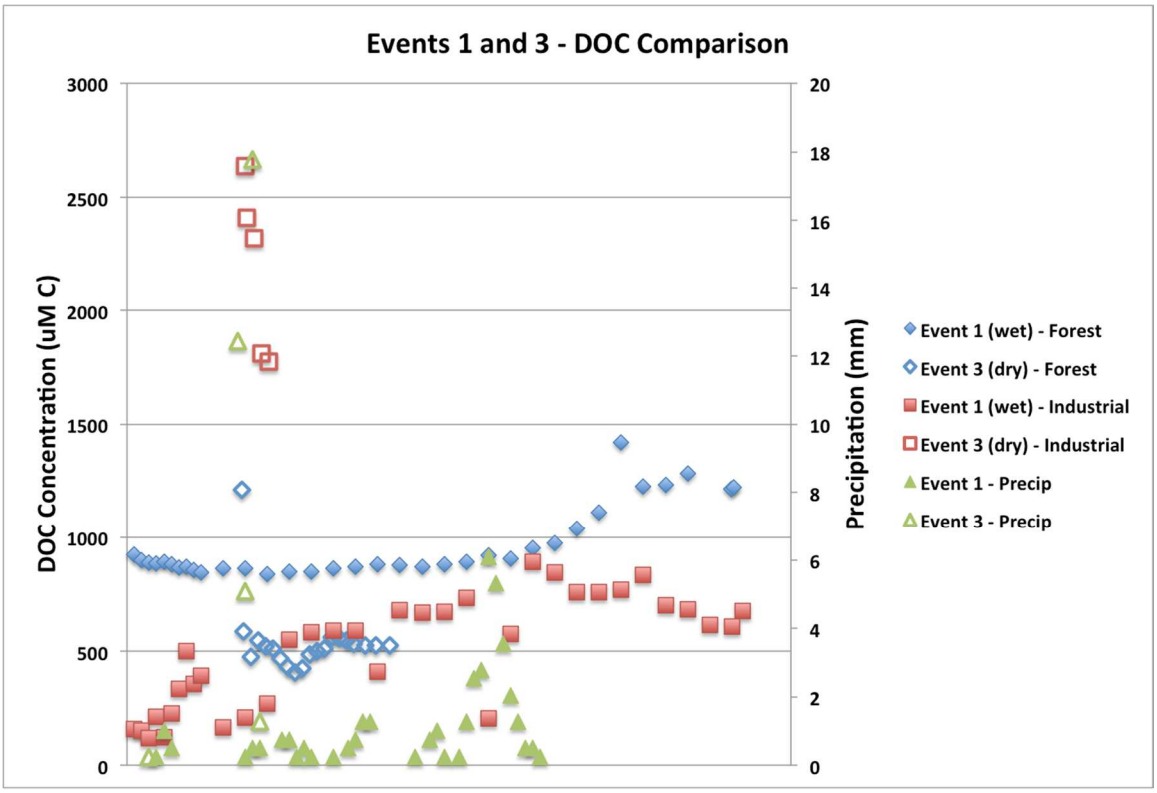

Figure 4.14: Event 1 and Event 3 DOC concentration comparison. Precipitation for both events is also graphed

Evidence of Dilution

Dilution might be expected during periods of high flow due to precipitation events or snowmelt. Event 5 shows a sharp decrease in DOC and CDOM concentrations at Industrial 3 within an hour of a high intensity period of the storm when more than 15 mm of rain fell in an hour (Figures 4.15 and 4.16). In contrast, DOC and CDOM concentrations at Forest 1 rise during this period of the storm. The high initial concentration at Industrial 3 at 1:00 AM on 9/19/12 drops sharply by the 2:00 AM sample. The high initial concentration may be the result of first flush runoff entering the stream at the beginning of the storm. The decrease an hour later may be the result of

dilution as runoff generated during the high intensity period enters the stream from farther areas of the subwatershed.

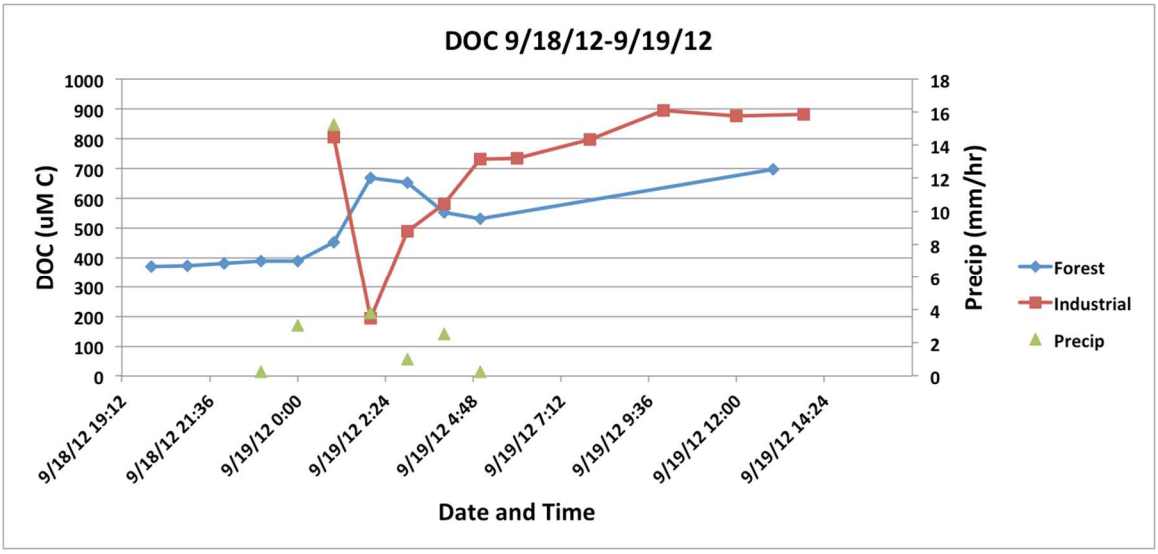

Figure 4.15: Discrete samples showing DOC concentration over time

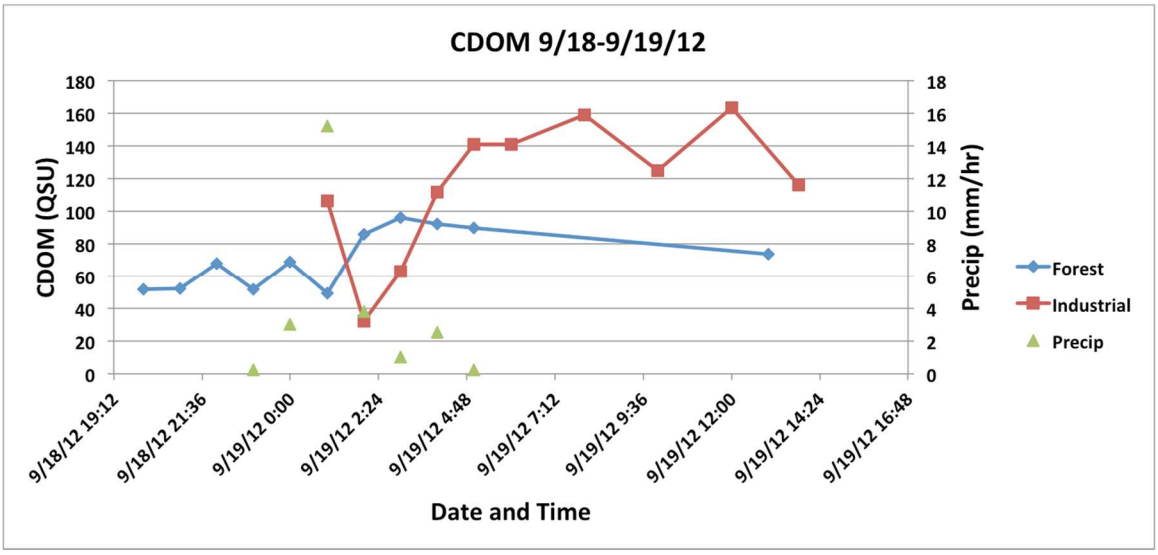

Figure 4.16: Discrete samples showing CDOM concentration over time

Dynamic Nature of DOC Concentrations – Sensors versus Discrete Samples

While discrete samples from the autosamplers allow for the elucidation of several trends in the concentrations, sensor data allows for even higher resolution sampling. The

sensor data also covers time periods when discrete samples were not collected. For example, during Event 6 at Forest 1, the discrete CDOM samples show an increasing concentration trend. The sensor data also captures this, but also captures the slight variability of the CDOM concentration during the storm, and then also shows the slight decrease in concentration following the storm (Figure 4.17).

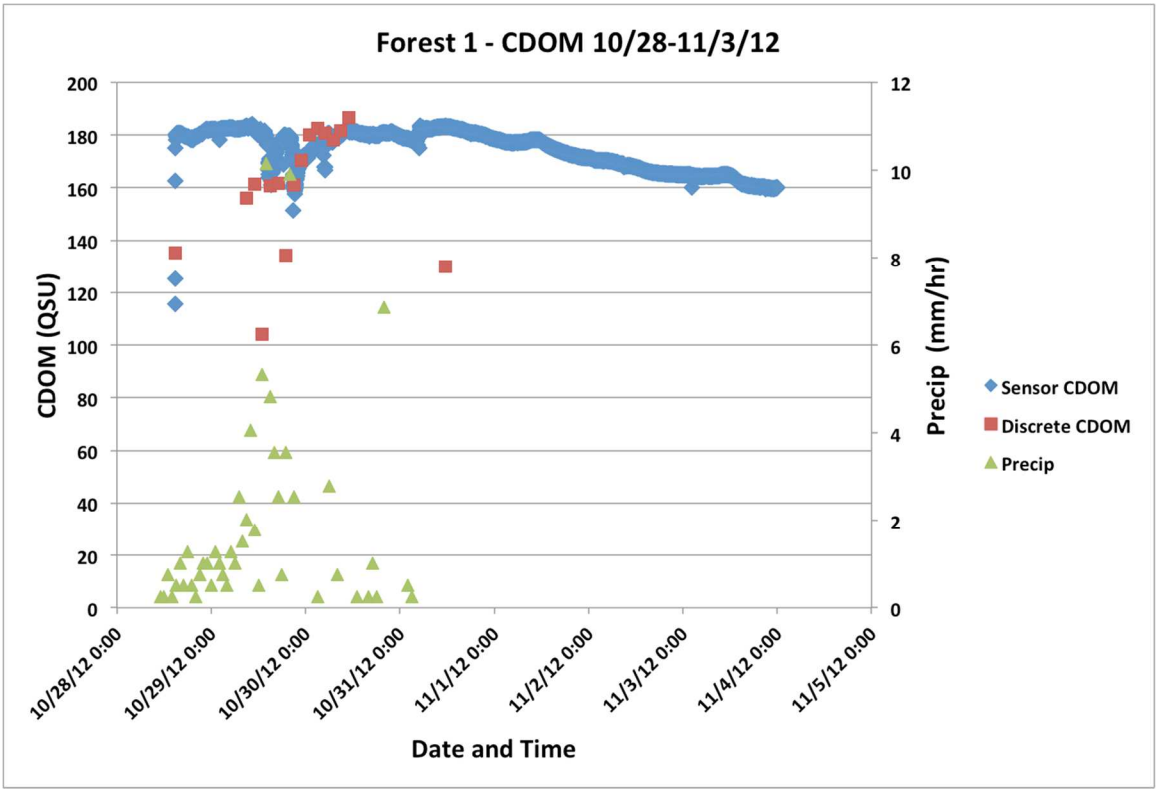

Figure 4.17: Forest 1 sensor data and discrete samples shown on the same axis. The sensor data has been converted to QSU using a calibration curve derived from discrete sample concentrations

During the same event at Industrial 3, the sensor data shows the high amount of variability in CDOM concentrations (Figure 4.18). This variability may be caused by increased runoff amounts, increased desorption, increasing connectivity within the

subwatershed, and dilution effects. The discrete samples capture some of this variability, but the sensor data captures an interesting concentration decrease about 12 hours after the storm ends. Several spikes in the concentration follow this decrease. Since the autosamplers were programmed to sample during the storm, they did not capture these post-storm phenomena. A hypothesis for the cause of these post-storm concentration increases is discussed in the *Other Data Trends* section.

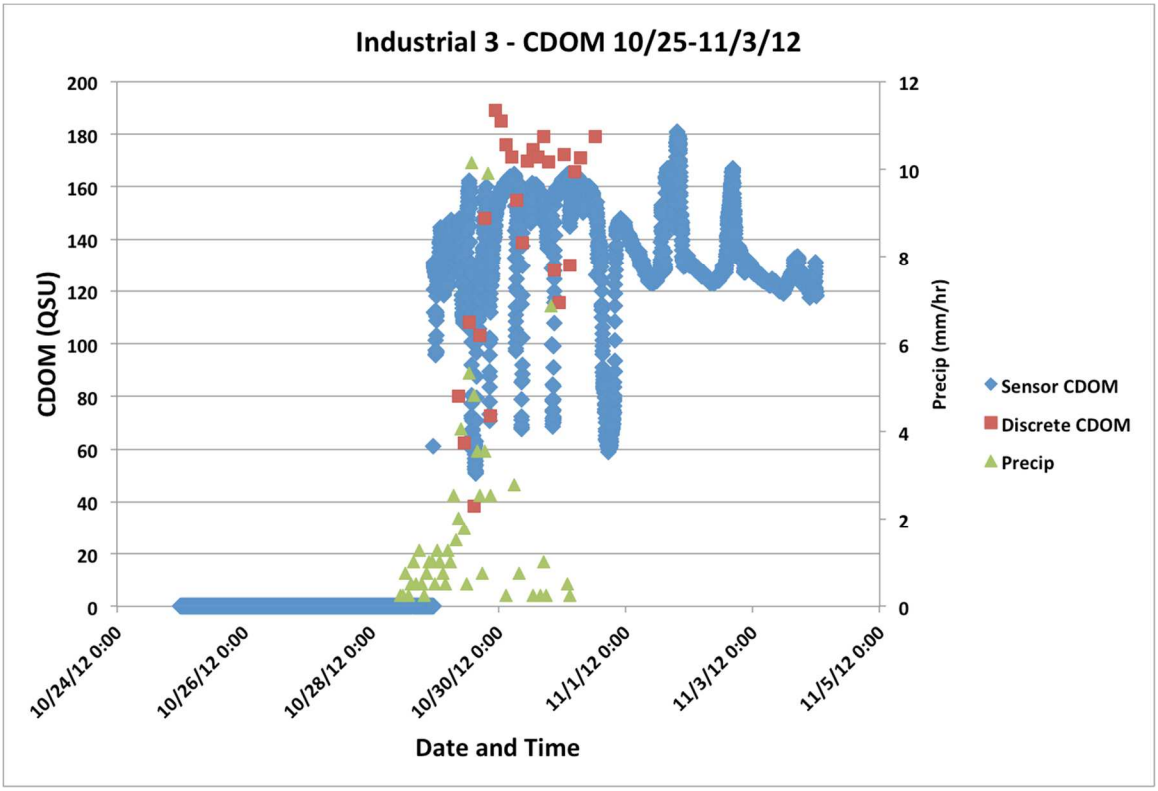

Figure 4.18: Industrial 3 sensor data and discrete samples shown on the same axis for Event 6. The sensor data has been converted to QSU using a calibration curve derived from discrete sample concentrations

During Event 7, both sites show good correlation between the sensor and discrete sample data. At Forest 1, there is little change in the sensor data during the storm, even during high intensity periods (Figure 4.19). At Industry 3, there is a small concentration

increase at the beginning of the sensor data, which is probably related to continued fluxes associated with Event 6 (Figure 4.20). Then, Event 7 starts and the concentrations fluctuate rapidly. The CDOM concentration spikes twice, then decreases sharply, increases to about 135 QSU, then decreases again to almost the minimum graphed concentration. All of these changes occur within about 15 hours. The concentration then increases over the final 24 hours of the graph. While Event 7 is a much smaller rain event than Event 6, the fluctuation magnitudes and observed concentrations are similar for both events.

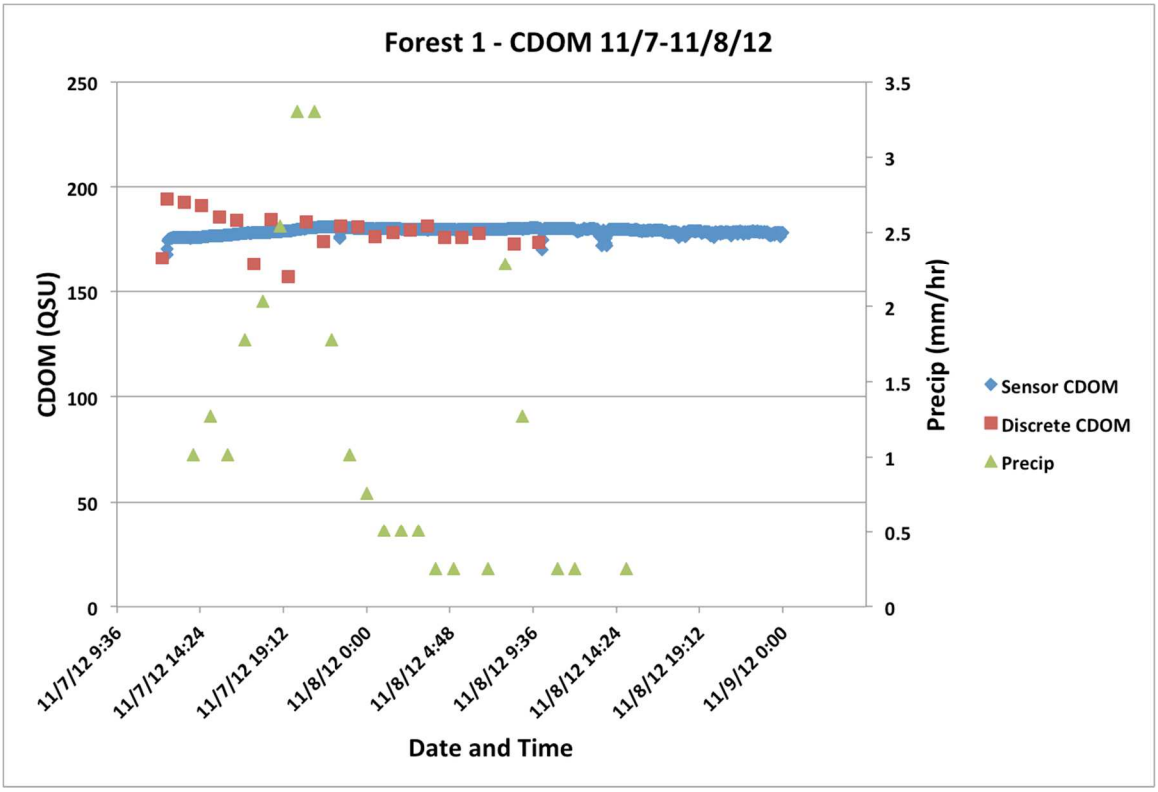

Figure 4.19: Forest 1 sensor data and discrete samples shown on the same axis

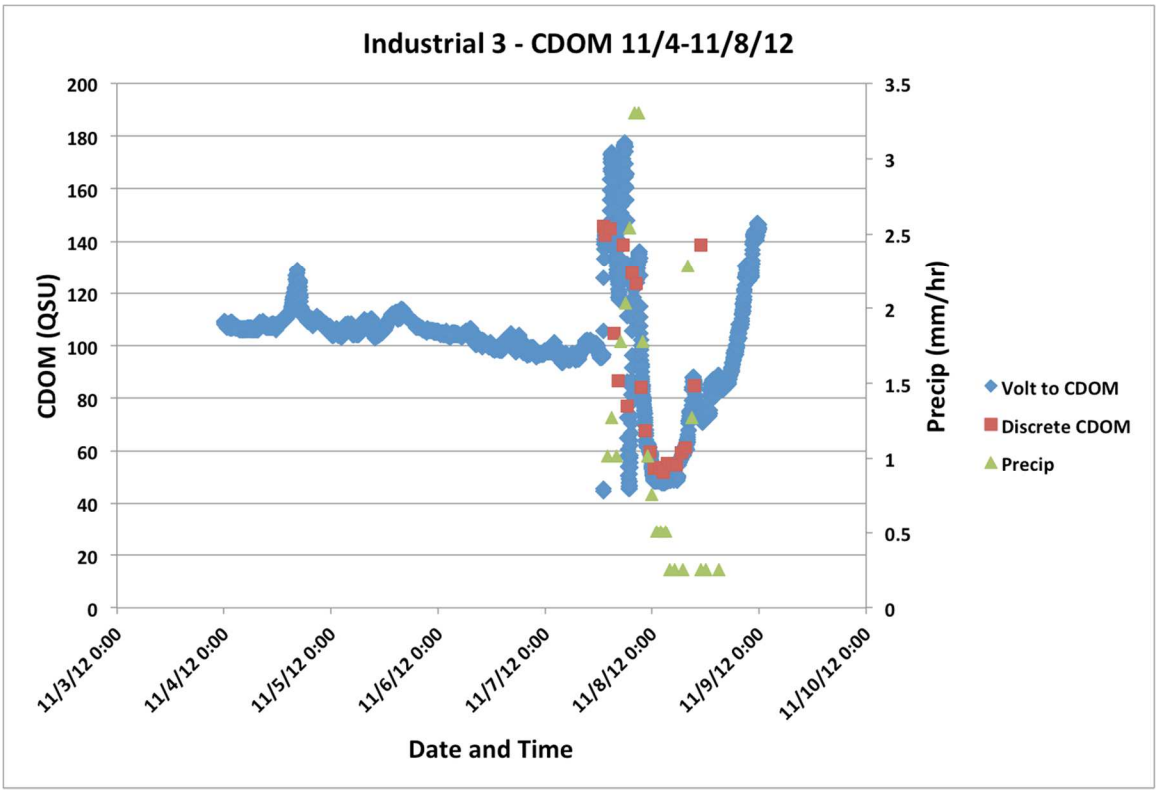

Figure 4.20: Industrial site sensor data and discrete samples shown on the same axis

Hurricane Sandy (Event 6)

Event 6, sampled from 10/29 through 10/31/12, is commonly known as Hurricane Sandy. Sandy made landfall along the southern New Jersey shore on 10/29/12, causing historic destruction and substantial loss of life. Sandy was a very large storm, with tropical storm force winds that affected areas within approximately 1000 miles. The greatest rainfall amounts occurred in New Jersey and Delaware, with eight locations reporting more than 279.4 mm. Most locations experienced less than 101.6 mm of rainfall (NOAA NWS Office of Climate, Weather and Water Services, 2013).

At Blue Hill, 83.6 mm of rain were measured during the storm. The storm had a long duration, occurring over 69 hours. Several periods of the storm had higher intensity rainfall, but much of the precipitation occurred at a rate of 2 mm per hour or less. This is the largest precipitation event sampled during this research.

DOC and CDOM concentrations are elevated at both sites during Event 6, with more variability at Industry 3 (Figure 4.21). CDOM concentrations are generally higher at the forested site (Figure 4.22).

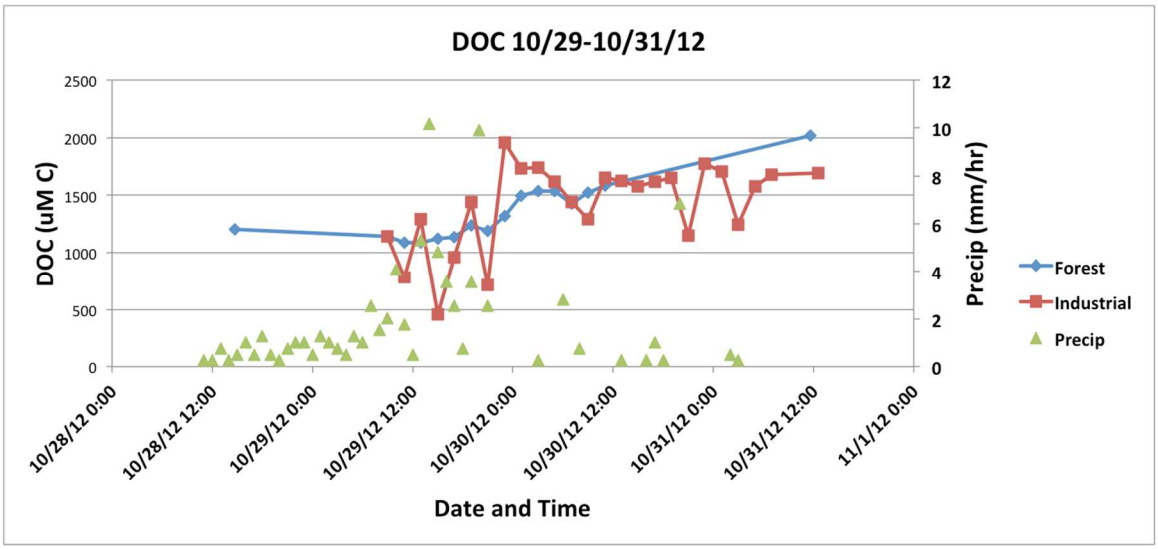

Figure 4.21: Discrete samples showing DOC concentration over time

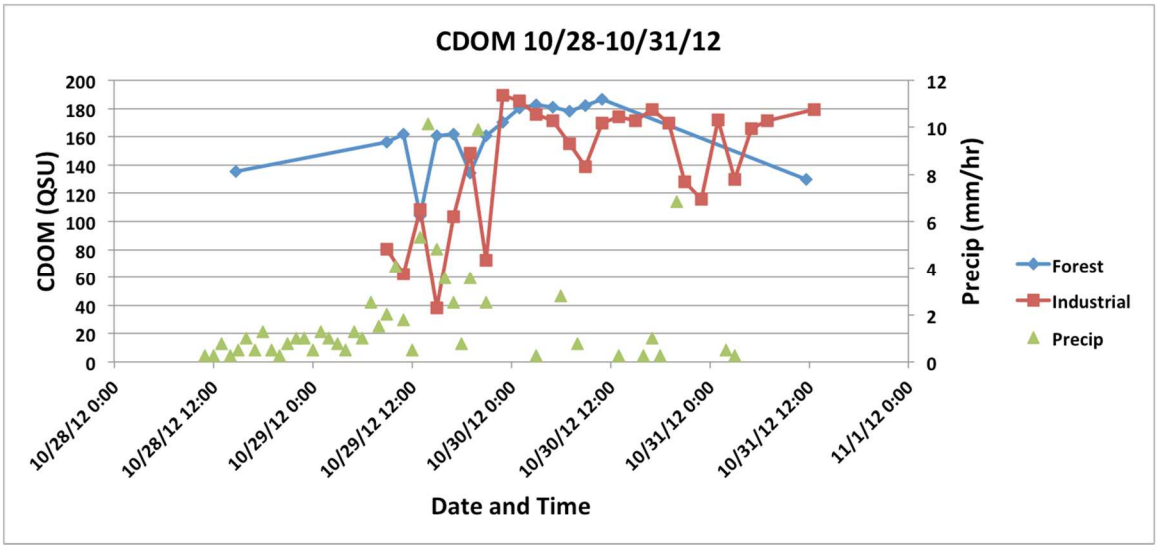

Figure 4.22: Discrete samples showing CDOM concentration over time

Characterization of DOM for Event 6

The CDOM versus DOC relationship is stronger at the industrial site, and the slopes are different for each site (Figure 4.23). This is similar to the overall trend for all of the storm samples. The higher CDOM-DOC relationship for the Forest 1 data may be due to

runoff within the subwatershed carrying higher levels of colored organic matter from the soil into the stream. There may also be in-stream production.

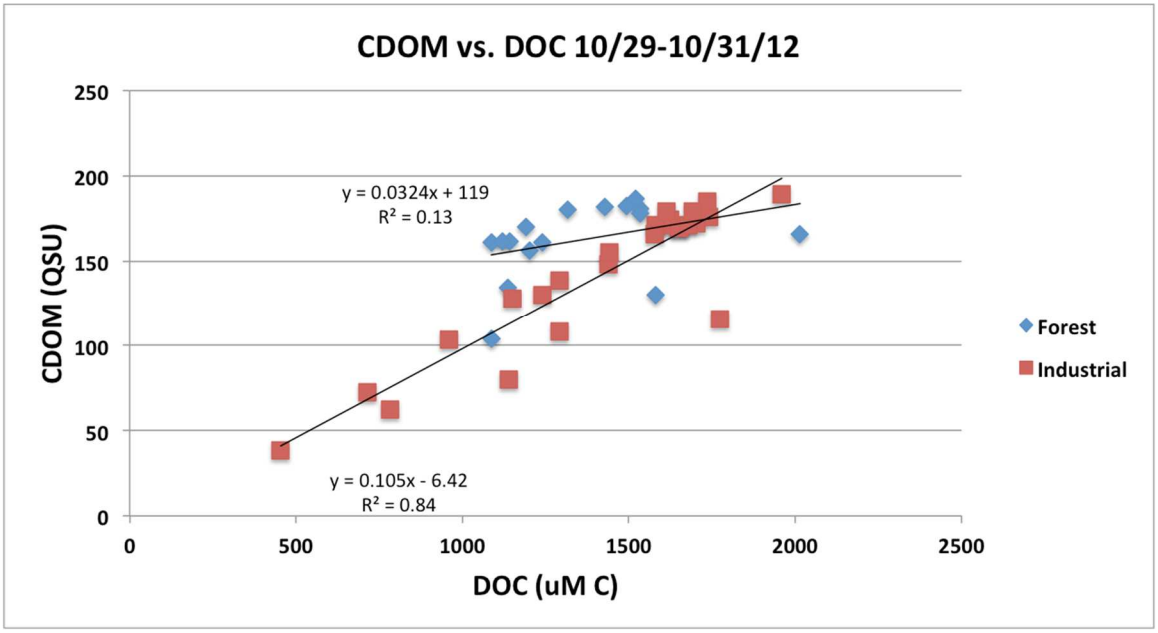

Figure 4.23: CDOM versus DOC

Forest 1 absorption coefficients increase sharply with time (Figure 4.24). The Industrial 3 absorption coefficients seem to increase as well, but not as quickly. Spectral slope ratios are similar at both sites, with noticeable increases at the forested site with high intensity precipitation. Slope ratios increase slightly at Forest 1 as the storm progresses, but decrease at Industry 3 (Figure 4.25).

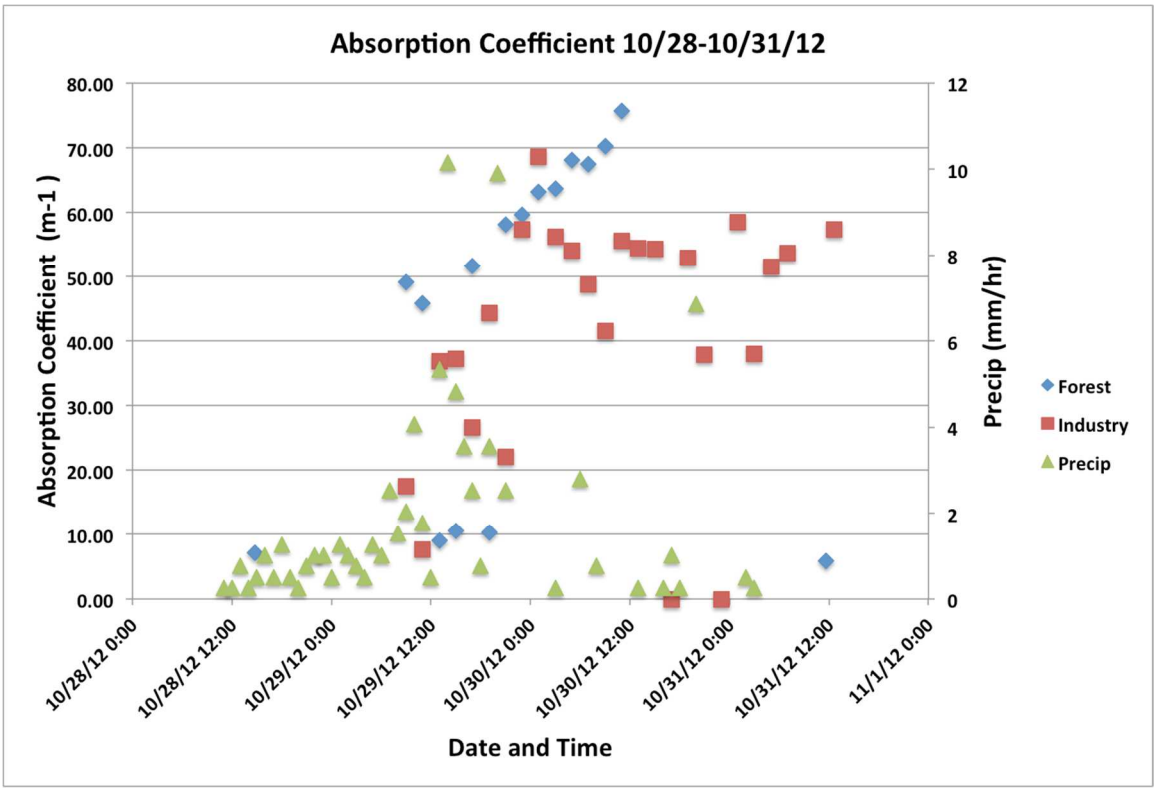

Figure 4.24: Absorption coefficients for discrete samples

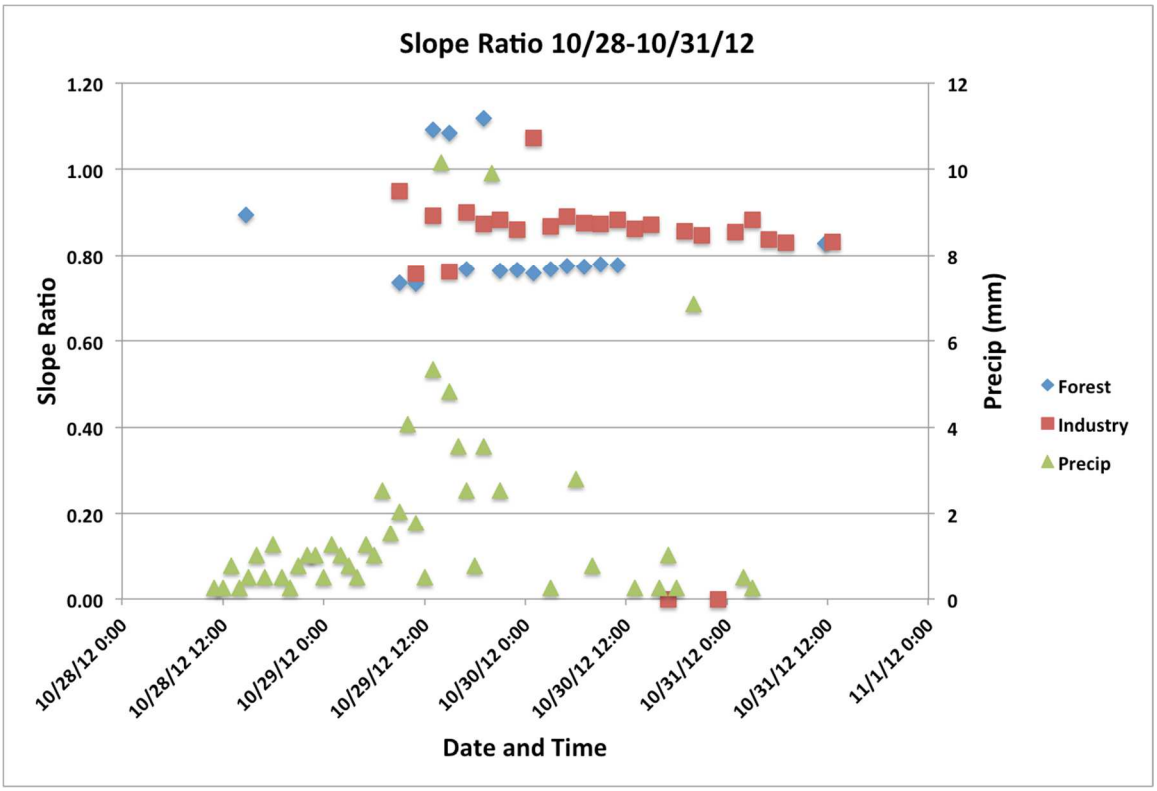

Figure 4.25: Spectral slope ratios for discrete samples

Event 6 Summary

As the largest storm event sampled, Hurricane Sandy offers a unique chance to see how the watershed responds to a large rain event. Both sites show elevated DOC and CDOM concentrations as the storm progresses. The industrial site is flashier, as shown during previous storms. It does not seem like the sampling subwatersheds have been depleted of carbon during the storm, as the increasing concentrations continue through the end of the discrete samples. In addition, there are pulses of high concentration water that are observed by the fluorescence sensors after the end of the storm, most obvious in Figure 4.18.

Other Data Trends

Event 1 discrete samples show an increasing DOC concentration trend for both sampling locations, with more variability in the Industrial concentrations (Figure 4.26).

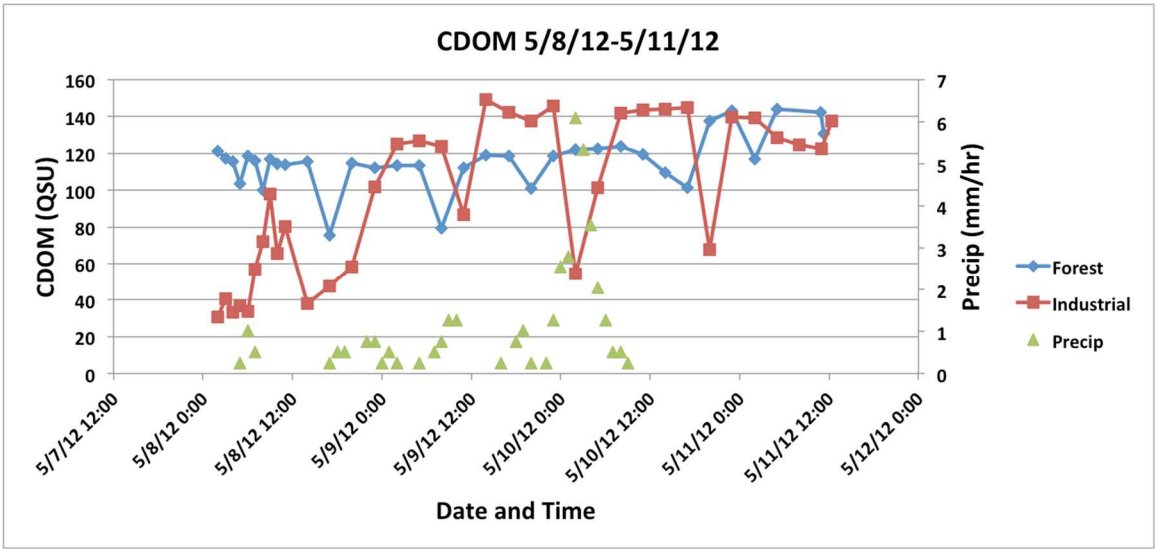

Figure 4.26: Discrete samples showing DOC concentration over time

During Event 1, the CDOM versus DOC slopes for the two sampling sites are different (Figure 4.27). This could be the influence of runoff from the different land use types.

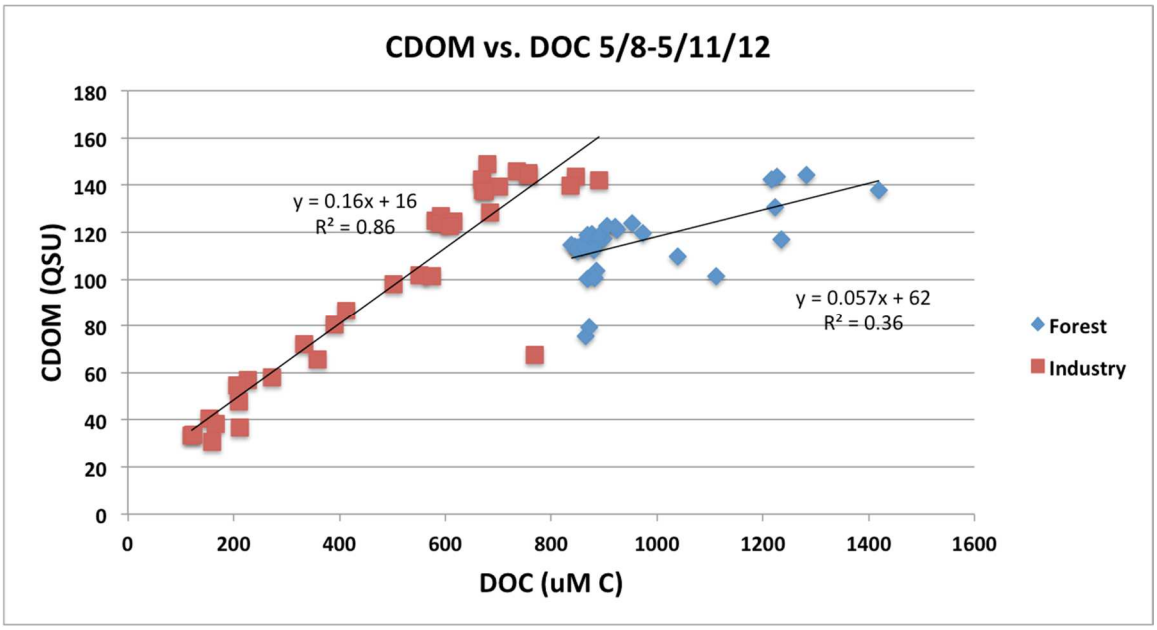

Figure 4.27: CDOM versus DOC

Large pulses of high concentration water were captured in Industrial 3 sensor data following the end of precipitation during Event 6 (Figure 4.18). This suggests a more complex watershed for Industrial 3, and may be the result of a slower runoff source, such as a wetland, or runoff traveling a greater distance before reaching the sampling point.

Discrete sample data at Industrial 3 from Event 7 also show a second concentration increase towards the end of the storm (Figures 4.28 and 4.29). Near the end of the storm, approximately 3.5 mm of rain falls over 2 hours. Smaller amounts of rain also occurred during the low concentration period of the sampled event. The sharp concentration rise toward the end of the storm could be the result of the additional rainfall causing increased desorption and increased runoff. It could also be the result of the additional precipitation increasing connectivity within the subwatershed. This

concentration increase is also captured by the sensor data from the Industrial 3 site (Figure 4.30).

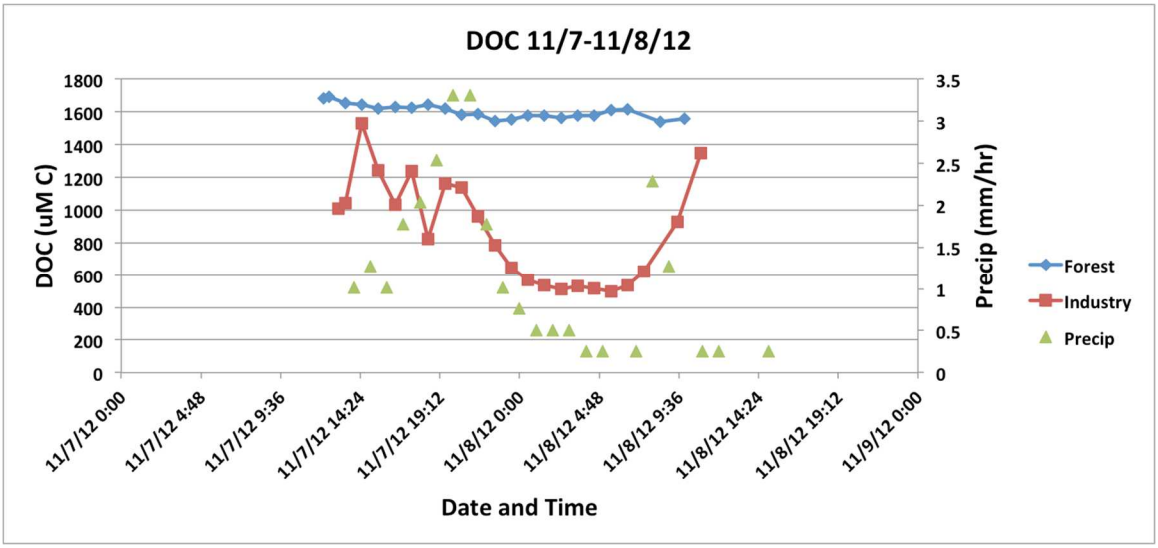

Figure 4.28: Discrete samples showing DOC concentration over time

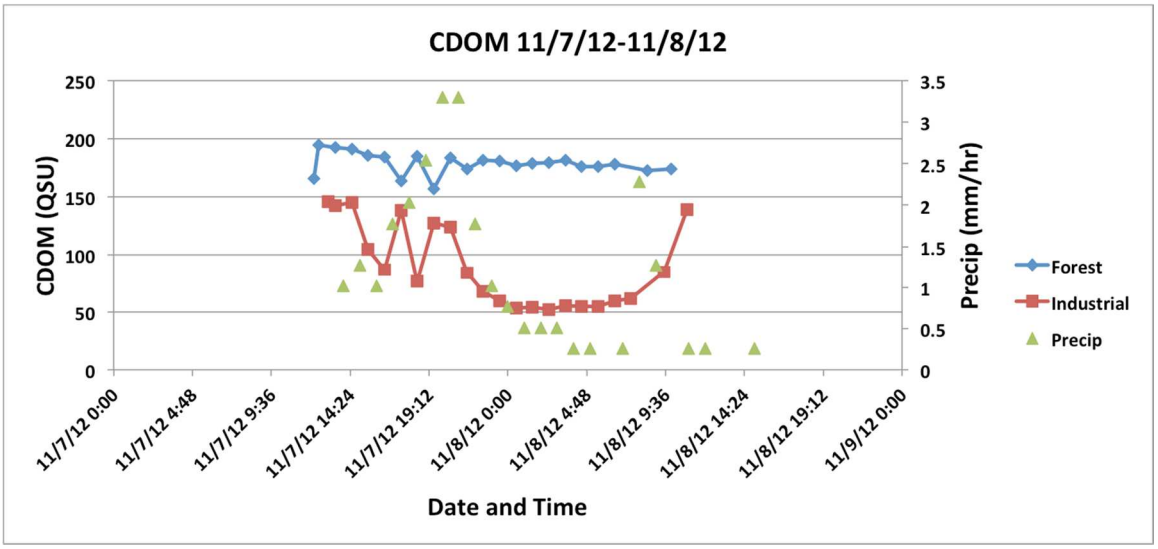

Figure 4.29: Discrete samples showing CDOM concentration over time

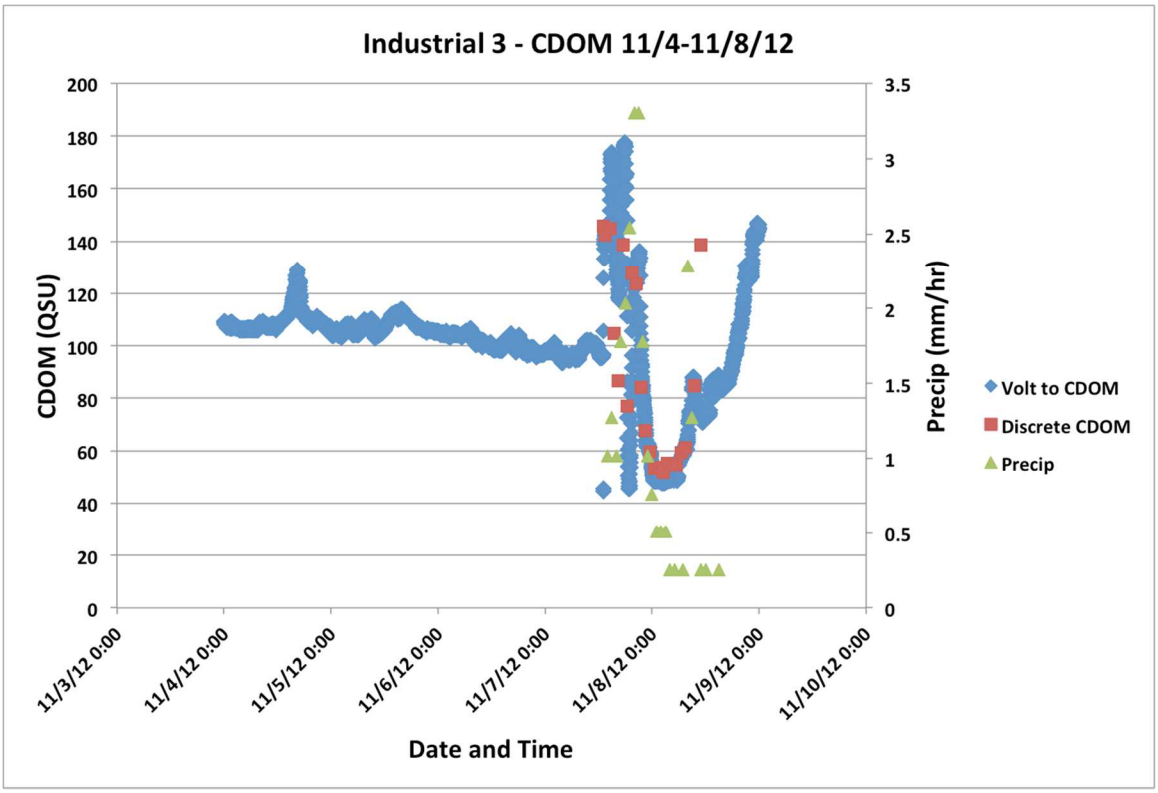

Figure 4.30: Industrial 3 sensor data and discrete samples from Event 7 shown on the same axis

This complexity is also visible in the CDOM-DOC plot of all the Forest 1 and Industrial 3 discrete samples collected in 2012 (Figure 4.31). The relationship for Forest 1 is fairly consistent. However, the Industrial 3 data shows variability, which may be the result of the two disparate water sources hypothesized above. While the entire subwatershed that the sampling site is located within has greater than 80% industrial land use, the sampling point is not representative of the entire subwatershed. This makes it even more likely that there could be runoff entering the sampling location from two, or more, distinct land use types. Additional GIS work should be utilized to determine the land use composition and areal extent of the source area for Industrial 3.

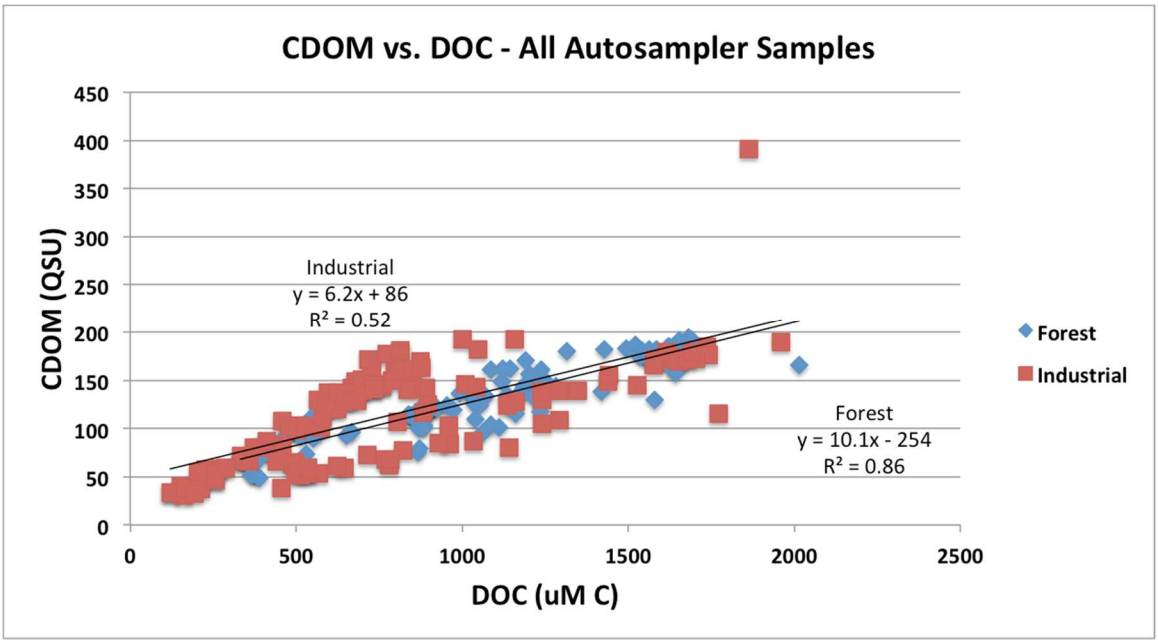

Figure 4.31: CDOM versus DOC for all discrete samples

Flux Calculations

DOC fluxes were calculated for each storm event utilizing sensor CDOM values and modeled flow values (Table 4.4). Sensor CDOM values were converted to DOC concentrations utilizing the CDOM-DOC relationship from discrete samples.

Table 4.4: Storm event DOC fluxes at Forest 1 and Industrial 3

Storm event	Dates	Forest 1 flux (g C)	Industrial 3 flux (g C)
1	5/8-5/11/12	400,000	15,000
2	6/12-6/14/12	No sensor data	3,200
3	7/18-7/19/12	2,200	140
4	8/27-8/28/12	5,200	500
5	9/18-9/19/12	890	210
6	10/29-10/31/12	520,000	110,000
7	11/7-11/8/12	110,000	26,000
Total	18 days	1,000,000	160,000

Monthly fluxes at Forest 1 and Industrial 3 were calculated using monthly watershed sampling data and modeled flow values (Table 4.5). An average flow was calculated for the month from daily modeled flow values, then that value was multiplied by the DOC concentration from the monthly sampling. This assumes that the monthly DOC concentration is representative of the entire month.

Table 4.5: Monthly DOC fluxes at Forest 1 and Industrial 3

Month	Forest 1 flux (g C)	Industrial 3 flux (g C)
January 2012	1,700,000	120,000
February 2012	940,000	120,000
March 2012	2,400,000	330,000
April 2012	2,700,000	370,000
May 2012	2,100,000	120,000
June 2012	690,000	44,000
July 2012	380,000	8,800
August 2012	280,000	No monthly sample data
September 2012	240,000	No monthly sample data
October 2012	340,000	180,000
November 2012	1,800,000	280,000
December 2012	No monthly sample data	54,000
Total	14,000,000	1,600,000

The calculated storm flux (6 storms) at Forest 1 is approximately 7.1% of the calculated yearly flux (11 months of data). The calculated storm flux (7 storms) at Industrial 3 is approximately 10% of the calculated yearly flux (10 months of data).

4.8 Conclusions

Data collected during storm events from co-located sensors and autosamplers can be utilized to examine the influence of stormwater runoff on riverine concentrations of

dissolved organic carbon. Sensor measurements are better able to capture more of the variability present in riverine DOC and CDOM concentrations due to runoff influxes. While there are many assumptions within the flux calculations, the comparison between sampled storm fluxes and monthly fluxes shows the significant impact that storm fluxes can have on DOC export from a small watershed. The seven sampled storm events account for 7 to 10 percent of the calculated yearly flux during 4 to 5 percent of the year.

These storms are a good representation of storms that occur from late spring through autumn. Several storm intensities and durations are sampled as well. However, the storm sampling does not account for storms that occur in the early spring that might increase fluxes from snowmelt. In 2012, the large storm at the end of April was not sampled. This storm resulted in more precipitation than Event 6, Hurricane Sandy.

For future deployments, the sensor package should include a flow sensor in order to better calculate carbon fluxes. One or more rain gauges should be deployed within the subwatershed being sampled, and at the sampling site, in order to determine when precipitation starts and ends. This would allow for calculation of the time of concentration for the subwatersheds. Precipitation data was obtained from records kept by the Blue Hill Observatory, which was located within the watershed. However, this data was only available hourly, and may not have been representative of the rainfall within the subwatersheds that were sampled. Finding ways to maximize battery life and recharging should also be a priority in order to collect consistent year-round data using sensors at these locations. This would allow for better estimation of yearly and storm-related DOC fluxes.

Additional measurements of soil moisture, streamflow, and local precipitation are needed in order to build a predictive model for DOC concentrations during storms. With further study, DOC fluxes during storms could be predicted from different land use types. This may be easier for impervious surfaces, but could also be achieved for natural surfaces with more data on antecedent rainfall, soil moisture, storm intensity and duration, land use, and topographic features such as slope.

CHAPTER 5

THE DYNAMICS OF DISSOLVED ORGANIC CARBON TRANSPORT FROM THE NEPONSET RIVER WATERSHED TO BOSTON HARBOR, MASSACHUSETTS, USA

5.1 Abstract

The flux of dissolved organic carbon from rivers into coastal areas is highly variable, and the amount and variability is expected to increase due to climate change (Evans et al., 2005; Dai et al., 2012). Dissolved organic carbon was sampled throughout the Neponset River Watershed (30 sites) monthly for seven years to determine the influence of rainwater runoff on dissolved organic carbon fluxes to coastal waters. Increased concentrations are observed following storm events and snowmelt, and are an average of 28% greater than concentrations observed during dry periods. Based on daily sampling data in September 2011, monthly fluxes may be underestimated by 38% or overestimated by 35%, although these percentages cannot be assumed to be true for other months or years. More frequent sampling allows for better certainty in estimations of monthly and yearly fluxes from the watershed, but must be balanced with logistical and cost restraints.

5.2 Introduction

Dissolved organic matter (DOM), including dissolved forms of carbon, nitrogen, and phosphorus, serves as a vehicle for the export of terrestrial carbon, nitrogen and

phosphorus to the ocean (Qualls et al., 1991; Hedin et al., 1998; Kalbitz et al., 2000). As a result, knowledge about the riverine concentration of dissolved organic carbon (DOC) and its transformation and movement through ecosystems is important. DOM represents an important source of nutrients for aquatic species (Jackson and Williams, 1985; Kemp et al., 1997; Gomi et al., 2002; Pace et al., 2004; Aller and Blair, 2006), enhances primary productivity (Rabalais et al., 2002), and absorbs harmful UV light (Green and Blough, 1994; Morris et al., 1995). Opsahl and Benner (1997) state that while terrigenous DOM represents only 0.7-2.4% of the total DOM in the ocean, the rapid remineralization of terrigenous DOM contributes to increased primary productivity in coastal waters.

Rivers transport approximately 0.17 to 0.45 Pg C y^{-1} (0.17 x 10^{15} g C to 0.45 x 10^{15}g C y^{-1}) as DOC from land to ocean annually (Schlunz and Schneider, 2000; Cole et al., 2007; Dai et al., 2012; Bauer et al., 2013; Schlesinger and Bernhardt, 2013). Many estimates are extrapolated from the measured fluxes from only the world's largest rivers (Schlunz and Schneider, 2000). For instance, Dai et al. (2012) used data from 118 rivers with available DOC concentrations, accounting for 48% of the global total riverine discharge, to estimate global DOC fluxes. This extrapolation may miss the influence of event-driven fluxes that may dominate water transport in many small watersheds that account for the other 52% of the global riverine discharge, but are currently unaccounted for in global river DOC fluxes.

Dissolved organic carbon in drinking water supplies can alter the efficacy of treatment efforts, and its presence can lead to harmful disinfection byproducts (Garvey and Tobiason, 2003; Evans et al., 2005; Kaplan et al., 2006). The fate and transport of

pollutants, such as mercury and other heavy metals, can be influenced by complexation with DOC (Ravichandran, 2004; Herngren et al., 2005; Selvendiran et al., 2008; Shanley et al., 2008). DOC also alters stream pH (Wigington Jr. et al., 1996).

The flux of DOC from rivers into coastal areas is highly variable and influenced by anthropologic perturbations, such as land use change, waterway modifications, and wetland loss (Findlay et al., 2001; Xenopoulos et al., 2003; Dai et al., 2012). Climate change also influences DOC export through changes in river discharge, sea-level height, and the severity of storms. Climate change is expected to increase riverine carbon fluxes, and also lead to increased variability in these fluxes (Evans et al., 2005; Dai et al., 2012).

A better quantitative and qualitative understanding of the carbon exported from land to the ocean is important for coastal and global carbon budgets, as well as informing management considerations and estimates of the global sink of anthropogenic carbon. Wahl, McKellar, and Williams (1997) compared DOC export from an urban stream and a forested stream in South Carolina. They found that mean annual DOC concentration in the urbanized stream was half that of the forested stream. However, due to greater runoff volumes in the urban catchment due to impervious surfaces, the annual DOC fluxes from the streams were within 10%. Tian et al. (2013) found that land surface processes (land-use type and density, hydrology and soil properties) are the primary factors controlling riverine DOC concentrations in small watersheds, particularly watersheds within a single climate zone and where the inter-annual mean temperature variation is small (less than 2° C). Yang et al. (2013) investigated the variation of DOC and dissolved nitrogen (DN) in surface runoff water during storms from different land use types in Florida. The land use

types included residential, agricultural (vegetable farm, nursery, ranch, citrus grove), golf course, and forest. They found that land use type and the size and intensity of rainfall events strongly influenced the concentrations of DOC and DN, as well as the export of nitrogen, phosphorus, and metals in runoff. The largest export of DOC occurred during rain events.

Chromophoric Dissolved Organic Matter (CDOM)

Dissolved organic matter is composed of thousands of compounds, most of which have not been classified into compounds or compound classes. CDOM is the colored fraction of dissolved organic matter that absorbs light over a broad range of wavelengths, both visible and UV. CDOM is typically yellowish in color and fluoresces blue when irradiated with UV light. Due to its light absorbing properties, CDOM affects the light penetration of natural waters and can influence biogeochemical processes. CDOM is also useful as a tracer for DOC, as well as a "proxy for mixing" (Coble, 2007), in aquatic environments (Green and Blough, 1994; Stedmon et al., 2003; Chen and Gardner, 2004; Coble, 2007).

When the CDOM – DOC relationship is known in terrestrially influenced areas for specific systems and/or time periods, CDOM measurements can be used as a proxy for DOC concentration (Figure 5.1). CDOM fluorescence can be easily measured *in situ* using optical sensors, while DOC concentration requires sample collection and laboratory analysis (Green and Blough, 1994; Coble, 2007). *In situ* measurement also allows for high resolution sampling. During episodic events, stormwater runoff can be a significant

contributor to CDOM concentrations in rivers (Baker and Spencer, 2004; Huang and Chen, 2009).

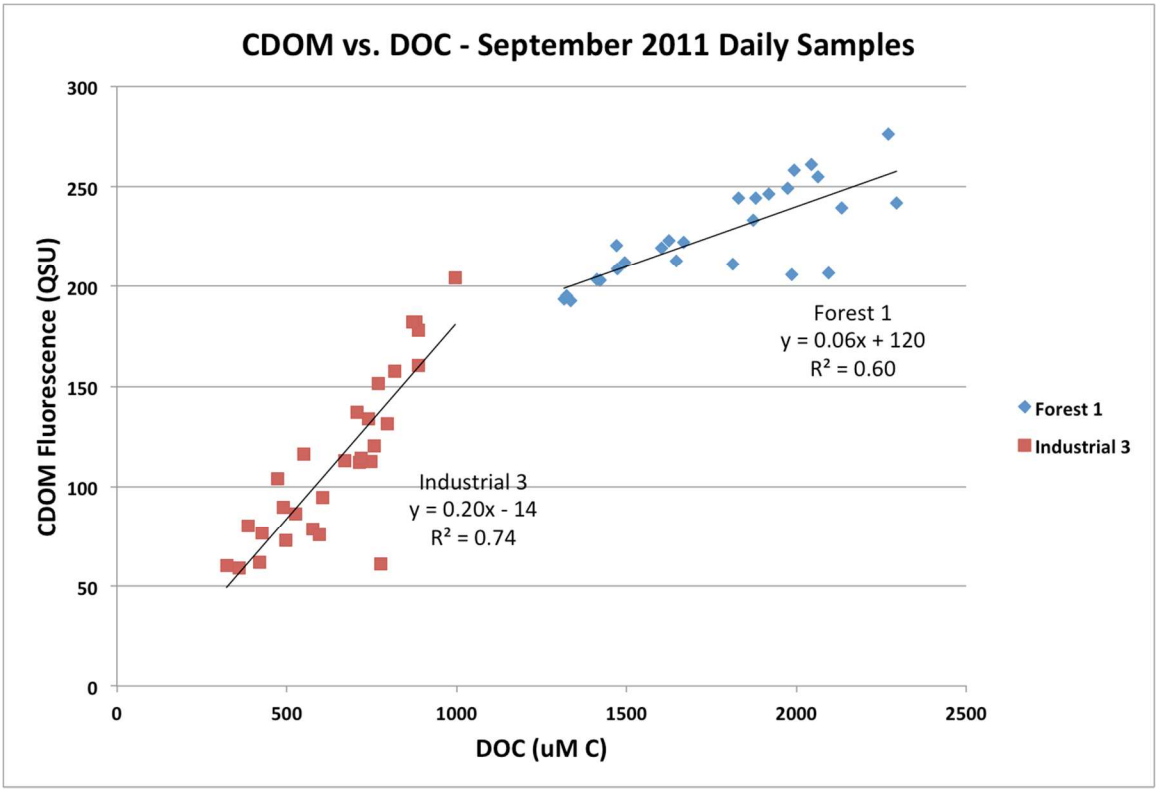

Figure 5.1: An example of the CDOM-DOC relationship from samples collected daily at two Neponset Watershed locations in September 2011

Neponset River Watershed

The Neponset River is located in an urban area close to Boston, Massachusetts and empties into Boston Harbor. The watershed covers about 300 square kilometers and is comprised of 14 cities and towns with a population of about 330,000 (Neponset River Watershed Association, 2014a). The Neponset River Estuary often fails to meet state water quality standards, due to the impacts of combined sewer overflows (CSO) and urban stormwater runoff (MWRA, 2014). Table 5.1 provides additional information about the Neponset River Watershed.

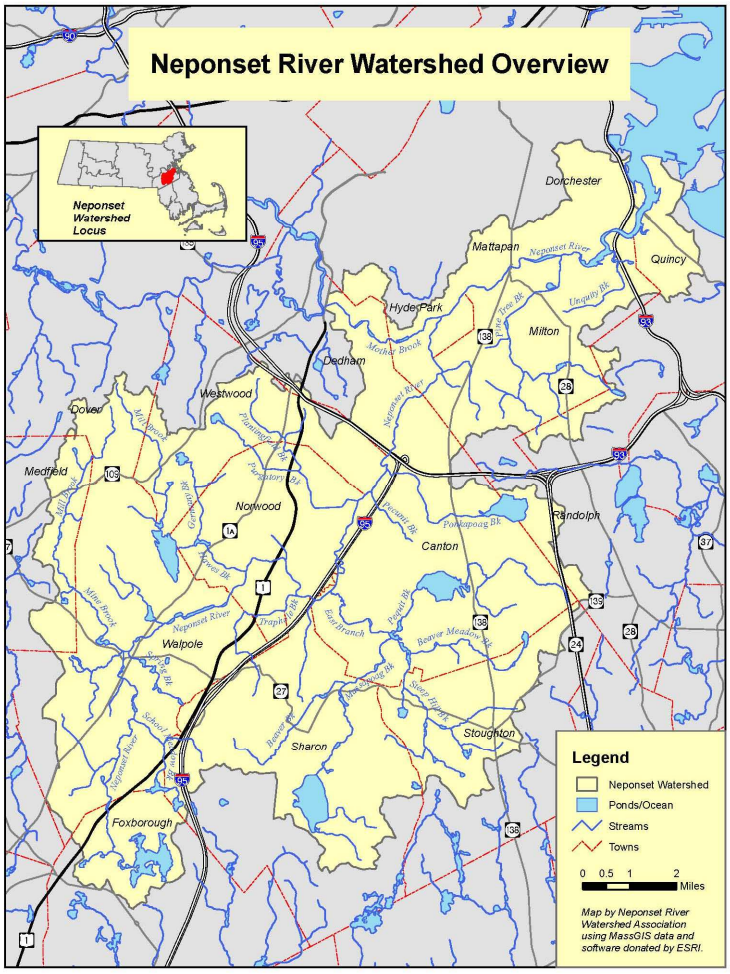

Figure 5.2: The Neponset Watershed is comprised of portions of 14 cities and towns and drains into Boston Harbor (Neponset River Watershed Association, 2014c)

Table 5.1: Summary data for Neponset River Watershed

Variable	Value	Source
Mean annual precipitation, Neponset River	123.49 cm (48.62 in)	http://www.bluehill.org
DOC concentration increase during storms	2-3 times	Neponset sample data (see Appendix B); Hood, Gooseff, and Johnson (2006)
Average baseline flow	2.83 m^3 sec^{-1} (100 ft^3 sec^{-1})	http://waterdata.usgs.gov/usa/nwis/uv?011055566
Average storm flow	8.5 m^3 sec^{-1} (300 ft^3 sec^{-1})	http://waterdata.usgs.gov/usa/nwis/uv?011055566

5.3 Methods

Watershed Sampling

Thirty-one freshwater sites within the Neponset River Watershed were sampled monthly from January 2008 to December 2012 (Figure 5.3). This was a continuation of a previous dataset with thirty sampling locations started in 2006 (Huang and Chen, 2009). Huang and Chen (2009) utilized land cover maps from MassGIS to determine the dominant land use types within the watershed. From their results, the watershed was found to be dominated by five land use types: residential (38%), forest (34%), industrial (5%), wetland (4%) and golf courses (2%). Sixteen other land use types classified in MassGIS accounted for less than 2% each. They then selected 30 sampling locations.

Fifteen freshwater sites were selected as endmembers with an endmember subwatershed defined as an area that drains at least 80% from a unique land-cover type. These sampling sites were named by land use and numbered to distinguish between sites in the same land use type (i.e. Forest 1, Wetland 3, etc.). Fifteen additional freshwater sites selected represent pour points, which are sites that represent drainage from a mixture of land use types. These sampling sites were labeled "PP" for pour point and then numbered (i.e. PP1, PP10, etc.). The thirty-first site was added in January 2009 at the location where part of the Charles River is diverted into the Neponset River watershed through Mother Brook. This site was named Mother Brook, or MB for short.

In September 2011, additional discrete samples were collected daily at a subset of 5 sampling sites. The five sites were PP1, PP6, PP8, Forest 1, and Industrial 3 (Figure 5.3). This sampling was conducted to investigate daily variability and provide higher temporal resolution context to the monthly sampling. Identical sampling procedures to the monthly procedures were utilized.

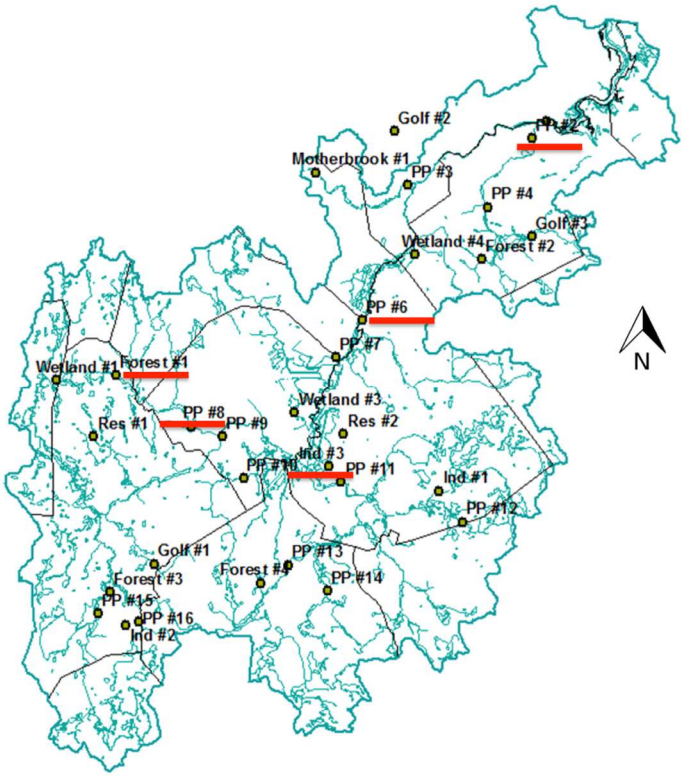

Figure 5.3: Map of the 31 monthly sampling sites within the Neponset River Watershed. Daily sampling locations from September 2011 are indicated by the red underline.

Other Data Sources

Climatic data, including precipitation, was obtained from records kept by the Blue Hill Observatory (http://www.bluehill.org) and available from the Blue Hill Observatory and NOAA's National Climatic Data Center (http://www.ncdc.noaa.gov/cdo-web/datasets/PRECIP_HLY/stations/COOP:190736/detail). Neponset Watershed discharge data was obtained from streamflow data available from the United States Geological Survey (USGS) (http://waterdata.usgs.gov/ma/nwis/current/?type=flow).

Discrete Samples

Discrete samples were collected on a single day using a stainless steel pitcher that was cleaned in the laboratory with deionized water and rinsed three times with water

from the sampling site. Discrete samples obtained during watershed sampling were transported to the laboratory in 300 ml pre-combusted (500°C, 5 hours) glass bottles with Teflon-lined caps. Within 24 hours of sampling, each sample was filtered (high purity N_2 pressure filtered, <15 psi) at the laboratory through pre-combusted 0.7 μm glass fiber filters (Whatman GF/F). Dissolved organic carbon (DOC) and chromophoric dissolved organic matter (CDOM) samples were filtered into pre-combusted (500°C, 5 hours) 40 ml borosilicate glass vials with Teflon-lined screw caps. DOC samples were acidified to pH less than 2 with phosphoric acid and stored in clear vials at 4°C until analysis (Kaplan 1994). Absorbance and fluorescence samples were stored in amber vials at -4°C until analysis. All samples were analyzed at room temperature (21°C ± 1°).

Dissolved Organic Carbon (DOC)

A Shimadzu TOC-V analyzer was utilized for DOC analysis (Qian and Mopper, 1996). DOC standards were prepared using potassium hydrogen phthalate (KHP, Sigma Chemical) based on the instrument manual. The instrument was turned on and allowed to warm-up for at least one hour. Milli-Q water injections were then run until the instrument baseline stabilized at a peak area less than 2, similar to values obtained during analysis of 1 μM C Low Carbon Water. The instrument was then calibrated with a seven-point standard curve. Samples were run following a linear regression of the standard curve ($r^2 \geq$ 0.995). On subsequent days, at least one random carbon standard was run and compared to the standard curve to ensure continued calibration.

While running samples, the instrument blank was checked with ultra high purity, low carbon Milli-Q UV water every 10 to 15 samples. The mean blank value was

subtracted from the sample measurements (Stedmon et al., 2000). Low Carbon Water (LCW) and Deep Sea Water (DSW) standards from Dennis Hansell's lab at the University of Miami were also run to ensure data quality (http://yyy.rsmas.miami.edu/groups/biogeochem/CRM.html).

CDOM Fluorescence

Fluorescence samples were thawed and then analyzed on a Photon Technologies International (PTI) Quantum Master 1 spectrofluorometer. Excitation scans were conducted with excitation (λ_{ex}) 337 nm, a 1 cm quartz cell, and emission scans from 350 nm to 650 nm. Slits widths were set to 4 nm. A blank (Milli-Q water) was run each day and subtracted from sample spectra to remove the Raman scattering peak. Fluorescence spectra were integrated in the wavelength range of 350 - 650 nm. A seven-point quinine sulfate standard curve (pH = 2) was used to convert the area of the emission spectra to quinine sulfate units (QSU) (Green and Blough, 1994; Siegener and Chen, 2002; Stedmon et al., 2003; Chen and Gardner, 2004). One QSU was equivalent to the fluorescence of 1 μg/l quinine sulfate at pH 2.

Spectral data were all corrected for the inner filter effect for samples with absorbance above 0.1. The inner filter effect occurs when dissolved species, including the fluorophore, absorb exciting or emitted radiation (Puchalski et al., 1991; Hu et al., 2002). To correct for this effect, dilution with Milli-Q water was conducted for all samples over 100 QSU (about 0.1 m^{-1}).

Sample Classification and Statistical Analysis

Prior to statistical analysis, each monthly sampling date was classified as wet, dry, or average. Sampling dates classified as wet were for samples that were collected within 36 hours of a preceding storm of 2.54 mm (0.1 in) or greater. Sampling dates classified as average had a storm of 2.54 mm (0.1 in) or greater 36 to 72 hours prior to sampling. Dates classified as dry had a preceding storm of 2.54 mm (0.1 in) or greater that occurred more than 72 hour prior to sampling. The Neponset River Watershed Association's (NepRWA) Citizens Water Monitoring Network (CWMN) samples six times per year at 41 sites within the watershed. CWMN samples for E. coli, total nitrogen and phosphorus, orthophosphate, nitrate, chlorophyll, dissolved oxygen, pH, and water temperature, but does not sample for DOC or CDOM (Neponset River Watershed Association, 2014b). NepRWA uses a similar wet/dry classification system, with greater than or equal to 0.05 inches of rain within 72 hours being classified as wet. Less than 0.05 inches within 72 hours of sampling is classified as dry.

There are many issues with the reporting and analysis of long-term datasets (Filella and Rodríguez-Murillo, 2014). Efforts are made here to report details about analytical procedures and statistical methods used. Two sample t-test, unequal variance, independent sample T-tests were utilized to compare the mean dissolved organic carbon concentrations of various wet/dry date combinations.

5.4 Results and Discussion

Monthly sampling

The dataset of monthly samples contains 2340 individual DOC samples from 31 sampling sites over approximately 78 months. Summary statistics for the entire dataset are presented in Table 5.2. All sample data are shown in Figure 5.4. A subset of data from five sampling locations is presented in Figure 5.6. The five locations were the same locations selected for daily sampling in 2011.

Table 5.2: Summary statistics for DOC sample concentration data, 2006-2012, by sampling location. All concentration values are in uM C.

Sample location	Number of samples*	Avg. 2006-2012	Std dev 2006-2012	Max value 2006-2012	Min value 2006-2012	2006 avg.	2007 avg.	2008 avg.	2009 avg.	2010 avg.	2011 avg.	2012 avg.
PP1	84	588	350	2239	269	524	459	1056	565	552	488	493
PP2	85	480	206	993	213	517	377	627	488	460	445	468
PP3	82	600	460	3251	258	527	472	986	575	717	486	464
PP4	84	610	382	2796	239	575	481	1040	521	637	509	541
PP6	84	576	309	2036	121	617	450	841	571	670	516	429
PP7	83	639	504	4050	307	651	566	852	607	958	518	456
PP8	85	561	487	3645	265	468	434	883	481	808	437	497
PP9	76	587	413	2914	260	568	408	1042	573	386	510	499
PP10	84	383	340	2400	66	350	270	778	302	423	342	230
PP11	85	467	274	2221	193	423	370	787	437	495	413	365
PP12	82	612	490	3447	113	471	688	1112	540	453	509	471
PP13	83	475	605	5569	120	394	350	1009	400	430	392	353
PP14	84	496	847	6745	195	353	288	842	859	490	349	318
PP15	81	565	274	1772	251	564	474	729	518	638	550	499
PP16	82	501	436	3559	79	524	295	986	514	327	477	410
Mother Brook	52	520	188	1269	271	NA	NA	811	561	520	521	435

*Some locations were dry or frozen on the sampling day and no sample was collected.

Sample location	Number of samples*	Avg. 2006-2012	Std dev 2006-2012	Max value 2006-2012	Min value 2006-2012	2006 avg.	2007 avg.	2008 avg.	2009 avg.	2010 avg.	2011 avg.	2012 avg.
Forest-1	82	938	591	3531	197	1182	536	1405	896	666	951	917
Forest-2	72	368	410	2062	77	NA	429	674	280	366	267	235
Forest-3	74	621	350	2090	126	NA	538	807	690	624	572	510
Forest-4	61	1061	1057	7650	248	NA	938	2005	848	777	807	790
Golf-1	75	335	252	1653	69	258	224	659	295	271	304	273
Golf-2	72	303	208	1496	133	NA	229	477	255	398	256	240
Golf-3	72	522	312	2401	278	NA	509	757	542	476	446	441
Industrial-1	84	810	479	2435	240	1125	559	948	798	739	863	682
Industrial-2	59	352	356	2485	43	NA	300	438	287	700	262	240
Industrial-3	66	452	281	1540	71	NA	457	569	398	447	428	461
Residential-1	82	453	339	2308	70	340	463	729	376	517	428	334
Residential-2	73	327	405	2539	13	NA	157	441	338	681	312	137
Wetland-1	67	1078	762	4547	121	1421	635	1564	866	1072	1153	742
Wetland-3	56	1358	1065	6752	72	NA	629	1370	2152	1499	1422	1154
Wetland-4	49	735	696	3228	93	NA	466	1126	912	579	715	498
Overall	2340	593	456	7650	13	592	448	915	595	606	537	470

*Some locations were dry or frozen on the sampling day and no sample was collected.

Sampling dates were not expressly selected to sample or avoid sampling precipitation events within the watershed (Figure 5.4). The sampled dates were classified as wet (precipitation within 1.5 days of sampling), medium (precipitation between 1.51 and 3 days prior to sampling), and dry (antecedent precipitation occurred greater than 3 days prior to sampling). Using this classification system, there were 45 wet, 8 medium, and 32 dry sampling dates. The wet sampling days represent 53% of the sampled days. From 2006 to 2012, 975 out of 2557 days (38%) had precipitation at Blue Hill Meteorological Observatory. Average monthly DOC concentration data for all sites is presented in Figure 5.5. In a comparison of average monthly DOC and monthly total precipitation, there is a trend of higher DOC concentrations with greater precipitation amounts (Figure 5.6).

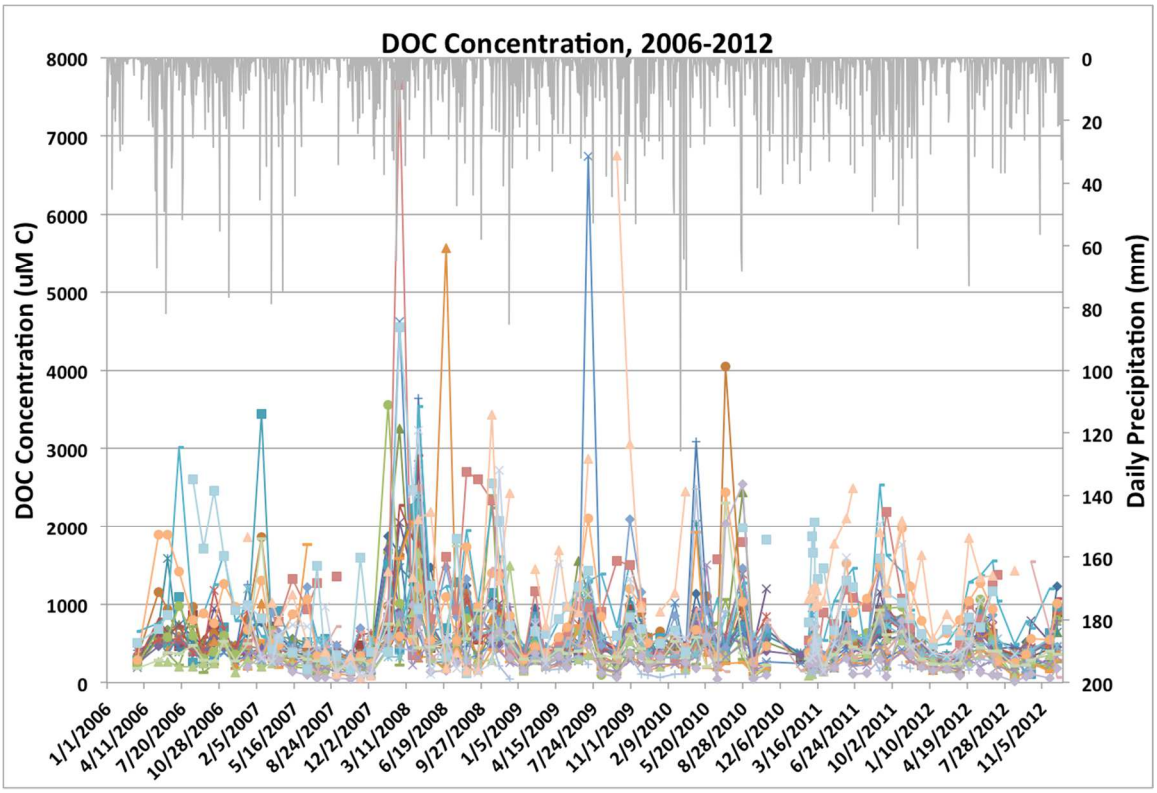

Figure 5.4: Graph of all DOC sample concentration data, 2006-2012. Precipitation is graphed on the secondary vertical axis.

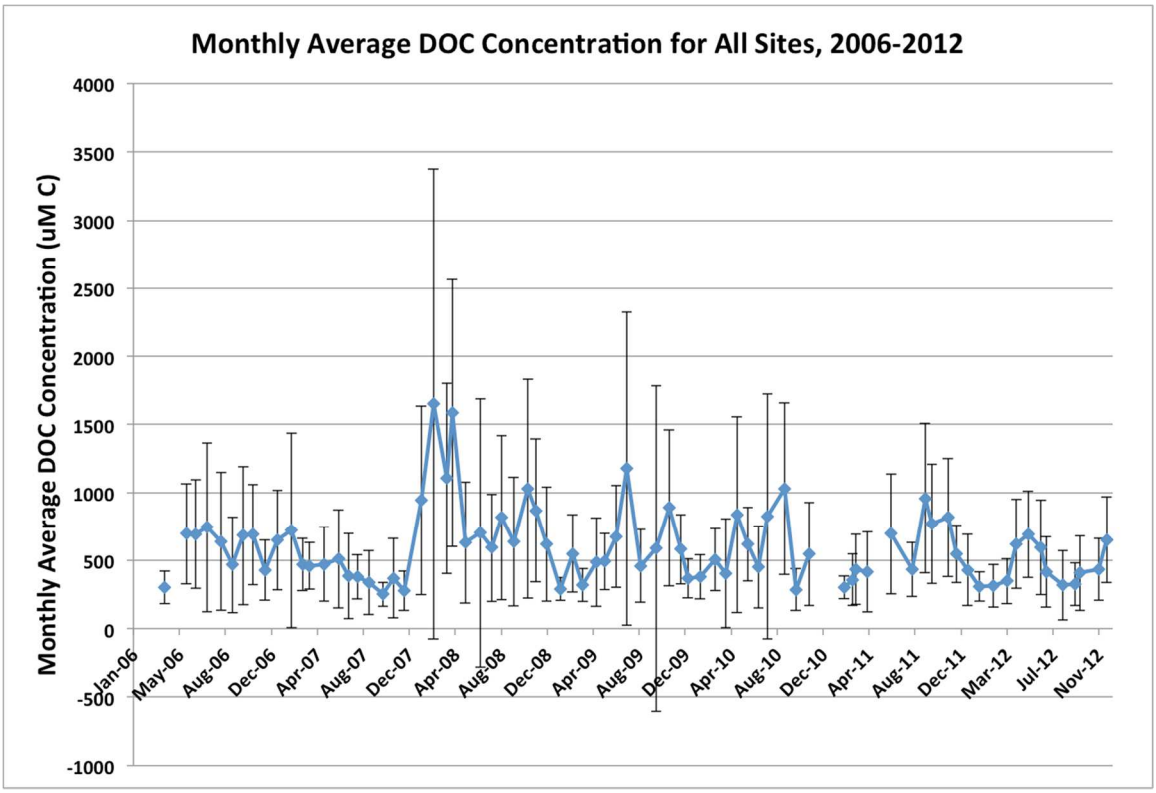

Figure 5.5: Monthly average DOC concentration for all sites from March 2006 through December 2012. Error bars represent 1 standard deviation.

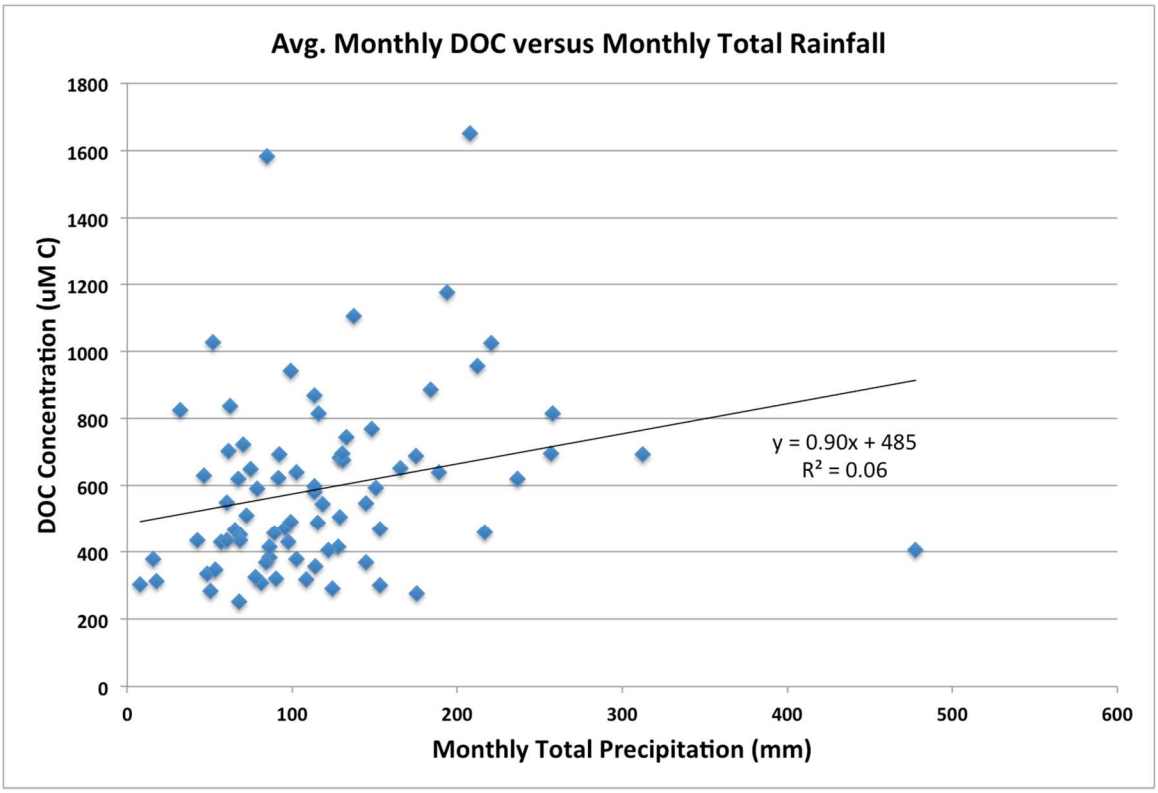

Figure 5.6: Comparison of average monthly DOC concentrations for all sampling locations with monthly total precipitation.

To further elucidate these trends, independent sample T-tests were utilized to compare the mean dissolved organic carbon concentrations of various wet/dry date combinations. These combinations, and their resulting *p* values, are presented in Table 5.3.

Table 5.3: Dataset comparisons using T-test p values

Group 1	Group 2	Two sample t-test, unequal variance, *p* value
All wet dates (45 sampling dates)	All dry dates (32 sampling dates)	6.7×10^{-10}
Winter wet dates 2/23/08, 1/20/09, 2/20/09, 1/19/10, 2/28/10, 2/24/12	Winter dry dates 12/10/06, 1/12/07, 2/18/07, 12/8/07, 1/22/08, 12/18/09, 2/21/11, 12/18/11, 12/15/12	0.42
Summer wet dates 8/08/07, 7/24/08, 7/12/09, 7/14/10, 8/27/10, 07/26/11, 8/29/11	Summer dry dates 9/07/07, 9/19/08, 9/26/09, 9/26/10, 9/16/11, 9/24/12	0.00011
3 selected wet dates - 2/23/08 (3^{rd} wettest February on record)	3 selected dry dates - 3/24/06 (2^{nd} driest	1.8×10^{-5}

- 3/27/10 (wettest March and wettest month on record) - 8/27/10 (5th wettest August on record)	March on record) - 5/13/07 (no rain for 2 weeks prior to sampling date) - 9/07/07 (2nd driest August on record; no rain for over 20 dates prior to sampling date)	
Wet – Forest	Dry – Forest	0.013
Wet – Golf	Dry – Golf	0.052
Wet – Industry	Dry – Industry	0.062
Wet – Residential	Dry – Residential	0.0023
Wet – Wetlands	Dry - Wetlands	0.11

Statistically significant differences in the sample means were observed for the following groups ($p < 0.05$):

- all wet sample dates versus all dry sample dates
- summer wet sample dates versus summer dry dates
- 3 selected wet sample dates versus 3 selected dry sample dates

- wet sampling dates (forest data) versus dry sampling dates (forest data), and
- wet sampling dates (residential data) versus dry sampling dates (residential data).

The statistically significant differences in the sample means may be the result of increased DOC concentrations occurring following precipitation events (wet sample dates).

The wet dates have an average DOC concentration that is 28% greater than the dry dates. The summer wet dates have an average DOC concentration that is 55% greater than the summer dry dates. The selected wet dates have an average DOC concentration that is 160% greater than the selected dry dates. The Forest wet dates have an average DOC concentration that is 31% greater than the Forest dry dates. The Residential wet dates have an average DOC concentration that is 63% greater than the Residential dry dates.

No statistical differences were noted for the following groups ($p > 0.05$):

- winter wet sample dates versus winter dry dates
- wet sampling dates (golf data) versus dry sampling dates (golf data)
- wet sampling dates (industrial data) versus dry sampling dates (industrial data)
- wet sampling dates (wetlands data) versus dry sampling dates (wetlands data)

The winter sample means may not be statistically different due to reduced temperatures, frozen ground, and precipitation falling as snow, rather than rain (Figure 5.7). In a comparison of average monthly DOC and monthly total snowfall, there is a trend of lower average DOC concentrations with greater monthly snowfall amounts (Figure 5.8). All of these factors would reduce DOC export from land to the waterway.

The mean concentrations from all sampling sites with golf, industrial, and wetland land uses were not statistically different when compared. However, statistical differences were noted in comparisons among data from a single sampling location (i.e. Industrial 1 wet versus Industrial 1 dry).

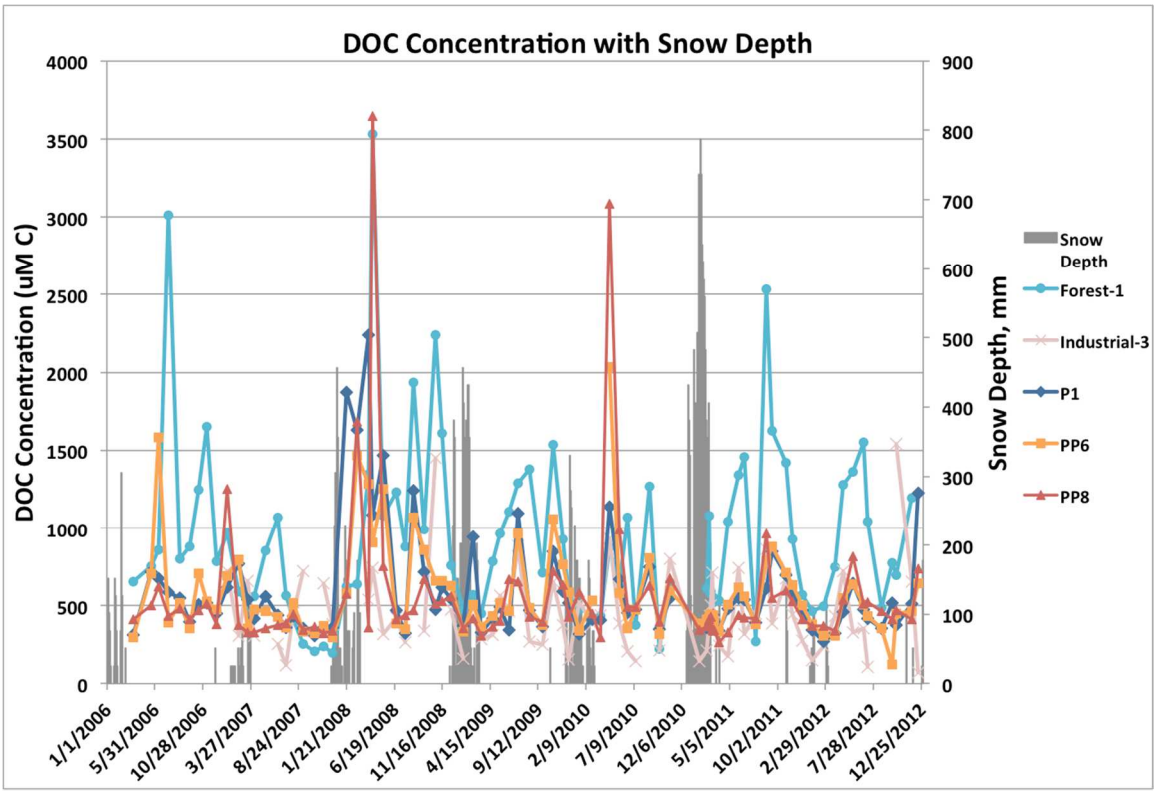

Figure 5.7: DOC concentration over time (2006-2012) for five watershed sampling locations. Snow depth at Blue Hill is also shown.

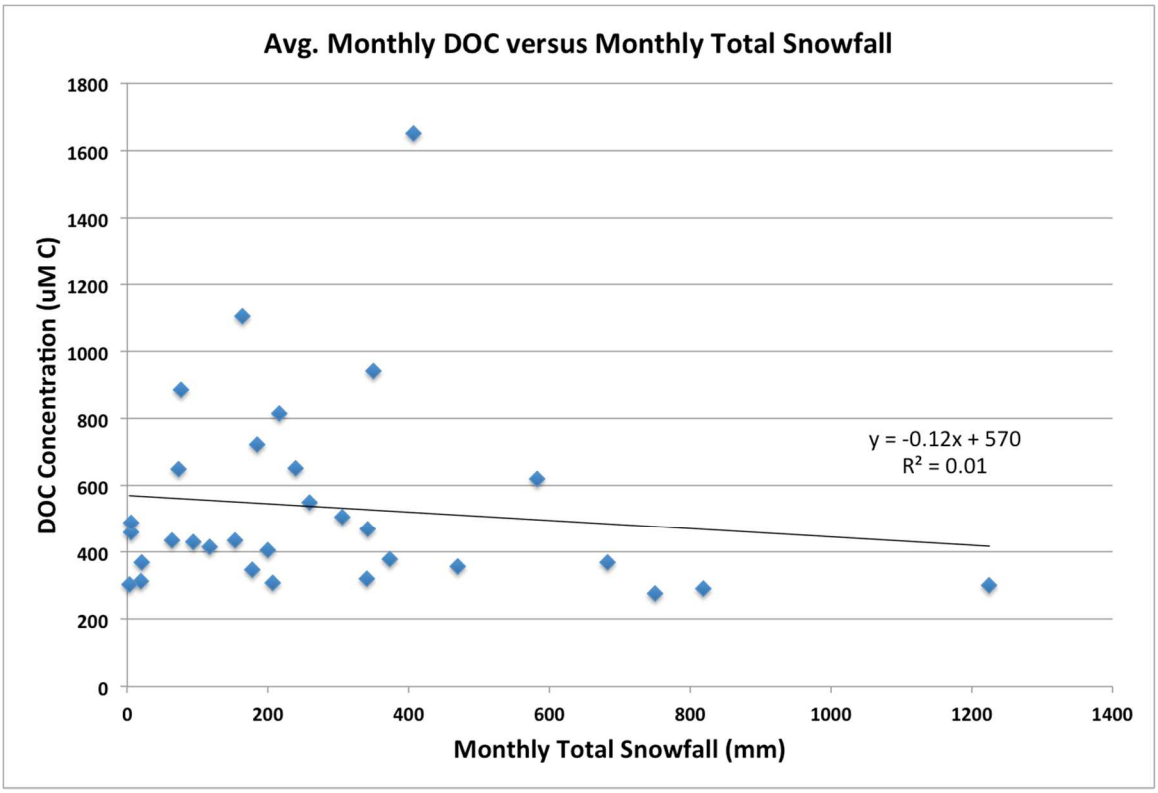

Figure 5.8: Comparison of average monthly DOC concentrations for all sampling locations with monthly total snowfall. Months without snowfall were excluded from the graph.

There is also a trend of increasing DOC concentrations with increasing temperatures (Figure 5.9). This would support the trend of lower DOC concentrations in the winter months.

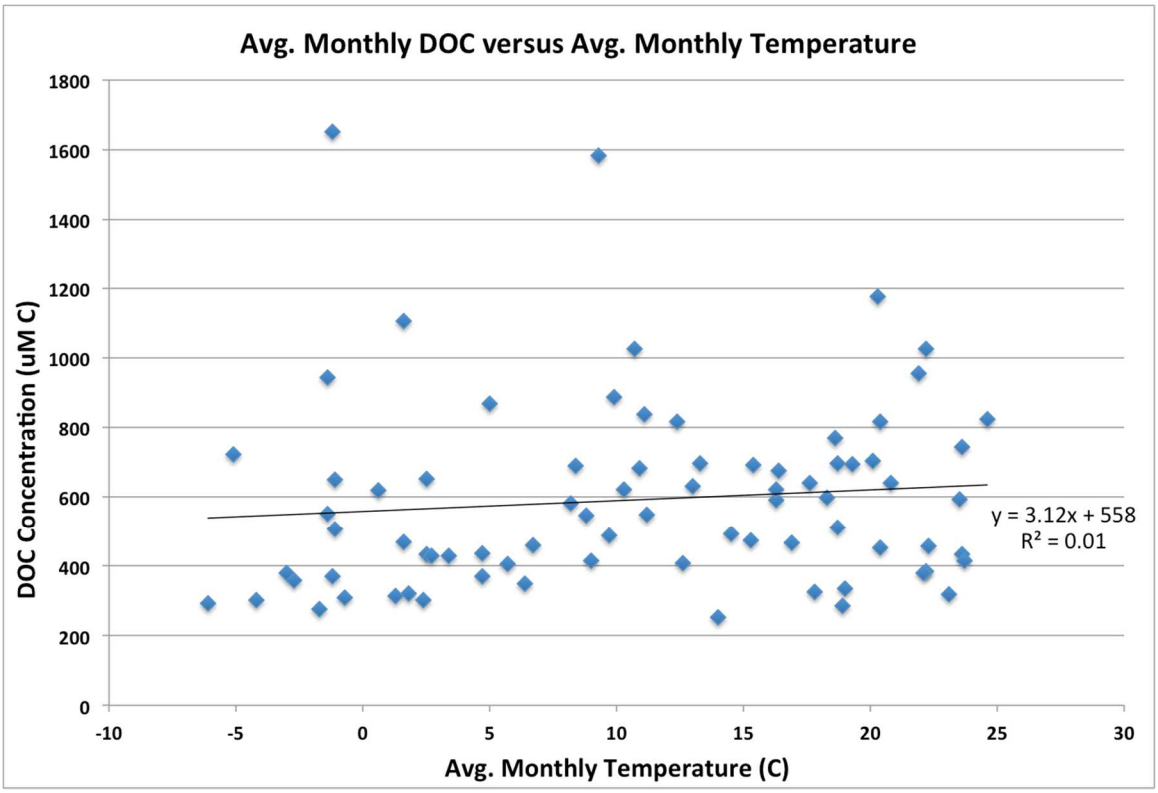

Figure 5.9: Comparison of average monthly DOC concentrations for all sampling locations with monthly average temperature.

Daily sampling – September 2011

Daily samples taken at the five watershed locations in September 2011 show a wide range of DOC and CDOM values (Figures 5.10 and 5.11). The CDOM/DOC graph also shows this range (Figure 5.15). For example, DOC fluctuated between 1316 µM C and 2294 µM C for Forest 1 (Figure 5.12) and 323 µM C and 996 µM C for Industrial 3 (Figure 5.13). CDOM values for Forest 1 varied between 193 QSU and 276 QSU, while Industrial 3 ranged between 59 QSU and 204 QSU. PP1 (Figure 5.14) and PP6 also showed concentration variations during the month. These variations may be the effect of runoff from rain events increasing DOC concentrations in the river. The CDOM/DOC

relationships for both Forest 1 and Industrial 3 are stronger for "wet" samples collected within 24 hours of a storm event. While the concentrations at Forest 1 are higher throughout the month than at Industrial 3, Industrial 3 appears to be flashier. The rain events on 9/14, 9/15, and 9/20 do not appear to increase CDOM and DOC concentrations at Forest 1. However, there are noticeable increases in the data from Industrial 3 on these dates. PP8 has more consistent concentrations throughout the month.

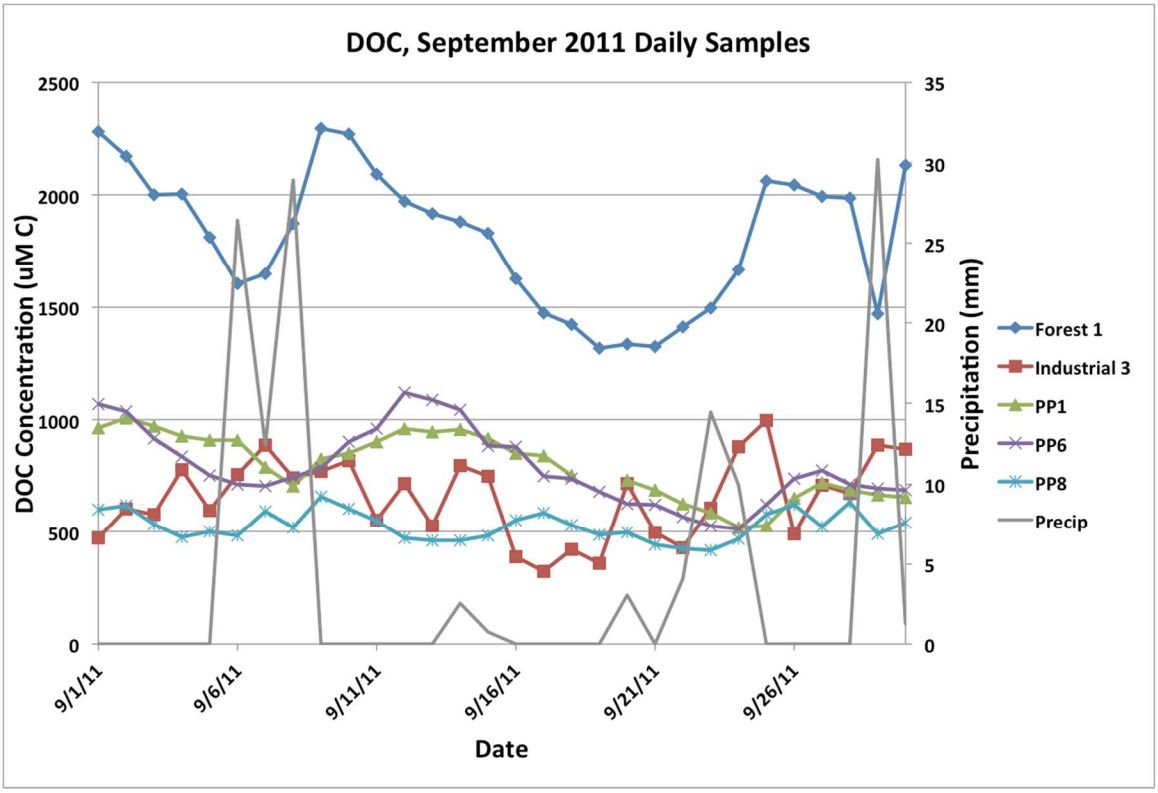

Figure 5.10: DOC concentrations from daily samples taken at five watershed locations in September 2011

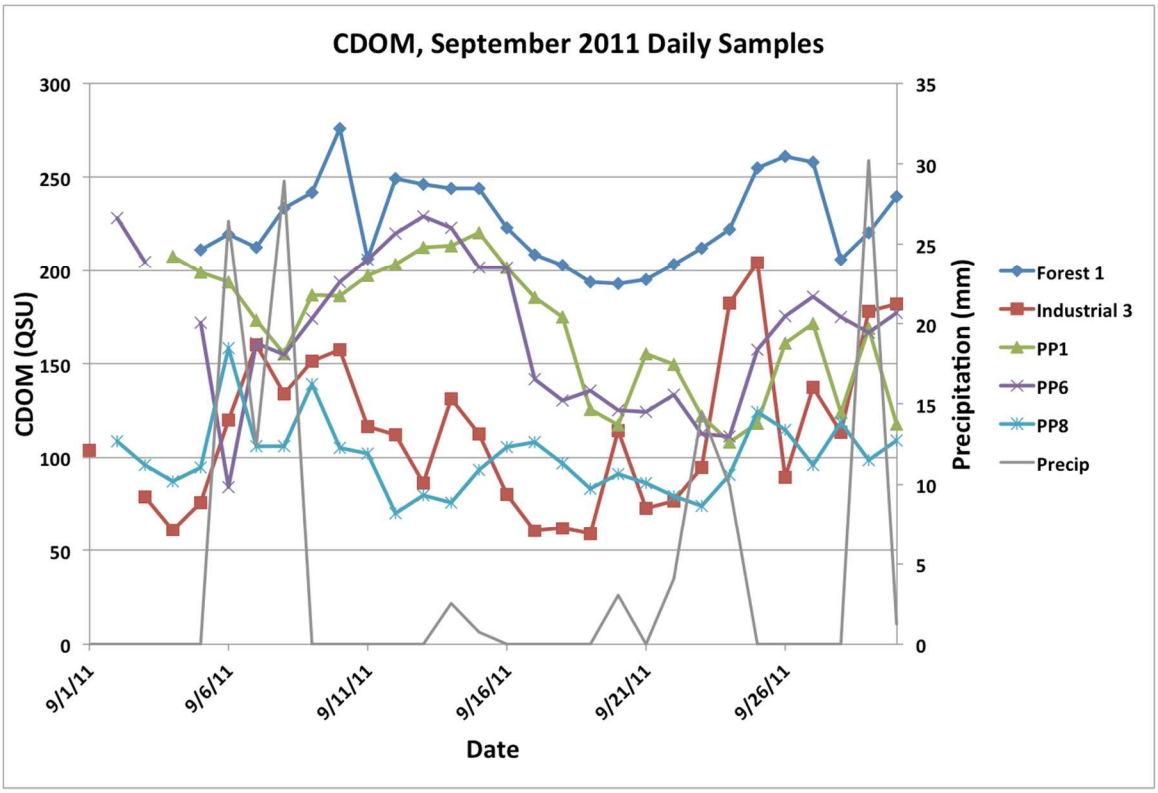

Figure 5.11: CDOM concentrations from daily samples taken at five watershed locations in September 2011

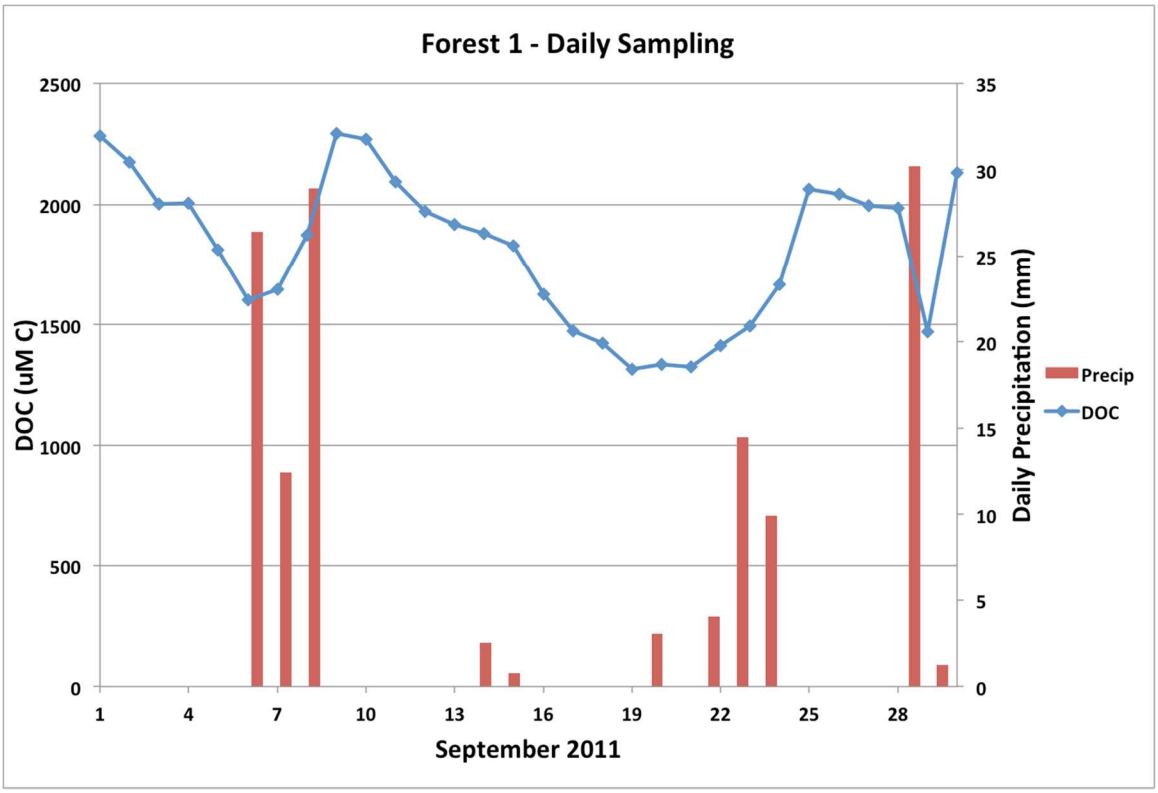

Figure 5.12: Forest 1 daily DOC concentrations during September 2011. Graph also shows daily precipitation amounts during the month

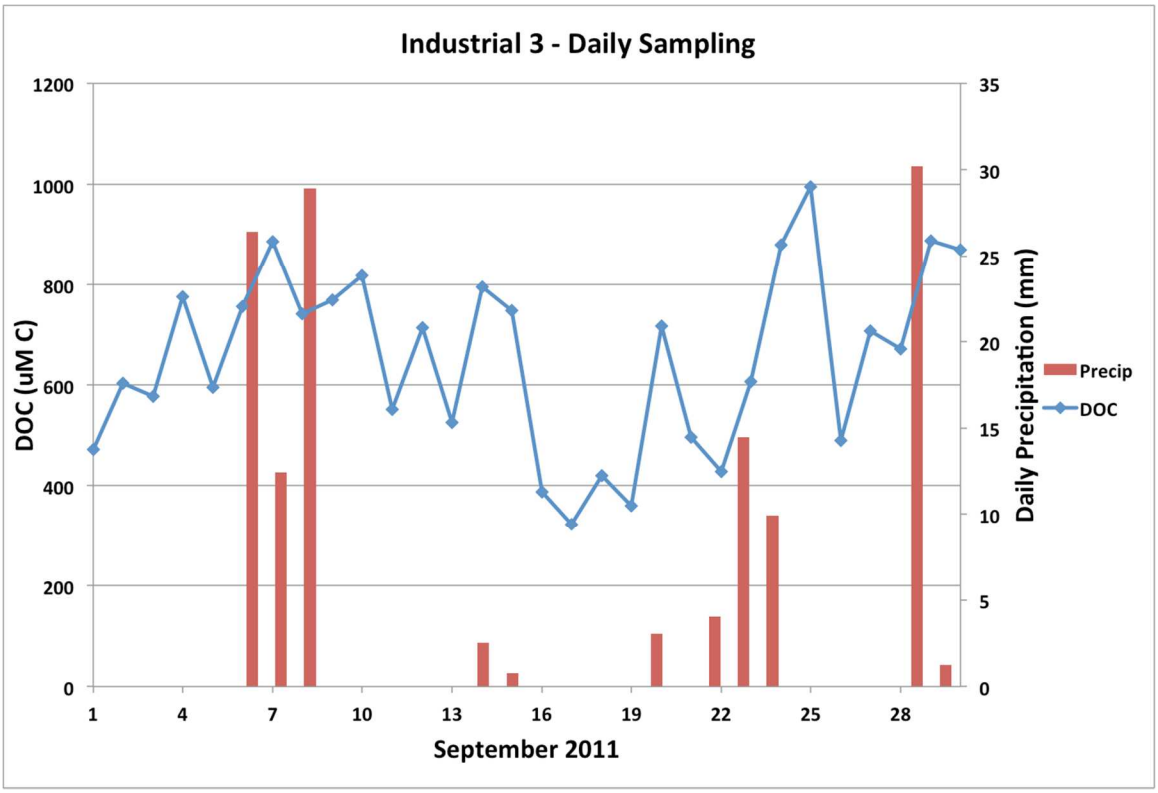

Figure 5.13: Industrial 3 daily DOC concentrations during September 2011. Graph also shows daily precipitation amounts during the month

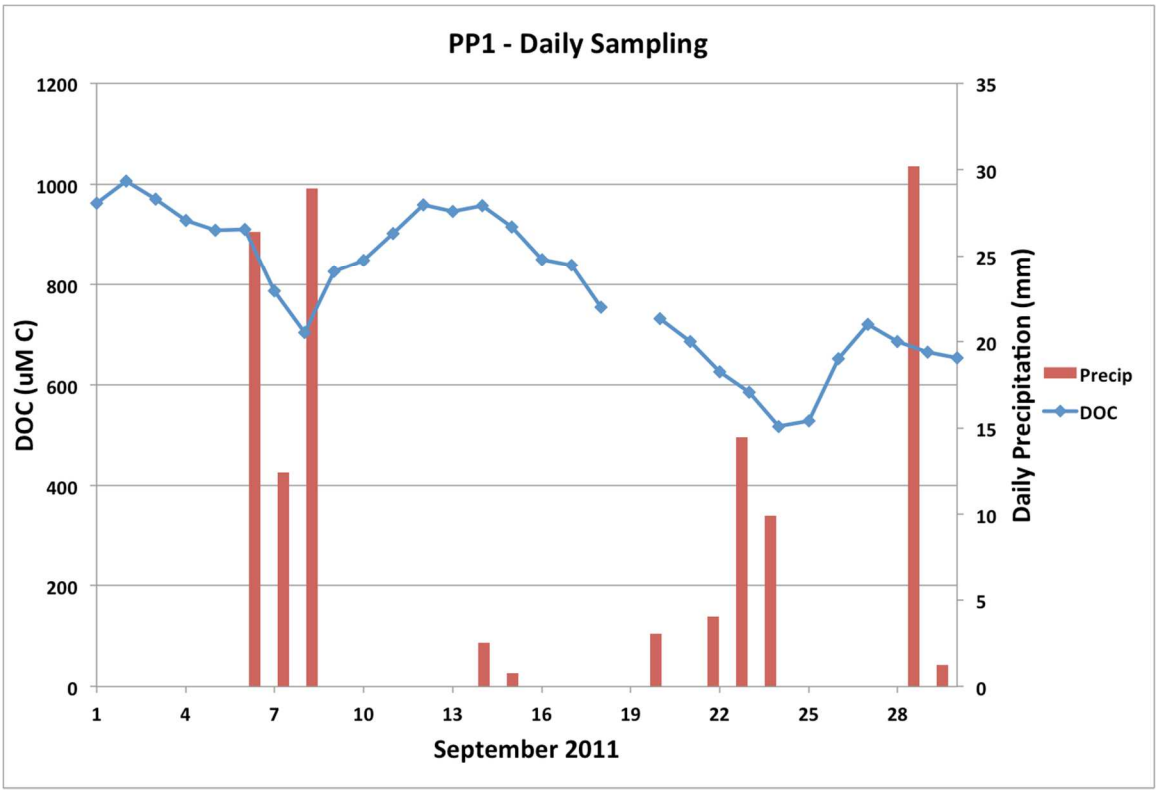

Figure 5.14: PP1 daily DOC concentrations during September 2011. Graph also shows daily precipitation amounts during the month

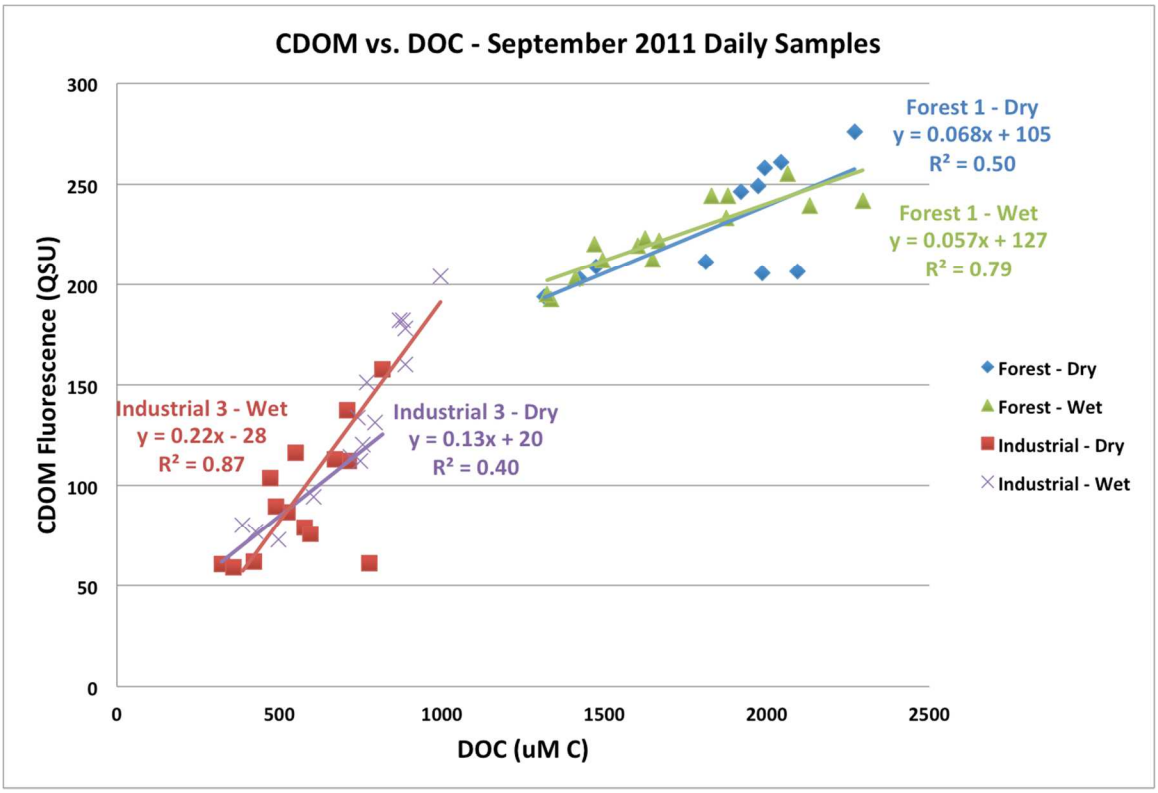

Figure 5.15: CDOM/DOC relationship from daily samples taken at five watershed locations in September 2011. Samples collected within approximately 24 hours of a rain event are labeled as "wet" samples. Dry samples were collected greater than 24 hours after a preceding storm.

During the September 6-9 storm, the maximum DOC and CDOM concentrations occur at different times at each site. Peak daily flow at PP1 occurred one day after the storm on 9/9/11. Table 5.4 shows the maximum concentration during or after the storm, and when that maximum concentration occurred. This lag may be due to the land use type(s) for each sampling site, as well as the size of the subwatershed draining through each sampling point.

Table 5.4: Peak DOC and CDOM concentrations for September 6-8 storm

Location	DOC Concentration Peak (uM C)	CDOM Concentration Peak (QSU)
Forest 1	2294; 1 day after	276; 2 days after
Industrial 3	887; during storm	160; during storm
PP1	960; 4 days after,	221; 7 days after
PP6	1121; 4 days after	229; 5 days after
PP8	659; 1 day after	158; during storm

Independent sample T-tests were utilized to compare daily sampling data from September 2011 to monthly sample data collected from 2006 through 2012 at the same five sites. Most September monthly sampling dates were classified as dry (6) or average (1), so antecedent rainfall is assumed to have a minimal impact on the comparison.

Table 5.5: Dataset comparisons using T-test p values

Sample Location	Daily Mean, Sept. 2011	Monthly Mean, Sept. 2006-2012	Two sample t-test, unequal variance, *p* value
Forest 1	1814	780	0.00082
Industrial 3	652	382	0.036
PP1	794	506	0.0079
PP6	790	462	0.024
PP8	527	454	0.15

Flux Estimates – September 2011

For September 2011, estimations of DOC flux at two sampling locations - PP1 and PP6 - were made utilizing discharge data from USGS gauge stations located at these

sites. These are the only sites within the watershed with USGS gauge stations. Using the September 2011 daily DOC concentrations and daily discharge, the September flux at PP1 was approximately 2.19 x 10^8 grams carbon. If sampling were conducted only once per month and then multiplied by the average discharge for the month, this monthly flux could be underestimated by 36% or overestimated by 23%, depending on the concentration the day that sampling was conducted.

Table 5.6: Estimated monthly DOC Flux for September 2011 at PP1 based on date DOC concentration data was obtained

Daily DOC concentrations x daily discharge	219,000,000 g C
Monthly sampling date (9/16/11)	230,000,000 g C
Monthly sampling, lowest concentration day (9/24/11)	140,000,000 g C
Monthly sampling, highest concentration day (9/2/11)	272,000,000 g C

Using the September 2011 daily DOC concentrations and daily discharge, the September flux at PP6 was approximately 1.29 x 10^8 grams carbon. If sampling were conducted only once per month and then multiplied by the average discharge for the month, this monthly flux could be underestimated by 38% or overestimated by 35%, depending on the concentration the day that sampling was conducted.

Table 5.7: Estimated monthly DOC Flux for September 2011 at PP6 based on date DOC concentration data was obtained

From daily sampling concentrations	129 x 10^6 g C
Monthly sampling date (9/16/11)	137 x 10^6 g C
Monthly Sampling, lowest concentration day (9/24/11)	80 x 10^6 g C
Monthly Sampling, highest concentration day (9/12/11)	174 x 10^6 g C

Flux Estimates – 2006-2012

Using average monthly discharge data from USGS and monthly DOC sample concentrations at PP1 (Figure 5.16), the freshwater DOC flux from the Neponset River into the Neponset Estuary was calculated from March 2006 through December 2012 (Figure 5.17). This dataset represents 78 months of complete data. Four months within this period have no DOC concentration data at PP1. Although the daily data at PP1 for September 2011 was available, it was not used in this calculation. The total estimated DOC flux during the 78 months with data is 1.42 x 10^{10} grams carbon. This is approximately 0.020 gC/m^2/day. This flux is at the low end of Yang's (2013) estimated Neponset Watershed carbon flux, which was 0.018 to 0.035 gC/m^2/day using daily flow estimates derived from a RHESSys model. If this flux has the same error shown in the September 2011 daily flux calculations, the flux could range between 0.013 and 0.028 gC/m^2/day.

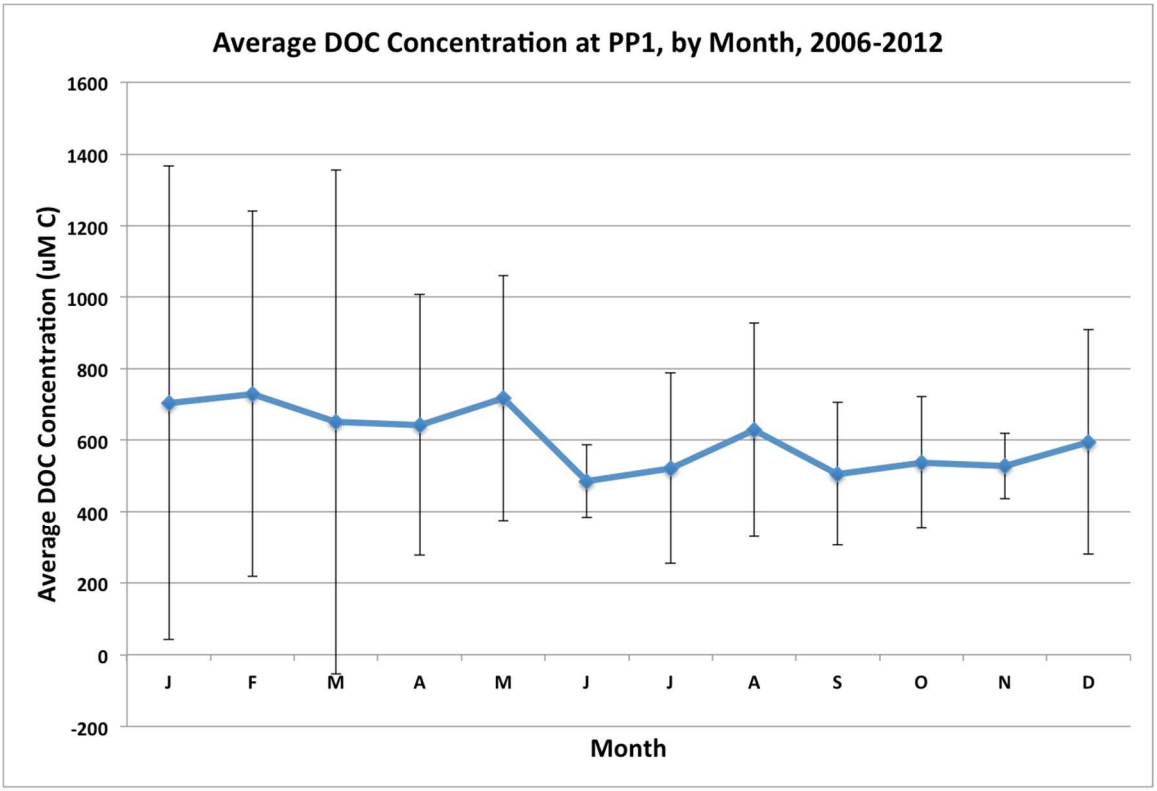

Figure 5.16: Average DOC concentration at PP1 by month, from 2006-2012. Error bars represent 1 standard deviation.

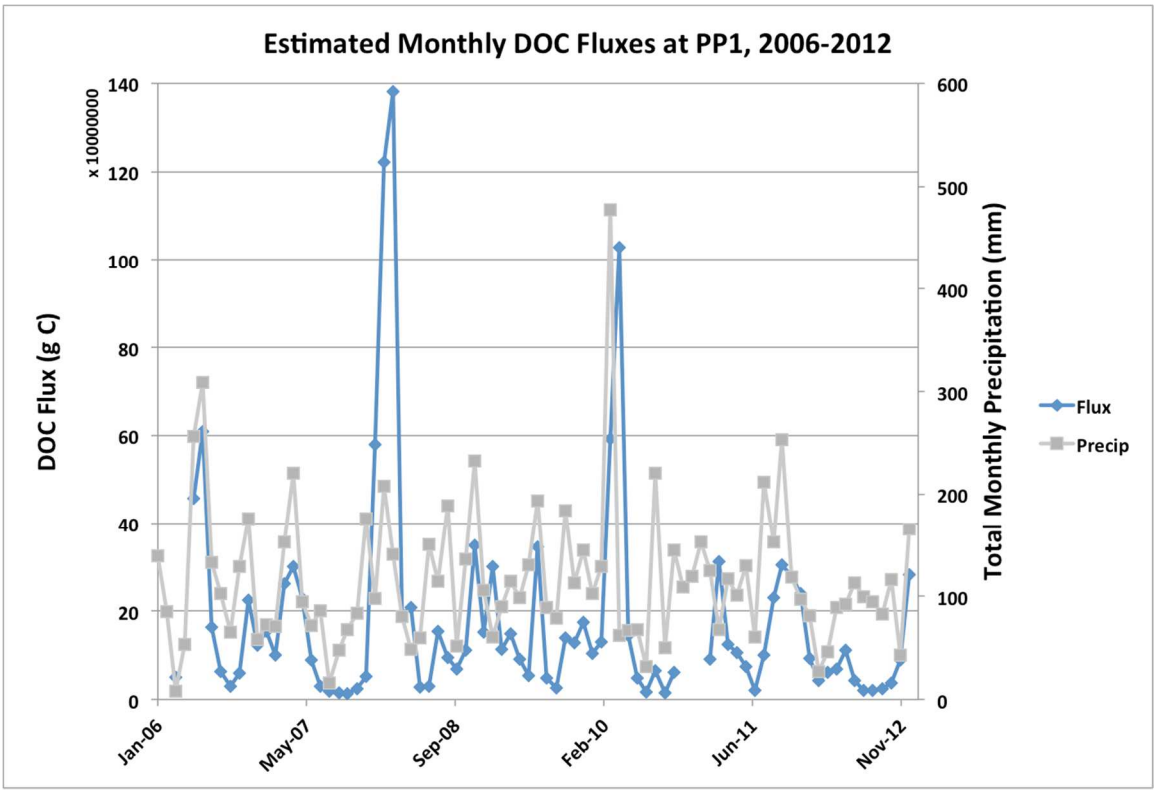

Figure 5.17: Estimated monthly DOC fluxes at PP1, March 2006 through December 2012, graphed with total monthly precipitation

The average monthly flux per year at PP1 is in Table 5.8. The average monthly flux, rather than total yearly flux, is provided to control for years with missing data. The values are comparable to the fluxes calculated with daily data in September 2011, but there are years with much higher and lower average monthly fluxes.

Table 5.8: Average monthly flux per year at PP1

Year	Avg. Monthly Flux (gC)
2006	198×10^6
2007	108×10^6
2008	369×10^6
2009	144×10^6
2010	221×10^6
2011	171×10^6
2012	74.5×10^6

5.5 Conclusions

Most studies consider a long-term data set to be 10 years or more of data (Evans et al., 2005). However, this research shows that dissolved organic carbon concentration variations may be observed on much shorter time spans. Due to the influence of rainwater runoff on DOC fluxes, weather and streamflow data can be used to determine the presence of increased or decreased fluxes. Since there is only one concentration value to represent the entire month, there is greater uncertainty in the DOC flux measurements calculated from monthly sampling data as compared to daily sampling data. The range of flux estimates using daily sample data shows the influence that variable DOC concentrations can have on flux calculations. While higher frequency sampling allows for better concentration data, and therefore better flux calculations, it also results in extra

logistical and financial considerations. Monthly sampling is better utilized to capture long-term trends, rather than short-term effects caused by stormwater runoff or snowmelt.

CHAPTER 6

SUMMARY

The purpose of this research was to determine the influence of first flush on dissolved organic carbon fluxes within the Neponset River Watershed. When the research began, it was not known if first flush was present within the watershed. By comparing high resolution samples obtained during episodic events to monthly watershed samples, the potential influence of storm events on yearly DOC fluxes was determined.

Using controlled experiments, first flush phenomena were observed on pervious (forested land) and impervious (parking lot) surfaces. Time series data suggest that first flush of dissolved organic carbon was present for all rainfall intensities during the parking lot controlled experiments. At the parking lot site, approximately 40-51% of DOC flux occurred within the first 20% of runoff. For the forested site, first flush was present in two of three simulations, but is only indicative of fluxes due to overland flow and does not capture soil water fluxes resulting from rainfall simulation. The soil fluxes would not be likely to contribute to a first flush effect, unless certain conditions were met, such as antecedent rainfall in close proximity resulting in high soil moisture. Natural land cover plays a key role in retaining water and DOC, and muting the effects of runoff caused by precipitation events.

Data collected during storm events from co-located sensors and autosamplers was used to examine the influence of stormwater runoff on riverine concentrations of dissolved organic carbon. The sensor data captured more of the riverine DOC and CDOM concentration variability present due to storm events. Storm fluxes calculated with the high resolution data show the significant impact that storm fluxes can have on DOC export from a small watershed. The calculated storm flux from 6 storms at the forested site is approximately 7.1% of the calculated annual (11 months of data) flux, which occurred during 4% of the year. The calculated storm flux from 7 storms at the industrial site is approximately 10% of the calculated yearly (10 months of data) flux, which occurred during 5% of the year.

While there are many assumptions within the flux calculations, the sampled storms represent only a fraction of the total storms that occurred during 2012 – approximately 13% (18 days sampled of 140 with precipitation). Elevated DOC concentrations may occur during the other storm events that were not sampled. With better monitoring data, the full influence of storms on riverine DOC concentrations and annual fluxes could be assessed.

When utilizing monthly data for DOC flux calculations, there is only one concentration value to represent the entire month, which results in greater uncertainty in DOC flux calculations. Based on daily samples collected in September 2011, monthly flux estimates in the Neponset River can be underestimated by 38% or overestimated by 35% when only one DOC concentration value is used. While higher frequency sampling provides more concentration data, and therefore more accurate flux calculations, it also

results in extra logistical and financial challenges. High resolution sampling better captures short-term effects caused by stormwater runoff or snowmelt. Monthly sampling should be utilized to capture long-term trends, on the scale of 10 years or greater. Monthly samples can also be used to observe seasonal trends, assess land use change effects on riverine constituents, and calibrate high resolution sensor measurements.

Connectivity

Hydrologic connectivity within the watershed is demonstrated by each component of this research. At the beginning of the simulated rain experiments, pooling of runoff was noticed in the parking lot (impervious) plot. Additional rain caused the pool to fill up and spill over, connecting the contents of the pool with the rest of the plot watershed and contributing to runoff at the collection point. Small concentration increases observed in the second and third runoff samples may be due to this process.

This same process seems to be present during storms within the Industrial 3 subwatershed (see Figures 4.18 and 4.20). After precipitation ends, there are additional concentration increases that are observed at the sampling point. This may be the result of a "pool" within the Industrial 3 subwatershed that gradually filled up with runoff from the storm, and was then released. The pool is not connected until a threshold is reached. This pool could be a storm drain retention basin, a wetland, or a more distant portion of the subwatershed. The delay in reaching the sampling point is related to the time of concentration of the subwatershed.

This complexity is also visible in the CDOM-DOC plot of all the Forest 1 and Industrial 3 discrete samples collected in 2012 (Figure 4.31). The relationship for Forest 1 is fairly consistent. However, the Industrial 3 data shows variability, which may be the result of the two disparate water sources hypothesized above.

Monthly samples are unable to capture the large range of concentrations that occur at a site during and after a storm. The different connectivities, and therefore time of concentration values, for each subwatershed are missed when only one sample is taken per month. During daily sampling of five locations in September 2011, concentration peaks following storms occurred at different times. Table 5.4 shows the maximum concentration during or after the storm, and when that maximum concentration occurred. The time lag may be due to the land use type(s) for each sampling site, as well as the size of the subwatershed draining through each sampling point. Also, assumptions are made in this research that precipitation data at Blue Hill Meteorological Observatory is representative of rainfall within the entire Neponset Watershed boundary. Most likely, this is not true, and some of the sampled subwatersheds may have received more or less rain, at different intensities, than those recorded at Blue Hill. This results in increased or decreased connectivity when compared with other subwatersheds within the Neponset Watershed.

Local Implications

This research shows the influence of storm events on local bodies of water. This information may be of use to local managers in order to implement controls for runoff

from impervious surfaces. The use of stormwater best management practices, such as bioretention cells, permeable pavers, and infiltration trenches (U.S. Environmental Protection Agency, 2012), would lead to reduced runoff entering local waterways. In the context of this research, this would also result in better water quality due to reduced fluxes of DOC to local bodies of water. Since DOC has multiple water quality effects, including complexation with heavy metals, water quality would be improved.

Broader Implications

Dai et al. (2012) used data from 118 rivers with available DOC concentrations to estimate global DOC fluxes. This calculation excluded small rivers that account for 52% of global riverine discharge. The results of this dissertation could assist with global carbon estimates, as they show the influence that episodic events can have on small rivers. For watersheds with similar land use and within similar climates, the potential influence of small rivers could be under- or overestimated by 30% or more, based on daily Neponset River sampling data from September 2011. However, additional investigation is needed to determine whether this variability is also present in other months or years.

Dissolved organic carbon fluxes may increase in coastal watersheds due to population growth and climate change. In 2010, approximately 39 percent of the United States' population lived in coastal areas. This population is expected to increase by an additional eight percent (10 million people) by 2020 (National Oceanic and Atmospheric Administration, 2012). Additional population pressure may result in land use change. As

demonstrated by this research, impervious surfaces result in greater fluxes of DOC to coastal areas.

Climate change is expected to increase riverine carbon fluxes due to changes in river discharge, sea-level height, and/or the severity and frequency of storms, and will also lead to increased variability in these fluxes (Evans et al., 2005; Dai et al., 2012). By controlling runoff through stormwater best management practices, more carbon could be stored within watersheds, thereby reducing carbon export to the oceans. If implemented globally, these runoff controls could increase the amount of carbon stored within soils. Most of the diverted carbon that would be stored in the soil is likely stored only temporarily. Increasing nutrients within watershed soils could lead to increased primary productivity and respiration, and these temporary sinks are still part of the active carbon pool. Things like deforestation, forest fires, and land use change could release these sinks.

While the data presented here cannot be extrapolated to other watersheds, some general trends may apply to other watersheds. First flush of DOC may be observed in watersheds with large impervious surface areas. Large first flushes with high DOC concentrations will occur during rain events following extended dry periods. This will be even more pronounced in regions where rain primarily occurs in the spring or fall. Wet climates may also have frequent first flushes due to high soil moisture content causing increased overland flow during storms.

Future studies

Monthly sampling should continue within the Neponset Watershed in order to assess long-term trends, such as interannual variability, climate change, and land use change. Large amounts of data that were collected during this research were not presented here, and further analysis of this data should be pursued. For example, total nitrogen concentrations for all of the DOC samples are available. Additional DOC quality analyses not presented here are also available. Data collected during this research and from Huang and Chen (2009) could be utilized to include the watershed in any future estimates of DOC export from small rivers.

This research is the first use of a rainfall simulator to test for the presence of a DOC first flush on various land use types. The rainfall simulator design is easily replicated and could be utilized to test for first flush of dissolved organic carbon from other land use types or in different climates. Prior to redeployment, the simulator should be retested for rainfall volume. Initial volumes measured from the nozzle were equal to the desired rainfall intensities for the experiments. However, based on runoff rates at the parking lot collection point, it appears that the 12.7 mm hr^{-1} and 6.35 mm hr^{-1} rain rates had intensities closer to 9.9 mm hr^{-1}. The 25.4 mm hr^{-1} rain rate may have had an intensity of approximately 45 mm hr^{-1}. In addition, testing other nozzle types may result in more even drop dispersion over the test plot.

The simulator could also be used to test for first flush of other dissolved and particulate constituents in runoff. Future work on permeable surfaces should include measurement of soil moisture before, during, and after simulated rainfall. This would

enable better assessment of the impact of antecedent rainfall on runoff volumes and concentrations. Future work should also investigate subsurface flows. This research estimates that only about 1% of simulated rainfall on a forested plot was captured as runoff. This may also be true for natural storms. The fate of the other 99% of precipitation is important for determining the influence of precipitation-driven groundwater fluxes to rivers.

The use of optical sensors to determine CDOM concentrations is unique for measuring DOC concentrations during storm events. By placing a CDOM sensor at each USGS gauging station, more precise estimates of DOC flux to coastal ecosystems could be obtained. Coupled with regular discrete sampling this would lead to better estimates of the contribution of small watersheds to the global carbon cycle. This would eliminate the remaining uncertainty around riverine DOC flux estimates. The results would also show the responses of different watersheds to runoff from storm events. This would allow decision-makers to implement stormwater best management practices in targeted watersheds.

APPENDIX A

SAMPLING LOCATION INFORMATION

Table A.1: Rain simulator locations

Site name	Latitude	Longitude	Location Description
Forested site	42.22116	-71.09069	Within Blue Hills Reservation
Parking lot site	42.31724	-71.03846	UMass Boston parking lot D

Table A.2: Sensor/autosampler locations

Site name	Latitude	Longitude	Watershed Size (km^2)	Characteristics
Forest #1	42.19228	-71.24872	1.96	>80% forested land use; remainder is a mix of low or very low density residential, forested wetland, and crop land
Industrial #3	42.16361	-71.15998	1.4 (approx.)	Mix of industrial, commercial, forest, and medium density residential land use types

Table A.3: Monthly sampling locations

Site name	Latitude	Longitude	Sampling period	Number of monthly samples
Forest #1	42.19228	-71.24872	3/2006-12/2012	82
Forest #2	42.22778	-71.09574	1/2007-12/2012	72
Forest #3	42.12481	-71.25144	1/2007-12/2012	74
Forest #4	42.12744	-71.18833	1/2007-	61

			12/2012	
Golf #1	42.13351	-71.23286	5/2006-12/2012	75
Golf #2	42.26776	-71.13180	1/2007-12/2012	72
Golf #3	42.23487	-71.07458	1/2007-12/2012	72
Ind #1	42.15573	-71.11398	3/2006-12/2012	84
Ind #2	42.11453	-71.24492	1/2007-12/2012	59
Ind #3	42.16361	-71.15998	1/2007-12/2012	66
Res #1	42.17310	-71.25820	3/2006-12/2012	82
Res #2	42.17360	-71.15397	1/2007-12/2012	73
Wetland #1	42.19078	-71.27366	3/2006-12/2012	67
Wetland #3	42.18032	-71.17419	1/2007-12/2012	56
Wetland #4	42.22955	-71.12372	1/2007-12/2012	49
Motherbrook	42.25500	-71.16472	11/2008-12/2012	52
PP #1	42.27064	-71.06831	3/2006-12/2012	84
PP #2	42.26532	-71.07457	3/2006-12/2012	85
PP #3	42.25094	-71.12650	3/2006-12/2012	82
PP #4	42.24404	-71.09317	3/2006-12/2012	84
PP #6	42.20910	-71.14574	3/2006-12/2012	84
PP #7	42.19760	-71.15679	3/2006-12/2012	83
PP #8	42.17613	-71.21716	3/2006-12/2012	85
PP #9	42.17287	-71.20442	3/2006-12/2012	76
PP #10	42.15996	-71.19552	3/2006-	84

			12/2012	
PP #11	42.15869	-71.15504	3/2006-12/2012	85
PP #12	42.14603	-71.10405	3/2006-12/2012	82
PP #13	42.13291	-71.17724	3/2006-12/2012	83
PP #14	42.12482	-71.16059	3/2006-12/2012	84
PP #15	42.11817	-71.25663	3/2006-12/2012	81
PP #16	42.11542	-71.23927	3/2006-12/2012	82

APPENDIX B

DATA COLLECTED DURING STORM EVENTS – CHAPTER 4

Event 1: 5/8-5/11/12 storm event

Forested site DOC concentrations are higher than at the industrial site throughout the event period. However, industrial site DOC concentrations are more variable, which could be driven by runoff generated by the precipitation (Figure B.1). Industrial CDOM concentrations start lower than at the forested site but fluctuate throughout the sampling period to values higher than the corresponding forest samples (Figure B.2). The CDOM versus DOC relationship is stronger for the industrial site (Figure B.3). The absorbance coefficients increase at the forested site as precipitation starts (Figure B.4). Spectral slope ratios decrease at the forested site as the precipitation starts, while ratios are consistent throughout the sampling period for the industrial site (Figure B.5). For CDOM fluorescence sensor data, the cleaning after the storm results in higher values at the forested site (Figure B.6). The sensor data at the industrial site tracks runoff influxes better than the discrete samples. A high peak is observed at the industrial site after precipitation has ended (Figure B.7). There is no noticeable rain effect observed at the forested site.

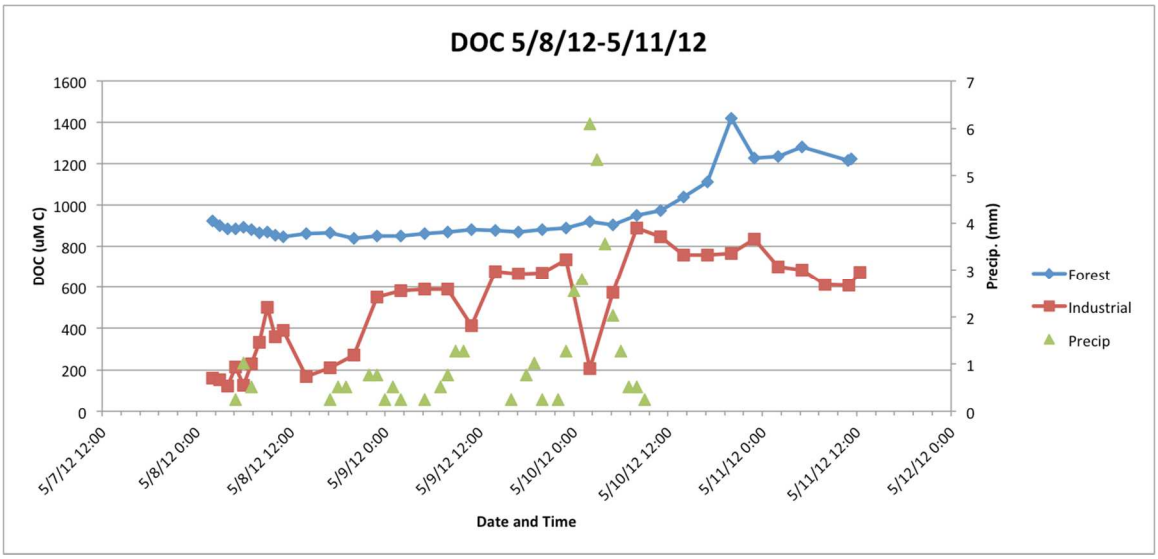

Figure B.1: Discrete samples showing DOC concentration over time

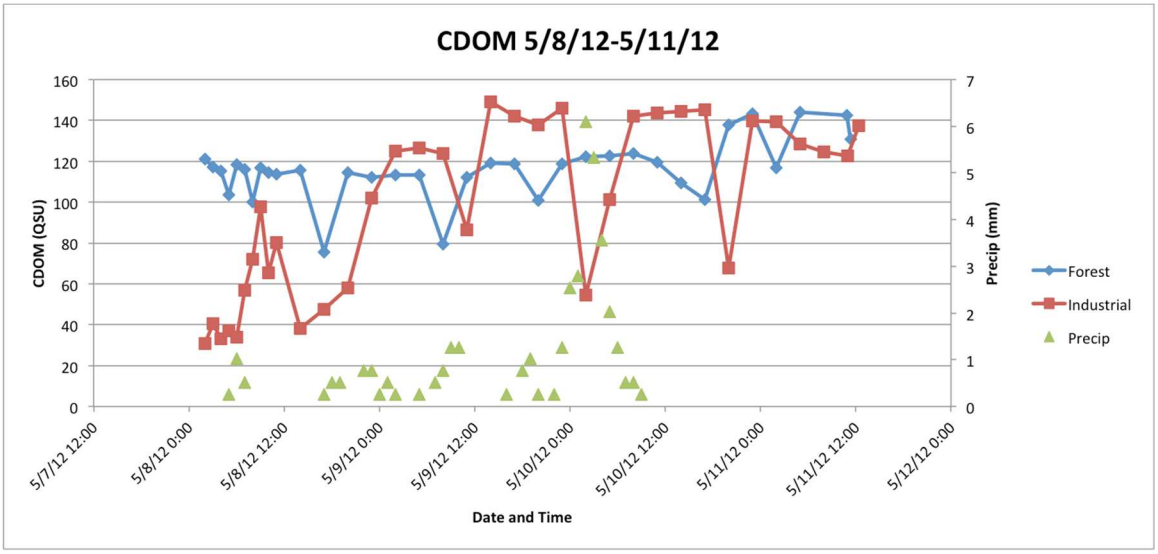

Figure B.2: Discrete samples showing CDOM concentration over time

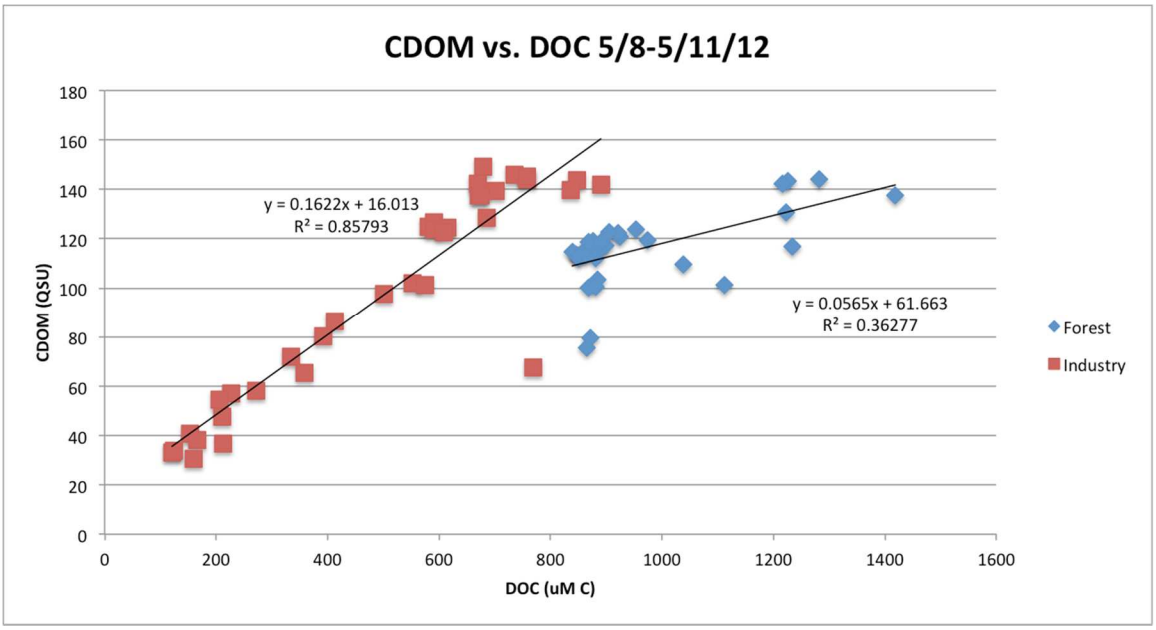

Figure B.3: CDOM versus DOC

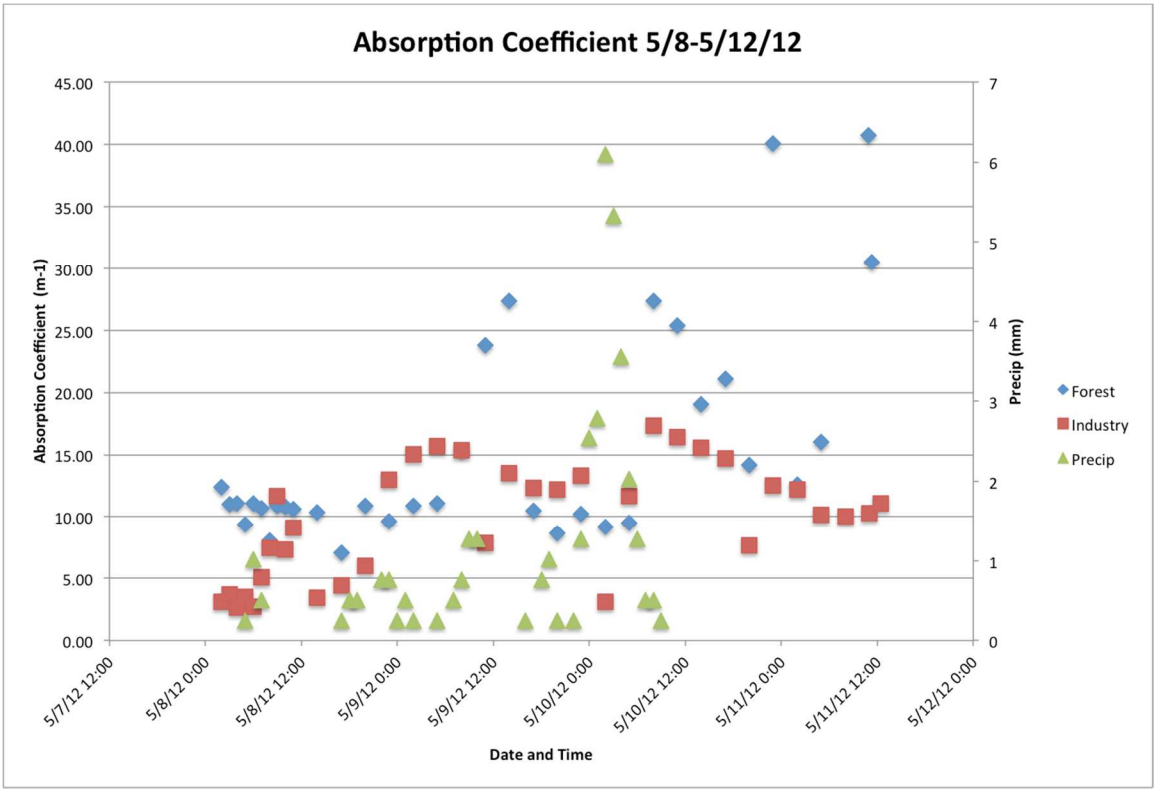

Figure B.4: Absorption coefficients for discrete samples

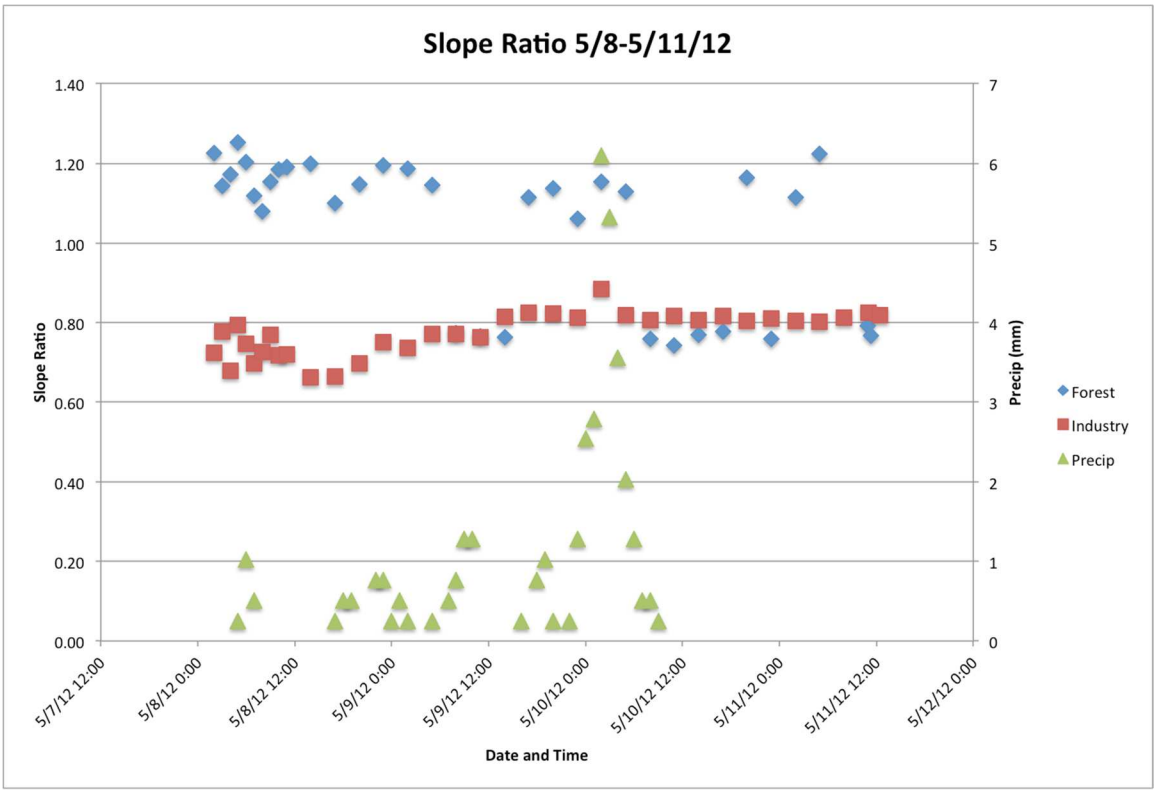

Figure B.5: Spectral slope ratios for discrete samples

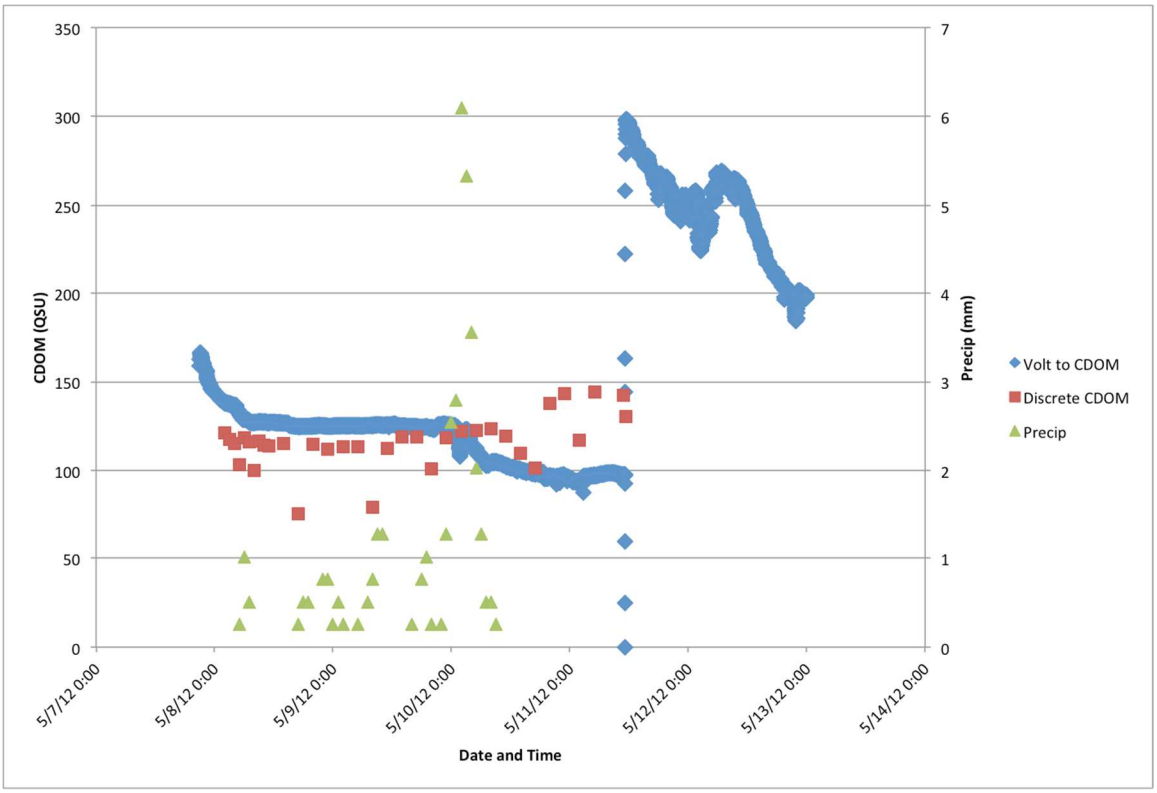

Figure B.6: Forested site sensor data and discrete samples shown on the same axis. The discontinuity on May 11 is the result of routine sensor cleaning.

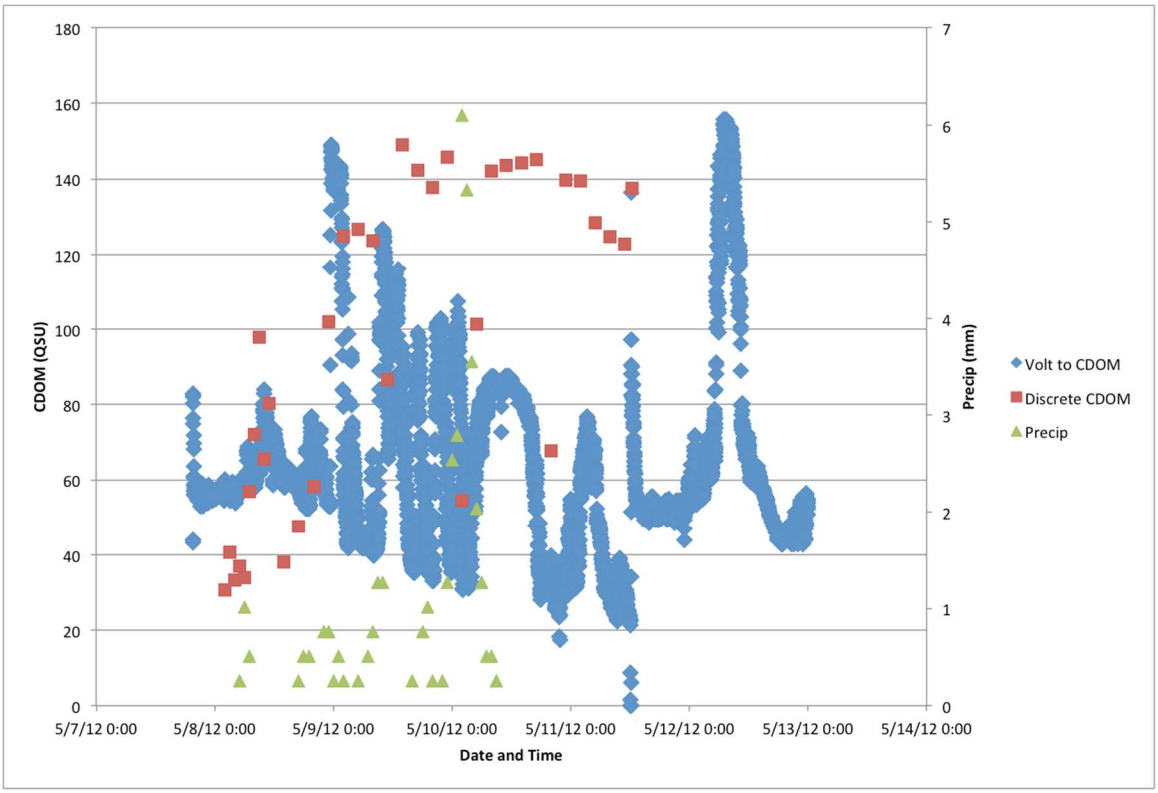

Figure B.7: Industrial site sensor data and discrete samples shown on the same axis.

Event 2: 6/12-6/14/12 storm event

Forested site DOC concentrations are higher than at the industrial site throughout the event period. There is a large peak in industrial site DOC concentration at the beginning of the storm (Figure B.8). Forest CDOM concentrations are generally decreasing throughout the sampling period, while industrial site concentrations are more variable with the influx of precipitation (Figure B.9). The CDOM versus DOC relationship is stronger for the industrial site (Figure B.10). The absorbance coefficients at the forested site are high throughout the sampling period, whereas the absorbance coefficients are very low at the industrial site (Figure B.11). Spectral slope ratios are consistent at the forested site, while there is variability at the industrial site, with increasing ratios as the precipitation starts (Figure B.12). For CDOM fluorescence sensor data, there is no usable sensor data at the forested site. The sensor data at the industrial site tracks runoff influxes well (Figure B.13). At the industrial site, there appears to be a dilution effect with rainfall amounts greater than about 1.5 mm per hour (Figure B.14). There is a slight decrease in the forested site discrete sample concentrations with precipitation.

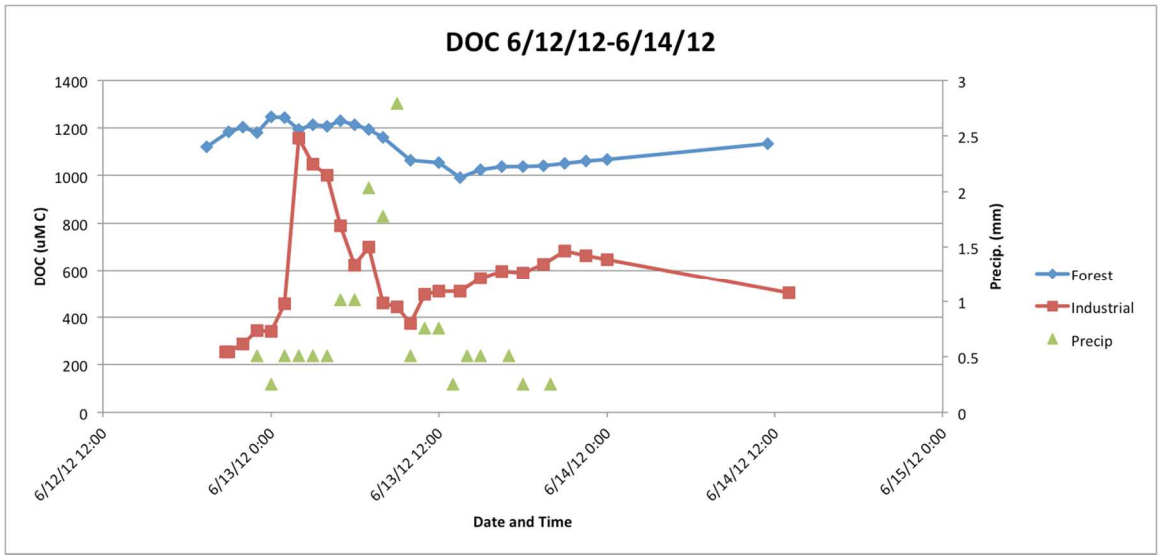

Figure B.8: Discrete samples showing DOC concentration over time

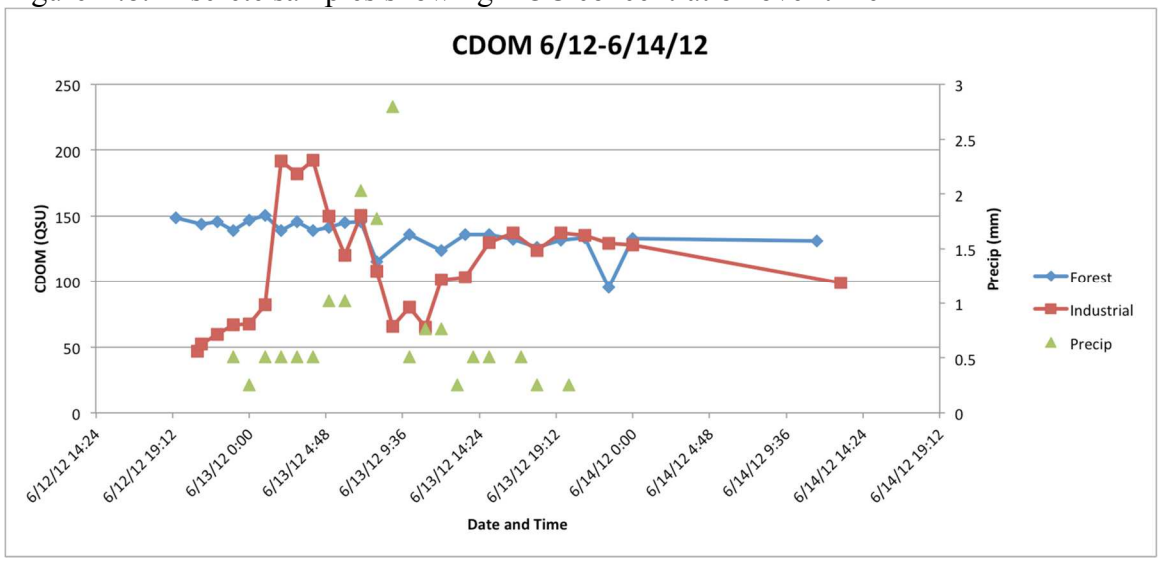

Figure B.9: Discrete samples showing CDOM concentration over time

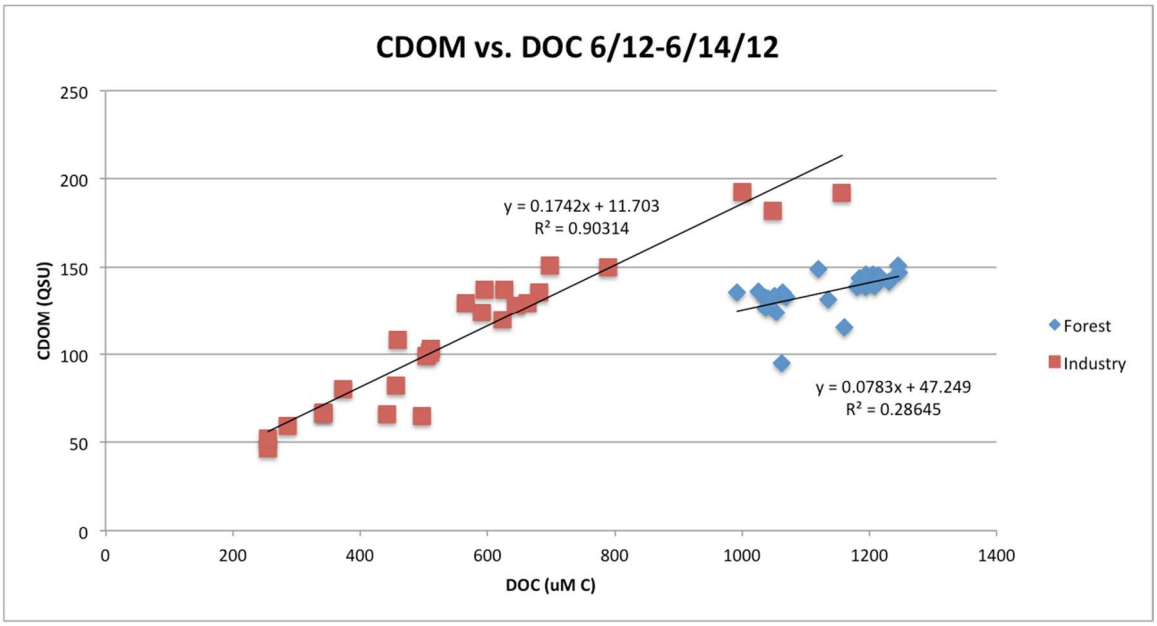

Figure B.10: CDOM versus DOC

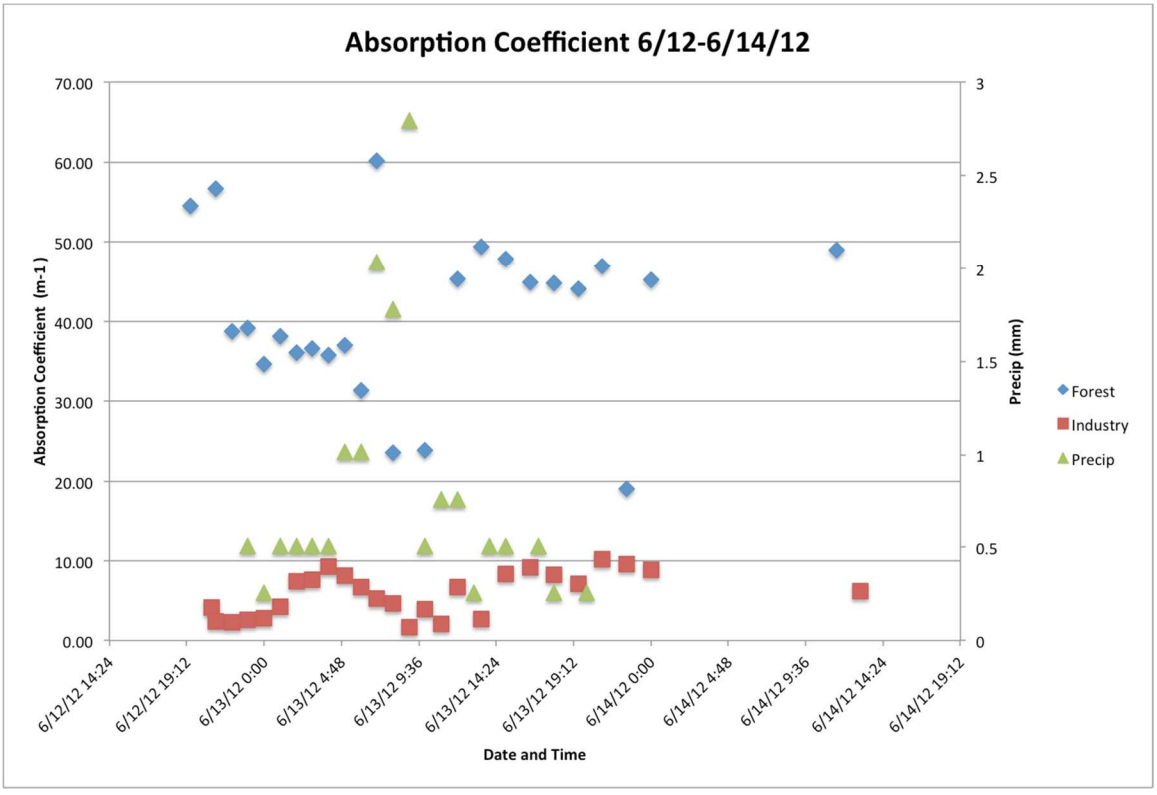

Figure B.11: Absorption coefficients for discrete samples

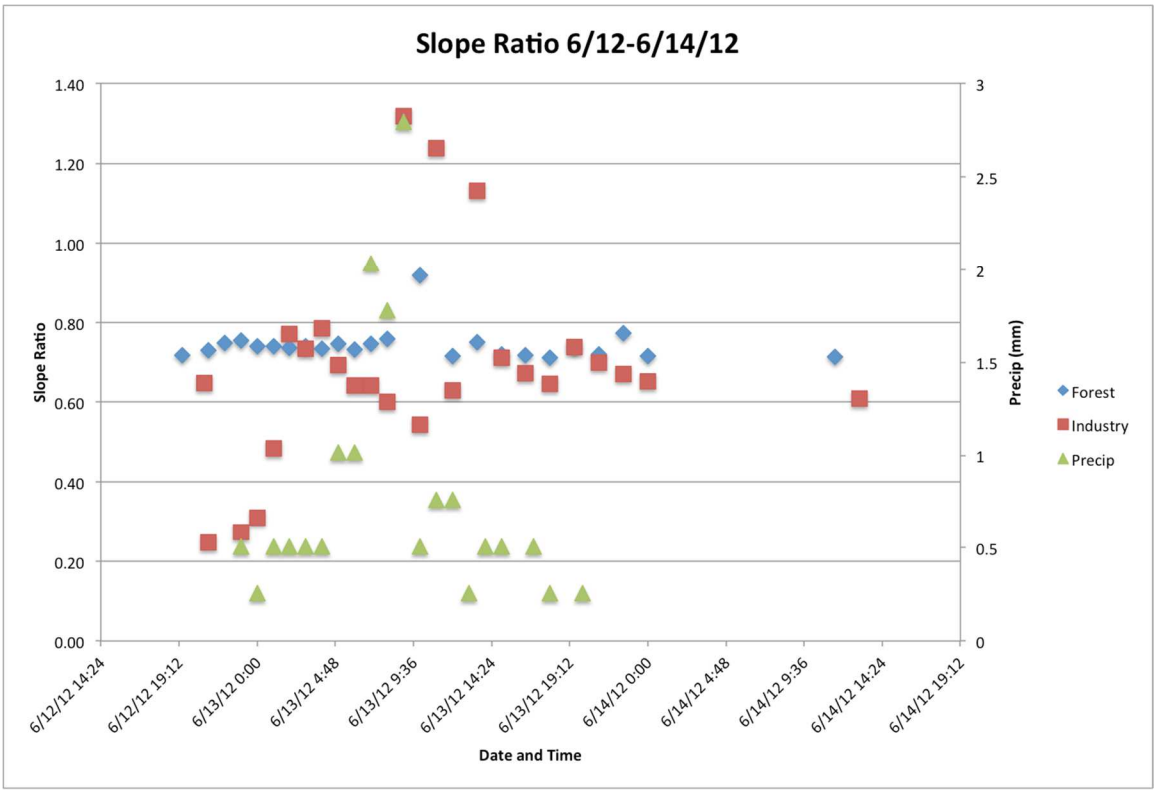

Figure B.12: Spectral slope ratios for discrete samples

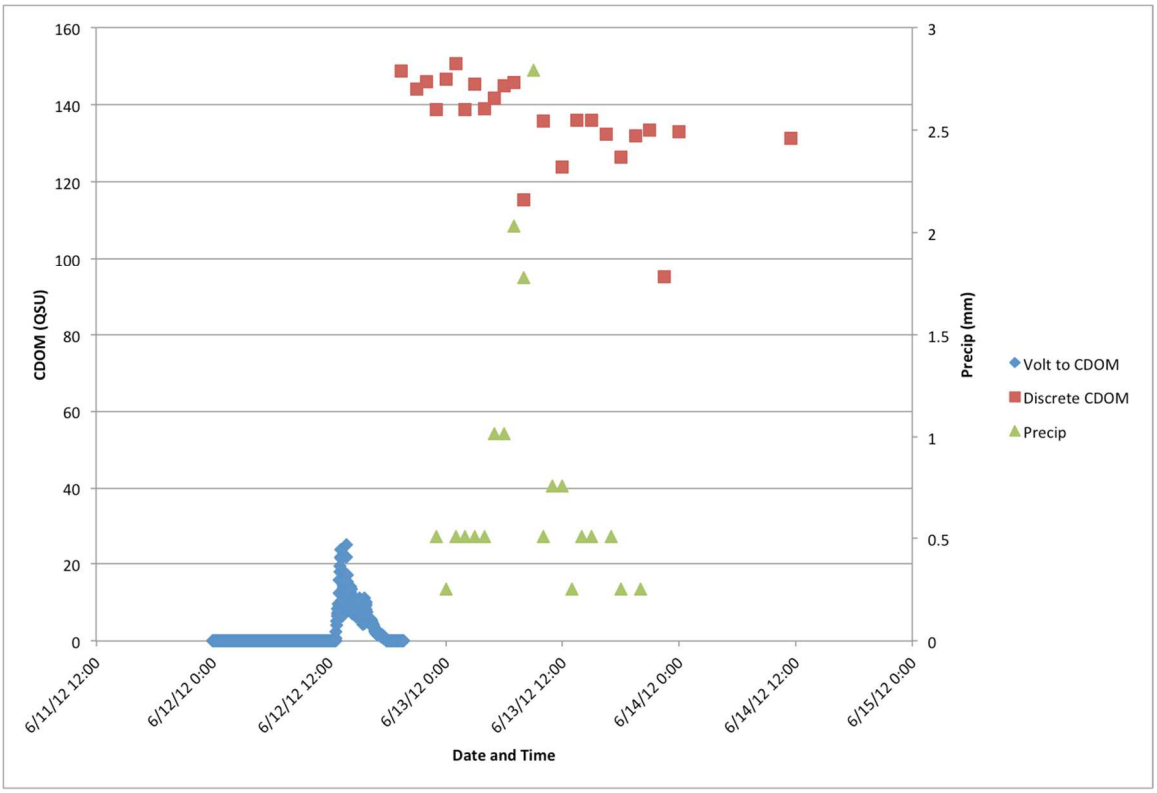

Figure B.13: Forested site sensor data and discrete samples shown on the same axis

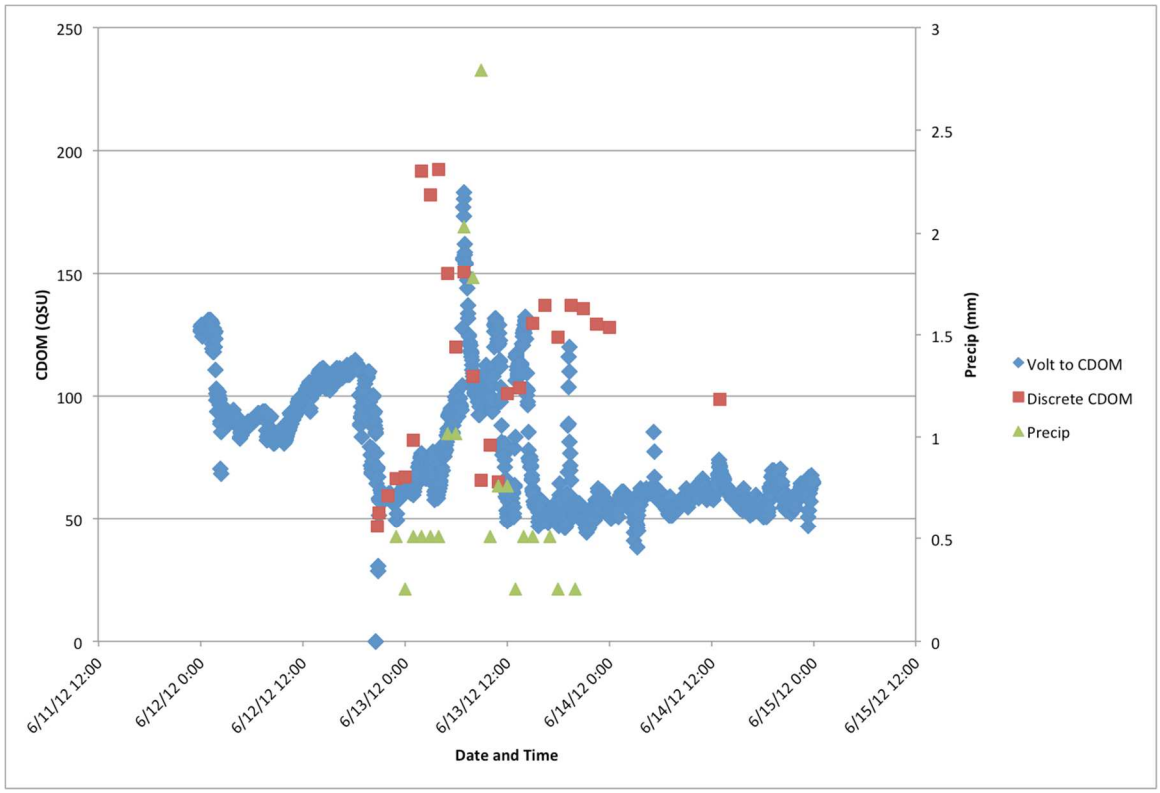

Figure B.14: Industrial site sensor data and discrete samples shown on the same axis

Event 3: 7/18-7/19/12 storm event

Forested site DOC and CDOM concentrations are consistent throughout the event period. There are only a few industrial discrete samples, but they are much higher concentrations than the forested site samples (Figures B.15 and B.16). The CDOM versus DOC relationship is much stronger for the forested site (Figure B.17). The absorbance coefficients generally decrease at the forested site, while in contrast the industrial site is variable during the sampling period (Figure B.18). Spectral slope ratios are similar for both sampling locations (Figure B.19). For CDOM fluorescence sensor data, the cleaning after the storm results in higher values at the forested site. The relationship between sensor data and discrete samples is good. The sensor data at the forested site shows some dilution with precipitation (Figure B.20). The industrial site sensor data shows a large storm influence. Concentrations return to pre-storm levels in about 24 hours after the storm ends (Figure B.21).

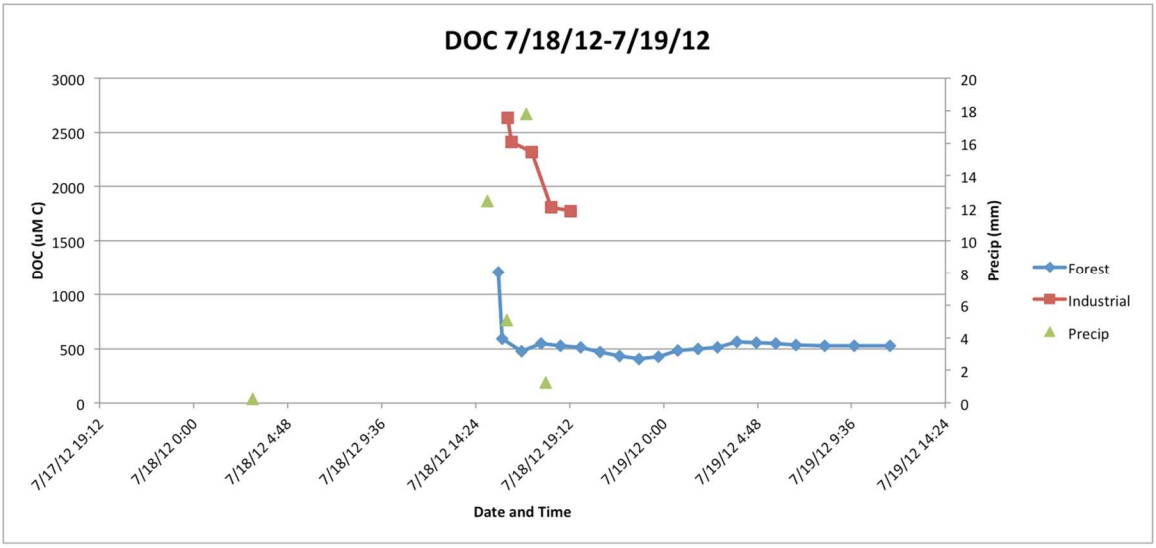

Figure B.15: Discrete samples showing DOC concentration over time

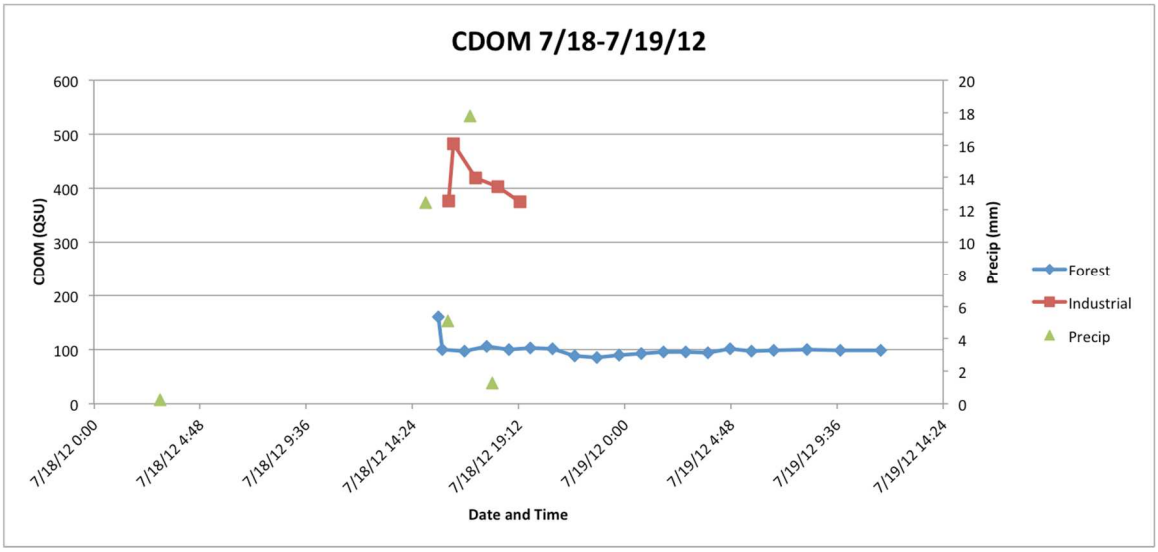

Figure B.16: Discrete samples showing CDOM concentration over time

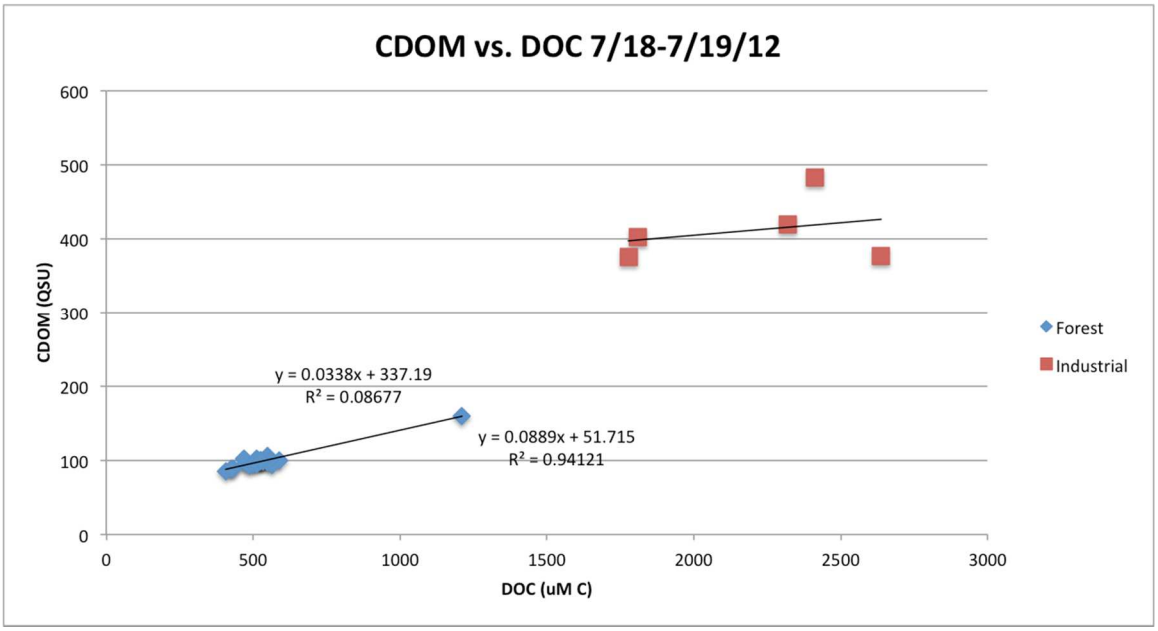

Figure B.17: CDOM versus DOC

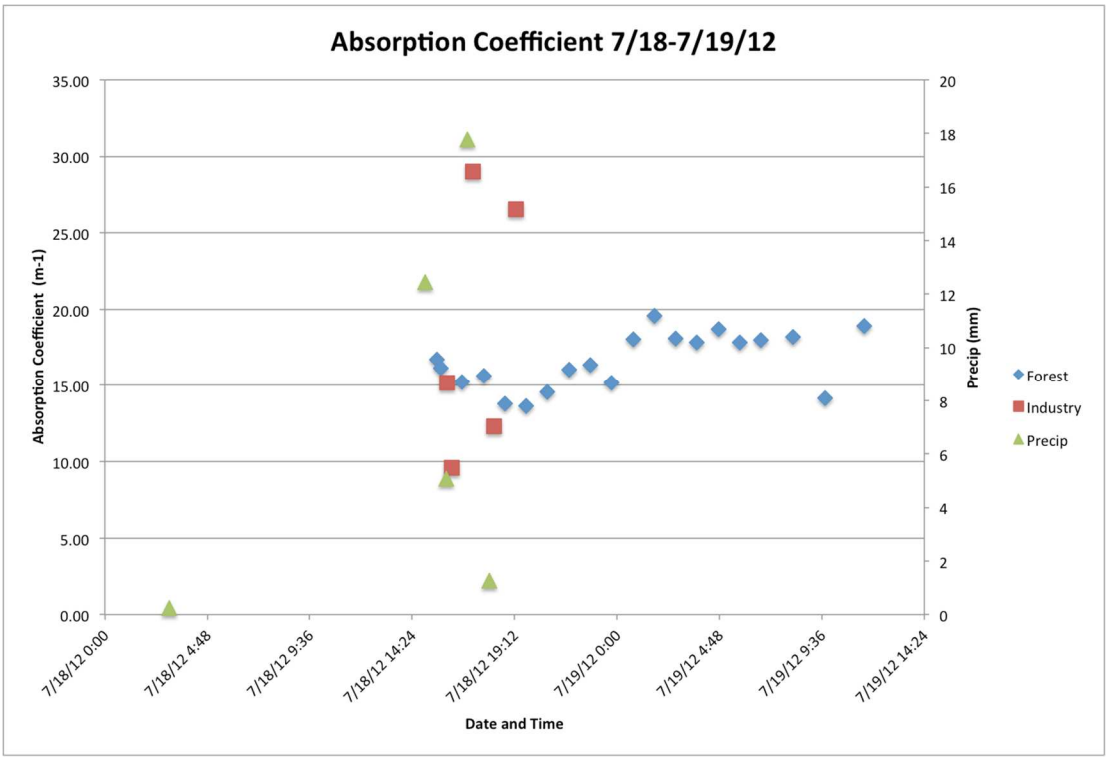

Figure B.18: Absorption coefficients for discrete samples

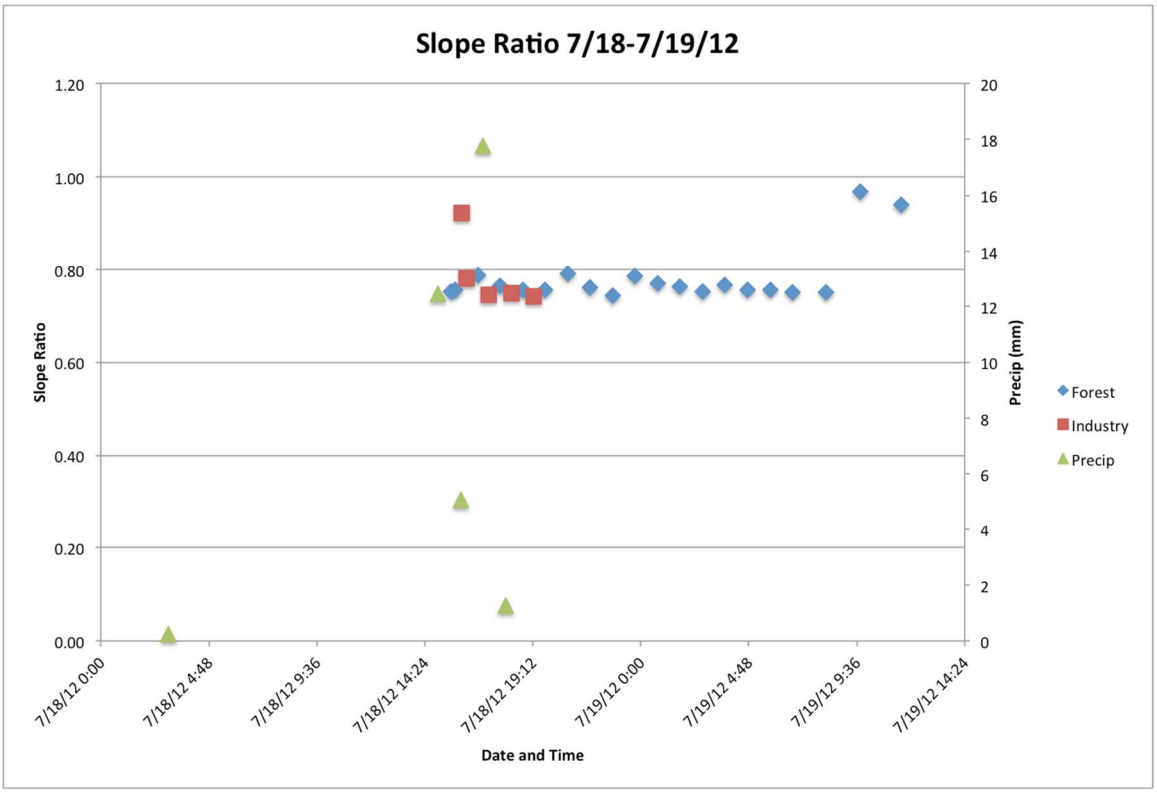

Figure B.19: Spectral slope ratios for discrete samples

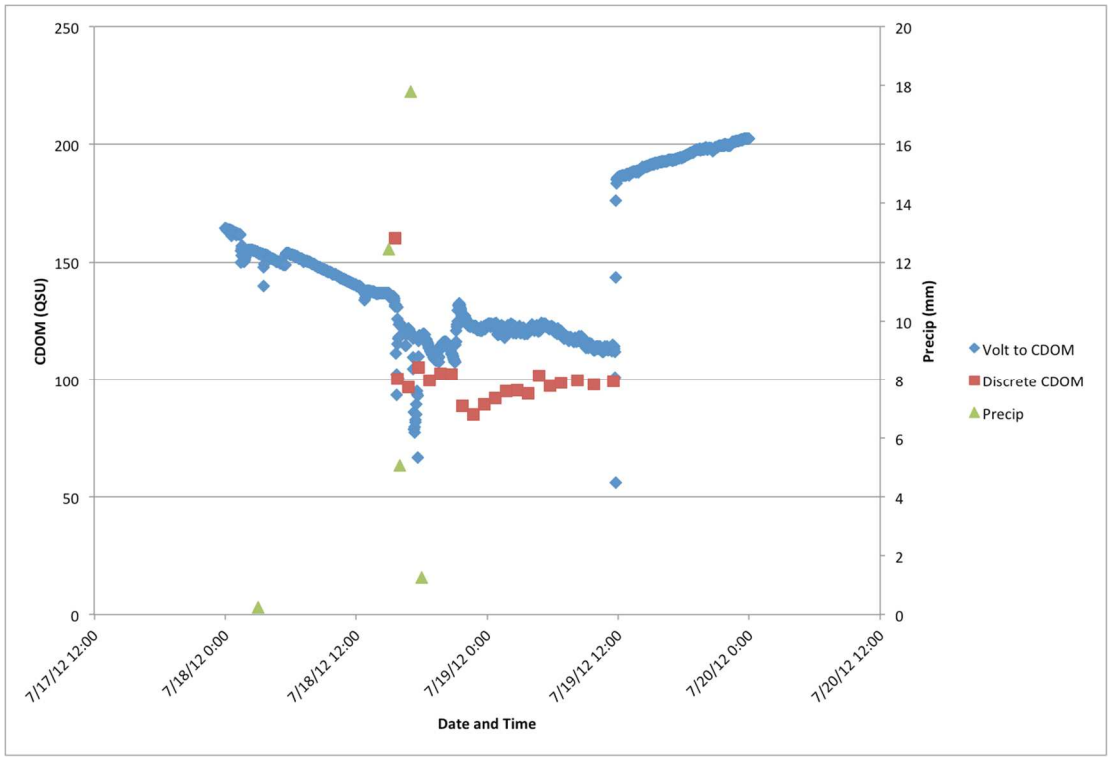

Figure B.20: Forested site sensor data and discrete samples shown on the same axis

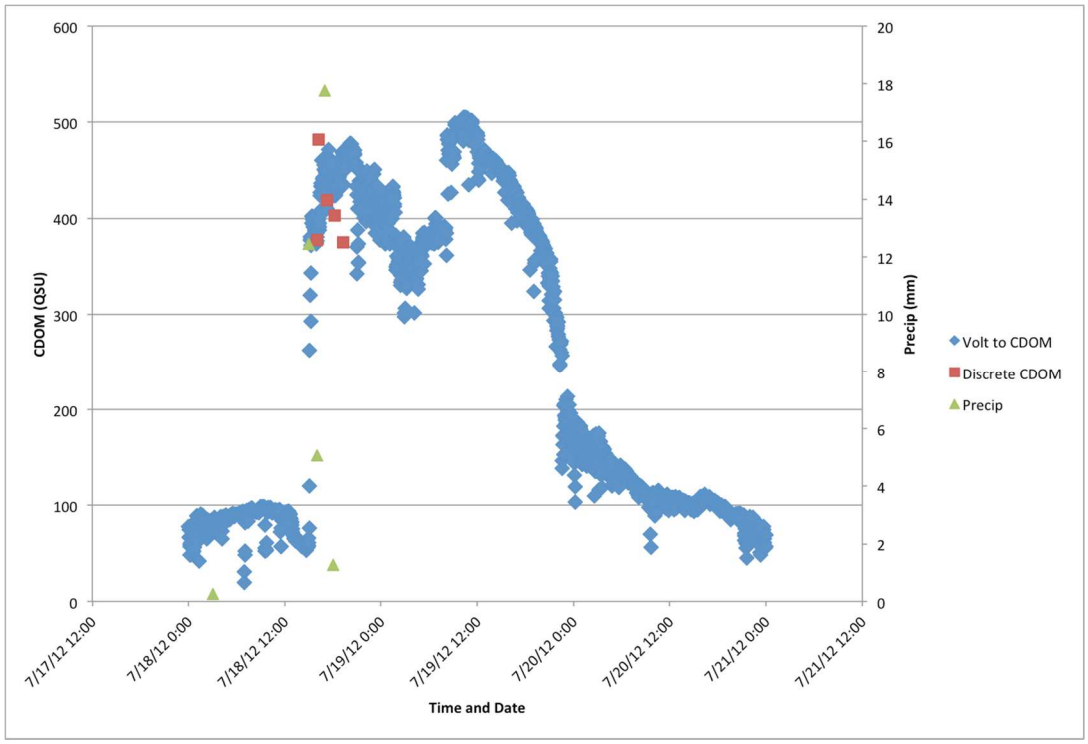

Figure B.21: Industrial site sensor data and discrete samples shown on the same axis .

Event 4: 8/27-8/28/12 storm event

Forested site DOC and CDOM concentrations are consistent throughout the event period. Industrial site DOC and CDOM concentrations start high, and decrease during the storm due to dilution (Figures B.22 and B.23). The CDOM versus DOC relationship is strong at both sites (Figure B.24). The absorbance coefficients increase after the storm, with a dilution effect during the storm (Figure B.25). Spectral slope ratios show a decreasing trend over time for both sampling locations (Figure B.26). At the forested site, concentrations vary during the storm and the CDOM fluorescence sensor data shows this (Figure B.27). At the industrial site, no sensor data was collected during the storm due to a dead battery. Sensor data for the period after the storm shows concentrations continuing to increase (Figure B.28).

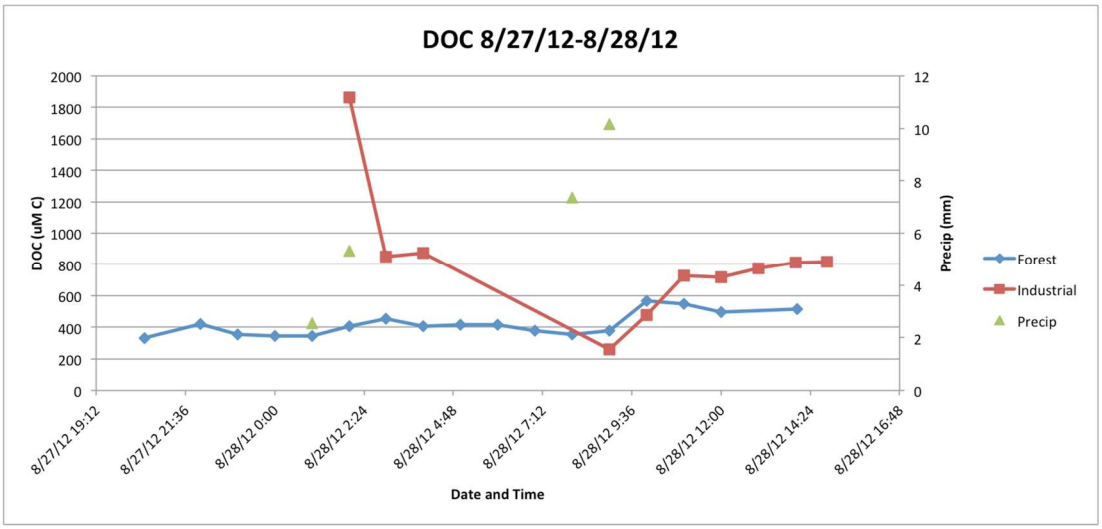

Figure B.22: Discrete samples showing DOC concentration over time

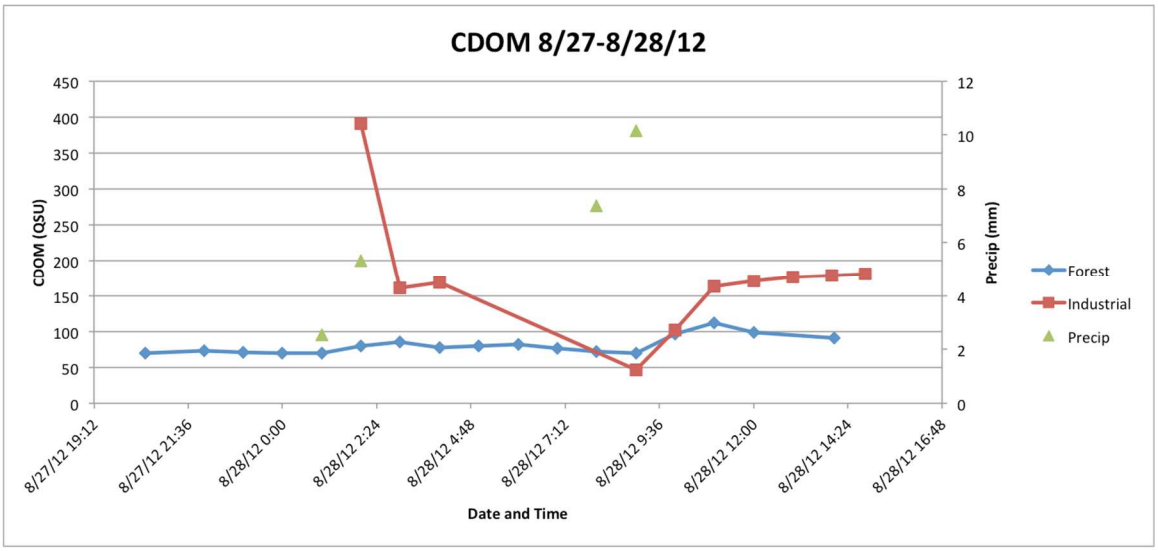

Figure B.23: Discrete samples showing CDOM concentration over time

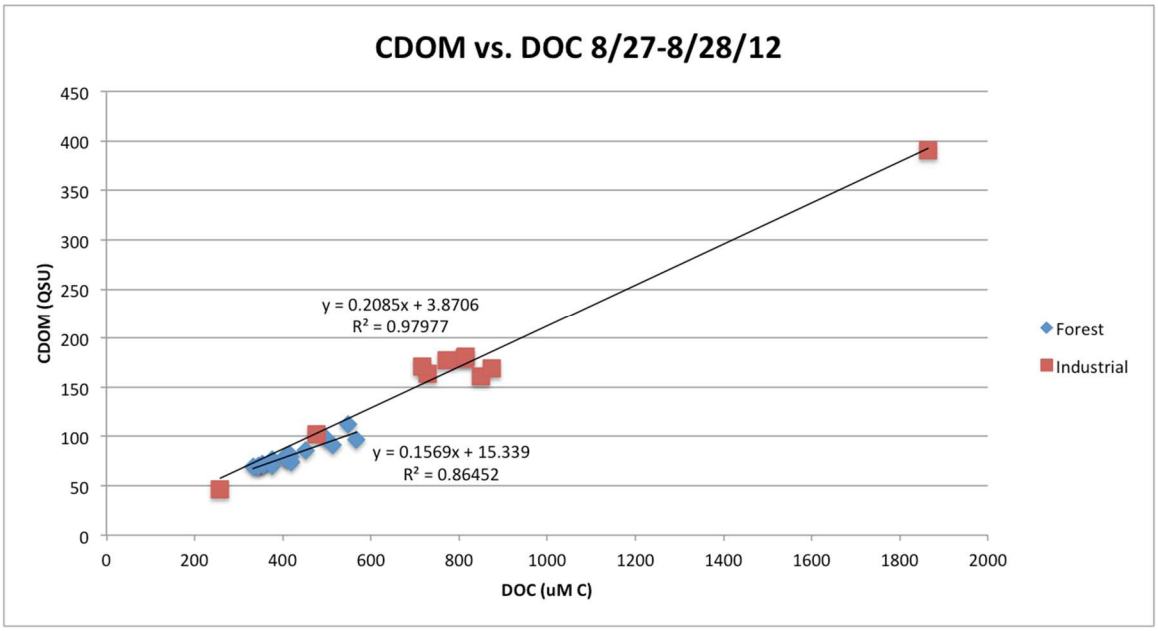

Figure B.24: CDOM versus DOC

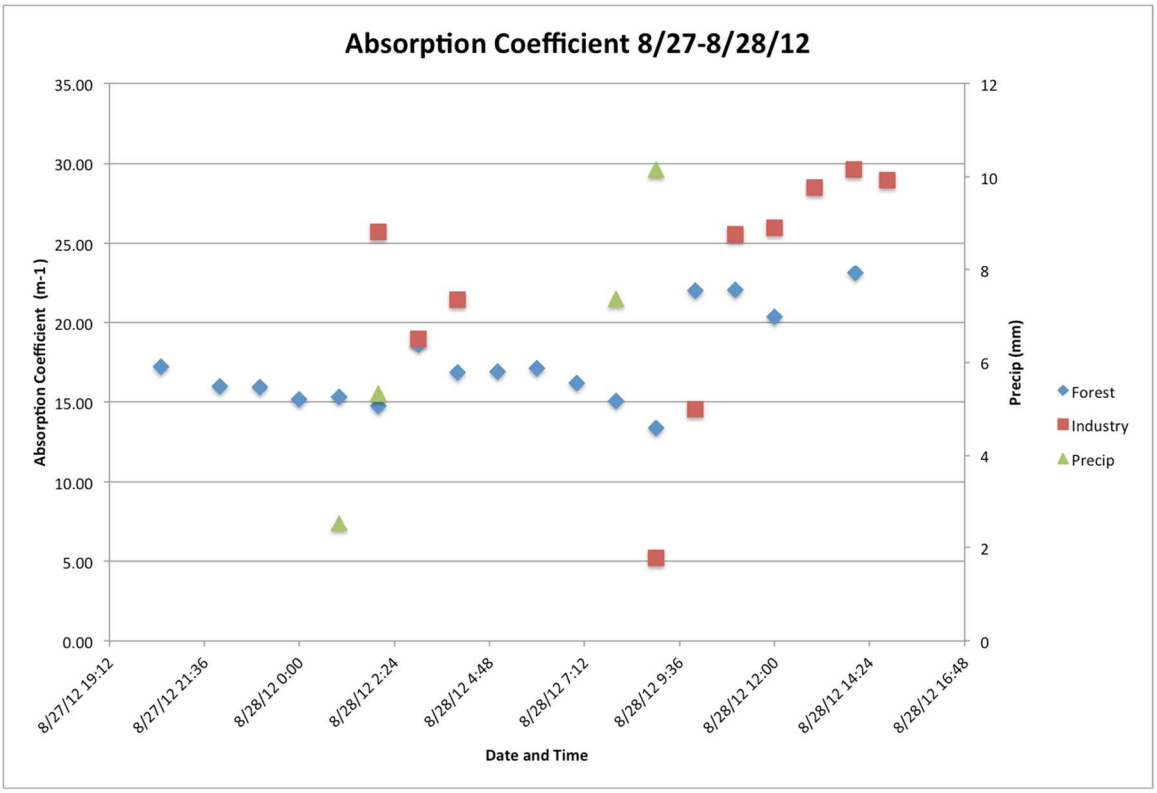

Figure B.25: Absorption coefficients for discrete samples

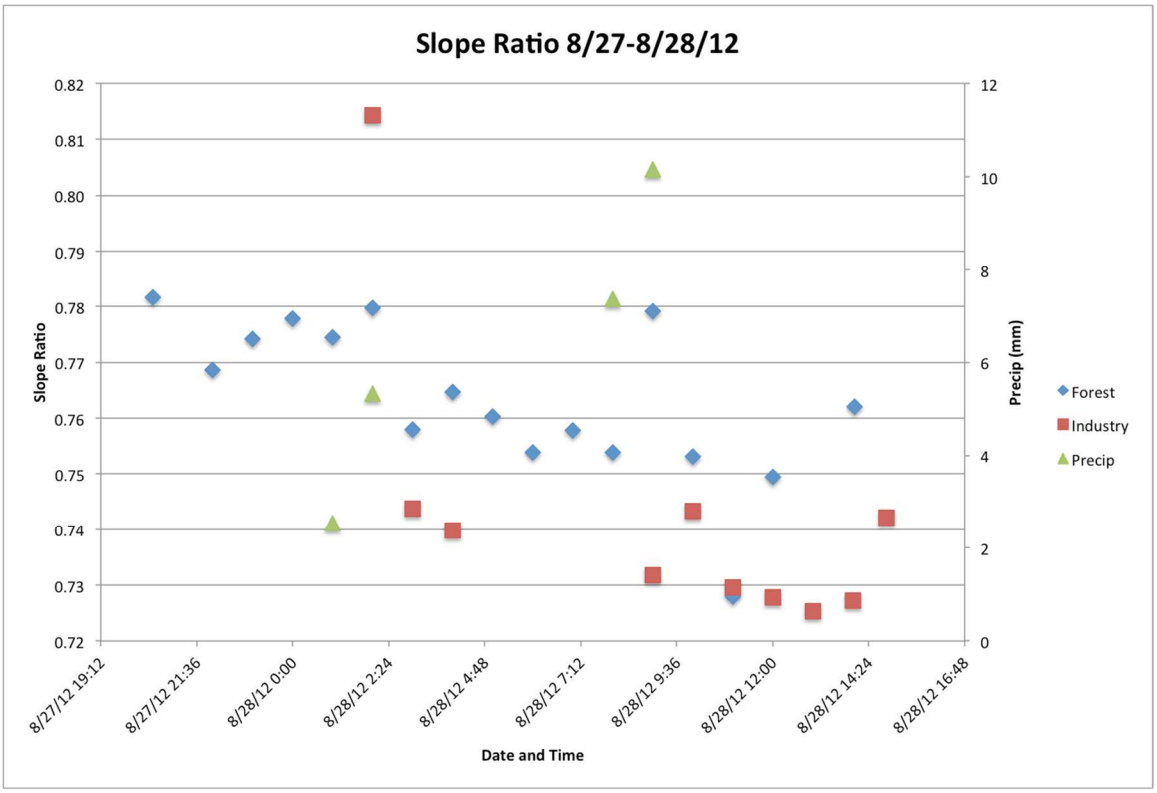

Figure B.26: Spectral slope ratios for discrete samples

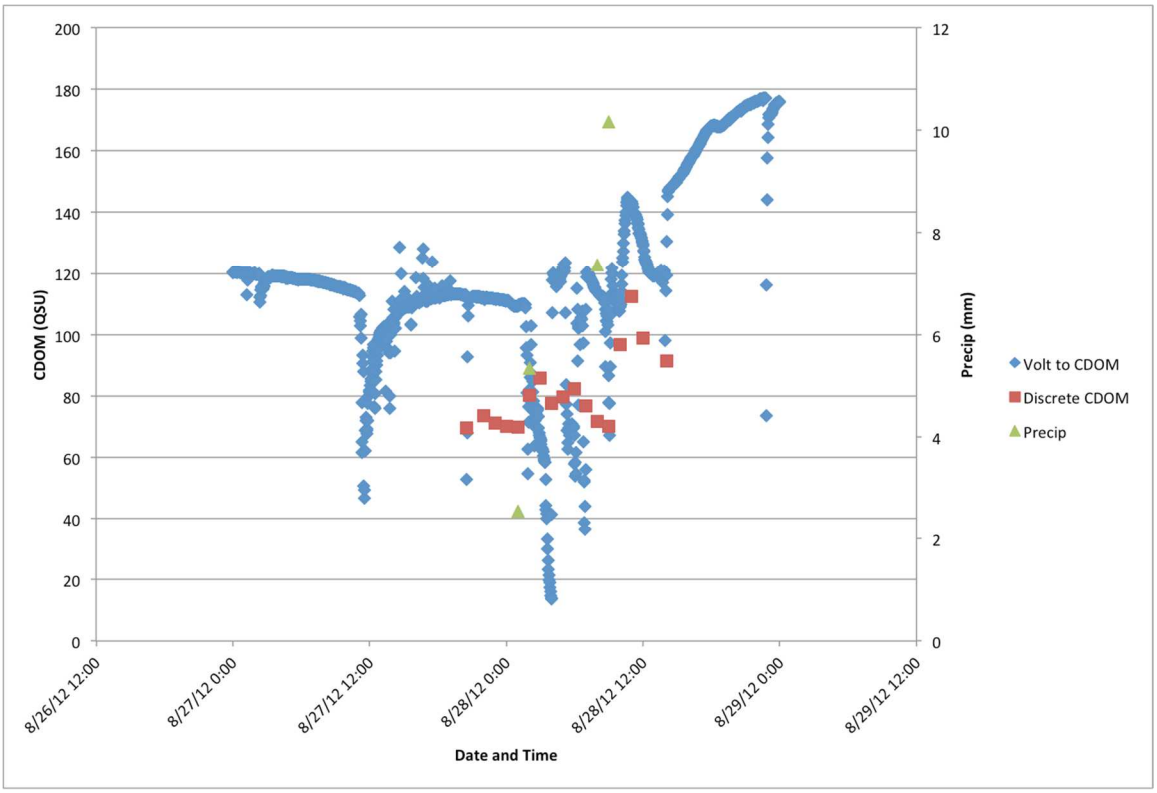

Figure B.27: Forested site sensor data and discrete samples shown on the same axis

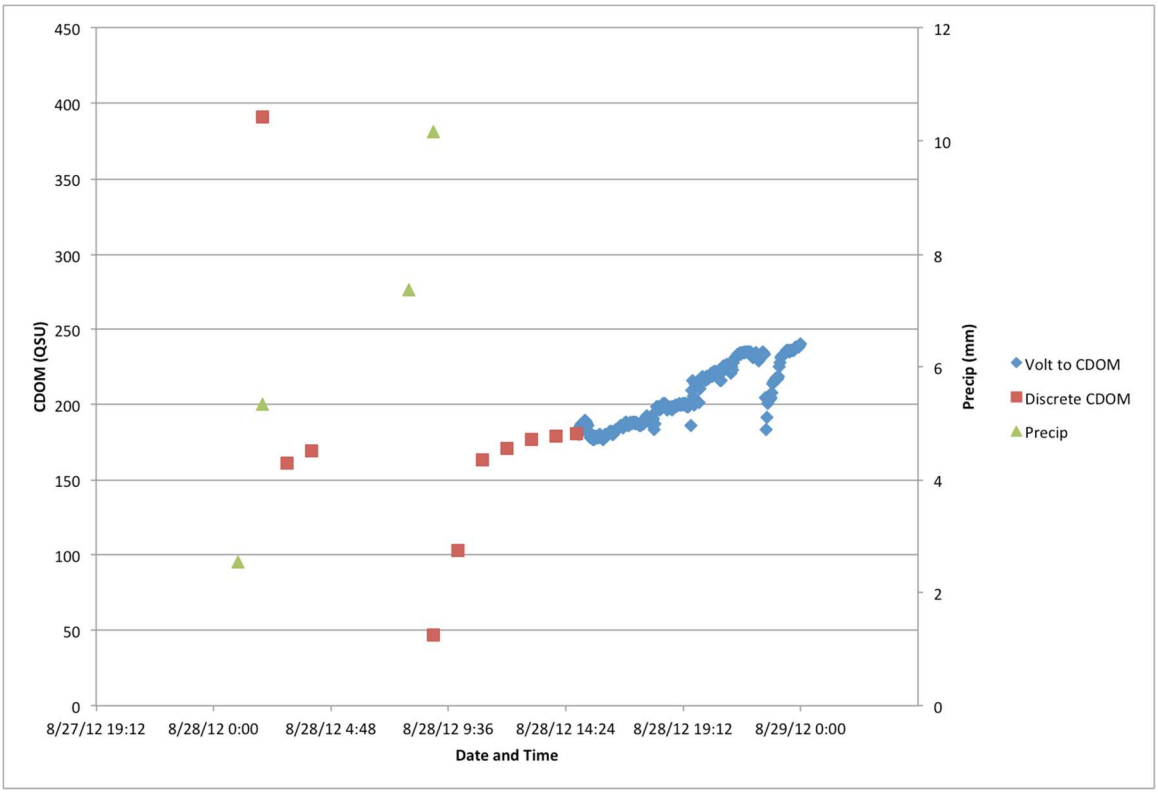

Figure B.28: Industrial site sensor data and discrete samples shown on the same axis

Event 5: 9/18-9/19/12 storm event

DOC and CDOM concentrations are very high at both sites during this storm. Industrial site values are generally higher, except during the storm. This is probably due to dilution (Figures B.29 and B.30). The CDOM versus DOC relationship is strong at both sites, with similar slopes (Figure B.31). The absorbance coefficients generally increase with precipitation at both sites. This effect is more noticeable at the industrial site (Figure B.32). Spectral slope ratios at the industrial site are highest during the storm, and then decrease. Slope ratios are consistent throughout at the forested site (Figure B.33). For CDOM fluorescence sensor data, the forested site shows an increasing trend after the storm (Figure B.34). At the industrial site, there was no water at the site until the storm. The concentration is elevated by the storm, and starts to decrease approximately 24 hours later. The industrial sensor data fluctuates during the storm, with some dilution effect (Figure B.35). In contrast, it appears that concentrations increase at the forested site with precipitation. This is noticeable in both the discrete and sensor data.

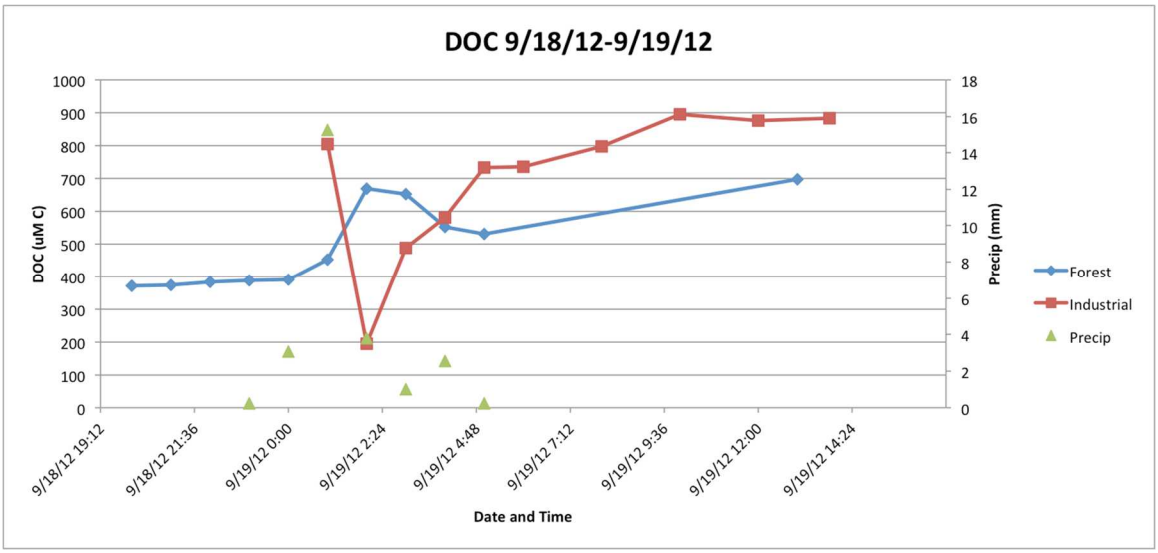

Figure B.29: Discrete samples showing DOC concentration over time

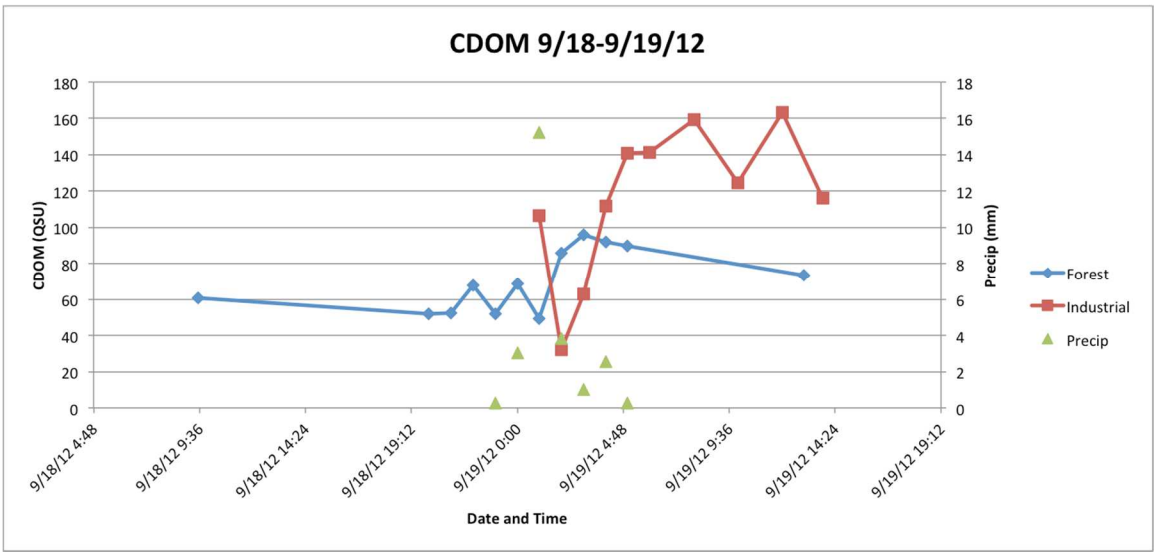

Figure B.30: Discrete samples showing CDOM concentration over time

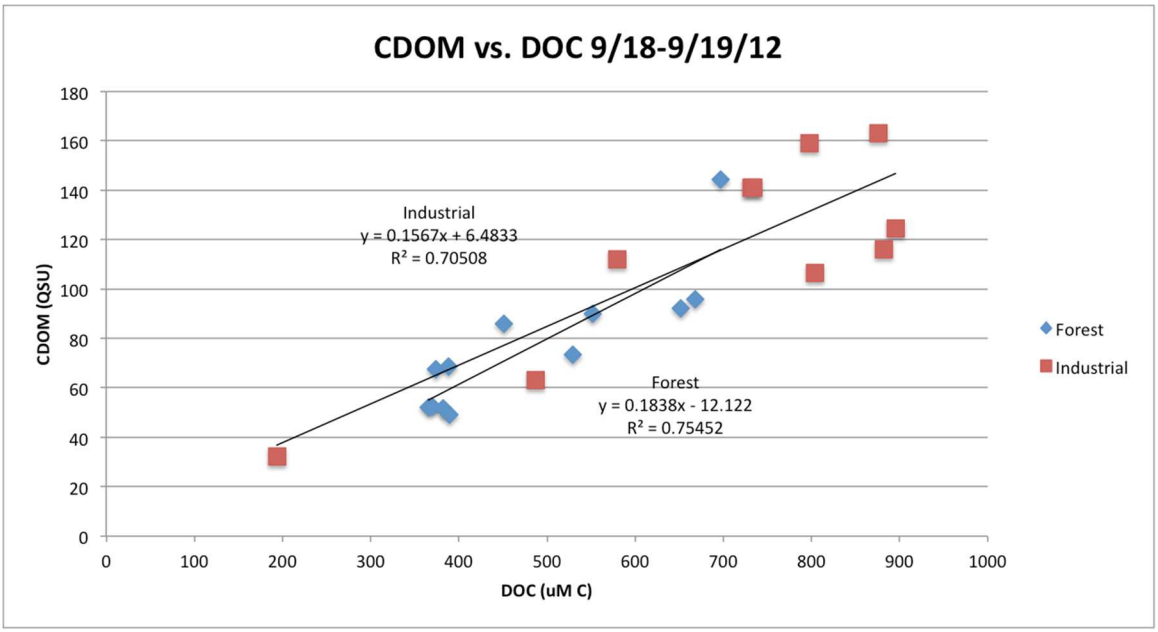

Figure B.31: CDOM versus DOC

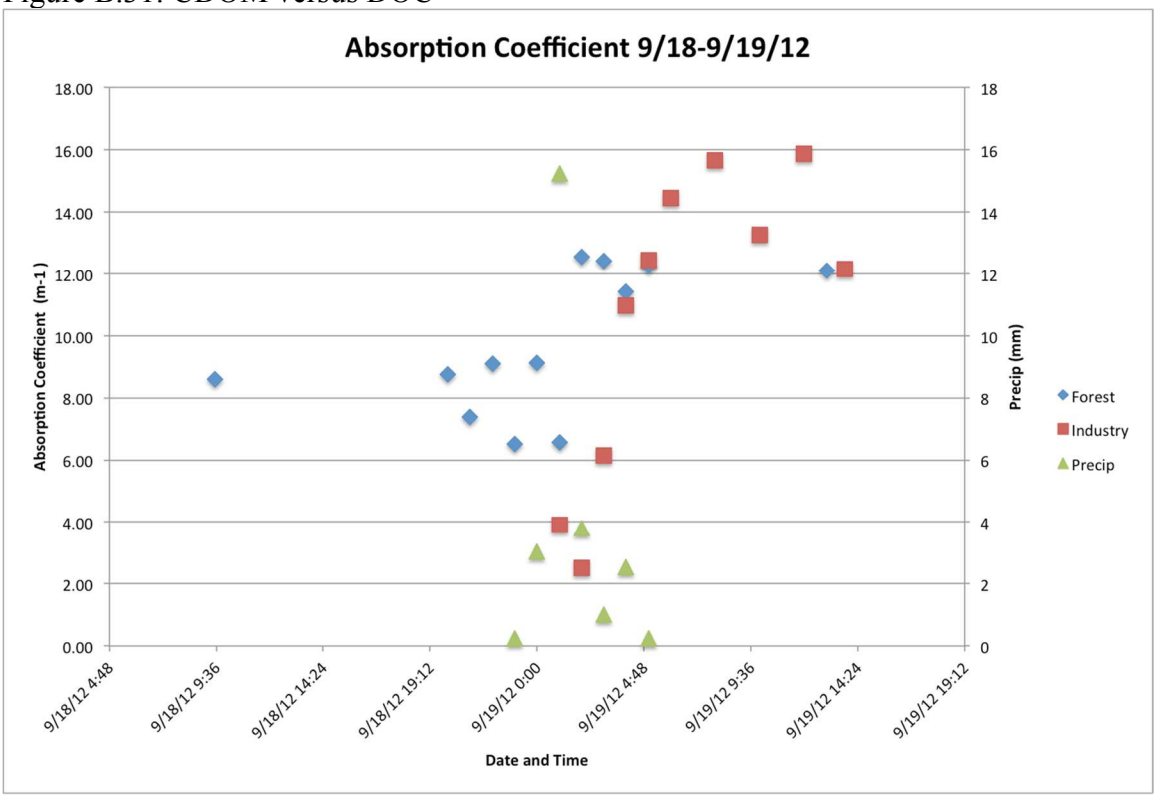

Figure B.32: Absorption coefficients for discrete samples

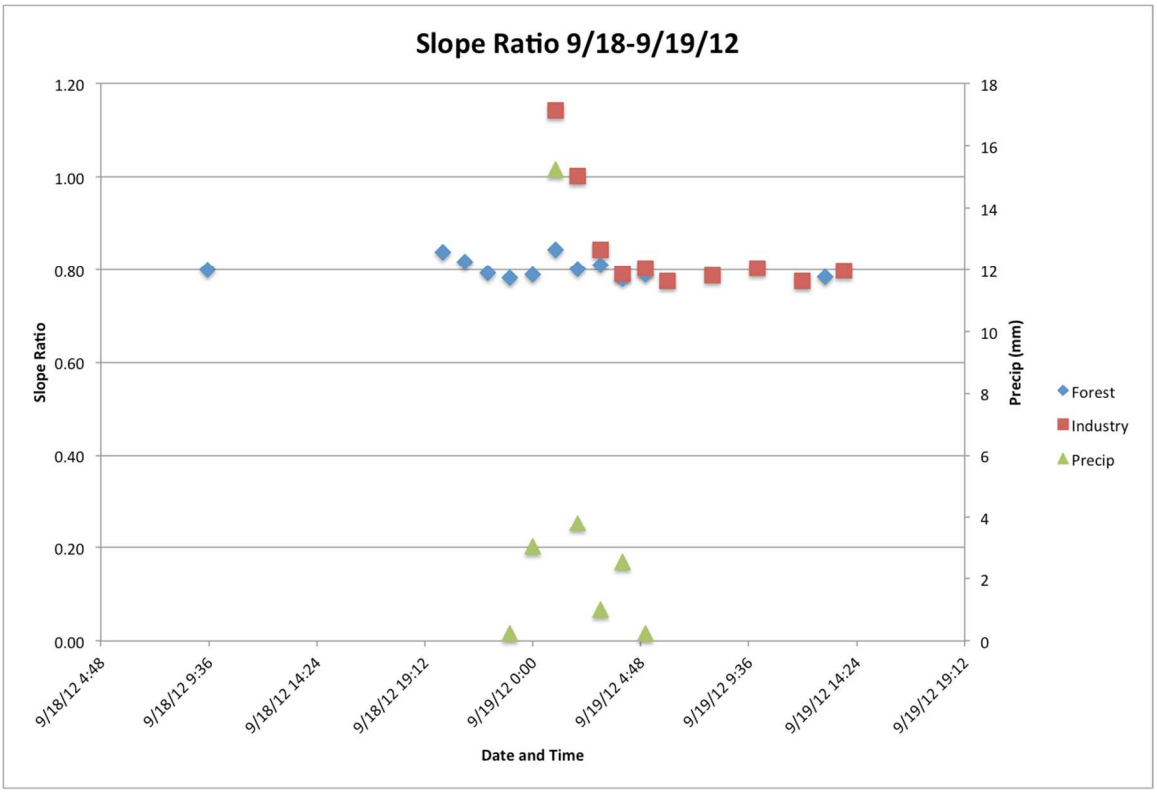

Figure B.33: Spectral slope ratios for discrete samples

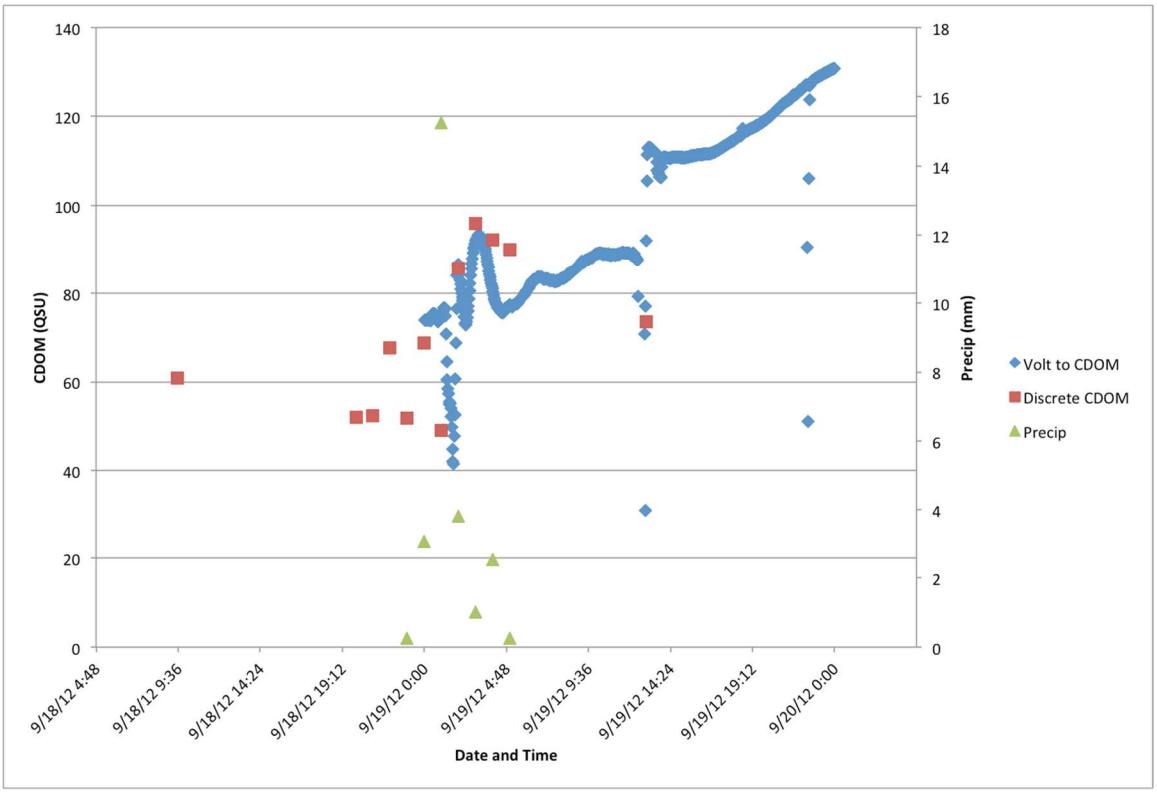

Figure B.34: Forested site sensor data and discrete samples shown on the same axis

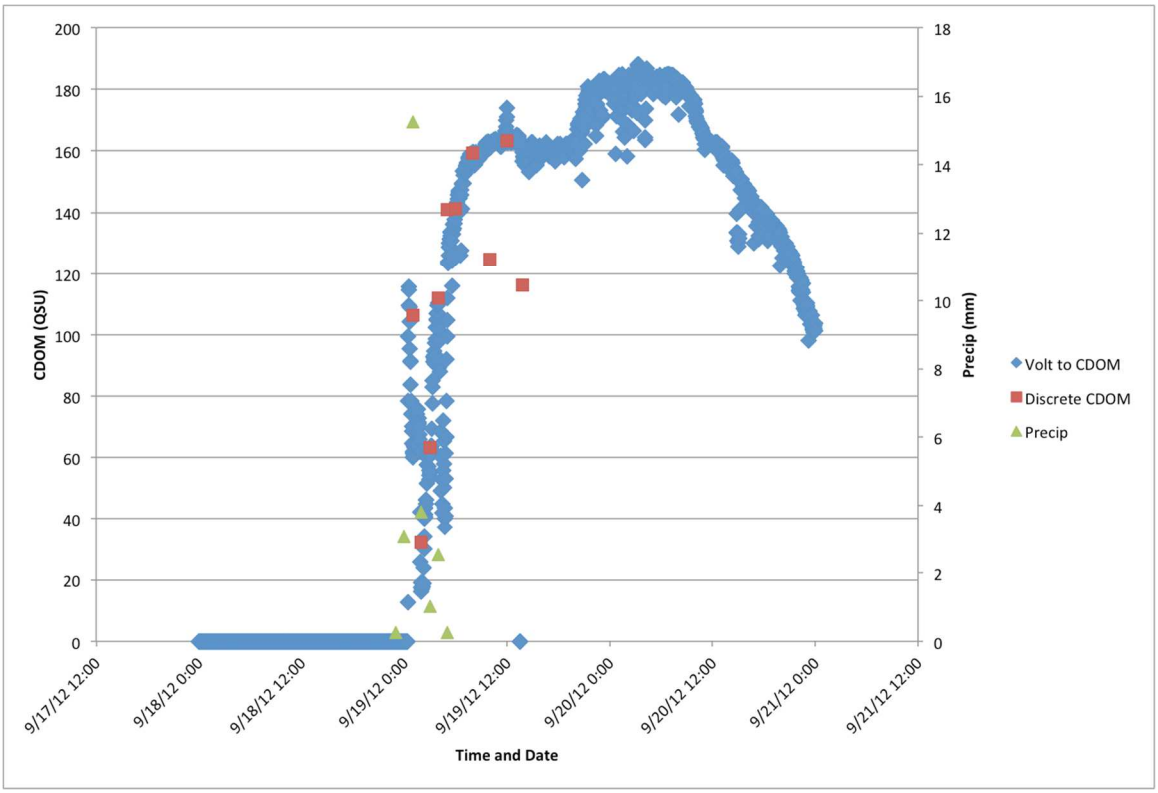

Figure B.35: Industrial site sensor data and discrete samples shown on the same axis

Event 6: 10/29-10/31/12 storm event – Hurricane Sandy

This is the largest precipitation event sampled during this research. DOC and CDOM concentrations are very high at both sites during this storm, with more variability at the industrial site (Figure B.36). CDOM concentrations are generally higher at the forested site (Figure B.37). The CDOM versus DOC relationship is stronger at the industrial site (Figure B.38). The absorbance coefficients at both sites increase as the storm progresses (Figure B.39). Spectral slope ratios are similar at both sites, with noticeable increases at the forested site with precipitation (Figure B.40). For CDOM fluorescence sensor data, the forested site shows little variation, while the industrial site data shows variations throughout the storm, and post-storm fluxes (Figures B.41 and B.42). There was no water at the industrial site prior to the storm.

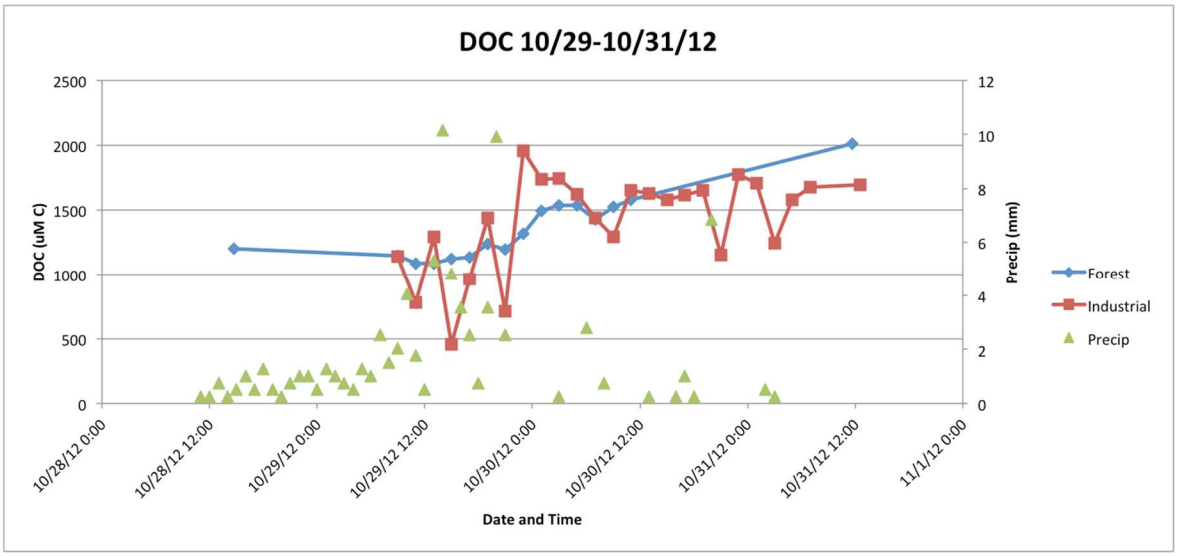

Figure B.36: Discrete samples showing DOC concentration over time

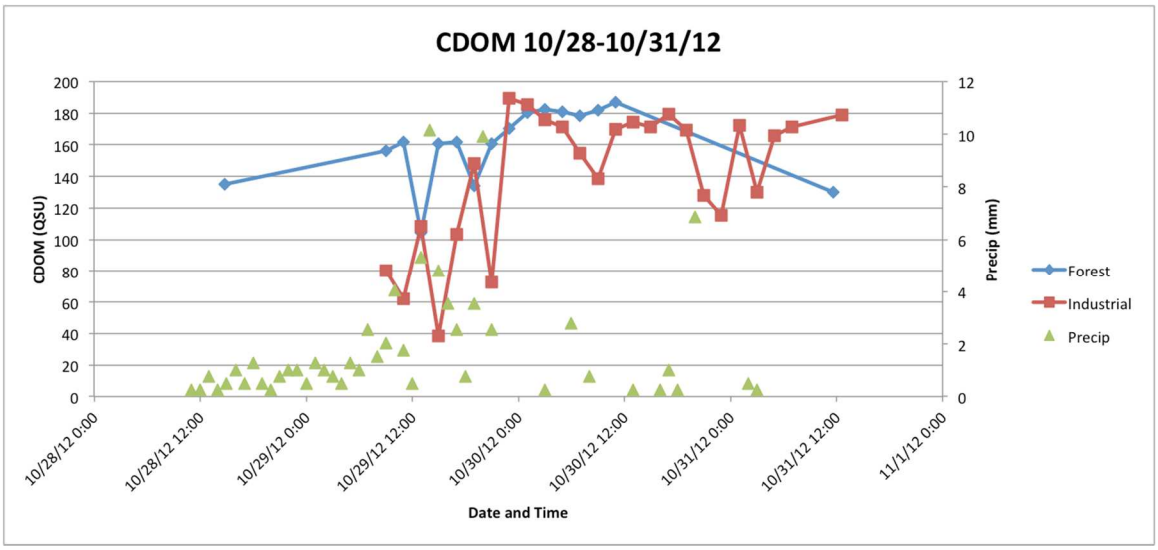

Figure B.37: Discrete samples showing CDOM concentration over time

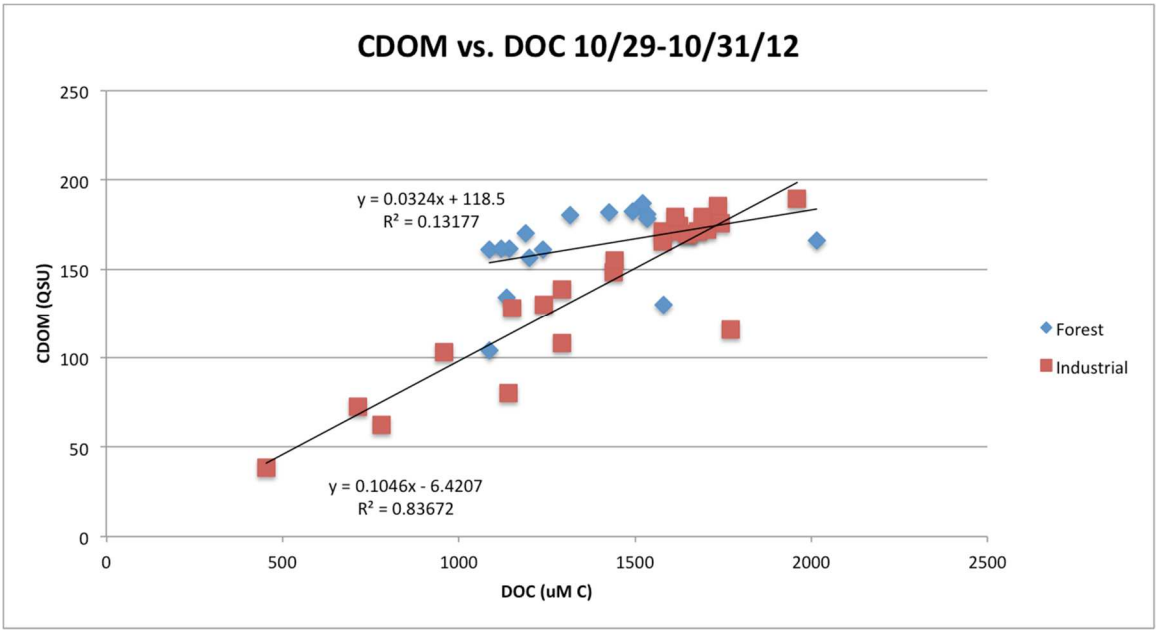

Figure B.38: CDOM versus DOC

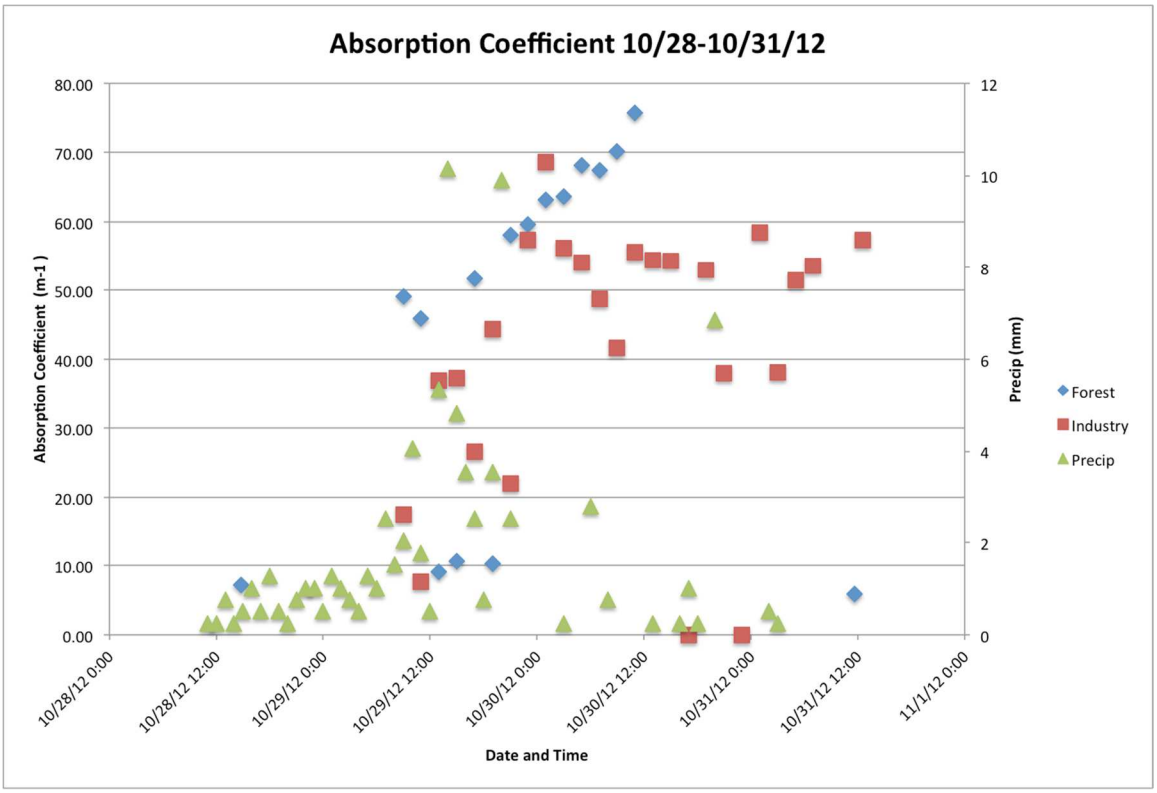

Figure B.39: Absorption coefficients for discrete samples

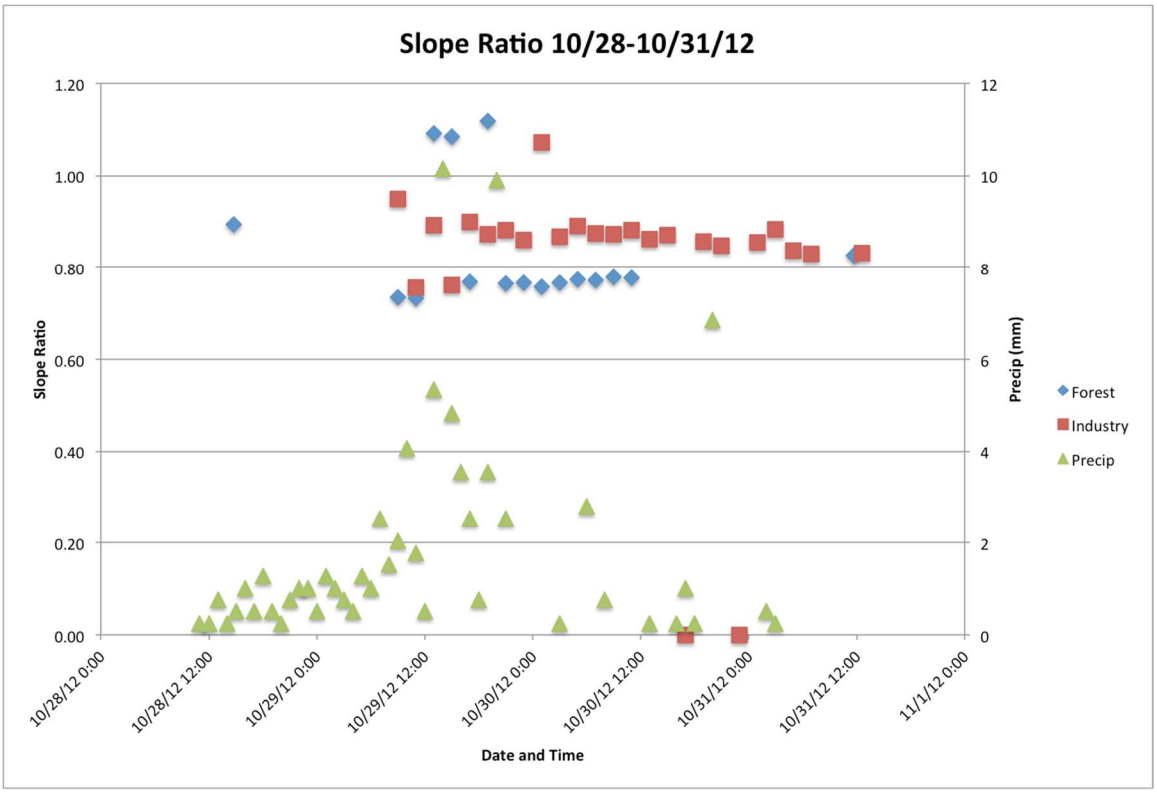

Figure B.40: Spectral slope ratios for discrete samples

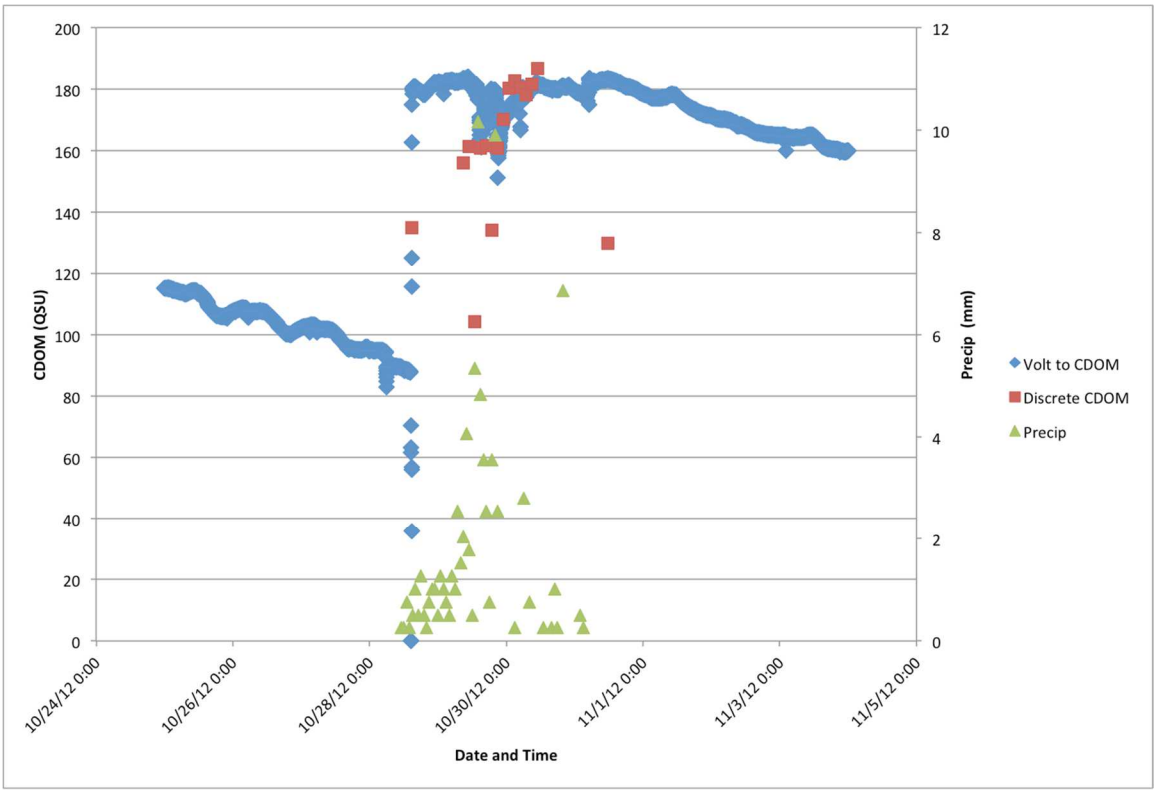

Figure B.41: Forested site sensor data and discrete samples shown on the same axis

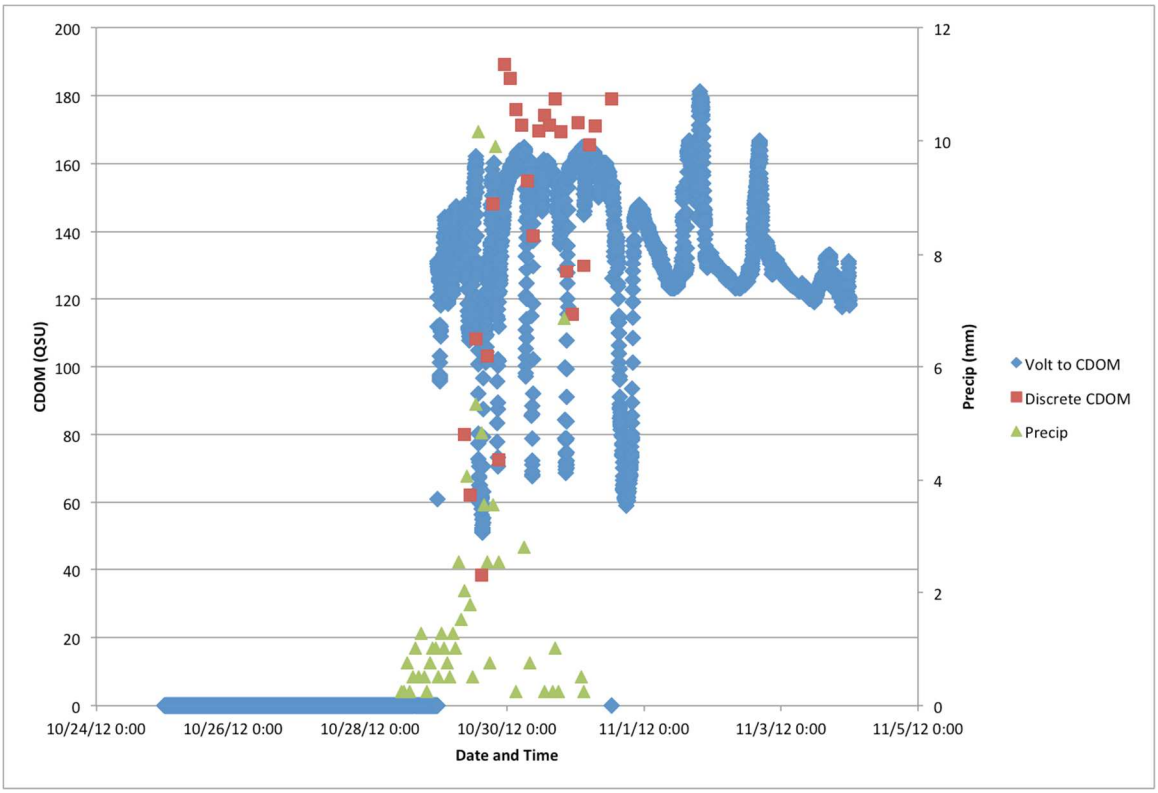

Figure B.42: Industrial site sensor data and discrete samples shown on the same axis

Event 7: 11/7-11/8/12 storm event

Forested site DOC and CDOM concentrations are higher than at the industrial site throughout the event period, with little effect from the storm. Larger rain amounts increase concentrations at the industrial site (Figures B.43 and B.44). The CDOM versus DOC relationship is stronger at the industrial site (Figure B.45). Absorption coefficients are higher for the forested site, with industrial site coefficients seemingly more influenced by precipitation (Figure B.46). Spectral slope ratios are similar at both sites, with little change during the storm (Figure B.47). For CDOM fluorescence sensor data, there is good agreement with the discrete samples. Industrial site concentrations are lower than at the forested site, and much more variable (Figures B.48 and B.49). Industrial site concentrations increase when the storm starts, decrease with precipitation, and then increase after the storm ends.

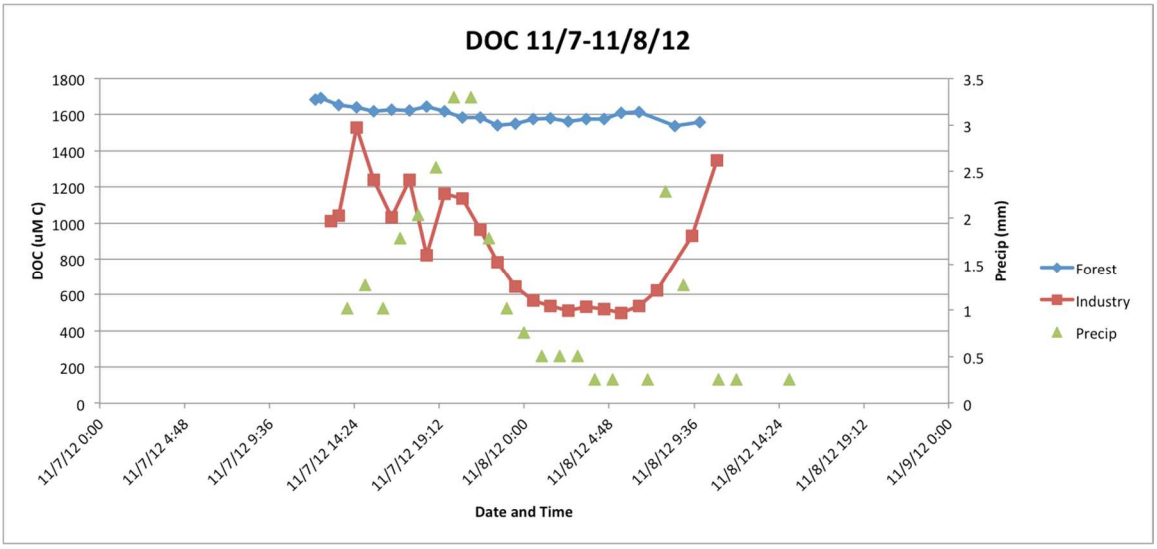

Figure B.43: Discrete samples showing DOC concentration over time

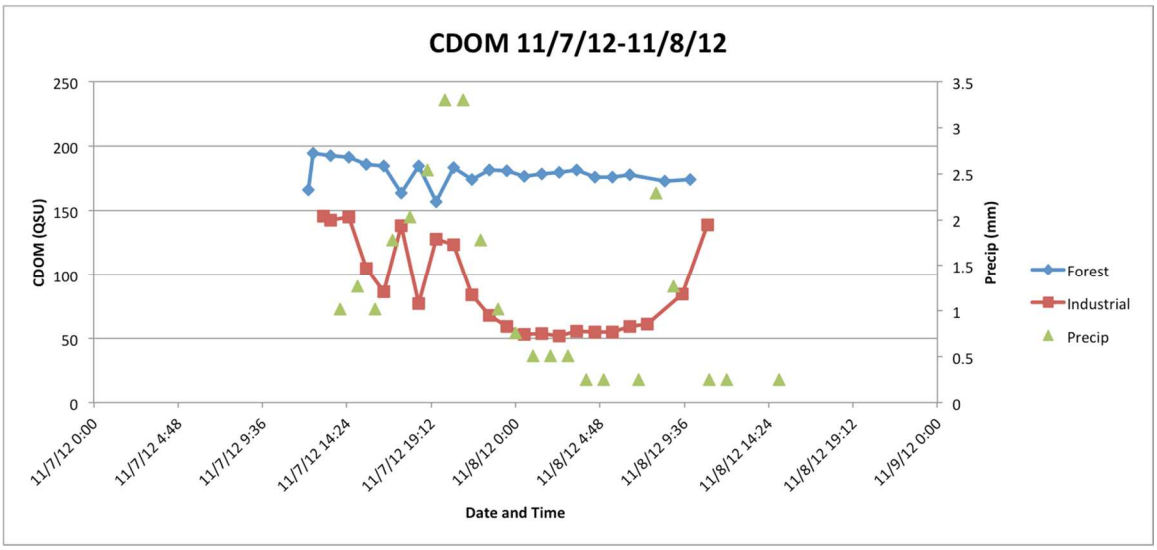

Figure B.44: Discrete samples showing CDOM concentration over time

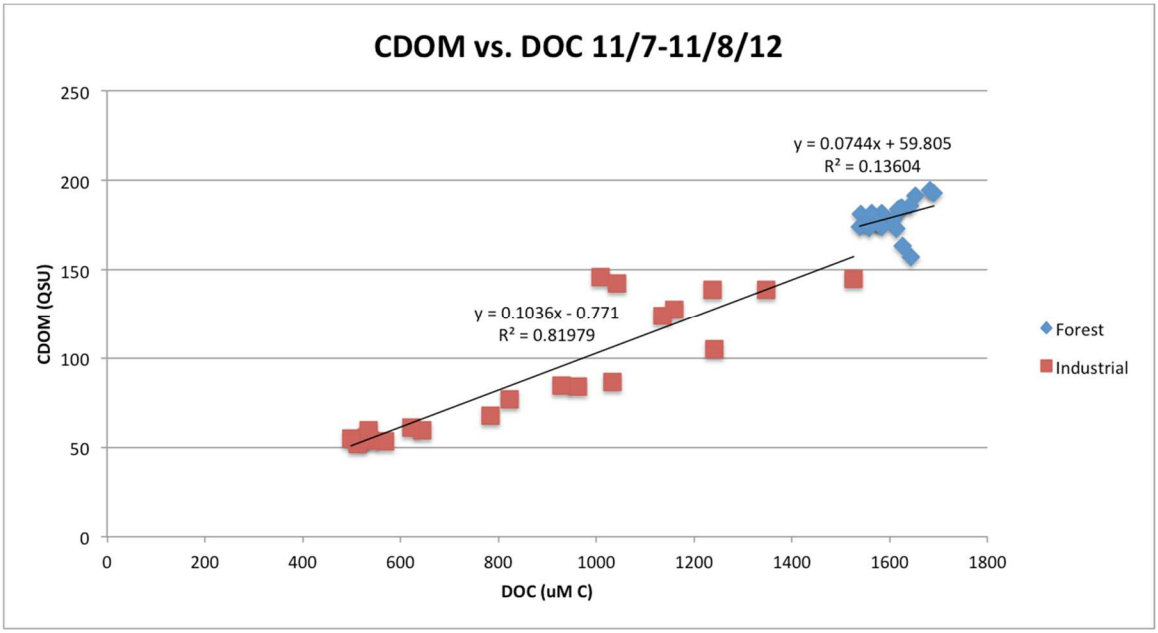

Figure B.45: CDOM versus DOC

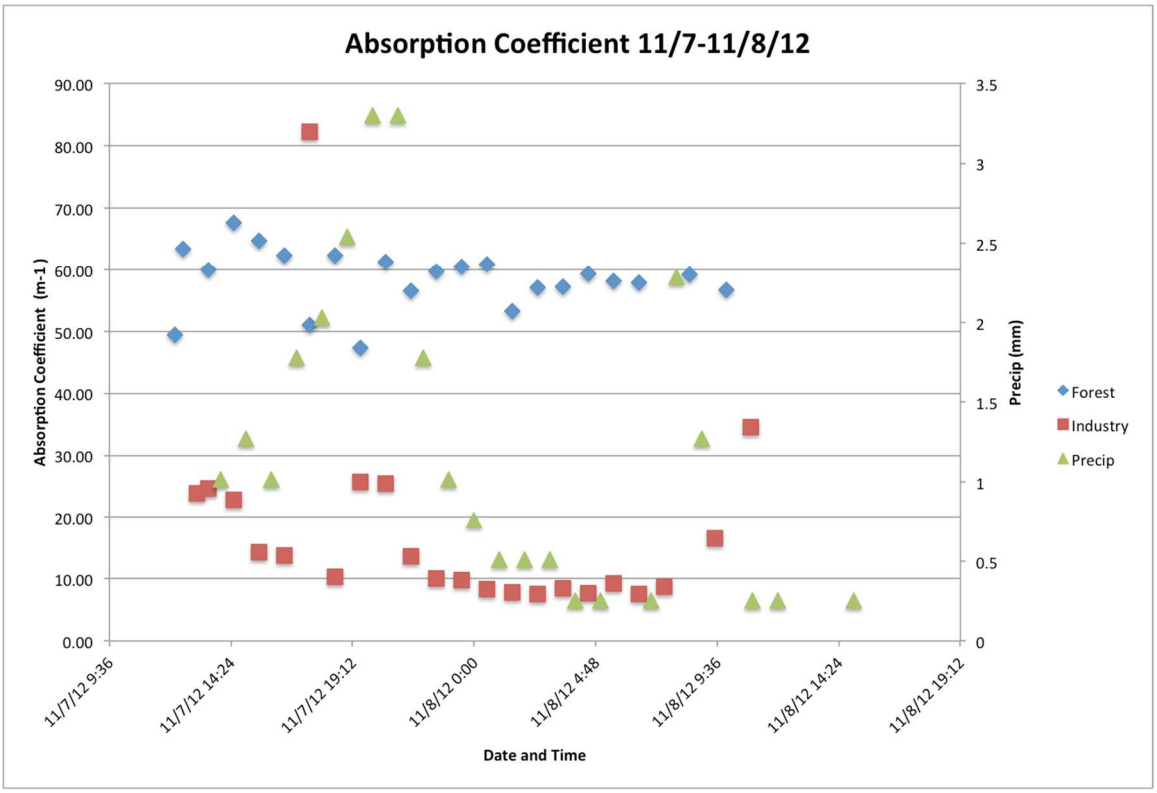

Figure B.46: Absorption coefficients for discrete samples

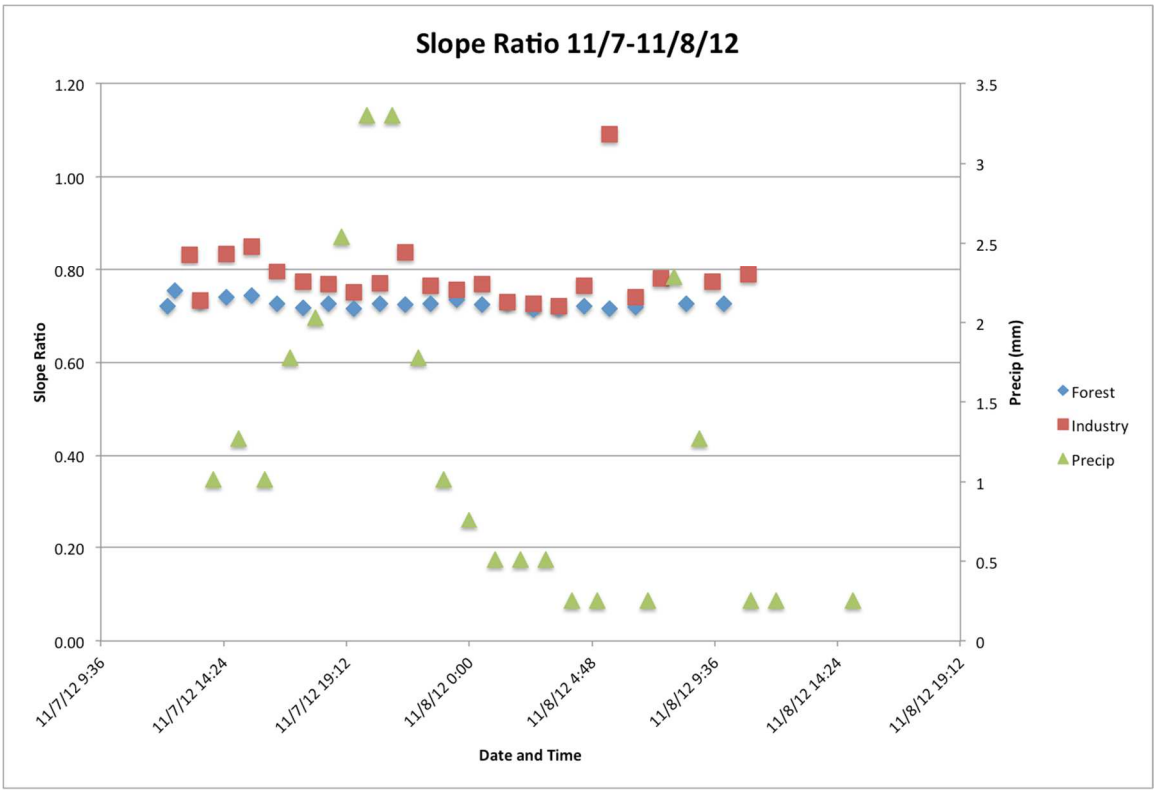

Figure B.47: Spectral slope ratios for discrete samples

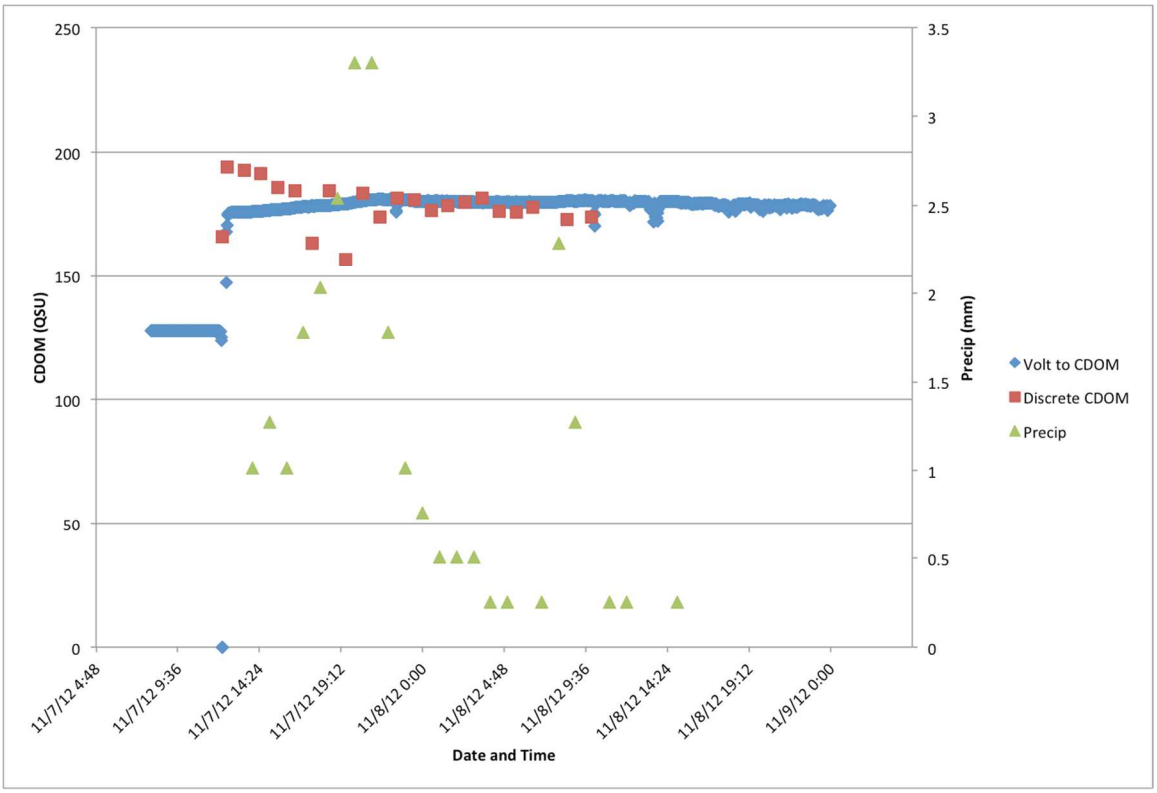

Figure B.48: Forested site sensor data and discrete samples shown on the same axis

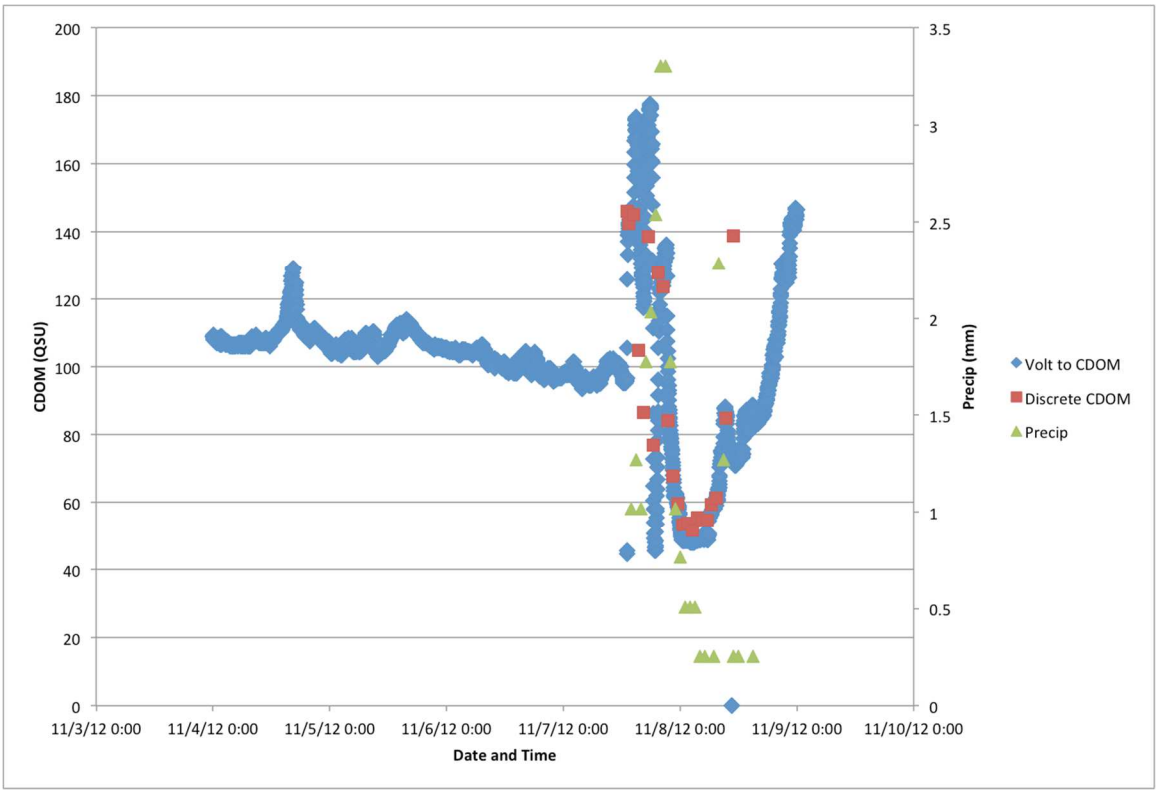

Figure B.49: Industrial site sensor data and discrete samples shown on the same axis

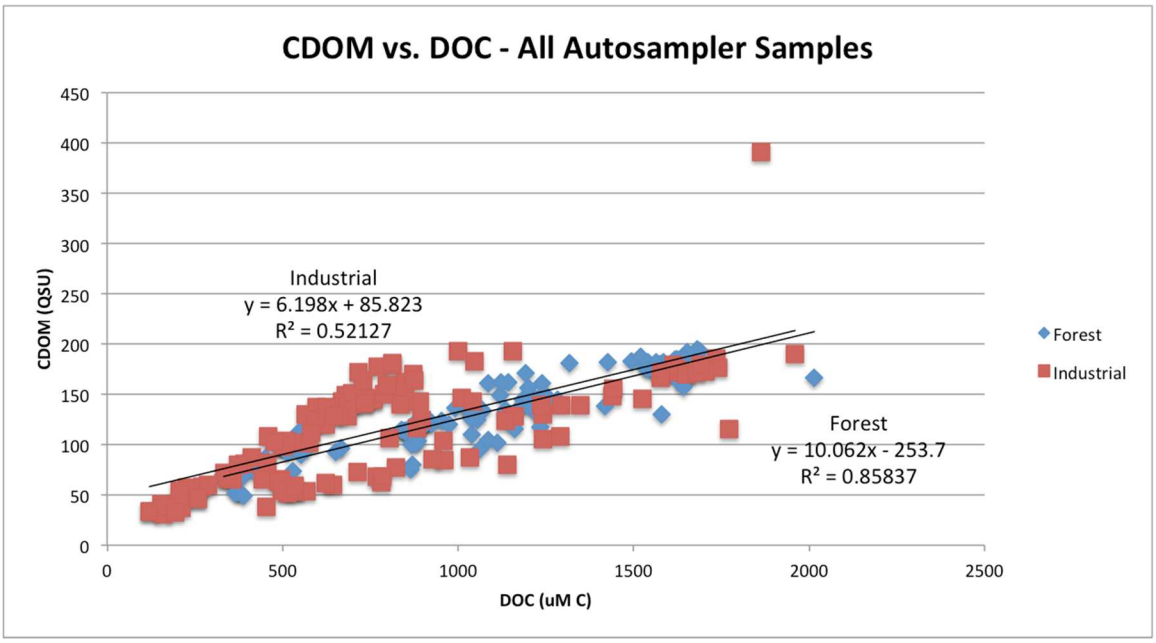

Figure B.50: CDOM versus DOC for all discrete storm samples

Table B.1: Event 1 (5/8-5/11/12), Forested site discrete samples

Sample	Date/Time	DOC (uM C)	CDOM (QSU)	Absorption coefficient
1	5/8/12 0200	925	121	12.40
2	5/8/12 0300	899	117	11.01
3	5/8/12 0400	888	115	11.07
4	5/8/12 0500	885	103	9.34
5	5/8/12 0600	892	119	11.10
6	5/8/12 0700	881	116	10.69
7	5/8/12 0800	868	100	8.03
8	5/8/12 0900	870	117	10.88
9	5/8/12 1000	857	114	10.85
10	5/8/12 1100	846	114	10.59
11	5/8/12 1400	864	115	10.36
12	5/8/12 1700	865	76	7.09
13	5/8/12 2000	839	115	10.89
14	5/8/12 2300	850	112	9.66
15	5/9/12 0200	850	113	10.89
16	5/9/12 0500	863	113	11.09
17	5/9/12 0800	871	79	15.34
18	5/9/12 1100	880	112	23.80

19	5/9/12 1400	876	119	27.35
20	5/9/12 1700	869	119	10.50
21	5/9/12 2000	881	101	8.68
22	5/9/12 2300	890	119	10.22
23	5/10/12 0200	921	122	9.20
24	5/10/12 0500	906	123	9.51
25	5/10/12 0800	953	124	27.32
26	5/10/12 1100	974	120	25.36
27	5/10/12 1400	1038	110	19.08
28	5/10/12 1700	1111	101	21.07
29	5/10/12 2000	1418	138	14.16
30	5/10/12 2300	1226	143	40.06
31	5/11/12 0200	1234	117	12.57
32	5/11/12 0500	1282	144	16.01
33	5/11/12 1055	1216	142	40.74
34	5/11/12 1120	1222	131	30.54

Table B.2: Event 1 (5/8-5/11/12), Industrial site discrete samples

Sample	Date/Time	DOC (uM C)	CDOM (QSU)	Absorption coefficient
1	5/8/12 0200	160	31	3.11
2	5/8/12 0300	154	41	3.73
3	5/8/12 0400	121	33	2.65
4	5/8/12 0500	212	37	3.54
5	5/8/12 0600	124	34	2.69
6	5/8/12 0700	227	57	5.08
7	5/8/12 0800	334	72	7.43
8	5/8/12 0900	502	98	11.66
9	5/8/12 1000	358	66	7.32
10	5/8/12 1100	391	80	9.12
11	5/8/12 1400	166	38	3.48
12	5/8/12 1700	210	48	4.42
13	5/8/12 2000	272	58	6.03
14	5/8/12 2300	552	102	12.99
15	5/9/12 0200	581	125	15.02
16	5/9/12 0500	591	127	15.67
17	5/9/12 0800	590	124	15.36
18	5/9/12 1100	412	87	7.83

19	5/9/12 1400	679	149	13.50
20	5/9/12 1700	669	142	12.32
21	5/9/12 2000	671	138	12.19
22	5/9/12 2300	735	146	13.33
23	5/10/12 0200	206	54	3.14
24	5/10/12 0500	575	101	11.65
25	5/10/12 0800	890	142	17.31
26	5/10/12 1100	847	144	16.40
27	5/10/12 1400	758	144	15.58
28	5/10/12 1700	758	145	14.69
29	5/10/12 2000	768	68	7.68
30	5/10/12 2300	836	140	12.56
31	5/11/12 0200	702	139	12.19
32	5/11/12 0500	685	128	10.13
33	5/11/12 0800	615	125	10.00
34	5/11/12 1100	609	123	10.27
35	5/11/12 1225	675	138	11.08

Table B.3: Event 2 (6/12-6/14/12), Forested site discrete samples

Sample	Date/Time	DOC (uM C)	CDOM (QSU)	Absorption coefficient
1	6/12/12 1925	1120	149	54.55
2	6/12/12 2100	1184	144	56.71
3	6/12/12 2200	1205	146	38.71
4	6/12/12 2300	1181	139	39.14
5	6/13/12 0000	1246	147	34.64
6	6/13/12 0100	1245	151	38.10
7	6/13/12 0200	1194	139	36.09
8	6/13/12 0300	1214	145	36.56
9	6/13/12 0400	1208	139	35.74
10	6/13/12 0500	1230	142	37.04
11	6/13/12 0600	1215	145	31.33
12	6/13/12 0700	1194	146	60.13
13	6/13/12 0800	1160	115	23.54
14	6/13/12 0900	Sample lost	Sample lost	Sample lost
15	6/13/12 1000	1063	136	23.86
16	6/13/12 1100	Sample lost	Sample lost	Sample lost
17	6/13/12 1200	1054	124	45.32
18	6/13/12 1330	992	136	49.43

19	6/13/12 1500	1025	136	47.92
20	6/13/12 1630	1036	132	44.94
21	6/13/12 1800	1036	126	44.80
22	6/13/12 1930	1041	132	44.07
23	6/13/12 2100	1052	133	46.92
24	6/13/12 2230	1062	95	19.11
25	6/14/12 0000	1069	133	45.25
26	6/14/12 1130	1135	131	48.97

Table B.4: Event 2 (6/12-6/14/12), Industrial site discrete samples

Sample	Date/Time	DOC (uM C)	CDOM (QSU)	Absorption coefficient
1	6/12/12 2045	256	47	4.16
2	6/12/12 2100	256	52	2.35
3	6/12/12 2200	287	60	2.27
4	6/12/12 2300	343	67	2.58
5	6/13/12 0000	342	67	2.84
6	6/13/12 0100	457	82	4.28
7	6/13/12 0200	1157	192	7.39
8	6/13/12 0300	1048	182	7.63
9	6/13/12 0400	1001	192	9.22

10	6/13/12 0500	789	150	8.13
11	6/13/12 0600	623	120	6.70
12	6/13/12 0700	698	151	5.30
13	6/13/12 0800	459	108	4.62
14	6/13/12 0900	443	66	1.66
15	6/13/12 1000	374	80	3.92
16	6/13/12 1100	497	65	2.04
17	6/13/12 1200	510	101	6.73
18	6/13/12 1330	511	103	2.69
19	6/13/12 1500	565	130	8.31
20	6/13/12 1630	596	137	9.16
21	6/13/12 1800	591	124	8.19
22	6/13/12 1930	626	137	7.08
23	6/13/12 2100	682	136	10.22
24	6/13/12 2230	663	129	9.56
25	6/14/12 0000	645	128	8.80
26	6/14/12 1300	503	99	6.18

Table B.5: Event 3 (7/18-7/19/12), Forested site discrete samples

Sample	Date/Time	DOC (uM C)	CDOM (QSU)	Absorption coefficient
1	7/18/12 1534	1211	160	16.73
2	7/18/12 1545	588	100	16.13
3	7/18/12 1645	474	97	15.25
4	7/18/12 1745	549	105	15.62
5	7/18/12 1845	523	100	13.81
6	7/18/12 1945	512	103	13.67
7	7/18/12 2045	470	102	14.57
8	7/18/12 2145	433	89	16.07
9	7/18/12 2245	407	85	16.36
10	7/18/12 2345	424	89	15.17
11	7/19/12 0045	486	92	18.06
12	7/19/12 0145	499	95	19.61
13	7/19/12 0245	513	95	18.11
14	7/19/12 0345	563	94	17.84
15	7/19/12 0445	556	102	18.72
16	7/19/12 0545	548	97	17.84
17	7/19/12 0645	534	99	17.98
18	7/19/12 0815	525	99	18.21

19	7/19/12 0945	524	98	14.14
20	7/19/12 1135	526	99	18.93

Table B.6: Event 3 (7/18-7/19/12), Industrial site discrete samples

Sample	Date/Time	DOC (uM C)	CDOM (QSU)	Absorption coefficient
1	7/18/12 1603	2637	377	15.16
2	7/18/12 1615	2412	482	9.59
3	7/18/12 1715	2321	419	29.00
4	7/18/12 1815	1810	403	12.30
5	7/18/12 1915	1777	375	26.57

No liquid detected for all other attempted autosampler samples. Site was almost dry when samples were retrieved.

Table B.7: Event 4 (8/27-8/28/12), Forested site discrete samples

Sample	Date/Time	DOC (uM C)	CDOM (QSU)	Absorption coefficient
1	8/27/12 2030	332	70	17.23
2	8/27/12 2200	419	73	16.00
3	8/27/12 2300	356	71	15.94
4	8/28/12 0000	346	70	15.19
5	8/28/12 0100	343	70	15.32
6	8/28/12 0200	406	80	14.79
7	8/28/12 0300	451	86	18.60
8	8/28/12 0400	406	78	16.86
9	8/28/12 0500	416	80	16.92
10	8/28/12 0600	414	82	17.14
11	8/28/12 0700	376	77	16.21
12	8/28/12 0800	352	72	15.09
13	8/28/12 0900	376	70	13.36
14	8/28/12 1000	567	97	22.01
15	8/28/12 1100	548	113	22.03
16	8/28/12 1200	497	99	20.33
17	8/28/12 1403	514	91	23.12

This event looked like a large storm, as the plants near the stream at the forest site were laid flat due to force of higher water during the storm.

Table B.8: Event 4 (8/27-8/28/12), Industrial site discrete samples

Sample	Date/Time	DOC (uM C)	CDOM (QSU)	Absorption coefficient
1	8/28/12 0200	1864	391	25.71
2	8/28/12 0300	848	161	18.97
3	8/28/12 0400	873	169	21.41
4	8/28/12 0900	258	47	5.20
5	8/28/12 1000	477	102	14.56
6	8/28/12 1100	728	163	25.60
7	8/28/12 1200	717	171	26.00
8	8/28/12 1300	772	177	28.50
9	8/28/12 1400	814	179	29.60
10	8/28/12 1451	814	181	28.95

Sampling started at 2200 on 8/27/12, no samples retrieved until 0200 8/28/12; then no samples between 0500 and 0800 on 8/28/12 – probably due to not enough water at sampling site

Table B.9: Event 5 (9/18-9/19/12), Forested site discrete samples

Sample	Date/Time	DOC (uM C)	CDOM (QSU)	Absorption coefficient
1	9/18/12 0932	366	61	8.59
2	9/18/12 2000	370	52	8.76
3	9/18/12 2100	374	52	7.39
4	9/18/12 2200	382	68	9.09
5	9/18/12 2300	388	52	6.50
6	9/19/12 0000	389	69	9.13
7	9/19/12 0100	451	49	6.56
8	9/19/12 0200	668	86	12.55
9	9/19/12 0300	652	96	12.43
10	9/19/12 0400	552	92	11.41
11	9/19/12 0500	530	90	12.27
12	9/19/12 1300	697	74	12.11

Autosampler samples started at 9/18/12 1200, first 8 samples not kept due to no rain occurring while they were collected

Table B.10: Event 5 (9/18-9/19/12), Industrial site discrete samples

Sample	Date/Time	DOC (uM C)	CDOM (QSU)	Absorption coefficient
1	9/19/12 0100	804	106	3.92
2	9/19/12 0200	194	32	2.52
3	9/19/12 0300	488	63	6.16
4	9/19/12 0400	580	112	10.97
5	9/19/12 0500	732	141	12.44
6	9/19/12 0600	734	141	14.44
7	9/19/12 0800	797	159	15.66
8	9/19/12 1000	895	125	13.27
9	9/19/12 1200	876	163	15.87
10	9/19/12 1350	882	116	12.14

Autosampler samples started at 9/18/12 1200, no liquid detected for samples until sample collected on 9/19/12 0100

Table B.11: Event 6 (10/29-10/31/12), Forested site discrete samples

Sample	Date/Time	DOC (uM C)	CDOM (QSU)	Absorption coefficient
1	10/28/12 1445	1201	135	7.18
2	10/29/12 0900	1143	156	49.11
3	10/29/12 1100	1087	162	45.88
4	10/29/12 1300	1087	104	9.04
5	10/29/12 1500	1121	161	10.60
6	10/29/12 1700	1135	162	51.69
7	10/29/12 1900	1239	134	10.27
8	10/29/12 2100	1191	161	58.09
9	10/29/12 2300	1316	170	59.67
10	10/30/12 0100	1493	180	63.21
11	10/30/12 0300	1533	183	63.66
12	10/30/12 0500	1533	181	68.13
13	10/30/12 0700	1427	178	67.51
14	10/30/12 0900	1521	182	70.23
15	10/30/12 1100	1580	187	75.73
16	10/31/12 1140	2015	130	5.90

Autosampler battery died after sample on 10/30/12 1100. Last sample was a grab sample taken during sample retrieval.

Table B.12: Event 6 (10/29-10/31/12), Industrial site discrete samples

Sample	Date/Time	DOC (uM C)	CDOM (QSU)	Absorption coefficient
1	10/29/12 0900	1140	80	17.46
2	10/29/12 1100	781	62	7.66
3	10/29/12 1300	1292	108	36.86
4	10/29/12 1500	454	38	37.24
5	10/29/12 1700	959	103	26.66
6	10/29/12 1900	1440	148	44.37
7	10/29/12 2100	715	73	22.06
8	10/29/12 2300	1960	189	57.39
9	10/30/12 0100	1735	185	68.65
10	10/30/12 0300	1742	176	56.25
11	10/30/12 0500	1619	171	54.11
12	10/30/12 0700	1441	155	48.74
13	10/30/12 0900	1293	139	41.61
14	10/30/12 1100	1651	170	55.60
15	10/30/12 1300	1625	174	54.48
16	10/30/12 1500	1580	171	54.29
17	10/30/12 1700	1614	179	No sample
18	10/30/12 1900	1651	169	52.97

19	10/30/12 2100	1150	128	37.94
20	10/30/12 2300	1772	116	No sample
21	10/31/12 0100	1704	172	58.51
22	10/31/12 0300	1241	130	38.06
23	10/31/12 0500	1577	166	51.50
24	10/31/12 0700	1678	171	53.66
25	10/31/12 1235	1692	179	57.37

Autosampler functioned well during sampling. Last sample is a grab sample taken during sample retrieval.

Table B.13: Event 7 (11/7-11/8/12), Forested site discrete samples

Sample	Date/Time	DOC (uM C)	CDOM (QSU)	Absorption coefficient
1	11/7/12 1212	1682	166	49.37
2	11/7/12 1230	1690	194	63.34
3	11/7/12 1330	1653	193	59.97
4	11/7/12 1430	1642	191	67.56
5	11/7/12 1530	1620	186	64.73
6	11/7/12 1630	1627	184	62.37
7	11/7/12 1730	1624	163	51.07
8	11/7/12 1830	1643	185	62.37
9	11/7/12 1930	1617	157	47.27
10	11/7/12 2030	1583	184	61.23
11	11/7/12 2130	1584	174	56.51
12	11/7/12 2230	1541	181	59.65
13	11/7/12 2330	1552	181	60.49
14	11/8/12 0030	1574	176	60.84
15	11/8/12 0130	1578	179	53.20
16	11/8/12 0230	1563	180	57.06
17	11/8/12 0330	1577	181	57.23
18	11/8/12 0430	1575	176	59.32

19	11/8/12 0530	1608	176	58.15
20	11/8/12 0630	1614	178	57.83
21	11/8/12 0830	1538	173	59.19
22	11/8/12 0957	1558	174	56.71

Table B.14: Event 7 (11/7-11/8/12), Industrial site discrete samples

Sample	Date/Time	DOC (uM C)	CDOM (QSU)	Absorption coefficient
1	11/7/12 1304	1010	146	23.88
2	11/7/12 1330	1042	142	24.66
3	11/7/12 1430	1526	145	22.81
4	11/7/12 1530	1241	105	14.20
5	11/7/12 1630	1034	87	13.76
6	11/7/12 1730	1237	139	82.28
7	11/7/12 1830	822	77	10.29
8	11/7/12 1930	1160	128	25.69
9	11/7/12 2030	1136	124	25.46
10	11/7/12 2130	962	84	13.59
11	11/7/12 2230	784	68	10.05
12	11/7/12 2330	644	59	9.85
13	11/8/12 0030	568	53	8.40

14	11/8/12 0130	537	54	7.88
15	11/8/12 0230	513	52	7.56
16	11/8/12 0330	531	55	8.48
17	11/8/12 0430	518	55	7.66
18	11/8/12 0530	499	55	9.23
19	11/8/12 0630	535	59	7.49
20	11/8/12 0730	622	61	8.77
21	11/8/12 0930	928	85	16.46
22	11/8/12 1055	1348	139	34.48

APPENDIX C

SEPTEMBER 2011 DAILY SAMPLING DATA

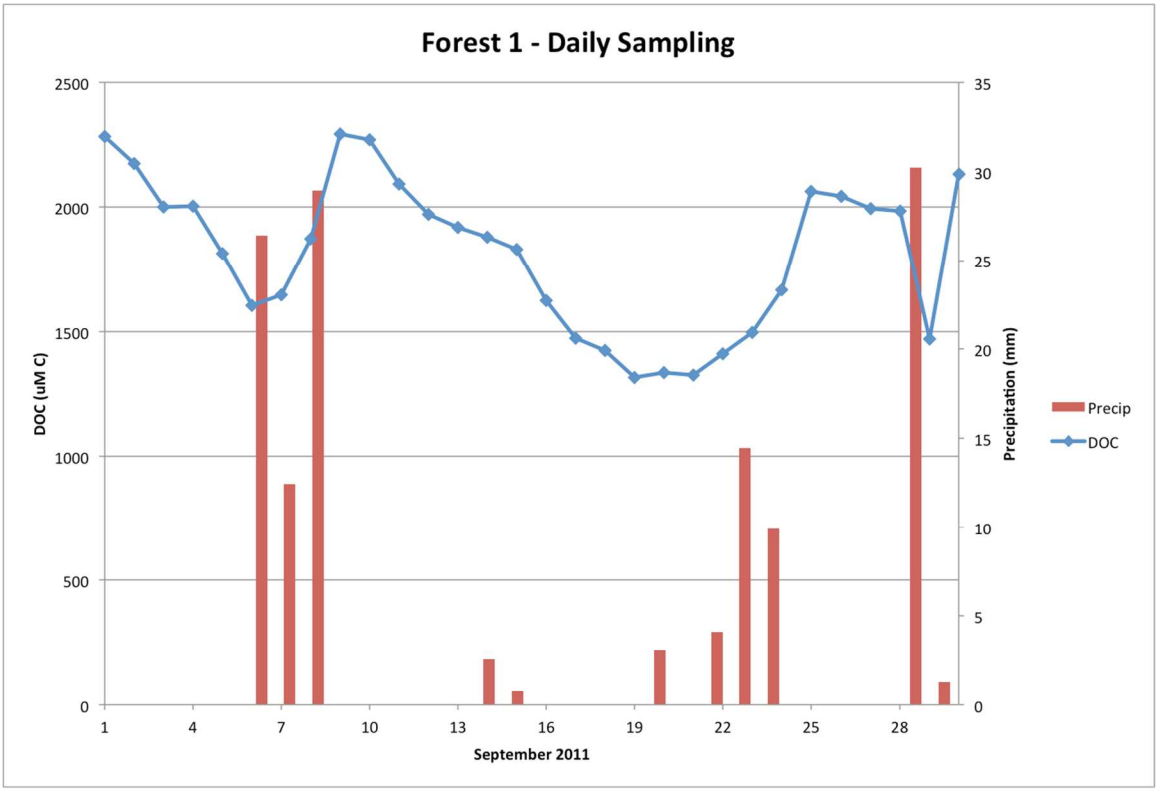

Figure C.1: Forest 1 daily DOC concentrations during September 2011. Graph also shows daily precipitation amounts during the month

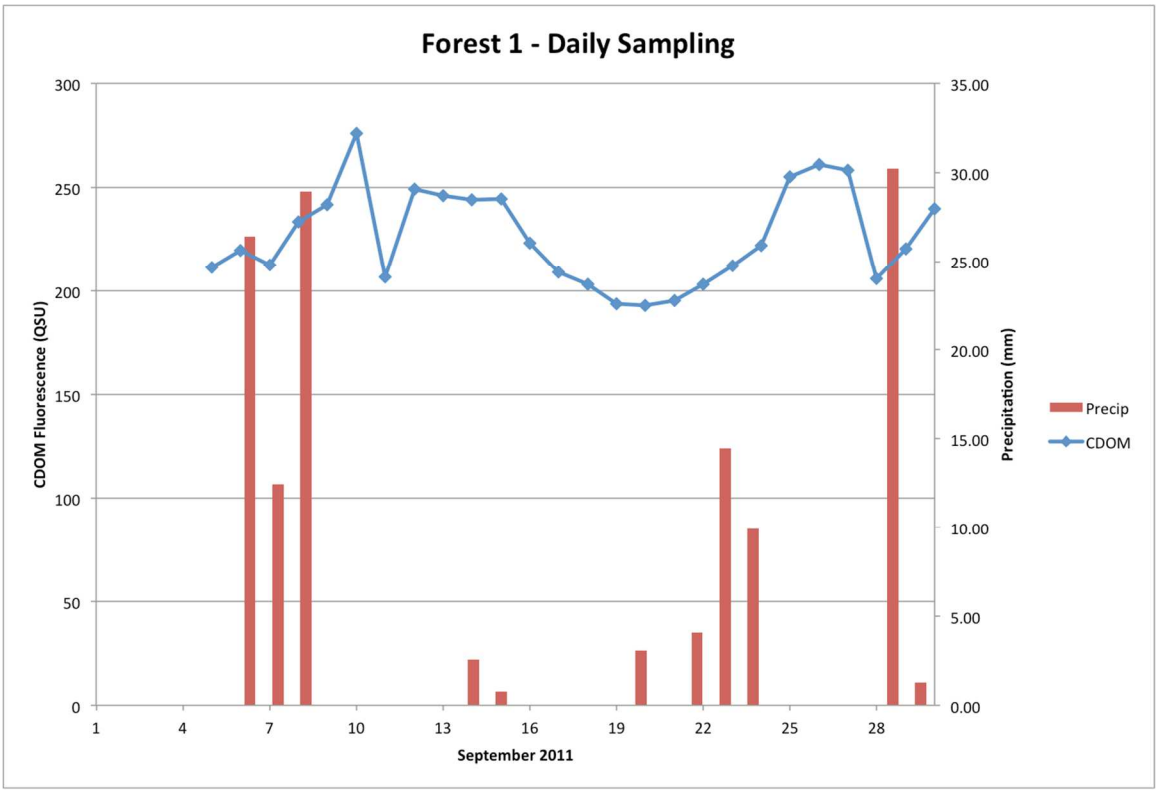

Figure C.2: Forest 1 daily CDOM concentrations during September 2011. Graph also shows daily precipitation amounts during the month

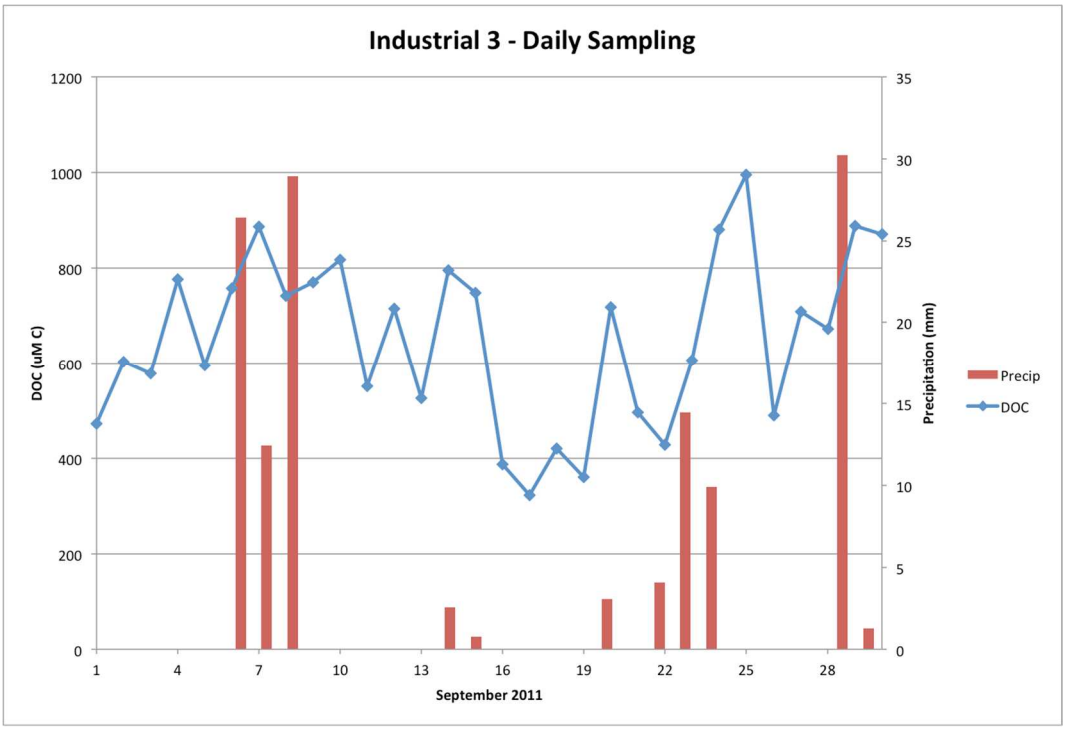

Figure C.3: Industrial 3 daily DOC concentrations during September 2011. Graph also shows daily precipitation amounts during the month

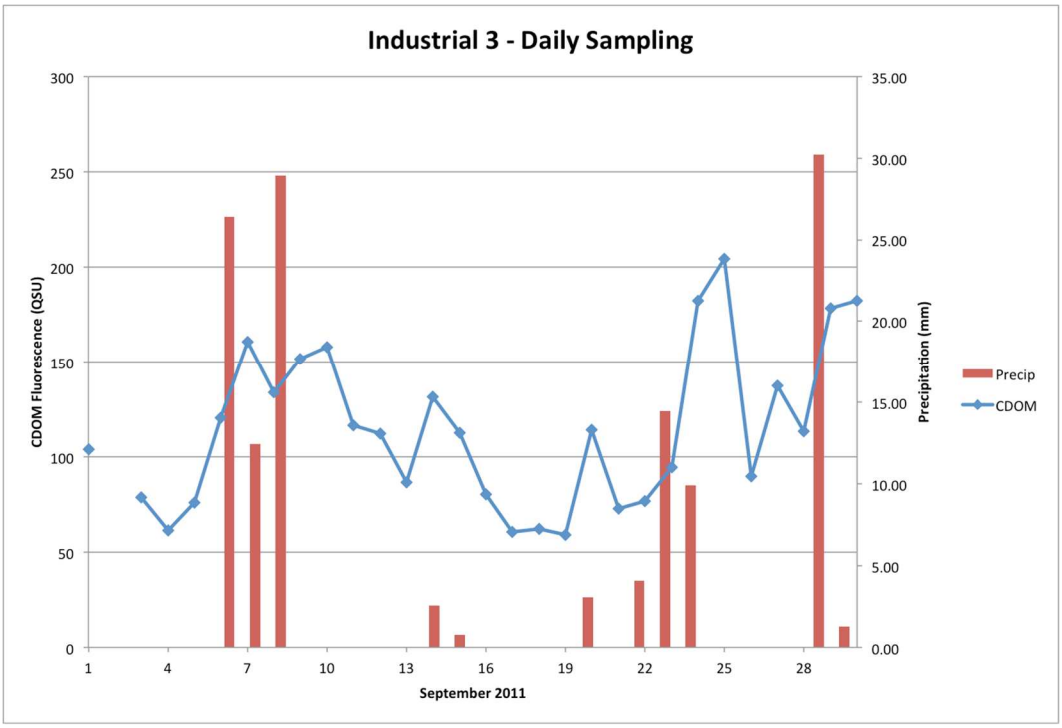

Figure C.4: Industrial 3 daily CDOM concentrations during September 2011. Graph also shows daily precipitation amounts during the month

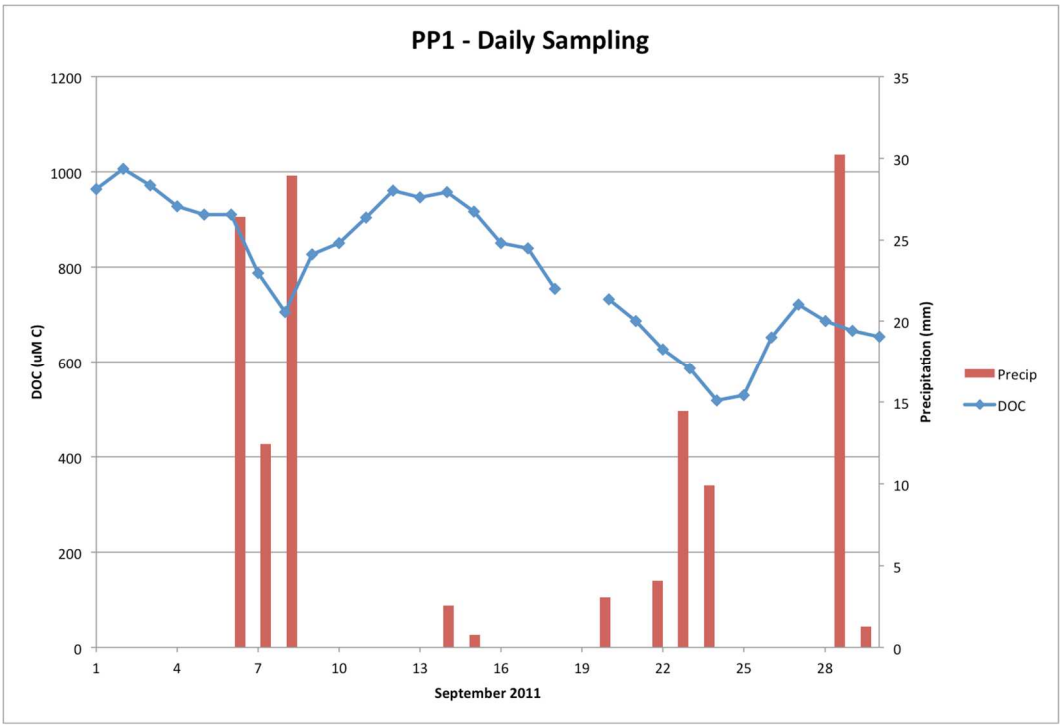

Figure C.5: PP1 daily DOC concentrations during September 2011. Graph also shows daily precipitation amounts during the month

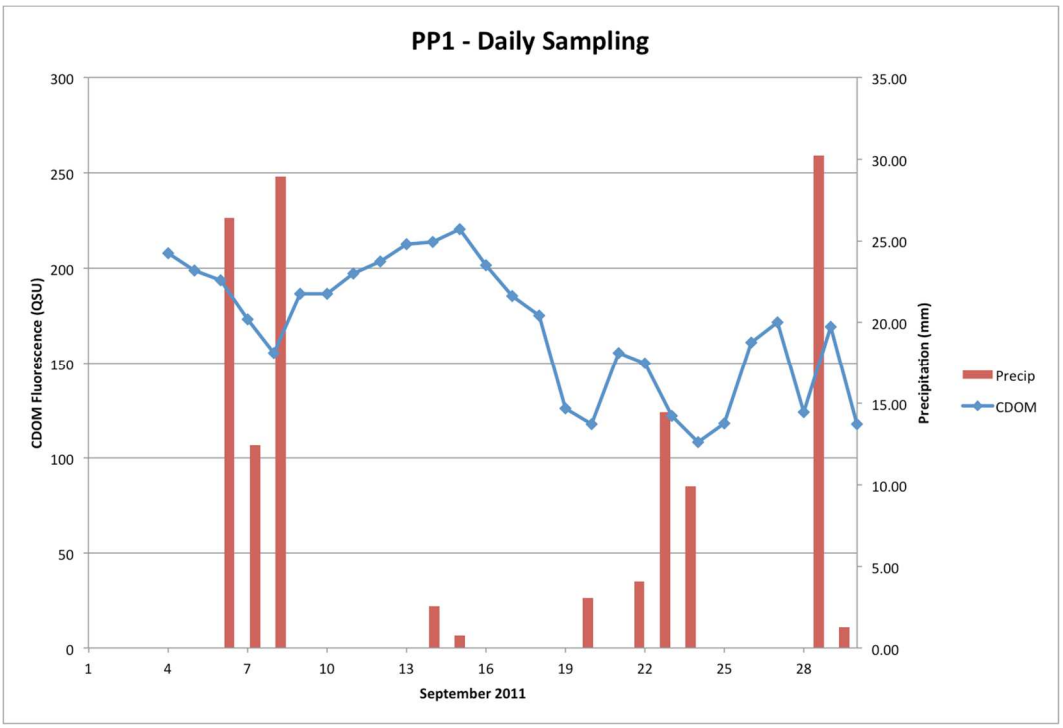

Figure C.6: PP1 daily CDOM concentrations during September 2011. Graph also shows daily precipitation amounts during the month

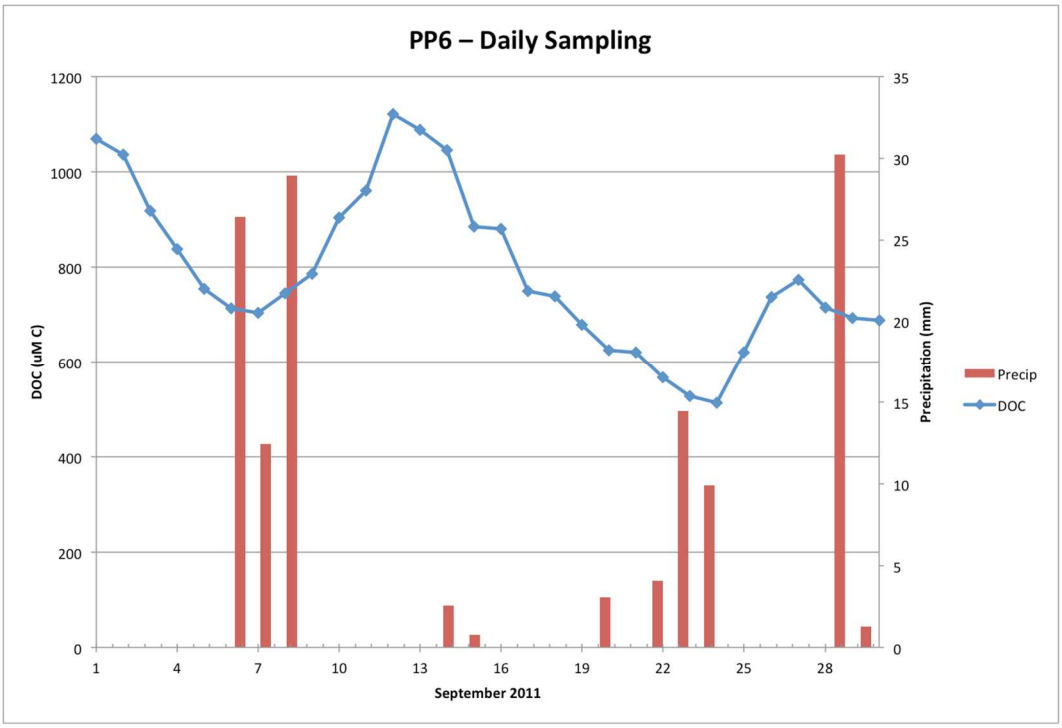

Figure C.7: PP6 daily DOC concentrations during September 2011. Graph also shows daily precipitation amounts during the month

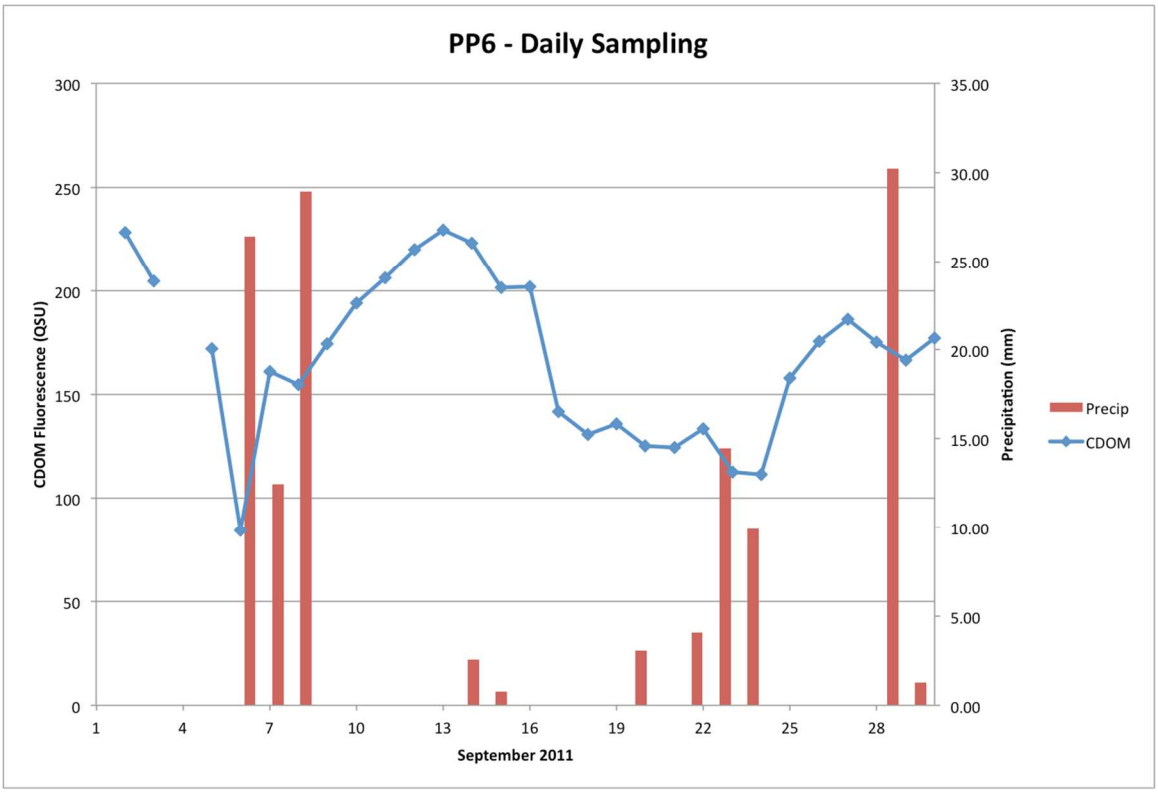

Figure C.8: PP6 daily CDOM concentrations during September 2011. Graph also shows daily precipitation amounts during the month

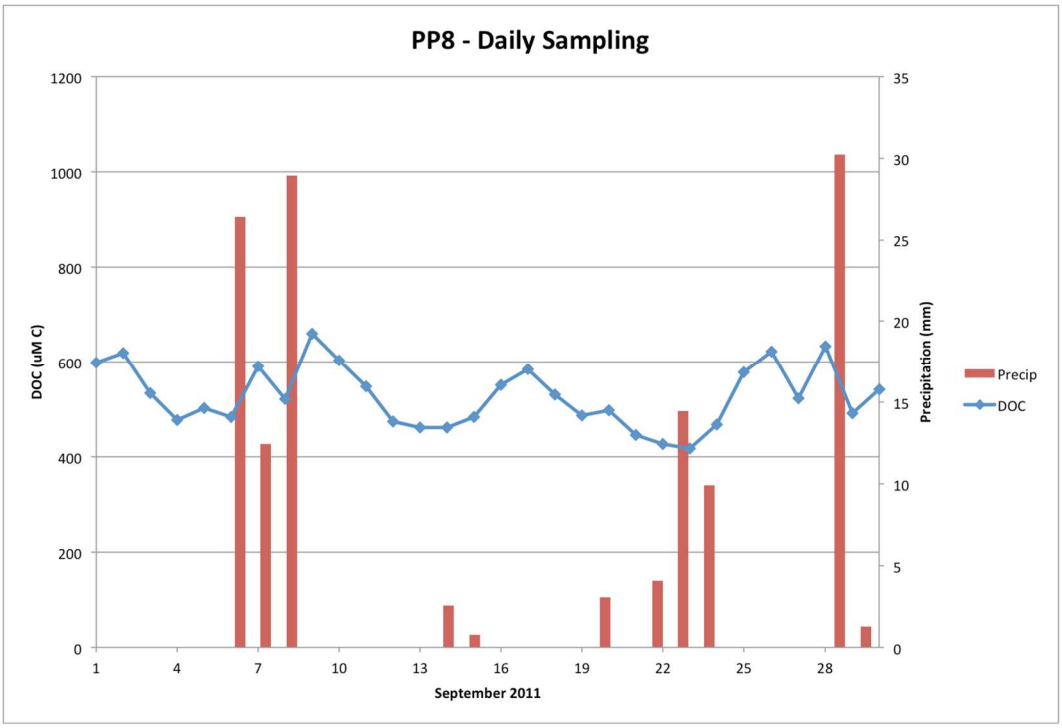

Figure C.9: PP8 daily DOC concentrations during September 2011. Graph also shows daily precipitation amounts during the month

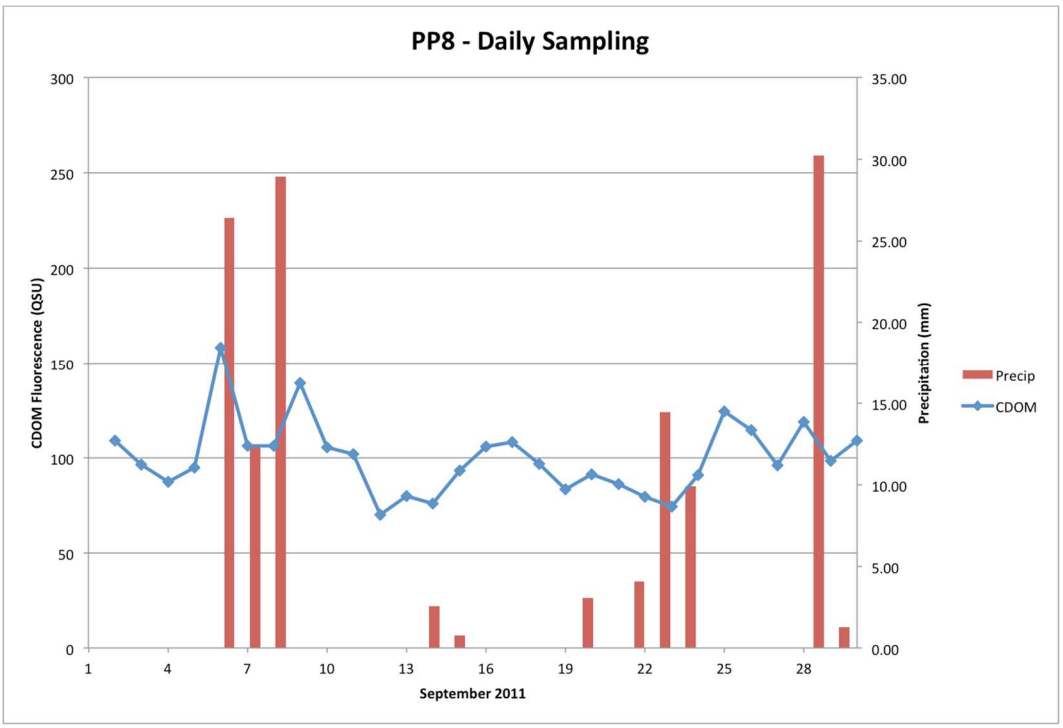

Figure C.10: PP8 daily CDOM concentrations during September 2011. Graph also shows daily precipitation amounts during the month

REFERENCE LIST

Ahn, J.H., Grant, S.B., Surbeck, C.Q., DiGiacomo, P.M., Nezlin, N.P., Jiang, S., 2005. Coastal water quality impact of stormwater runoff from an urban watershed in southern California. Environmental Science & Technology 39, 5940–5953.

Aldurrah, M., Bradford, J., 1982. The Mechanism of Raindrop Splash on Soil Surfaces. Soil Sci. Soc. Am. J. 46, 1086–1090.

Aller, R.C., Blair, N.E., 2006. Carbon remineralization in the Amazon-Guianas tropical mobile mudbelt: A sedimentary incinerator. Continental Shelf Research 26, 2241–2259.

Anderegg, W.R.L., Prall, J.W., Harold, J., Schneider, S.H., 2010. Expert credibility in climate change. PNAS 12107–12109.

Appel, P.L., Hudak, P.F., 2001. Automated sampling of stormwater runoff in an urban watershed, north-central Texas. Journal of Environmental Science and Health, Part A 36, 897–907.

Bach, P.M., McCarthy, D.T., Deletic, A., 2010. Redefining the stormwater first flush phenomenon. Water Research 44, 2487–2498.

Baker, A., Spencer, R.G.M., 2004. Characterization of dissolved organic matter from source to sea using fluorescence and absorbance spectroscopy. Science of The Total Environment 333, 217–232.

Barrett, M.E., Irish Jr., L.B., Malina Jr., J.F., Charbeneau, R.J., 1998. Characterization of highway runoff in Austin, Texas, Area. Journal of Environmental Engineering 124, 131.

Bauer, J.E., Cai, W.-J., Raymond, P.A., Bianchi, T.S., Hopkinson, C.S., Regnier, P.A.G., 2013. The changing carbon cycle of the coastal ocean. Nature 504, 61–70.

Beven, K.J., 2011. Rainfall-runoff modelling: the primer. John Wiley & Sons.

Blanquies, J., Scharff, M., Hallock, B., 2003. The Design and Construction of a Rainfall Simulator. International Erosion Control Association (IECA), 34th Annual Conference and Expo: Las Vegas, Nevada.

Boehm, A.B., Grant, S.B., Kim, J.H., Mowbray, S.L., McGee, C.D., Clark, C.D., Foley, D.M., Wellman, D.E., 2002. Decadal and shorter period variability of surf zone water quality at Huntington Beach, California. Environmental Science & Technology 36, 3885–3892.

Boissier, J.M., Fontvieille, D., 1995. Biological characteristics of forest soils and seepage waters during simulated rainfalls of high intensity. Soil Biology and Biochemistry 27, 139–145.

Boissier, J.M., Fontvieille, D., 1993. Biodegradable dissolved organic carbon in seepage waters from two forest soils. Soil Biology and Biochemistry 25, 1257–1261.

Bowers, D.G., Brett, H.L., 2008. The relationship between CDOM and salinity in estuaries: An analytical and graphical solution. Journal of Marine Systems 73, 1–7.

Bubenzer, G.D., 1979. Inventory of rainfall simulators. Proceedings of the Rainfall Simulator Workshop. Tucson, Arizona. 120–130.

Bubenzer, G.D., Molnau, M., McCool, D.K., 1985. Low intensity rainfall with a rotating disk simulator. Transactions of the ASAE-American Society of Agricultural Engineers 28.

Buffleben, M.S., Zayeed, K., Kimbrough, D., Stenstrom, M.K., Suffet, I.H., 2002. Evaluation of urban non-point source runoff of hazardous metals entering Santa Monica Bay, California. Water Science and Technology 263–268.

Cai, W.-J., Hu, X., Huang, W.-J., Murrell, M.C., Lehrter, J.C., Lohrenz, S.E., Chou, W.-C., Zhai, W., Hollibaugh, J.T., Wang, Y., Zhao, P., Guo, X., Gundersen, K., Dai, M., Gong, G.-C., 2011. Acidification of subsurface coastal waters enhanced by eutrophication. Nature Geosci 4, 766–770.

Chang, R., Goldsby, K.A., 2012. Chemistry, 11th Edition, 11th edition. ed. McGraw-Hill Science/Engineering/Math, New York.

Characklis, G.W., Wiesner, M.R., 1997. Particles, metals, and water quality in runoff from large urban watershed. Journal of Environmental Engineering 123, 753.

Chen, R.F., 1999. In situ fluorescence measurements in coastal waters. Organic Geochemistry 30, 397–409.

Chen, R.F., Gardner, G.B., 2004. High-resolution measurements of chromophoric dissolved organic matter in the Mississippi and Atchafalaya River plume regions. Marine Chemistry 89, 103–125.

Christiansen, J.E., 1942. Irrigation by sprinkling. California Agricultural Experiment Station Bulletin 670.

Coble, P.G., 2007. Marine optical biogeochemistry: The chemistry of ocean color. Chemical Reviews 107, 402–418.

Cole, J.J., Prairie, Y.T., Caraco, N.F., McDowell, W.H., Tranvik, L.J., Striegl, R.G., Duarte, C.M., Kortelainen, P., Downing, J.A., Middelburg, J.J., Melack, J., 2007. Plumbing the Global Carbon Cycle: Integrating Inland Waters into the Terrestrial Carbon Budget. Ecosystems 10, 172–185.

Conmy, R.N., Coble, P.G., Chen, R.F., Gardner, G.B., 2004. Optical properties of colored dissolved organic matter in the Northern Gulf of Mexico. Marine Chemistry 89, 127–144.

Cook, J., Nuccitelli, D., Green, S.A., Richardson, M., Winkler, B., Painting, R., Way, R., Jacobs, P., Skuce, A., 2013. Quantifying the consensus on anthropogenic global warming in the scientific literature. Environ. Res. Lett. 8.

Dai, M., Yin, Z., Meng, F., Liu, Q., Cai, W.-J., 2012. Spatial distribution of riverine DOC inputs to the ocean: an updated global synthesis. Current Opinion in Environmental Sustainability 4, 170–178.

Deletic, A., 1998. The first flush load of urban surface runoff. Water Research 32, 2462–2470.

Delpla, I., Baures, E., Jung, A.V., Thomas, O., 2011. Impacts of rainfall events on runoff water quality in an agricultural environment in temperate areas. Science of the Total Environment.

Del Vecchio, R., Blough, N.V., 2004. Spatial and seasonal distribution of chromophoric dissolved organic matter and dissolved organic carbon in the Middle Atlantic Bight. Marine Chemistry 89, 169–187.

Del Vecchio, R., Blough, N.V., 2002. Photobleaching of chromophoric dissolved organic matter in natural waters: kinetics and modeling. Marine Chemistry 78, 231–253.

Doney, S.C., Fabry, V.J., Feely, R.A., Kleypas, J.A., 2009. Ocean Acidification: The Other CO_2 Problem. Annual Review of Marine Science 1, 169–192.

Downing, B.D., Boss, E., Bergamaschi, B.A., Fleck, J.A., Lionberger, M.A., Ganju, N.K., Schoellhamer, D.H., Fujii, R., 2009. Quantifying fluxes and characterizing compositional changes of dissolved organic matter in aquatic systems in situ using combined acoustic and optical measurements. Limnology and Oceanography: Methods 7, 119–131.

Driscoll, E.D., Shelley, P.E., Strecker, E.W., 1990. Pollutant Loadings and Impacts from Highway Stormwater Runoff. National Technical Information Service.

Eckley, C.S., Branfireun, B., 2009. Simulated rain events on an urban roadway to understand the dynamics of mercury mobilization in stormwater runoff. Water Research 43, 3635–3646.

Eckley, C.S., Branfireun, B., 2008. Mercury mobilization in urban stormwater runoff. Science of the Total Environment 403, 164–177.

Eckley, C.S., Branfireun, B., Diamond, M., Van Metre, P.C., Heitmuller, F., 2008. Atmospheric mercury accumulation and washoff processes on impervious urban surfaces. Atmospheric Environment 42, 7429–7438.

Edwards, D.R., Sharpley, A.N., Humphry, J.B., Daniel, T.C., 2002. A Portable Rainfall Simulator for Plot-Scale Runoff Studies. Applied Engineering in Agriculture 18, 199–204.

Egodawatta, P., Thomas, E., Goonetilleke, A., 2007. Mathematical interpretation of pollutant wash-off from urban road surfaces using simulated rainfall. Water Research 41, 3025–3031.

Eigel, J.D., Moore, I.D., 1983. A simplified technique for measuring raindrop size and distribution. Transactions of the American Society of Agricultural Engineers 26.

Evans, C., Davies, T.D., 1998. Causes of concentration/discharge hysteresis and its potential as a tool for analysis of episode hydrochemistry. Water Resour. Res. 34, 129–137.

Evans, C.D., Monteith, D.T., Cooper, D.M., 2005. Long-term increases in surface water dissolved organic carbon: Observations, possible causes and environmental impacts. Environmental Pollution 137, 55–71.

Fabry, V.J., Seibel, B.A., Feely, R.A., Orr, J.C., 2008. Impacts of ocean acidification on marine fauna and ecosystem processes. ICES J. Mar. Sci. 65, 414–432.

Ferrari, G.M., 2000. The relationship between chromophoric dissolved organic matter and dissolved organic carbon in the European Atlantic coastal area and in the West Mediterranean Sea (Gulf of Lions). Marine Chemistry 70, 339–357.

Filella, M., Rodríguez-Murillo, J.C., 2014. Long-term Trends of Organic Carbon Concentrations in Freshwaters: Strengths and Weaknesses of Existing Evidence. Water 6, 1360–1418.

Findlay, S., Quinn, J.M., Hickey, C.W., Burrell, G., Downes, M., 2001. Effects of land use and riparian flowpath on delivery of dissolved organic carbon to streams. Limnology and Oceanography 46, 345–355.

Gardner, G.B., Chen, R.F., Berry, A., 2005. High-resolution measurements of chromophoric dissolved organic matter (CDOM) in the Neponset River Estuary, Boston Harbor, MA. Marine Chemistry 96, 137–154.

Garvey, E.A., Tobiason, J.E., 2003. Relationships between measures of NOM in Quabbin Watershed. Journal American Water Works Association 95, 73–84.

Gersberg, R.M., Daft, D., Yorkey, D., 2004. Temporal pattern of toxicity in runoff from the Tijuana River Watershed. Water Research 38, 559–568.

Gomi, T., Sidle, R.C., Richardson, J.S., 2002. Understanding processes and downstream linkages of headwater systems. BioScience 52, 905–916.

Grant, S.B., Sanders, B.F., Boehm, A.B., Redman, J.A., Kim, J.H., Mrše, R.D., Chu, A.K., Gouldin, M., McGee, C.D., Gardiner, N.A., others, 2001. Generation of enterococci bacteria in a coastal saltwater marsh and its impact on surf zone water quality. Environmental Science & Technology 35, 2407–2416.

Greenley, D.A., Walsh, R.G., Young, R.A., 1981. Option value: empirical evidence from a case study of recreation and water quality. The Quarterly Journal of Economics 96, 657.

Green, S.A., Blough, N.V., 1994. Optical absorption and fluorescence properties of chromophoric dissolved organic matter in natural waters. Limnology and Oceanography 39, 1903–1916.

Gunn, R., Kinzer, G.D., 1949. The Terminal Velocity of Fall for Water Droplets in Stagnant Air. Journal of Atmospheric Sciences 6, 243–248.

Hairsine, P., Rose, C., 1991. Rainfall Detachment and Deposition - Sediment Transport in the Absence of Flow-Driven Processes. Soil Sci. Soc. Am. J. 55, 320–324.

Hart, J.K., Martinez, K., 2006. Environmental Sensor Networks: A revolution in the earth system science? Earth-Science Reviews 78, 177–191.

Hathaway, J.M., Hunt, W.F., 2010. Evaluation of First Flush for Indicator Bacteria and Total Suspended Solids in Urban Stormwater Runoff. Water, Air, & Soil Pollution 1–13.

Hedges, J.I., Keil, R.G., Benner, R., 1997. What happens to terrestrial organic matter in the ocean? Organic Geochemistry 27, 195–212.

Hedin, L.O., von Fischer, J.C., Ostrom, N.E., Kennedy, B.P., Brown, M.G., Robertson, G.P., 1998. Thermodynamic Constraints on Nitrogen Transformations and Other Biogeochemical Processes at Soil-Stream Interfaces. Ecology 79, 684–703.

He, J., Valeo, C., Chu, A., Neumann, N.F., 2010. Characteristics of Suspended Solids, Microorganisms, and Chemical Water Quality in Event-Based Stormwater Runoff from an Urban Residential Area. Water Environment Research 82, 2333–2345.

Hellweger, F.L., 2007. Ensemble modeling of E. coli in the Charles River, Boston, Massachusetts, USA. Water Science and Technology 56, 39–46.

Hellweger, F.L., Masopust, P., 2008. Investigating the Fate and Transport of Escherichia coli in the Charles River, Boston, Using High-Resolution Observation and Modeling1. Journal of the American Water Resources Association 44, 509–522.

Helms, J.R., Stubbins, A., Ritchie, J.D., Minor, E.C., Kieber, D.J., Mopper, K., 2008. Absorption spectral slopes and slope ratios as indicators of molecular weight, source, and photobleaching of chromophoric dissolved organic matter. Limnology and Oceanography 53, 955.

Herngren, L., Goonetilleke, A., Ayoko, G.A., 2005. Understanding Heavy Metal and Suspended Solids Relationships in Urban Stormwater Using Simulated Rainfall. Journal of Environmental Management 76, 149–158.

Hewlett, J.D., Hibbert, A.R., 1967. Factors affecting the response of small watersheds to precipitation in humid areas. Forest Hydrology 275–290.

Hinton, M.J., Schiff, S.L., English, M.C., 1998. Sources and Flowpaths of Dissolved Organic Carbon during Storms in Two Forested Watersheds of the Precambrian Shield. Biogeochemistry 41, 175–197.

Hongve, D., 1999. Production of dissolved organic carbon in forested catchments. Journal of Hydrology 224, 91–99.

Hood, E., Gooseff, M.N., Johnson, S.L., 2006. Changes in the character of stream water dissolved organic carbon during flushing in three small watersheds, Oregon. Journal of Geophysical Research: Biogeosciences 111.

Howarth, R.W., Sharpley, A., Walker, D., 2002. Sources of nutrient pollution to coastal waters in the United States: Implications for achieving coastal water quality goals. Estuaries and Coasts 25, 656–676.

Huang, W., Chen, R.F., 2009. Sources and transformations of chromophoric dissolved organic matter in the Neponset River Watershed. Journal of Geophysical Research 114.

Hu, C., Muller-Karger, F.E., Zepp, R.G., 2002. Absorbance, absorption coefficient, and apparent quantum yield: A comment on common ambiguity in the use of these optical concepts. Limnology and Oceanography 47, 1261–1267.

Hudson, N., 1993. Field Measurement of Soil Erosion and Runoff. Food & Agriculture Organization of the United Nations.

Intergovernmental Panel on Climate Change, 2013. Climate Change 2013: The Physical Science Basis. Contribution of Working Group I to the Fifth Assessment Report of the Intergovernmental Panel on Climate Change 2013. Cambridge University Press, Cambridge, UK, and New York.

Intergovernmental Panel on Climate Change, 2007. Climate change 2007: the physical science basis: contribution of Working Group I to the Fourth Assessment Report of the Intergovernmental Panel on Climate Change. Cambridge University Press, Cambridge, UK, and New York.

Jackson, G.A., Williams, P.M., 1985. Importance of dissolved organic nitrogen and phosphorus to biological nutrient cycling. Deep Sea Research Part A. Oceanographic Research Papers 32, 223–235.

Jakeman, A.J., Hornberger, G.M., 1993. How much complexity is warranted in a rainfall-runoff model? Water Resources Research 29, 2637–2649.

Jeong, Y., Sanders, B.F., Grant, S.B., 2006. The information content of high-frequency environmental monitoring data signals pollution events in the coastal ocean. Environmental Science & Technology 40, 6215–6220.

Kalbitz, K., Solinger, S., Park, J.H., Michalzik, B., Matzner, E., 2000. Controls on the dynamics of dissolved organic matter in soils: a review. Soil Science 165, 277.

Kang, J.H., Kayhanian, M., Stenstrom, M.K., 2008. Predicting the existence of stormwater first flush from the time of concentration. Water Research 42, 220–228.

Kaplan, L.A., Newbold, J.D., Van Horn, D.J., Dow, C.L., Aufdenkampe, A.K., Jackson, J.K., 2006. Organic matter transport in New York City drinking-water-supply watersheds. J. N. Am. Benthol. Soc. 25.

Karl, T.R., Trenberth, K.E., 2003. Modern global climate change. Science 302, 1719–1723.

Kayhanian, M., Stenstrom, M.K., 2008. First-Flush Characterization for Stormwater Treatment [WWW Document]. URL http://www.stormh2o.com/SW/Articles/100.aspx (accessed 2.21.14).

Keith, D.J., Yoder, J.A., Freeman, S.A., 2002. Spatial and temporal distribution of coloured dissolved organic matter (CDOM) in Narragansett Bay, Rhode Island: implications for phytoplankton in coastal waters. Estuarine, Coastal and Shelf Science 55, 705–717.

Kemp, W.M., Smith, E.M., Marvin-DiPasquale, M., Boynton, W.R., 1997. Organic carbon balance and net ecosystem metabolism in Chesapeake Bay. Marine Ecology Progress Series 150, 229–248.

Lascano, R.J., Vorheis, J.T., Baumhardt, R.L., Salisbury, D.R., 1997. Computer-controlled variable intensity rain simulator. Soil Science Society of America Journal 61, 1182–1189.

Laws, J.O., 1941. Measurements of the fall-velocity of water -drops and raindrops. Transactions, American Geophysical Union 22, 709.

Laws, J.O., Parsons, D.A., 1943. The relation of raindrop-size to intensity. Transactions, American Geophysical Union 24, 452–460.

Lee, J.H., Bang, K.W., 2000. Characterization of urban stormwater runoff. Water Research 34, 1773–1780.

Lee, J.H., Bang, K.W., Ketchum, L.H., others, 2002. First flush analysis of urban storm runoff. The Science of the Total Environment 293, 163–175.

Lee, J.Y., Kim, Y., Han, M.Y., Kim, H., 2011. Characteristics of the event mean concentration (EMC) from rainfall runoff on an urban highway. Environmental Pollution.

Levin, I., Hesshaimer, V., 2000. Radiocarbon - a unique tracer of global carbon cycle dynamics. Radiocarbon 42, 69–80.

Loch, R.J., Robotham, B.G., Zeller, L., Masterman, N., Orange, D.N., Bridge, B.J., Sheridan, G., Bourke, J.J., 2001. A multi-purpose rainfall simulator for field infiltration and erosion studies. Soil Res. 39, 599–610.

Long, R.P., Demars, K.R., 2005. Design considerations for a prototype erosion control testing plot. The New England Transportation Consortium.

Makepeace, D.K., Smith, D.W., Stanley, S.J., 1995. Urban stormwater quality: Summary of contaminant data. Critical Reviews in Environmental Science and Technology 25, 93–139.

McKnight, D.M., Smith, R.L., Harnish, R.A., Miller, C.L., Bencala, K.E., 1993. Seasonal Relationships between Planktonic Microorganisms and Dissolved Organic Material in an Alpine Stream. Biogeochemistry 21, 39–59.

McLaughlin, C., Kaplan, L.A., 2013. Biological lability of dissolved organic carbon in stream water and contributing terrestrial sources. Freshwater Science 32, 1219–1230.

Meyer, L.D., 1979. Methods for attaining desired rainfall characteristics in rainfall simulators., in: Agricultural Reviews and Manuals. Presented at the Rainfall Simulator Workshop. Tucson (USA).

Meyer, L.D., Harmon, W.C., 1979. Multiple-intensity rainfall simulator for erosion research on row sideslopes. Transactions of the American Society of Agricultural Engineers 22.

Michaud, J., 1994. A Citizen's Guide to Understanding and Monitoring Lakes and Streams [WWW Document]. Washington State Department of Ecology. URL http://www.ecy.wa.gov/programs/wq/plants/management/joysmanual/ (accessed 8.10.13).

Miller, J.L., Gardner, L.R., 1981. Sheet flow in a salt-marsh basin, North Inlet, South Carolina. Estuaries and Coasts 4, 234–237.

Miller, W.P., 1987. A Solenoid-Operated, Variable Intensity Rainfall Simulator. Soil Science Society of America Journal 51, 832–834.

Morris, D.P., Zagarese, H., Williamson, C.E., Balseiro, E.G., Hargreaves, B.R., Modenutti, B., Moeller, R., Queimalinos, C., 1995. The attenuation of solar UV radiation in lakes and the role of dissolved organic carbon. Limnology and Oceanography 1381–1391.

MWRA, 2014. MWRA's Neponset River Page [WWW Document]. URL http://www.mwra.state.ma.us/harbor/html/nr_wq.htm (accessed 3.23.15).

National Oceanic and Atmospheric Administration, 2012. NOAA's State of the Coast: State of the Coast, Population Indicator [WWW Document]. URL http://stateofthecoast.noaa.gov/population/welcome.html (accessed 2.23.15).

Neff, J.C., Asner, G.P., 2001. Dissolved organic carbon in terrestrial ecosystems: synthesis and a model. Ecosystems 4, 29–48.

Neponset River Watershed Association, 2014a. NepRWA Action Plan [WWW Document]. Neponset River Watershed Association. URL http://www.neponset.org/about/action-plan/ (accessed 3.23.15).

Neponset River Watershed Association, 2014b. Neponset River Water Quality Data [WWW Document]. Neponset River Watershed Association. URL https://www.neponset.org/projects/water-quality/water-quality-and-cwmn/cwmn-data/ (accessed 3.23.15).

Neponset River Watershed Association, 2014c. Neponset Watershed Map [WWW Document]. Neponset River Watershed Association. URL http://www.neponset.org/your-watershed/your-watershed-map/ (accessed 3.23.15).

NOAA NWS Office of Climate, Weather and Water Services, 2013. Hurricane/Post-Tropical Cyclone Sandy, October 22-29, 2012 Service Assessment.

Opsahl, S., Benner, R., 1997. Distribution and cycling of terrigenous dissolved organic matter in the ocean. Nature 386, 480–482.

Pace, M.L., Cole, J.J., Carpenter, S.R., Kitchell, J.F., Hodgson, J.R., Van de Bogert, M.C., Bade, D.L., Kritzberg, E.S., Bastviken, D., 2004. Whole-lake carbon-13 additions reveal terrestrial support of aquatic food webs. Nature 427, 240–243.

Pachauri, R.K., Reisinger, A., 2007. Climate Change 2007: Synthesis Report. Contribution of Working Groups I, II and III to the Fourth Assessment Report of the Intergovernmental Panel on Climate Change. Intergovernmental Panel on Climate Change 1.

Parsakhoo, A., Lotfalian, M., Kavian, A., Hoseini, S.A., Demir, M., 2012. Calibration of a portable single nozzle rainfall simulator for soil erodibility study in hyrcanian forests. African Journal of Agricultural Research 7, 3957–3963.

Peeler, K.A., Opsahl, S.P., Chanton, J.P., 2006. Tracking anthropogenic inputs using caffeine, indicator bacteria, and nutrients in rural freshwater and urban marine systems. Environmental Science & Technology 40, 7616–7622.

Pérez-Latorre, F.J., de Castro, L., Delgado, A., 2010. A comparison of two variable intensity rainfall simulators for runoff studies. Soil and Tillage Research 107, 11–16.

Pitt, R., 1999. Small storm hydrology and why it is important for the design of stormwater control practices, in: James, W (Ed.), Advances in Modeling the Management of Stormwater Impacts. Ontario and Lewis Publishers/CRC Press, pp. 61–91.

Pruss, A., 1998. Review of epidemiological studies on health effects from exposure to recreational water. International Journal of Epidemiology 27, 1–9.

Puchalski, M.M., Morra, M.J., Wandruszka, R. von, 1991. Assessment of inner filter effect corrections in fluorimetry. Fresenius J Anal Chem 340, 341–344.

Qian, J., Mopper, K., 1996. Automated high-performance, high-temperature combustion total organic carbon analyzer. Analytical Chemistry 68, 3090–3097.

Qualls, R.G., Haines, B.L., Swank, W.T., 1991. Fluxes of dissolved organic nutrients and humic substances in a deciduous forest. Ecology 254–266.

Rabalais, N.N., Turner, R.E., Wiseman Jr, W.J., 2002. Gulf of Mexico Hypoxia, AKA" The Dead Zone." Annual Review of Ecology and Systematics 235–263.

Ravichandran, M., 2004. Interactions between mercury and dissolved organic matter—-a review. Chemosphere 55, 319–331.

Raymond, P.A., Saiers, J.E., 2010. Event controlled DOC export from forested watersheds. Biogeochemistry 100, 197–209.

Riebeek, H., 2011. NASA Earth Observatory : [WWW Document]. URL http://earthobservatory.nasa.gov/Features/CarbonCycle/page1.php (accessed 2.20.14).

Rundel, P.W., Graham, E.A., Allen, M.F., Fisher, J.C., Harmon, T.C., 2009. Environmental Sensor Networks in Ecological Research. New Phytologist 182, 589–607.

Saraceno, J.F., Pellerin, B.A., Downing, B.D., Boss, E., Bachand, P.A., Bergamaschi, B.A., 2009. High-frequency in situ optical measurements during a storm event: Assessing relationships between dissolved organic matter, sediment concentrations, and hydrologic processes. Journal of Geophysical Research: Biogeosciences 114.

Schiff, K.C., Tiefenthaler, L.L., 2003. Seasonal Flushing of Pollutant Concentrations and Loads in Urban Stormwater1. Journal of the American Water Resources Association.

Schlesinger, W.H., Bernhardt, E.S., 2013. Biogeochemistry: An Analysis of Global Change. Academic Press.

Schlunz, B., Schneider, R.R., 2000. Transport of terrestrial organic carbon to the oceans by rivers: re-estimating flux- and burial rates. International Journal of Earth Sciences 88, 599–606.

Schneider, S.H., 1989. The Greenhouse Effect: Science and Policy. Science 243, 771–81.

Selvendiran, P., Driscoll, C.T., Bushey, J.T., Montesdeoca, M.R., 2008. Wetland influence on mercury fate and transport in a temperate forested watershed. Environmental Pollution 154, 46–55.

Shanley, J.B., Alisa Mast, M., Campbell, D.H., Aiken, G.R., Krabbenhoft, D.P., Hunt, R.J., Walker, J.F., Schuster, P.F., Chalmers, A., Aulenbach, B.T., others, 2008. Comparison of total mercury and methylmercury cycling at five sites using the small watershed approach. Environmental Pollution 154, 143–154.

Shaw, S.B., Walter, M.T., Steenhuis, T.S., 2006. A physical model of particulate wash-off from rough impervious surfaces. Journal of Hydrology 327, 618–626.

Shelton, C.H., Von Bernuth, R.D., Rajbhandari, S.P., 1985. A continuous-application rainfall simulator. Transactions of the American Society of Agricultural Engineers 28.

Sheng, Y., Ying, G., Sansalone, J., 2008. Differentiation of transport for particulate and dissolved water chemistry load indices in rainfall-runoff from urban source area watersheds. Journal of Hydrology 361, 144–158.

Siegener, R., Chen, R.F., 2002. Caffeine in Boston Harbor seawater. Marine Pollution Bulletin 44, 383–387.

Smith, R.E., Goodrich, D.C., 2005. Rainfall excess overland flow, in: Encyclopedia of Hydrological Sciences. John Wiley & Sons, pp. 1707–1718.

Stedmon, C.A., Markager, S., Bro, R., 2003. Tracing dissolved organic matter in aquatic environments using a new approach to fluorescence spectroscopy. Marine Chemistry 82, 239–254.

Stedmon, C.A., Markager, S., Kaas, H., 2000. Optical properties and signatures of chromophoric dissolved organic matter (CDOM) in Danish coastal waters. Estuarine, Coastal and Shelf Science 51, 267–278.

Stenstrom, M., Kayhanian, M., 2005. First Flush Phenomenon Characterization (Final report No. CTSW-RT-05-73-02.6). California Department of Transportation, Sacramento, CA.

Stewart, J.R., Gast, R.J., Fujioka, R.S., Solo-Gabriele, H.M., Meschke, J.S., Amaral-Zettler, L.A., Del Castillo, E., Polz, M.F., Collier, T.K., Strom, M.S., others, 2008. The coastal environment and human health: microbial indicators, pathogens, sentinels and reservoirs. Environmental Health 7, S3.

Stieglitz, M., Shaman, J., McNamara, J., Engel, V., Shanley, J., Kling, G.W., 2003. An approach to understanding hydrologic connectivity on the hillslope and the implications for nutrient transport. Global Biogeochem. Cycles 17, 1105.

Thomas, N.P., El Swaify, S.A., 1989. Construction and calibration of a rainfall simulator. Journal of Agricultural Engineering Research 43, 1–9.

Tian, Y.Q., Yu, Q., Feig, A.D., Ye, C., Blunden, A., 2013. Effects of climate and land-surface processes on terrestrial dissolved organic carbon export to major U.S. coastal rivers. Ecological Engineering 54, 192–201.

Tiefenthaler, L.L., Schiff, K.C., 2003. Effects of rainfall intensity and duration on first flush of stormwater pollutants. Southern California Coastal Water Research Projects.

Tiefenthaler, L.L., Schiff, K.C., Bay, S.M., 2001a. Characteristics of parking lot runoff produced by simulated rainfall. Southern California Coastal Water Research Project.

Tiefenthaler, L.L., Schiff, K.C., Leecaster, M.K., 2001b. Temporal variability patterns of stormwater concentrations in urban stormwater runoff. Southern California Coastal Water Research Projects.

USDA, 2013a. Web Soil Survey [WWW Document]. URL http://websoilsurvey.nrcs.usda.gov/app/WebSoilSurvey.aspx (accessed 4.5.15).

USDA, 2013b. Rapid Assessment of U.S. Soil Carbon (RaCA) | NRCS [WWW Document]. URL http://www.nrcs.usda.gov/wps/portal/nrcs/detail/soils/survey/?cid=nrcs142p2_054164 (accessed 4.5.15).

U.S. Environmental Protection Agency, 2012. Stormwater Management Best Practices [WWW Document]. URL http://www.epa.gov/greeningepa/stormwater/best_practices.htm (accessed 2.23.15).

Van Dijk, A., Bruijnzeel, L.A., Rosewell, C.J., 2002. Rainfall intensity–kinetic energy relationships: a critical literature appraisal. Journal of Hydrology 261, 1–23.

Vaze, J., Chiew, F.H.S., 2003. Study of pollutant washoff from small impervious experimental plots. Water Resour. Res. 39, 1160.

Vaze, J., Chiew, F.H.S., 2002. Experimental study of pollutant accumulation on an urban road surface. Urban Water 4, 379–389.

Wada, K., Yamanaka, S., Yamamoto, M., Toyooka, K., 2006. The characteristics and measuring technique of refractory dissolved organic substances in urban runoff. Water Science and Technology 53, 193.

Wade, T.J., Calderon, R.L., Sams, E., Beach, M., Brenner, K.P., Williams, A.H., Dufour, A.P., 2006. Rapidly measured indicators of recreational water quality are predictive of swimming-associated gastrointestinal illness. Environmental Health Perspectives 114, 24.

Wade, T.J., Pai, N., Eisenberg, J.N.S., Colford Jr, J.M., 2003. Do US Environmental Protection Agency water quality guidelines for recreational waters prevent gastrointestinal illness? A systematic review and meta-analysis. Environmental Health Perspectives 111, 1102.

Wahl, M.H., McKellar, H.N., Williams, T.M., 1997. Patterns of nutrient loading in forested and urbanized coastal streams. Journal of Experimental Marine Biology and Ecology, Urbanization and Southeastern Estuaries 213, 111–131.

Wang, X.-C., Chen, R.F., Gardner, G.B., 2004. Sources and transport of dissolved and particulate organic carbon in the Mississippi River estuary and adjacent coastal waters of the northern Gulf of Mexico. Marine Chemistry 89, 241–256.

Westerhoff, P., Anning, D., 2000. Concentrations and characteristics of organic carbon in surface water in Arizona: influence of urbanization. Journal of Hydrology 236, 202–222.

Wigington Jr, P.J., Baker, J.P., DeWalle, D.R., Kretser, W.A., Murdoch, P.S., Simonin, H.A., Van Sickle, J., McDowell, M.K., Peck, D.V., Barchet, W.R., 1996. Episodic acidification of small streams in the northeastern United States: Episodic Response Project. Ecological Applications 374–388.

Wilcox, B.P., Wood, M.K., Tromble, J.T., Ward, T.J., 1986. A hand-portable single nozzle rainfall simulator designed for use on steep slopes. Journal of Range Management 375–377.

Wiley, P.C., Leeworthy, V.R., Stone, E.A., 2006. Economic Impact of Beach Closures and Changes in Water Quality for Beaches in Southern California. National Oceanic and Atmospheric Administration.

Xenopoulos, M.A., Lodge, D.M., Frentress, J., Kreps, T.A., Bridgham, S.D., Grossman, E., Jackson, C.J., 2003. Regional comparisons of watershed determinants of dissolved organic carbon in temperate lakes from the Upper Great Lakes region and selected regions globally. Limnology and Oceanography 48, 2321–2334.

Yamashita, Y., Jaffé, R., 2008. Characterizing the Interactions between Trace Metals and Dissolved Organic Matter Using Excitation- Emission Matrix and Parallel Factor Analysis. Environmental Science & Technology 42, 7374–7379.

Yamashita, Y., Jaffé, R., Maie, N., Tanoue, E., 2008. Assessing the dynamics of dissolved organic matter (DOM) in coastal environments by excitation emission matrix fluorescence and parallel factor analysis (EEM-PARAFAC). Limnology and Oceanography 53, 1900–1908.

Yang, Y., 2013. Studying Soil Moisture and Land-to-Water Carbon Export in Urbanized Coastal Areas Using Remotely Sensed Data and a Regional Hydro-Ecological Model (Doctoral Dissertation). University of Massachusetts Boston.

Yang, Y., He, Z., Wang, Y., Fan, J., Liang, Z., Stoffella, P.J., 2013. Dissolved organic matter in relation to nutrients (N and P) and heavy metals in surface runoff water as affected by temporal variation and land uses – A case study from Indian River Area, south Florida, USA. Agricultural Water Management 118, 38–49.

Yau, V., Wade, T.J., de Wilde, C.K., Colford Jr, J.M., 2009. Skin-related symptoms following exposure to recreational water: a systematic review and meta-analysis. Water Quality, Exposure and Health 1, 79–103.

Zhang, W., Zhang, S., Yue, D., Wan, C., Ye, Y., Wang, X., 2008. Characterization and loading estimation of polycyclic aromatic hydrocarbons in road runoff from urban regions of Beijing, China. Environmental Toxicology and Chemistry 27, 31–37.

Zhang, Y., Qin, B., Zhu, G., Zhang, L., Yang, L., 2007. Chromophoric dissolved organic matter (CDOM) absorption characteristics in relation to fluorescence in Lake Taihu, China, a large shallow subtropical lake. Hydrobiologia 581, 43–52.

Zia, H., Harris, N.R., Merrett, G.V., Rivers, M., Coles, N., 2013. The impact of agricultural activities on water quality: A case for collaborative catchment-scale management using integrated wireless sensor networks. Computers and Electronics in Agriculture 96, 126–138.